

**Antarctic climate and vegetation  
during the Neogene: a  
geochemical and modelling  
approach**

**Rhian Laura Rees-Owen**

Submitted in accordance with the requirements for the degree of  
Doctor of Philosophy

The University of Leeds  
School of Earth and Environment

August 2016



The candidate confirms that the work submitted is her own and that appropriate credit has been given where reference has been made to the work of others.

This copy has been supplied on the understanding that it is copyright material and that no quotation from the thesis may be published without proper acknowledgement.

Copyright © **2016** The University of Leeds and **Rhian Rees-Owen**

The right of **Rhian Rees-Owen** to be identified as Author of this work has been asserted by her in accordance with the Copyright, Designs and Patents Act 1988.



# Acknowledgements

First and foremost, I would like to thank my supervisors; Rob Newton, Ruza Ivanovic, Jane Francis and James Riding, for their invaluable support, expertise and encouragement over the last four years. I have learnt an incredible amount under their guidance, and they have enabled me to spend as much time gallivanting as I liked.

I am grateful to my collaborators; Fiona Gill, Julia Tindall, Paul Valdes, Rich Pancost, Jens Holtvoeth, Christopher Vane, Raquel Lopes dos Santos and Alina Marca for sharing their knowledge and expertise. Lauren Grégoire, Amanda Maycock, Tracy Aze, Dan Hill, Andy Connolly, Fiona Keay, Santi Clerici and Stephen Reid and other members of the Palaeo@Leeds, Cohen Geochemistry and Physical Climate Change Groups also deserve many thanks for technical support and very useful scientific discussions.

The British Geological Survey are thanked for their CASE support, which has made life infinitely easier. The Trans-Antarctic Association, Geochemistry Group, Palaeontological Association, UK-IODP, University of Utah and ESSi are thanked for travel and subsistence funding which allowed me to attend several conferences and summer schools, and carry out fieldwork in Chile. I could not have carried out my research without Omora Ethnobotanical Park giving me permission to sample their trees and use their field station, or Marcelo Leppe at INACH giving me invaluable support and advice on conducting fieldwork in Chile. Roel Brienen was kind enough to loan me his tree ring expertise, increment borers, microtomes and lab space on many occasions. My thanks are also extended to the British Antarctic Survey for the loan of fossil samples.

There are many people within the School of Earth and Environment who have made the last four years a brilliant experience. Special thanks go to Caroline Prescott, James Witts and Edine Pape for both enlightening and mood-lightening chats, as well as to my lovely office mates through the years; Jo, Maggie, Chris, Laura, Tom and Autumn, you've been stellar. I am grateful to Hannah Goddard for proofreading more geochemistry than any non-geochemist should ever have to read.

Joe Forth deserves a particularly special mention for his technical advice and support both in and out of the field. Finally, I could not have completed this thesis without my family and friends, whose encouragement, patience and dance moves have made the

## Acknowledgements

---

last four years a pleasure.

# Abstract

During the mid- to late Neogene (20 - 2.5 million years ago), episodic retreat of the Antarctic Ice Sheet (AIS) coincided with periods of higher-than-present atmospheric CO<sub>2</sub>, indicating ice sheet sensitivity to climatic conditions similar to those projected for the coming decades. Understanding Antarctic climate and vegetation during such a period of AIS retreat is crucial for our fundamental understanding of high latitude environments in warmer-than-present climate scenarios. This thesis presents a detailed geochemical study of sediments and plant fossils from the terrestrial Sirius Group of Oliver Bluffs, Transantarctic Mountains, located at 85° S today and during the Neogene.

Biomarker analysis of the sediments show strong evidence for a warmer Antarctica, where summer temperatures reached 5 °C. These relatively favourable conditions supported a low diversity mixed vegetation. In contrast to the macrofossil record, there is geochemical evidence for conifers, suggesting that Antarctic vegetation was strongly controlled by local environmental variability. The warmer conditions are associated with a dynamic carbon cycle, evidenced by anomalously high and variable atmospheric  $\delta^{13}\text{C}$  and possibly linked to atmospheric CO<sub>2</sub> levels. Precipitation isotopes are reconstructed from plant compound isotope analysis of the fossils, and indicate markedly different hydrological cycling. This result is supported by climate modelling experiments which suggest that Antarctic hydrological cycling is most strongly governed by the extent of the ice sheet rather than by greenhouse gas radiative forcing. This thesis presents a new approach to exploring Antarctic climate and vegetation and provides important novel information on this crucial region of the world.



# Contents

<b>List of Figures</b>	<b>xi</b>
<b>List of Tables</b>	<b>xvii</b>
<b>Abbreviations</b>	<b>xix</b>
<b>1 Introduction</b>	<b>1</b>
1.1 Background to this thesis . . . . .	1
1.1.1 Rationale . . . . .	1
1.1.2 Geological setting . . . . .	2
1.1.3 Antarctic climate and vegetation during AIS retreat . . . . .	7
1.2 Aims and objectives . . . . .	13
1.2.1 Can a geochemical approach advance understanding of local and regional vegetation community structures? (Chapter 2) . . . . .	15
1.2.2 What were continental temperatures during EAIS retreat? (Chapter 2) . . . . .	17
1.2.3 Can oxygen isotopes in Antarctic fossil prostrate trees be used to trace hydrological change? (Chapter 3) . . . . .	18
1.2.4 Were there changes in carbon cycling during EAIS retreat? (Chapter 3) . . . . .	23
1.2.5 Was there a different hydrological cycle during EAIS retreat? (Chapter 4) . . . . .	23
1.3 Thesis structure and author contributions . . . . .	25
<b>2 The last forests on Antarctica: reconstructing flora and temperatures from the Neogene Sirius Group, Transantarctic Mountains</b>	<b>27</b>
Abstract . . . . .	28

2.1	Introduction . . . . .	28
2.2	Materials and Methods . . . . .	31
2.2.1	Geological setting . . . . .	31
2.2.2	Plant lipid analysis by Gas Chromatography/Mass Spectrometry	33
2.2.3	GDGT analysis by Liquid Chromatography/Mass Spectrometry	34
2.3	Results . . . . .	35
2.3.1	Plant lipid contents . . . . .	35
2.3.2	Bacterial tetraether lipid distributions . . . . .	45
2.4	Discussion . . . . .	46
2.4.1	Reconstructing vegetation from plant biomarkers . . . . .	46
2.4.2	Temperature reconstruction from bacterial biomarkers . . . . .	54
2.5	Conclusions . . . . .	55
2.6	Supplementary Information 1 . . . . .	57
<b>3</b>	<b>Climatic signals recorded in carbon and oxygen isotopes of fossil southern beech trees from Antarctica</b>	<b>59</b>
	Abstract . . . . .	60
3.1	Introduction . . . . .	60
3.2	Materials and methods . . . . .	63
3.2.1	Oliver Bluffs; fossil site . . . . .	63
3.2.2	Isla Navarino; modern analogue site . . . . .	64
3.2.3	Sample preparation and isotopic analysis . . . . .	67
3.3	Results and discussion . . . . .	69
3.3.1	Oxygen and carbon isotope ratios in modern <i>Nothofagus</i> . . . . .	69
3.3.2	Source water $\delta^{18}\text{O}$ in modern <i>Nothofagus</i> . . . . .	71
3.3.3	Reconstructing ancient precipitation $\delta^{18}\text{O}$ from fossil <i>Nothofagus</i>	72
3.3.4	Reconstructing atmospheric $\delta^{13}\text{C}$ from fossil <i>Nothofagus</i> . . . . .	77
3.4	Conclusions . . . . .	83
3.5	Supplementary Information 2 . . . . .	85
3.5.1	Modification of carbon and oxygen isotopes by continuous light .	85
<b>4</b>	<b>Smaller ice sheets drive a shift in the Antarctic temperature-water isotope relationship in a warmer world</b>	<b>95</b>

---

Abstract . . . . .	96
4.1 Introduction . . . . .	96
4.2 Reconstructing precipitation isotopes . . . . .	98
4.3 Changes in moisture delivery to the continent . . . . .	103
4.4 Conclusions . . . . .	111
4.5 Methods . . . . .	113
4.5.1 Proxy data . . . . .	113
4.5.2 Climate modelling . . . . .	114
4.6 Supplementary Information 3 . . . . .	119
4.6.1 Proxy reconstruction of precipitation isotopes . . . . .	119
4.6.2 Modelling hydrological change . . . . .	123
4.6.3 Supplementary figures . . . . .	126
4.6.4 Supplementary tables . . . . .	129
<b>5 Conclusions, wider implications and future work</b>	<b>131</b>
5.1 Revisiting the aims and objectives . . . . .	131
5.2 Answering the research questions . . . . .	131
5.2.1 Can a geochemical approach advance understanding of local and regional vegetation community structures? (Chapter 2) . . . . .	131
5.2.2 What were continental temperatures during EAIS retreat? (Chapter 2) . . . . .	133
5.2.3 Can oxygen isotopes in Antarctic fossil prostrate trees be used to trace hydrological change? (Chapter 3) . . . . .	134
5.2.4 Were there changes in carbon cycling during EAIS retreat? (Chapter 3) . . . . .	136
5.2.5 Was there a different hydrological cycle during EAIS retreat? (Chapter 4) . . . . .	138
5.2.6 What are the bigger implications of this work? . . . . .	142
5.3 Scientific advances and overall conclusions . . . . .	144
5.4 Future work . . . . .	148
5.4.1 Dating improvements . . . . .	148
5.4.2 How representative are the geochemical results in this thesis? . . . . .	150
5.4.3 Improved climate modelling . . . . .	151

5.4.4 Expanding the scope of the work . . . . . 152

**References** . . . . . **155**

# List of Figures

1.1	(A) Current areas of glacier thinning and ice mass loss from the Antarctic Ice Sheet, denoted by red circles, where the size of the circle shows the speed of mass loss, from Paolo et al. (2015). (B) Early estimates of Pliocene AIS retreat by Webb et al. (1984) corresponding to loss of more than half of the ice sheet volume, and demonstrating the presence of open marine basins in the interior of the continent. (C) mid-Miocene AIS retreat under CO <sub>2</sub> levels of 500 ppmv (Gasson et al., 2016). (D) Pliocene AIS retreat at 400 ppmv atmospheric CO <sub>2</sub> and using a dynamic topography scheme (Austermann et al., 2015). . . . .	3
1.2	Antarctic data sites mentioned in this literature review. OB = Oliver Bluffs (Francis and Hill, 1996, McKelvey et al., 1991), AND = ANDRILL-2A core (Feakins et al., 2012, Gasson et al., 2016, Griener et al., 2015, Levy et al., 2016, Warny et al., 2009), MDV = McMurdo Dry Valleys (Ashworth et al., 2007, Lewis et al., 2007, 2008, Marchant et al., 1993a, Sugden et al., 1995), DSDP274 = Deep Sea Drilling Program Site 274 (Fleming and Barron, 1996), WL = Wilkes Land (Cook et al., 2013), PB = Prydz Bay (Clark et al., 2013, Cook et al., 2014, Escutia et al., 2009, Passchier et al., 2011), SG = Shackleton Glacier (Hambrey et al., 2003).	6
1.3	The oxygen isotope composition of cellulose is primarily governed by three processes: (a) the isotopic composition of precipitation, combined with evaporation processes from the soil and groundwater mixing; (b) evapotranspiration from leaves, which itself is dependent upon temperature and relative humidity; and (c), various well-constrained biological fractionation factors. . . . .	21
2.1	Map of Beardmore Glacier region with Oliver Bluffs marked. Grey areas denote outcrops. White areas denote ice-covered land and the Ross Ice Shelf. . . . .	32

2.2	GC-MS (Total Ion Current; TIC) traces of polar, aromatic and apolar fractions from one sample from Oliver Bluffs, Transantarctic Mountains. For peak annotations see Table 2.1. $\circ$ = alkanolic acid, $\blacksquare$ = alkanols, $\blacktriangle$ = alkanes. . . . .	36
2.3	Average fractional abundance of n-alkanes, n-alkanols, n-alkanoic acids. Error bars = 1 sd. . . . .	45
2.4	Average branched GDGT distributions in sediment samples (n=15). Error bars = 1 sd. . . . .	46
2.5	Distributions of reconstructed palaeotemperature for Oliver Bluffs using two calibrations from Peterse et al. (2012). . . . .	47
2.6	Structures of the terpenoid compounds identified in sediments at Oliver Bluffs. . . . .	58
3.1	( <b>A</b> ) Location of sampling sites on Isla Navarino in Tierra del Fuego, Chile. Yellow triangle = marks the location of the GNIP station at Ushuaia; open circles = mark the tree ring sampling sites. ( <b>B</b> ) Fossil wood location at Oliver Bluffs (black filled circle), Transantarctic Mountains, Antarctica. White represents ice; grey shapes are Transantarctic Mountain outcrops. ( <b>C</b> ) Photograph of exceptionally preserved fossil <i>Nothofagus</i> from Oliver Bluffs. ( <b>D</b> ) Scanning Electron Microscope image of fossil <i>Nothofagus</i> , demonstrating excellent preservation of wood fibres. ( <b>E</b> ) Prostrate <i>Nothofagus antarctica</i> from Isla Navarino. . . . .	65
3.2	( <b>A</b> ) Standard deviation of $\delta^{13}\text{C}_{cell}$ (closed circles) and $\delta^{18}\text{O}_{cell}$ (open circles) with altitude for <i>Nothofagus</i> from Isla Navarino, demonstrating a decrease in variability for $\delta^{18}\text{O}_{cell}$ for prostrate trees. Dotted line is a linear trendline for the oxygen data. ( <b>B</b> ) Mean $\delta^{18}\text{O}_{cell}$ data for modern <i>Nothofagus</i> separated into arboreal and prostrate form, and fossil <i>Nothofagus</i> . ( <b>C</b> ) As panel ( <b>B</b> ) but for $\delta^{13}\text{C}_{cell}$ . . . . .	69
3.3	The relationship between modelled source water $\delta^{18}\text{O}$ and measured $\delta^{18}\text{O}_{source}$ from soils (circles), roots (squares) and Global Network of Isotopes in Precipitation $\delta^{18}\text{O}_{precip}$ (summer precipitation; diamond). Modelled source water $\delta^{18}\text{O}$ was calculated from measured $\delta^{18}\text{O}_{cell}$ (modern <i>Nothofagus</i> ) using the same method as Anderson et al. (2002). Markers give the mean modelled $\delta^{18}\text{O}$ , y-error bars show the full measured data range, x-errors show fully propagated model errors, and a 1:1 ratio is given by the dotted line for comparison. Modelled data is calculated using $\text{RH} = 0.7$ , $f = 0.2$ . . . . .	74

3.4	Cellulose $\delta^{18}\text{O}$ from the Sirius Group fossil <i>Nothofagus</i> , with modelled $\delta^{18}\text{O}$ of palaeo precipitation and modern Antarctic snow. Modern measurements from Masson-Delmotte et al. (2008); data restricted to $>75^\circ\text{S}$ and below 700 masl. The median is given by the line, the first and third quartiles by the box, and the whiskers denote the full range of data. . . . .	75
3.5	<b>A)</b> Atmospheric $\delta^{13}\text{C}$ through time based on the benthic $\delta^{13}\text{C}$ records (Tippie et al., 2010). Dark grey line gives the 3 Ma moving average, and 95% confidence intervals are given by the grey shading. <b>B)</b> Reconstructed $\delta^{13}\text{C}_{atmos}$ for the Sirius Group, with $\delta^{13}\text{C}_{atmos}$ for the mid-Miocene and Pliocene based on benthic $\delta^{13}\text{C}$ records (Tippie et al., 2010). The median is given by the line, the first and third quartiles by the box, and the whiskers denote the full range of data. . . . .	81
4.1	Location of the Sirius Group sediments at Oliver Bluffs (yellow star), which is on the poleward side of the Transantarctic Mountains (TAM). Grey shading shows rocky outcrops of the mountains. . . . .	97
4.2	. . . . .	101
4.2	<b>(A)</b> The relationship between $\delta^{18}\text{O}$ and $\delta^2\text{H}$ for modern Antarctic snow (open pink circles) demonstrating the linear relationship between $\delta^{18}\text{O}$ and $\delta^2\text{H}$ at high latitude (local meteoric water line). Filled red circles are modern data for sites south of $75^\circ\text{S}$ and below 700 m above sea level. Sirius Group data is summarised by the green box and whisker plot in the x- and y- directions showing median (line), 25th and 75th percentiles (box) and range (error bars). Modern data from Masson-Delmotte et al. (2008). <b>(B)</b> $\delta^{18}\text{O}$ versus temperature for modern Antarctic snow (Masson-Delmotte et al., 2008), Sirius Group data (green box and whiskers, as in panel A) and data from the palaeo HadCM3 climate model simulation (blue squares for grid cells where surface temperature $< 0^\circ\text{C}$ and grey diamonds for surface temperature $> 0^\circ\text{C}$ ). <b>(C)</b> $\delta^2\text{H}$ and surface air temperature in modern Antarctic snow (Masson-Delmotte et al., 2008), with Sirius Group data indicated by the box and whisker plot, as in panel (A). . . . .	102

- 4.3 **(A)** Tracer initialisation sectors (T1-T12; see Methods). Each tracer was initialised at the surface of the labelled sectors. The tracer sectors overlay the mean difference in summer evaporation from the sea surface of the palaeo scenario with respect to the preindustrial (simulations a and b; see Methods). **(B)** Stacked bar charts of absolute tracer abundance for latitudinal sectors where white = 0 - 30 °S, light grey = 30 - 60 °S, dark grey = 60 - 80 °S. **(C)** Tracer abundance profiles for the preindustrial and palaeo simulations for a set of grid cells on East Antarctica representative of the Sirius Group site (see Supplementary Information 3). Tracer amounts were calculated on the 10<sup>th</sup> day of the simulation, which is the residence time of water vapour in the atmosphere. . . . . 104
- 4.4 Mean summer difference in the palaeo scenario with respect to the preindustrial (simulations a and b; see Methods) for **(A)** precipitation  $\delta^{18}\text{O}$ ; **(B)** atmospheric vapour  $\delta^{18}\text{O}$  in the lower atmosphere; **(C)** surface temperature; **(D)** evaporation from the sea; **(E)** total precipitation; **(F)** precipitation falling as rain. Climate fields are calculated from a 30 year climate mean (last 30 years of the simulations). The Sirius Group site is shown by the black dot. Note reversed scalebar in **E** and **F**. . . . . 107
- 4.5 **(A)** Current precipitation regime over Antarctica, where all precipitation falls as snow. **(B)** Inferred precipitation regime under reduced ice sheet conditions where precipitation falls as rain over deglaciated coastal areas, depleting the remaining vapour as it moves inland relative to scenario (A). 109
- 4.6 Mean summer difference for precipitation  $\delta^{18}\text{O}$  (repeat of Fig. 4.4A) in the palaeo scenario with respect to the preindustrial (simulations a and b; see Methods) and the locations of ice cores with records longer than 1000 years . B = Byrd, DF = Dome Fuji, DC = EPICA Dome C, K = Komsomaskay, SA = Siple Dome A, TD = Taylor Dome, TA = TALDICE, V = Vostok, W = WAIS Divide. Climate means are calculated from the last 30 years of the simulations. . . . . 110
- 4.7 **(A)**  $\delta^{18}\text{O}$  from the Sirius Group precipitation, modern Antarctic precipitation at sites above 75 °S and below 700 masl, precipitation over the entire continent, and simulated precipitation for deglaciated regions from the HadCM3 palaeo simulation. **(B)** from the Sirius Group precipitation, modern Antarctic precipitation at sites above 75 °S and below 700 masl, precipitation over the entire continent. Modern data from Masson-Delmotte et al. (2008). . . . . 126
- 4.8 Seasonal (summer) mean surface wind vectors for **(A)** preindustrial and **(B)** palaeo simulations. . . . . 126

4.9	(A) Mean summer temperature difference for the intermediate simulation (c) with respect to the preindustrial (a) for a 30 year climate mean (taken from the last 30 years of the simulation). (B) Mean summer precipitation $\delta^{18}\text{O}$ difference for the intermediate simulation (c) with respect to the preindustrial (a) for a 30 year climate mean (taken from the last 30 years of the simulation). . . . .	127
4.10	Latitudinal bounds for tracers superimposed over the mean summer evaporation difference for the palaeo simulation with respect to the preindustrial. . . . .	127
4.11	(A) Ice sheet extent for palaeo boundary conditions; the grey box shows the grid boxes used to calculate tracer concentrations. (B) Ice sheet extent for preindustrial boundary conditions. . . . .	128
5.1	Cellulose $\delta^{18}\text{O}$ from the Sirius Group fossil <i>Nothofagus</i> , with modelled $\delta^{18}\text{O}$ of palaeo precipitation and modern Antarctic snow. Modern measurements from Masson-Delmotte et al. (2008); data restricted to $>75^\circ\text{S}$ and below 700 masl. The median is given by the line, the first and third quartiles by the box, and the whiskers denote the full range of data. Reproduced from Chapter 3. . . . .	136
5.2	(A) The relationship between $\delta^{18}\text{O}$ and $\delta^2\text{H}$ for modern Antarctic snow (open pink circles) demonstrating the linear relationship between $\delta^{18}\text{O}$ and $\delta^2\text{H}$ at high latitude (local meteoric water line). Filled red circles are modern data for sites south of $75^\circ\text{S}$ and below 700 m above sea level. Sirius Group data is summarised by the green box and whisker plot in the x- and y- directions showing median (line), 25 <sup>th</sup> and 75 <sup>th</sup> (box) and range (error bars). Modern data from Masson-Delmotte et al. (2008). (B) $\delta^{18}\text{O}$ versus temperature for modern Antarctic snow (Masson-Delmotte et al., 2008), Sirius Group data (green box and whiskers, as in panel A) and data from the palaeo HadCM3 climate model simulation (blue squares for grid cells where surface temperature $< 0^\circ\text{C}$ and grey diamonds for surface temperature $> 0^\circ\text{C}$ ). (C) $\delta^2\text{H}$ and surface air temperature in modern Antarctic snow (Masson-Delmotte et al., 2008), with Sirius Group data indicated by the box and whisker plot, as in panel (A). Reproduced from Chapter 4. . . . .	140
5.3	(A) Current precipitation regime over Antarctica, where all precipitation falls as snow. (B) Inferred precipitation regime under reduced ice sheet conditions where precipitation falls as rain over deglaciated coastal areas, depleting the remaining vapour as it moves inland relative to scenario (A). Reproduced from Chapter 4. . . . .	141



# List of Tables

1.1	Summary of the outstanding uncertainties in the published research undertaken to understand Antarctic palaeoclimate and vegetation during EAIS retreat, forming the basis of this thesis. . . . .	14
1.2	Research Questions addressed in this thesis. . . . .	15
2.1	Compounds identified in the sediments from Oliver Bluffs, Transantarctic Mountains. L = identified by comparison with the literature; M/R = identified by comparison of mass spectra or retention times with NIST and internal library; S = interpretation of mass spectra. (a) Rontani and Aubert (2004), (b) Otto and Simoneit (2001), (c) Philp (1985), (d) Simoneit and Mazurek (1982), (e) Simoneit (1977), (f) Enzell and Ryhage (1967), (g) AOCs lipid library, (h) Branco et al. (2004), (i) Sousa et al. (2006), (j) Lorenz et al. (2008), (k) Huang et al. (2013), (l) Trendel et al. (1989), (m) LaFlamme and Hites (1979). . . . .	39
2.2	Differing biomarker distributions indicating microenvironments in the Beardmore Glacier region. . . . .	51
2.3	Summary of organic proxy data . . . . .	57
3.1	Summary of sample sites on Isla Navarino with mean site $\delta^{18}\text{O}_{soil}$ . . .	71
3.2	Isotope and morphology data for modern <i>Nothofagus</i> trees from Isla Navarino. *p is <i>N. pumilio</i> and a is <i>N. antarctica</i> . . . . .	87
3.3	Isotopic data for Sirius Group samples. . . . .	90
4.1	Plant leaf wax $\delta^{13}\text{C}$ results of the samples used in this study. Data for the <i>n</i> -C <sub>23</sub> , <i>n</i> -C <sub>25</sub> , <i>n</i> -C <sub>27</sub> , <i>n</i> -C <sub>29</sub> and <i>n</i> -C <sub>31</sub> alkanes is given for each, along with the analytical error (standard deviation for duplicate or triplicate measurements). All numbers are in per mille (‰). . . . .	129

4.2	Plant leaf wax $\delta^2\text{H}$ results of the samples used in this study. Data for the $n\text{-C}_{23}$ , $n\text{-C}_{25}$ , $n\text{-C}_{27}$ , $n\text{-C}_{29}$ and $n\text{-C}_{31}$ alkanes is given for each, along with the analytical error (standard deviation for duplicate or triplicate measurements). All numbers are in per mille (‰). . . . .	130
5.1	Research questions addressed in this thesis (reproduced from Chapter 1).	132
5.2	Summary of the outstanding uncertainties in the published research undertaken to understand Antarctic palaeoclimate and vegetation during EAIS retreat, forming the basis of this thesis. Reproduced from Chapter 1. . . . .	145
5.3	Summary of the progress made in advancing the science of this field and in addressing the uncertainties raised in Table 5.2. . . . .	146

# Abbreviations

ACL - Average Chain Length

AIS - Antarctic Ice Sheet

AMOC - Atlantic Meridional Overturning Current

br-GDGT - branched Glycerol Dialkyl Glycerol Tetraether

BSTFA - *bis*(trimethyl)trifluoroacetamide

CBT - Cyclisation of Branched Tetraethers

CPI - Carbon Preference Index

DCM - Dichloromethane

EAIS - East Antarctic Ice Sheet

GCM - General Circulation Model

GC/MS - Gas Chromatography/Mass Spectrometry

GIS - Greenland Ice Sheet

GNIP - Global Network of Isotopes in Precipitation

HMW - High Molecular Weight

kyr - Thousand years

LC/MS - Liquid Chromatography/Mass Spectrometry

LMW - Low Molecular Weight

Ma - Million years ago

MAP - Mean Annual Precipitation

MAAT - Mean Annual Air Temperature

MBT - Methylation of Branched Tetraethers

MeOH - Methanol

## Abbreviations

---

MW - Molecular Weight

OEP - Odd-Even Preference

RH - Relative Humidity

s.d. - Standard deviation

s.e.m. - Standard error of the mean

TMS - Trimethylsilyl

VSMOW - Vienna Standard Mean Ocean Water

# Chapter 1

## Introduction

### 1.1 Background to this thesis

#### 1.1.1 Rationale

As a result of anthropogenic greenhouse gas emissions, average global surface temperatures are projected to increase by up to 4.8 °C; this unprecedented warming is predicted to have far-reaching consequences for the Earth's climate system (under the Representative Concentration Pathway 8.5 scenario; IPCC, 2013). High latitude environments, including ice sheets, are particularly sensitive to climate change, and have experienced temperature increases much larger than the global average with potentially severe repercussions for continental ice sheets (Fig. 1.1A; Jacka and Budd, 1998, Rohling et al., 2012, Singarayer and Valdes, 2010). Considerable effort has therefore gone into understanding present-day dynamics of the Antarctic Ice Sheet (AIS), and forming projections of its behaviour under future warming scenarios. However, much less is understood about how aspects of the terrestrial Antarctic climate and environment, particularly surface temperature, hydrological cycling and vegetation, might change during future ice sheet retreat. Improved understanding of Antarctic climate during periods of significant ice sheet retreat in the geological past is crucial for understanding the fundamental behaviour of high latitude climates during warmer-than-present climate scenarios.

There is both direct and indirect evidence that, in the past, the AIS exhibited large changes in volume and extent during the Neogene (23 - 2.5 million years ago; Ma), from both the West and East Antarctic Ice Sheets (Fig. 1.1B, C and D; Levy et al., 2016, Naish et al., 2009, Pollard and Deconto, 2016). Looking to these past episodes of ice sheet retreat could therefore provide valuable new information about the behaviour of Antarctic climate and vegetation in warmer, reduced ice worlds.

One such episode of ice sheet retreat is represented by the terrestrial Sirius Group sediments at Oliver Bluffs in the Transantarctic Mountains, which provide a unique opportunity to explore Antarctic terrestrial climate. A fossil-bearing layer within the formation represents a period of AIS retreat during which a tundra shrub grew 480 km from the South Pole (Carlquist, 1987, Francis and Hill, 1996, Hill and Trustwell, 1993, Hill et al., 1996, Webb and Harwood, 1987), indicating that mean summer temperatures were significantly warmer than the present day (Ashworth and Preece, 2003, Ashworth and Kuschel, 2003, Ashworth and Cantrill, 2004, Francis and Hill, 1996). Presently, the AIS exerts a strong influence on regional climate, particularly through surface albedo feedbacks on temperature, but also by influencing the water vapour holding capacity of the atmosphere, which affects hydrological cycling on the continent (Krinner et al., 2007). It could be anticipated that ice sheet retreat in the past would have significantly affected these climate variables, but Antarctic terrestrial climate in the past is poorly constrained and there is a clear need for detailed datasets to assess the impacts ice sheet retreat. The purpose of this thesis is to reconstruct the climate and vegetation on the continent during this episode of AIS retreat, as well as to explore the impact of ice sheet retreat on climate. The findings will have relevance for both our understanding of past warm periods, as well as for constraining the fundamental behaviour of the climate system under future warming scenarios.

### **1.1.2 Geological setting**

Much of this thesis uses fossil and sediment samples from the Sirius Group sediments in the Transantarctic Mountains, Antarctica to reconstruct terrestrial climate and flora

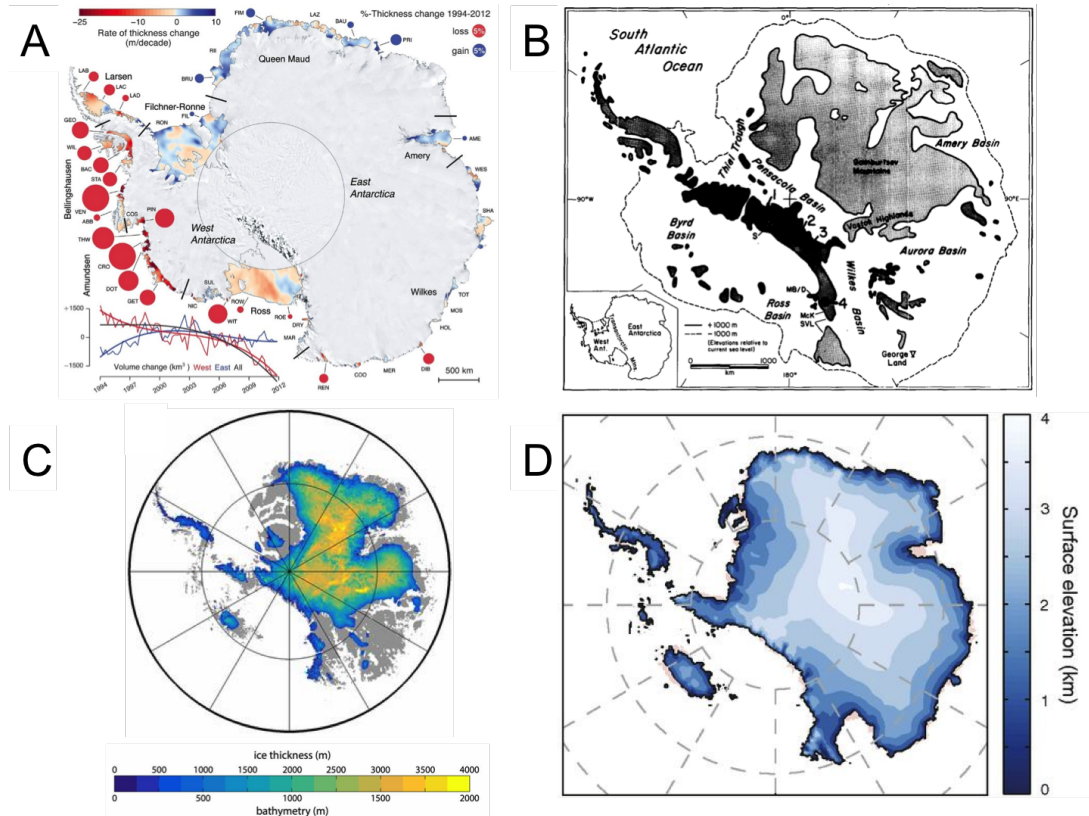


**Figure 1.1:** (A) Current areas of glacier thinning and ice mass loss from the Antarctic Ice Sheet, denoted by red circles, where the size of the circle shows the speed of mass loss, from Paolo et al. (2015). (B) Early estimates of Pliocene AIS retreat by Webb et al. (1984) corresponding to loss of more than half of the ice sheet volume, and demonstrating the presence of open marine basins in the interior of the continent. (C) mid-Miocene AIS retreat under CO<sub>2</sub> levels of 500 ppmv (Gasson et al., 2016). (D) Pliocene AIS retreat at 400 ppmv atmospheric CO<sub>2</sub> and using a dynamic topography scheme (Austermann et al., 2015).

during a period of Neogene AIS retreat. Well-preserved terrestrial sequences are rare, but can provide valuable information about past climate systems, so these samples are a unique opportunity to gain new insights into Antarctic climates. The Sirius Group sediments are a set of Neogene glacial sedimentary deposits outcropping over 1300 km throughout the Transantarctic Mountains. While there are other locations where plant fossils have been reported (dated between the Oligocene and Pliocene; Hambrey et al., 2003), I focus particularly on one outcrop at Oliver Bluffs in the Beardmore Glacier region (85° S, 166° E). Here a plant fossil-bearing horizon represents a brief period where the AIS retreated far enough, and temperatures were warm enough, for a vegetation to grow, although the age of these deposits and plant fossils is uncertain.

The age of the Sirius Group has been the focus of a long-running debate, and has played a key role in determining the stability (or otherwise) of the EAIS since its expansion  $\sim 13.85$  Ma (for detailed discussion, see Barrett, 2013). The Sirius Group as a whole is considered by Passchier (2001, 2004) to be the product of multiple ice sheet retreat and advance events, and as such, deposits at different locations may be of different ages. The Sirius Group at Oliver Bluffs consists predominantly of glacial tillites, as well as thin mudstones, siltstones and sandstones, deposited during glacial advance and retreat (Passchier, 2001, 2004, Webb et al., 1996). The deposits were assigned a Pliocene age based on the understanding that marine diatoms recovered from diatomaceous clasts in glacial sediments record the incursion of seawater deep into the continent, and therefore that the East Antarctic Ice Sheet responded dynamically to Pliocene warmth (therefore sediments were deposited  $\sim 3.8$  Ma; Webb et al., 1996; Fig. 1.1B). Retallack et al. (2001) assigned an age of 1.3 - 4.1 Ma to palaeosols in the same formation. However, this age is complicated by arguments that the Pliocene diatoms were windblown contamination (Burckle and Potter, 1996, Stroeve et al., 1996), implying that the sediments are much older, although Passchier (2004) disputes this on the basis of provenance and geochemical data of the diatomaceous clasts. *Nothofagus* pollen discovered in DSDP Site 274 with a biostratigraphic age of  $\sim 3$  Ma also supports a Pliocene age, as the most likely source for the pollen would have been from *Nothofagus* growing on the Ross Sea coast (i.e. the fossil plants at Oliver Bluffs; Fleming and

Barron, 1996), but this result has not been replicated in other studies.

Other researchers suggest a much older age for the deposits. The presence of unweathered volcanic ash in the McMurdo Dry Valleys dated to between 4 and 15 Ma are thought to indicate a persistently cold and arid climate since the mid-Miocene, and therefore that the deposits at Oliver Bluffs can be no younger than  $\sim 14$  Ma (Marchant et al., 1993a,b,c, 1996, Sugden et al., 1995). This is supported by more recent work from the Olympus Range at the head of the McMurdo Dry Valleys, where sediment and moraines record the transition from wet-based to cold-based glaciation between 14 and 13.6 Ma (Lewis et al., 2007, 2008). Exposure dating of surfaces associated with the nearby Koski fault at Oliver Bluffs indicates that the sediments are much older than 3.8 Ma (Ackert, Jr. and Kurz, 2004). Furthermore, with the exception of the pollen record from DSDP Site 274, there is a considerable lack of marine evidence for a vegetated continent during the Pliocene: terrestrial pollen in Pliocene intervals from marine cores from the Ross Sea are considered to be derived from eroded Paleogene strata (Taviani et al., 2008, Warny et al., 2006), and a similar result is suggested for pollen data from the Antarctic Peninsula, although in situ Pliocene pollen in this core cannot be ruled out (Warny and Askin, 2011). In contrast, the marine cores dated to the mid-Miocene (17 - 15 Ma) contain abundant terrestrial pollen (Warny et al., 2009) and it seems unlikely that vegetation could survive on Antarctica into the Pliocene without leaving some sort of palynological trace. Notably, during the mid-Miocene, the AIS underwent episodic ice sheet retreat coincident with elevated  $\text{CO}_2$  (Foster et al., 2012, Levy et al., 2016) and increased vegetation cover on the continent (Warny et al., 2009).

In summary, it seems most likely that the Sirius Group at Oliver Bluffs are mid-Miocene ( $\sim 17 - 15$  Ma) rather than Pliocene in age, although this cannot be confirmed and remains a hotly debated topic. Regardless of age, the sediments and fossil assemblages at Oliver Bluffs indicate a period of warming and ice sheet retreat such that the ice sheet margins were no more than 500 km from the South Pole. The deposits at this site are unique in terms of both their excellent preservation and the type of climate event that they represent and can provide new perspectives on our fundamental

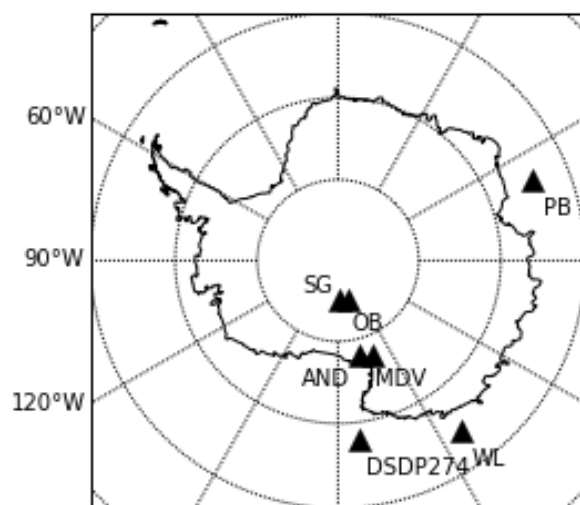


**Figure 1.2:** Antarctic data sites mentioned in this literature review. OB = Oliver Bluffs (Francis and Hill, 1996, McKelvey et al., 1991), AND = ANDRILL-2A core (Feakins et al., 2012, Gasson et al., 2016, Griener et al., 2015, Levy et al., 2016, Warny et al., 2009), MDV = McMurdo Dry Valleys (Ashworth et al., 2007, Lewis et al., 2007, 2008, Marchant et al., 1993a, Sugden et al., 1995), DSDP274 = Deep Sea Drilling Program Site 274 (Fleming and Barron, 1996), WL = Wilkes Land (Cook et al., 2013, Passchier et al., 2013a), PB = Prydz Bay (Clark et al., 2013, Cook et al., 2014, Escutia et al., 2009, Passchier et al., 2011), SG = Shackleton Glacier (Hambrey et al., 2003).

understanding of high latitude climates during warmer worlds.

### **1.1.3 Antarctic climate and vegetation during AIS retreat**

This section provides background and context to the topics explored in Chapters 2, 3 and 4. Each section gives the state of current knowledge from the Sirius Group at Oliver Bluffs and places it within the wider context of Antarctic research for both of the possible age scenarios for the deposits (the mid-Miocene, ~17 - 15 Ma, and the early to mid- Pliocene, 5 - 3 Ma).

#### **1.1.3.1 Ice sheet retreat**

The fossil plants from the Sirius Group sediments represent a time period when the AIS margin had retreated far inland. The depositional environment is thought to have been an active glacial margin at the head of a fjord more than 100 km from the Ross Sea, where now the sequence is exposed on the flanks of the modern Beardmore Glacier. Furthermore, the stratigraphy at the Oliver Bluffs is indicative of a highly dynamic ice margin, where the glacier advanced and retreated on several occasions (Ashworth and Cantrill, 2004). Both of the possible age scenarios for the Sirius Group at Oliver Bluffs correspond to time periods during the Neogene where there is strong independent evidence for considerable fluctuations in both the volume and extent of the AIS.

The variable nature of the ice-sheet during the mid-Miocene is demonstrated by sequence stratigraphy (Fielding et al., 2011), mineral provenance (Hauptvogel and Passchier, 2012, Iacoviello et al., 2015) and sedimentology (Passchier et al., 2011, 2013b) from marine cores in the Ross Sea, pointing to warm intervals when ice sheet margins retreated inland as far as the Transantarctic Mountains (Hauptvogel and Passchier, 2012, Passchier et al., 2011). During colder intervals, the grounding line extended well into the Ross Sea basin (Hauptvogel and Passchier, 2012). Overall, well-dated glacial and fossil records from the Olympus Range in the McMurdo Dry Valleys, East Antarctica indicate a significantly smaller ice sheet accompanied by wet-based glaciers prior to 13.94 Ma (Lewis et al., 2007, 2008). This ice sheet retreat is replicated in modelling

studies, which are able to produce significant and variable AIS retreat, equivalent to 30 - 36 m of sea level rise (Gasson et al., 2016, Pekar and DeConto, 2006).

The mid-Miocene ice sheet fluctuations appear to be primarily driven by orbital variations (Griener et al., 2015, Passchier et al., 2013b), but the AIS was clearly highly sensitive to relatively small and rapid fluctuations in atmospheric CO<sub>2</sub> (Foster et al., 2012, Gasson et al., 2016, Levy et al., 2016); multiple geochemical records indicate a threshold for Miocene AIS retreat of around 500 ppmv (Greenop et al., 2014, Holbourn et al., 2015, Kürschner et al., 2008, Levy et al., 2016). Since these ice sheet fluctuations occurred for a range of atmospheric CO<sub>2</sub> from preindustrial CO<sub>2</sub> levels to projections for the year 2050 (280-500 ppmv), it is important to understand how Antarctic climate might have been affected by them (Gasson et al., 2016). Furthermore, these rapid fluctuations in atmospheric CO<sub>2</sub> drove variability in the marine carbon isotope record (Holbourn et al., 2007, 2013, Vincent and Berger, 1985, Woodruff and Savin, 1989), suggesting a long-term coupling between the carbon cycle, ice sheet and climate throughout the middle Miocene (Holbourn et al., 2015). The exact nature of this relationship is unknown, particularly with respect to carbon cycling during episodes of ice sheet retreat.

Similarly to the mid-Miocene, evidence from mineral provenance, ice-rafted debris, sediment facies and grain size, microfossils and mineralogy from multiple sub-glacial basins demonstrate that the EAIS had a dynamic margin during the Pliocene, largely due to orbital forcing (Cook et al., 2013, 2014, Escutia et al., 2009, Hansen et al., 2015, Passchier et al., 2011, Patterson et al., 2014, Reinardy et al., 2015, Williams et al., 2010). Until recently, attempts to model EAIS retreat that are consistent with estimates of Pliocene sea level increases (of up to 25 m higher than present day) suggested it could not have happened (Pollard and DeConto, 2009). However, a number of additional processes related to ice sheet instability have since been added to the ice sheet model used by Pollard and DeConto (2009), and under warm conditions the model now predicts considerable ice loss in East Antarctica (equivalent to 17 m of sea level rise; Pollard et al., 2015, Pollard and DeConto, 2016). Ice sheet retreat also seems more likely when taking into account Pliocene-specific mantle topography under the

ice sheet, which implies a much larger deglaciated area than under modern conditions (Austermann et al., 2015). The AIS appears to be less sensitive to CO<sub>2</sub> during the Pliocene; peak warmth during the mid-Pliocene Warm Period is associated with CO<sub>2</sub> levels of 365 - 415 ppmv (Pagani et al., 2010), much lower than peak CO<sub>2</sub> levels of the mid-Miocene. Nevertheless, long-term variability in the AIS is believed to have varied coherently with the carbon cycle throughout the Pliocene (de Boer et al., 2014), but again, the dynamics of the carbon cycle during these fluctuations is not clear.

### 1.1.3.2 Vegetation

The site at Oliver Bluffs is most notable for an exceptionally preserved fossil flora, consisting of fossil mosses, cushion plants, flowers, and the wood, pollen and leaves of a new species of *Nothofagus*, *Nothofagus beardmorensis* (Ashworth and Cantrill, 2004, Askin and Markgraf, 1986, Carlquist, 1987, Hill and Trustwell, 1993, Hill et al., 1996, Webb and Harwood, 1987, 1993). The fossil plants stand out especially for their high degree of preservation: the plants are desiccated and there is very little permineralisation (infilling of fossil casts by water-borne minerals), meaning that much original woody structure is preserved (Francis and Hill, 1996). The discovery of such well-preserved plant fossils, 500 km from the South Pole, has been described as one of the most important palaeobotanical discoveries to have been made in Antarctica (Ashworth and Cantrill, 2004). The fossil plants represent a tundra vegetation, and all woody plants were identified as a single species of *Nothofagus* (Carlquist, 1987), although a few rare grains of podocarp pollen were also identified (Askin and Markgraf, 1986, Askin and Raine, 2000, Hill and Trustwell, 1993, Raine, 1998). The discovery of podocarp pollen without accompanying macrofossils at a site with abundant, well-preserved *Nothofagus* macrofossils and pollen raises questions about the make-up of Antarctic vegetation: was Antarctic flora entirely dominated by one species of *Nothofagus*, or do biases in the fossil record mask a more diverse mixed angiosperm-conifer vegetation?

This discrepancy is also reflected in the wider record of Antarctic vegetation during the Neogene. Pollen records from mid-Miocene marine sediment cores from both the

Ross Sea and the Antarctic Peninsula record a tundra shrub dominated by *Nothofagus* with sparse podocarps (Anderson et al., 2011, Askin and Raine, 2000, Feakins et al., 2012, Levy et al., 2016, Raine, 1998, Warny and Askin, 2011, Warny et al., 2009). A *Nothofagus* dominated flora is also supported by well-dated terrestrial deposits from the McMurdo Dry Valleys, where fossil assemblages record a tundra habitat, along with numerous bryophytes, lycophytes and algal species, similar to the flora of modern day Tierra del Fuego, Chile (Ashworth et al., 2007, Lewis et al., 2008). However, in contrast to the Ross Sea coastal vegetation, there is no evidence for the presence of podocarps in the Dry Valleys, indicating complex spatial and temporal patterns in Antarctic vegetation change. It is suggested that tundra vegetation became extinct  $\sim 13.85$  Ma on East Antarctica (Lewis et al., 2008) and by 12.8 Ma on the Peninsula (Anderson et al., 2011) as a result of the growing ice sheet, although it cannot be ruled out that vegetation survived in refugia into the Pliocene (Warny and Askin, 2011). A lack of well-dated terrestrial Pliocene deposits means there is a shortage of vegetation information about the Antarctic continent, although *Nothofagus* pollen dated to the mid-Pliocene has been recovered from a sedimentary core  $\sim 250$  km offshore from Cape Adare (Deep Sea Drilling Project Site 274; Fleming and Barron, 1996); this result has not been repeated in subsequent Antarctic cores (e.g. Warny et al., 2006). Therefore, while the pollen record from the Ross Sea in particular appears to provide a thorough record of Neogene vegetation on Antarctica (Feakins et al., 2012, Warny et al., 2009), it is clear from other records that there are many pieces of the puzzle still missing, which a new approach could help to find.

### 1.1.3.3 Climate

The occurrence of vegetation at such high latitudes in the Transantarctic Mountains at Oliver Bluffs is indicative of considerable warming and ice sheet retreat. The fossil wood has very narrow growth rings, implying slow growth during a short summer growing season where temperatures reached  $\sim 5$  °C (Francis and Hill, 1996); 10 °C warmer than Antarctic summer temperatures in the present day. This is comparable with the lower biological limits of fossil fauna found at the same site, all implying a minimum summer

temperature of 4 - 5 °C (Ashworth and Kuschel, 2003, Ashworth and Preece, 2003), while analysis of palaeosols in the same sequence implied MATs of -3 to -11 °C (Retallack et al., 2001). Warmer than present-day continental temperatures are supported by geological evidence from elsewhere on the continent for the mid-Miocene. Pollen records from the Ross Sea suggest that at peak warmth, mid-Miocene air temperatures could have reached 10 °C (Feakins et al., 2012, Griener et al., 2015, Warny et al., 2009), and data from soil chemofunctions suggests mean annual temperatures were perhaps 4 - 8 °C (Passchier et al., 2013a). The presence of wet-based glaciation suggests temperatures in the Dry Valleys were 25 - 30 °C higher than present-day, but a switch in glacier thermal regime means air temperatures may have reached present-day temperatures (-30 °C) by 13.94 Ma (Lewis et al., 2007). Similarly warm temperatures for the Pliocene (8 °C in the summer) are also supported by atmospheric GCM modelling, driven by Southern Ocean sea surface temperature warming, and reduced terrestrial ice cover and surface albedo (Francis et al., 2007).

With the exception of the pollen and geochemistry-derived temperatures from the Ross Sea (which, because of the age uncertainty, are not directly comparable to Oliver Bluffs), the temperature reconstructions for Antarctica during the Neogene are largely limited to analyses based on qualitative comparisons of modern fauna and flora (Ashworth and Kuschel, 2003, Ashworth and Preece, 2003, Francis and Hill, 1996). These reconstructions therefore do not provide quantitative estimates of palaeotemperatures, and fossil-derived palaeotemperatures are generally less precise than geochemically-derived temperature estimates (Ballantyne et al., 2005). A geochemistry based palaeothermometer applied to the Oliver Bluffs sediments could provide far more precise estimates of continental temperature during this period of ice sheet retreat, and is the aim of part of this thesis.

There is some evidence for hydrological cycle change during Neogene AIS retreat. Mean annual precipitation of 120 - 220 mm is also estimated from palaeosol analysis at Oliver Bluffs (Retallack et al., 2001), which is drier than precipitation estimates from the Pliocene atmospheric GCM (72 - 360 mm; Francis et al., 2007). Both of these estimates indicate that Antarctica experienced significantly higher mean annual

precipitation than during the present-day (variable, but up to 100 mm). This was further explored by Tindall and Haywood (2015), who used a fully coupled oxygen isotope-enabled ocean-atmosphere GCM to explore global precipitation isotope patterns during the mid-Pliocene Warm Period. At high latitudes, increased temperatures lead to increased precipitation  $\delta^{18}\text{O}$ , but the relationship between the two was spatially variable and non-linear (as opposed to the present day, linear relationship; Craig, 1961, Tindall and Haywood, 2015).

Hydrological change is also noted for the mid-Miocene. Reconstructions of precipitation based on soil chemofunctions suggest that mean annual precipitation could have been as high as 600 mm (Passchier et al., 2013a); during ice sheet minima, increased precipitation improved water availability, allowing the periodic expansion of vegetation between 20 and 16 Ma (Griener et al., 2015). Using an aqua-planet model (an entirely ocean-covered Earth surface), it was inferred that increased precipitation was driven by evaporation from high latitude oceans, leading to an increase in locally derived moisture relative to the present day (Feakins et al., 2012), although the results of this study are not specific to periods of ice sheet retreat, and are instead averaged over a much expanded time period (20 - 16 Ma). The evidence from both the Pliocene and mid-Miocene suggest that high latitude hydrological cycling may function differently in warmer worlds with reduced ice sheets, but a detailed study exploring mechanistic change specific to ice sheet retreat is clearly lacking. While Feakins et al. (2012) provided a more thorough examination of Antarctic hydrological cycling than that of Tindall and Haywood (2015), aqua-planet models cannot capture land surface-climate interactions or the influence of ice sheets on climate. These interactions could be particularly important at high latitudes, where the impact of the ice sheet on albedo, atmospheric moisture content and atmospheric circulation have been shown to be particularly important for both past and present-day climate (Francis et al., 2007, Holland and Bitz, 2003, Krinner et al., 2007, Jacka and Budd, 1998, Rohling et al., 2012, Singarayer and Valdes, 2010). Instead, a fully coupled ocean-atmosphere GCM (as in Tindall and Haywood, 2015) would enable a rigorous examination of the climate and hydrological response to ice sheet reduction.

#### 1.1.3.4 Research opportunities and outstanding uncertainties

Regardless of age, the sediments and fossil assemblages at Oliver Bluffs indicate a period of warming and ice sheet retreat so that the ice sheet margins were no more than 500 km from the South Pole. The deposits at this site are unique in terms of both their excellent preservation and the type of climate event that they represent. They provide numerous untapped opportunities for examining Antarctic palaeoclimate through further proxy work, which will build on previous research on the deposits that has so far mostly provided qualitative temperature estimates. Firstly, the exceptional preservation of the fossil prostrate trees means that tree ring isotope analysis may be applied, building on previous dendrochronological work (Francis and Hill, 1996, McCarroll and Loader, 2004). Application of this technique to the Oliver Bluffs fossils would provide novel proxy archives for Antarctica, but, prostrate plants have not been tested for their use in tree ring isotope studies and further work developing this proxy is needed. Secondly, the fossil plants were deposited in situ, which means that it is likely that there are high levels of contemporaneous organic matter in the surrounding sedimentary matrix, making biomarker-based temperature and vegetation reconstructions possible for the first time on the Antarctic continent. Thus, the deposits present a unique opportunity to study a snapshot of Antarctic climate and vegetation during a period of significant ice retreat, and to provide rare terrestrial Neogene palaeoclimate data.

There are several substantial gaps in current knowledge of Antarctic climate processes and vegetation cover during periods of ice sheet retreat, (mostly summarised in section 1.1.3). Given the important influence of AIS both globally and regionally (briefly outlined in section 1.1.1) it is the intent of this thesis to address these outstanding uncertainties, as indicated in table 1.1.

## 1.2 Aims and objectives

The aim of this thesis is to answer the broad research question:

**What was Antarctic climate and vegetation during a period of Neogene**

**Table 1.1:** Summary of the outstanding uncertainties in the published research undertaken to understand Antarctic palaeoclimate and vegetation during EAIS retreat, forming the basis of this thesis.

---

---

Outstanding uncertainties in the research carried out to date
1. Uncertainties over the composition of Neogene Antarctic vegetation communities due to discrepancies between the macrofossil and pollen record in both terrestrial and marine geological records.
2. Limited geochemical-based temperature data to provide more precise, quantitative estimates of continental temperatures during ice sheet retreat.
3. Prostrate fossil trees could provide novel proxy archives of environmental signals but it is unknown whether tree ring isotopes in prostrate trees or shrubs record climate signals.
4. Limited understanding of carbon cycle dynamics during EAIS retreat, although ice sheet fluctuations are known to be linked to atmospheric CO <sub>2</sub> levels.
5. No constraints in hydrological change during EAIS retreat or detailed examination of Antarctic climate response to EAIS retreat: the only Neogene Antarctic hydrological reconstruction to date is too early (20 - 15 Ma) and has no temporal resolution.

---

### **East Antarctic Ice Sheet retreat?**

This thesis takes an integrated, multidisciplinary approach, and uses both geochemical and climate modelling methods to address this aim. Numerous geochemical techniques are applied to a terrestrial archive of AIS retreat recovered from the Sirius Group sediments to elucidate information about temperature, vegetation, hydrological cycling and atmospheric CO<sub>2</sub>. In addition, there is a climate modelling component that builds on some of the geochemical results to investigate in greater detail the impact of EAIS retreat on the Antarctic hydrological cycle. This data-model approach has the benefit of being able to test the assumptions made in generating the geochemical data and gaining a more comprehensive understanding of the palaeoclimate system under examination.

The overarching research aim above can be addressed by a number of objectives, which have been framed as Research Questions, given in Table 1.2. Each of the following chapters (Chapters 2, 3 and 4) explicitly address these questions, with at least one Research Question addressed per chapter. Chapter 2 addresses Research Questions 1

**Table 1.2:** Research questions addressed in this thesis.

Research Question	Chapter
1. Can a geochemical approach advance understanding of local and regional vegetation community structures?	2
2. What were continental temperatures during EAIS retreat?	2
3. Can oxygen isotopes in Antarctic fossil prostrate trees be used to trace hydrological change?	3
4. Were there changes in carbon cycling during EAIS retreat?	3
5. Was there a different hydrological cycle during EAIS retreat?	4

and 2: organic geochemical methods are used to examine in detail environmental and vegetation changes during Antarctic ice sheet retreat, and a geochemical temperature proxy is used to elucidate continental summer temperatures. Chapter 3 addresses Research Questions 3 and 4 and takes an isotopic approach to constraining precipitation and the composition of atmospheric CO<sub>2</sub>. Chapter 4 combines several of the insights from Chapters 2 and 3, and adds a reconstruction of precipitation hydrogen isotopes to examine how a reduced AIS could impact hydrological cycling, and to take these insights forward at both a local and continental scale. The results vastly broaden our understanding of how Antarctic continental climate is impacted by ice sheet retreat. The rest of this chapter explores the scientific background of each research question and briefly discusses the methodologies used to address them.

### 1.2.1 Can a geochemical approach advance understanding of local and regional vegetation community structures? (Chapter 2)

There are many challenges associated with reconstructing past Antarctic vegetation, not least because much of the geological record is hidden by the ice sheet. Vegetation on the Antarctic continent was probably sporadic in nature during the Neogene: advancing inland as the EAIS retreated and returning to form coastal refugia as it expanded again (Levy et al., 2016). Discrepancies between the pollen and macrofossil record of Antarctic vegetation during the Neogene have led to uncertainties over the composition and ecology of this vegetation. The Sirius Group macrofossil record suggests a low

diversity tundra shrub, dominated by *Nothofagus* (southern beech; Carlquist, 1987, Francis and Hill, 1996, Hill and Trustwell, 1993, Hill et al., 1996, Webb and Harwood, 1987). Rare podocarpaceous pollen from the Sirius Group indicate the presence of conifers, but this is not reflected in the macrofossil record (Askin and Raine, 2000). Similar discrepancies in the presence or absence of conifers are noted elsewhere in the Transantarctic Mountains (Ashworth et al., 2007, Lewis et al., 2008). This could be explained by several possibilities: there may have been spatially complex vegetation-environment patterns which are not well understood, or biases in either the macrofossil or pollen record for Antarctica (or both) which have not yet been identified. The application of organic geochemical methods to Antarctic sediments could provide new constraints on Neogene Antarctic vegetation.

Terrestrial plants are major producers of biological compounds, which can be deposited *in situ* or transported into sedimentary basins. During transport and deposition, compounds can lose much of their functionality, but their carbon skeletons are preserved in sediments as biomarkers. The distributions of certain classes of biomarker (e.g., *n*-alkanes, terpenoids) are characteristic of different types of vegetation, and therefore biomarker distributions in sediments be used as proxies for vegetation composition and diversity at the time of deposition. Furthermore, the use of biomarkers as a proxy for vegetation has some advantages over looking only at the fossil record. The fossil record (both macro- and micro-) necessarily suffers from various biases due to differences in degradation and preservation, transportation, and in the case of pollen, differing rates of pollen production between plant types. The biomarker record also suffers from the same biases, but they act in different ways upon the biomarker record compared to the fossil record. The biomarker-based approach used in this thesis to reconstruct vegetation can therefore provide a different perspective on vegetation communities. This approach provides new insights into Antarctic flora during the Neogene and will contribute to our broader understanding of the history of vegetation on Antarctica. Details of the analytical geochemistry techniques used here are given in Chapter 2.

### 1.2.2 What were continental temperatures during EAIS retreat? (Chapter 2)

Since the discovery of a fossil flora in the Sirius Group sediments at Oliver Bluffs, numerous researchers have reconstructed continental temperatures in an attempt to understand how vegetation could be sustained at such high latitudes. At 85° S, vegetation growing at Oliver Bluffs would have received ~42% of the radiation received over Tierra del Fuego (54° S), resulting in low temperatures even during the summer. A mean summer temperature of ~5 °C has been proposed based on the minimal thermal requirements of freshwater molluscs (Ashworth and Preece, 2003), listroderine weevils (Ashworth and Kuschel, 2003) and extant *Nothofagus* species (Francis and Hill, 1996, Hill and Trustwell, 1993, Hill et al., 1996, Hill and Jordan, 1996, Webb and Harwood, 1993), and climate modelling suggests summer temperatures could have been 8 °C (Francis et al., 2007). Palaeosol structures for the Sirius Group suggest mean annual temperatures of between -11 and -3 °C (Retallack et al., 2001). While these reconstructions are numerous, there is a clear need for a more quantitative calculation of temperature using geochemical methods.

The use of a geochemistry-based proxy for palaeo-temperatures has numerous advantages over other methods. Fossil-based temperature proxies such as pollen, insects and leaf margin shape provide qualitative measures of climate change, but tend to be less precise than geochemical proxies, which can provide more quantitative estimates (Ballantyne et al., 2005).

Palaeothermometers based on branched glycerol dialkyl glycerol tetraethers (br-GDGTs) are very useful for terrestrial settings such as the Sirius Group, which contain only low levels of carbonate, precluding the use of isotopic temperature proxies. The MBT'/CBT proxy (Methylation of Branched Tetraethers and Cyclization of Branched Tetraethers, respectively; Peterse et al., 2012, Weijers et al., 2007) is based on the temperature-dependent distribution of br-GDGTs in soils and works well in cold high latitude climates (Peterse et al., 2009). The use of the MBT'/CBT proxy as a palaeothermometer is discussed further in Chapter 2, but will provide a precise

estimate of continental temperatures on Antarctica.

### **1.2.3 Can oxygen isotopes in Antarctic fossil prostrate trees be used to trace hydrological change? (Chapter 3)**

To examine how Antarctic climate behaved during EAIS retreat, it is useful to examine changes in the hydrological cycle, particularly looking at precipitation over the continent. Oxygen isotope ratios in precipitation act as a tracer of the hydrological cycle. Locally, precipitation  $\delta^{18}\text{O}$  is governed by condensation temperature and the amount of condensate formed from the parcel of water vapour (Dansgaard, 1964), but is also influenced more broadly by the characteristics of the moisture source (both location and isotopic composition) and the trajectories of the vapour in the atmosphere (Gat, 1996). Therefore, on geological timescales, there are multiple changes to the climate system that could affect precipitation isotopes, including changes in seasonality, sea surface temperature gradients, continental topography, and ice sheet volume and extent (Feakins et al., 2012, Kaandorp et al., 2005, Sepulchre et al., 2006, Ullman et al., 2014). Oxygen isotope ratios in tree ring cellulose have been shown to be a very useful tool for reconstructing precipitation isotopes in the modern (McCarroll and Loader, 2004). The exceptionally well-preserved prostrate trees at Oliver Bluffs therefore have excellent potential for use, but prostrate trees are generally not used in isotope studies. In Chapter 3, the ability of cellulose-oxygen isotopes in prostrate *Nothofagus* to record precipitation  $\delta^{18}\text{O}$  is tested using modern plants, and then applied to fossil *Nothofagus* from the Sirius Group, Antarctica.

#### **1.2.3.1 Prostrate trees**

Prostrate trees are woody plants with a stunted or twisted dwarf growth form (generally <2 m height), which frequently have a non-vertical trunk or grow laterally along the ground. They generally inhabit marginal habitats, e.g. at higher altitudes than arboreal trees, growing at or above the upper treeline on mountain slopes or at the tundra-taiga interface (Crawford, 2014). The stunted growth form may be genetically predetermined,

or it could occur because of phenotype plasticity. The latter cause is most likely the case for the prostrate *Nothofagus* fossils used in this study; at their southernmost extent in South America ( $\sim 54^\circ$  S), multiple *Nothofagus* species grow in prostrate form in areas most affected by strong winds, whereas they grow in erect form in more sheltered areas (Veblen et al., 1996). In addition, pollen records from the Ross Sea suggest that Antarctic vegetation increased in stature from a prostrate shrubby form to a more tree-like, upright growth form in response to brief warming during the Miocene (Warny et al., 2009), indicating that *Nothofagus* adopts a prostrate form as a phenotypic response to climate.

A common feature of prostrate trees is the formation of tension wood, formed in place of normal wood by trees, in response to gravity. Cambial activity is enhanced on the upper side of non-vertical trunk wood, producing more cells and therefore a thicker and denser growth ring. This can lead to elliptical or asymmetric growth rings, and in angiosperms, tension wood has a higher proportion of cellulose than normal wood. Prostrate plants are traditionally not used in dendroclimatological studies for this reason (Schweingruber, 2007), although increasingly tree ring widths in high altitude shrubs are being explored as climate archives (Hantemirov et al., 2011, Garcia-Cervigon Morales et al., 2012). To my knowledge, prostrate trees have never been tested for use in tree ring isotope studies. If they prove to be suitable archives of climate variables, tree ring isotopes from the fossil *Nothofagus* in this study could be used to reconstruct Antarctic palaeoclimate, with an emphasis on hard-to-reconstruct variables such as the isotopic composition of precipitation. Importantly, this advance would also make end-member environments that have heightened climate sensitivity, such as those at high latitudes and altitudes, more accessible for climate reconstructions.

### **1.2.3.2 Oxygen isotopes in tree rings**

Oxygen isotopes in tree ring cellulose are widely used as a proxy for palaeoclimate and can be used to reconstruct  $\delta^{18}\text{O}$  of ancient precipitation (Ballantyne et al., 2006, 2010, Csank et al., 2011, Jahren and Sternberg, 2003, 2008, Wolfe et al., 2012). Cellulose

$\delta^{18}\text{O}$  is largely governed by three dominant factors (summarised in Fig. 1.3):

- (a) The isotopic composition of the plants source water (Dawson and Ehleringer, 1993, Dawson and Pate, 1996);
- (b) Enrichment of heavy isotopes in leaf water via stomatal conductance, which is controlled by relative humidity (Barbour et al., 2000, Barbour and Farquhar, 2001, Barbour et al., 2002, Craig and Gordon, 1965, Dongmann et al., 1974);
- (c) Various biological fractionation factors during biosynthetic pathways and transport i.e., synthesis of leaf sugars from leaf water (factor b), transport of sugars to the cambium and their subsequent conversion to cellulose. (Barbour et al., 2000, Sternberg et al., 1986).

A plants main source of water (factor a) is through the soil and accordingly, part of the  $\delta^{18}\text{O}$  signal of trees is that of the soil moisture, generally from precipitation or groundwater. This signal is governed by several additional factors: soil residence time (as fractionation can occur via evaporation from the soil); the depth from which the roots acquire water (Dawson and Pate, 1996), and seasonal variation in  $\delta^{18}\text{O}$  of precipitation. No fractionation occurs when roots take up water, thus soil water  $\delta^{18}\text{O} = \text{source water } \delta^{18}\text{O}$  (Brunel et al., 1991).

Various models exist describing the relationship between source water  $\delta^{18}\text{O}$ , leaf water  $\delta^{18}\text{O}$  and relative humidity (i.e. factor b). The majority are steady-state models based, in one way or another, on the Craig-Gordon model of evaporation from a free water surface (Craig and Gordon, 1965, Dongmann et al., 1974, Farquhar et al., 1989b, Farquhar and Lloyd, 1993b) e.g. equation 1.1:

$$\Delta^{18}\text{O}_{evap} = \epsilon + \epsilon_k + \frac{e_a}{e_i}(\Delta^{18}\text{O}_{atmos} - \epsilon_k) \quad (1.1)$$

where  $\Delta^{18}\text{O}_{evap}$  gives the degree of enrichment of leaf water relative to source water at the site of evaporation,  $\epsilon$  is the depression of water vapour pressure by  $\text{H}_2^{18}\text{O}$ ,  $\epsilon_k$  is the fractionation at the stomata/leaf boundary layer,  $\Delta^{18}\text{O}_{atmos}$  gives the degree of

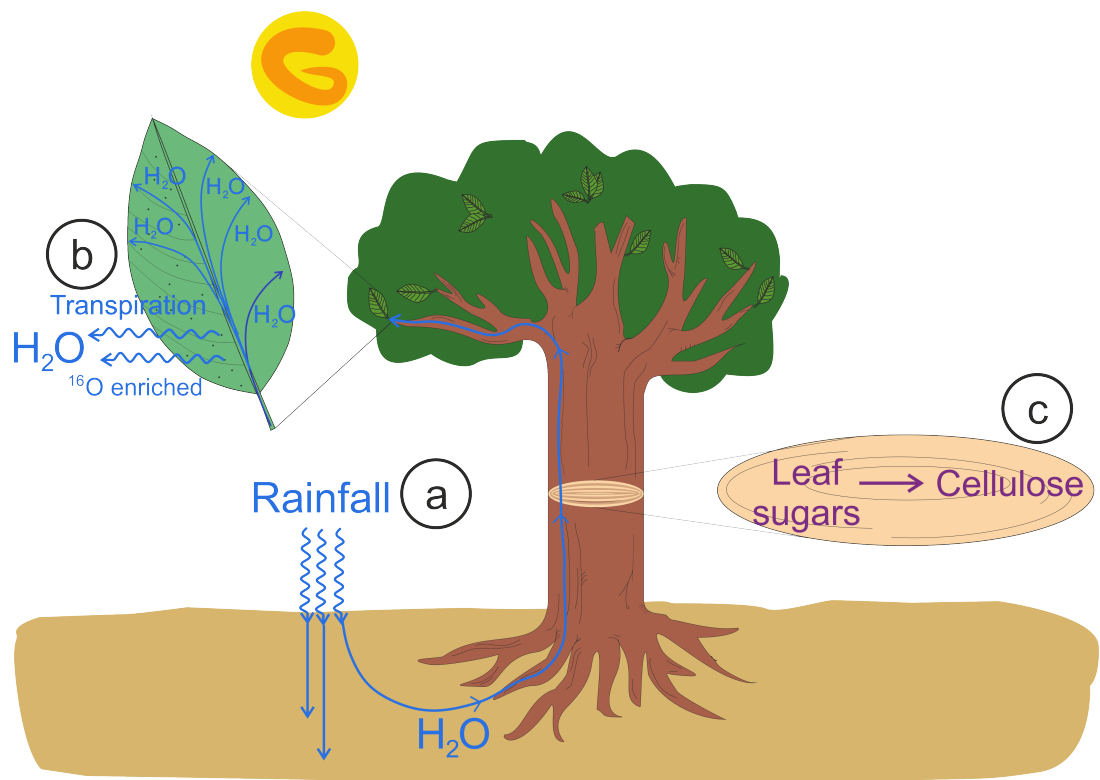


**Figure 1.3:** The oxygen isotope composition of cellulose is primarily governed by three processes: (a) the isotopic composition of precipitation, combined with evaporation processes from the soil and groundwater mixing; (b) evapotranspiration from leaves, which itself is dependent upon temperature and relative humidity; and (c), various well-constrained biological fractionation factors.

enrichment of atmospheric water vapour relative to the source water, and  $e_a$  and  $e_i$  give the ambient and intercellular vapour pressures respectively (Craig and Gordon, 1965). Numerous extensions to equation 1.1 have been proposed including enrichment along a series of evaporative cells (Gat and Bowser, 1991); the two-pool model, representing the mesophyll and veins (Allison et al., 1985); and the Péclet effect (Farquhar and Lloyd, 1993a), which describes the convection of depleted water to evaporating sites (stomata), opposed by backward diffusion of  $\text{H}_2^{18}\text{O}$  from enriched evaporative sites, supported by multiple observations (Barbour et al., 2004, Gan et al., 2002, Helliker and Ehleringer, 2000, Roden and Ehleringer, 1999, Wang and Yakir, 1995).

During the synthesis of leaf sugars (factor  $c$ ), carbonyl-bound oxygens exchange with leaf water resulting in an isotopic enrichment of 27 ‰ for sugar  $\delta^{18}\text{O}$  relative to leaf water  $\delta^{18}\text{O}$  (Sternberg et al., 1986). Further fractionation occurs during synthesis of cellulose from sucrose, where exchange occurs between the hydroxyl groups on the sugar rings and source water in xylem tissue (Sternberg et al., 1986).

Several models have been proposed combining factors (b) and (c) together, and can link  $\delta^{18}\text{O}$  of tree ring cellulose and plant source water. Early models were generally empirical or with basic terms describing evaporative enrichment, or the proportion of oxygen that exchanges with xylem water (Epstein et al., 1977, Sternberg et al., 1986, Yakir and DeNiro, 1990). More recent models are more mechanistic in nature and increasingly complex, including biological fractionation factors (Saurer et al., 1997, Roden and Ehleringer, 2000) and transpiration rates (Barbour et al., 2004). Comparisons between the latter three models found that the simplest approaches, such as that by (Saurer et al., 1997), give better predictions (Roden and Ehleringer, unpublished data). This is good news for palaeo-reconstructions, where the required input information on climate and biological parameters is scarce. For this reason, a simple adaptation of the Saurer model is used in Chapter 3 (Anderson et al., 2002).

#### **1.2.4 Were there changes in carbon cycling during EAIS retreat? (Chapter 3)**

During the Neogene, it appears that the Antarctic Ice Sheet had an atmospheric CO<sub>2</sub> threshold of ~500 ppmv before significant collapse occurred (Gasson et al., 2016, Levy et al., 2016); ice sheet volume and extent, and the carbon cycle are clearly linked to each other. In this section of the thesis, I attempt to constrain carbon cycling during AIS retreat using  $\delta^{13}\text{C}$  of plant material from the Sirius group fossils to reconstruct the isotopic composition of atmospheric CO<sub>2</sub>. The carbon isotopic composition of the atmospheric carbon reservoir varies through time with fluctuations in carbon fluxes through ocean and atmospheric reservoirs (Berner, 1998, Zachos et al., 2001). In most palaeoclimate studies, atmospheric  $\delta^{13}\text{C}$  is assumed to be equivalent to the preindustrial value of -6.5 ‰ (e.g. Feakins et al., 2005, 2007, Hopley et al., 2007, Zhang et al., 2009), but most likely varied through time in line with changes in the carbon cycle, such as rates of organic carbon burial and ocean overturning. Therefore calculating atmospheric  $\delta^{13}\text{C}$  provides additional constraints on carbon cycling during a period of ice sheet retreat.

Terrestrial plant material has been ignored generally as a potential proxy for atmospheric  $\delta^{13}\text{C}$  because it was thought that various physiological effects drowned out the atmospheric signal (reviewed in Farquhar et al., 1989a). However, Arens et al. (2000) found a strong linear relationship between  $\delta^{13}\text{C}$  of C3 land plant tissue and  $\delta^{13}\text{C}$  of atmospheric CO<sub>2</sub>, and this has been used several times to constrain ancient carbon cycling (Grocke et al., 1999, Jahren et al., 2001).

#### **1.2.5 Was there a different hydrological cycle during EAIS retreat? (Chapter 4)**

The presence of vegetation on Antarctica during the Neogene supports the notion that there was a different hydrological cycle, presumably with increased precipitation relative to today. Feakins et al. (2012) found enriched precipitation isotopes over the Antarctic coast throughout the warmth of the Miocene, and unexpected changes in precipitation

isotopes are also noted during the mid-Pliocene Warm period (Tindall and Haywood, 2015). Chapter 4 takes a data-model approach to answer Research Question 5. The geochemical data component builds on the oxygen isotope results of Chapter 3 by the addition of a second, independent proxy for precipitation isotopes (plant leaf wax hydrogen isotopes, giving precipitation  $\delta^2\text{H}$ ; a discussion of the proxy can be found in Chapter 4). This both provides greater confidence in the result from Chapter 3 and allows deeper analysis of hydrological cycling.

The geochemical results are then combined with climate modelling from an isotope-enabled ocean-atmosphere GCM in order to assess climate mechanisms behind the geochemical data. In order to fully understand our geochemical data, a climate model with oxygen isotopes implemented throughout the hydrological cycle is necessary. Thus far, modelling work specifically exploring Neogene Antarctic palaeoclimate has only used an isotope-enabled aqua-planet model (Feakins et al., 2012). This type of model does not take into account the impact of changes in albedo, sea ice or ice sheet volume and elevation on climate, which enact multiple feedbacks on temperature, atmospheric circulation and evaporation; all essential components to understanding hydrological cycling. Tindall and Haywood (2015) examined the mid-Pliocene global hydrological cycle using a fully coupled ocean-atmosphere GCM, which is able to capture land surface-climate interactions as well as the direct influence of the ice sheet on climate. However, a full examination of Antarctic hydrological cycling was not the purpose of that paper, but it provides an excellent starting point for the work carried out and presented in this thesis, which will provide in-depth understanding of climate mechanisms at play during ice sheet retreat. The addition of atmospheric dye-tracers into the model will further this work by providing a first order approximation of changes in moisture source region in a warmer world.

It is important to point out here that the boundary conditions used for the modelling component of this thesis are equivalent to those for the mid-Pliocene Warm Period, which could differ from the boundary conditions of the true time period represented by the geochemical results. Nevertheless, these still provide a reasonable representation of the boundary conditions important for answering our question; elevated atmospheric

CO<sub>2</sub> (400 ppmv) and a reduced AIS (2/3 the size of present-day). Furthermore, as discussed in section 1.1.3, the use of a fully coupled atmosphere-ocean GCM will address specific questions surrounding the impact of a reduced ice sheet on Antarctic hydrological cycling which will advance our understanding beyond the aqua-planet modelling of Feakins et al. (2012).

### 1.3 Thesis structure and author contributions

All written work presented in this thesis is my own. In addition to guidance and technical support from my supervisors, a number of collaborations resulting in co-authorships were established while undertaking the research in this thesis. Listed in order of appearance, these are:

- Dr Fiona Gill (University of Leeds, UK) who granted me access to her organic geochemistry lab and aided me in GC-FID and GC-MS analysis and quantification of biomarker lipids (Chapter 2).
- Drs. Christopher H. Vane and Raquel A. Lopes dos Santos (British Geological Survey, UK) who provided measurements of GDGT abundances and gave useful discussion on the MBT'/CBT palaeothermometer (Chapter 2).
- Dr Alina Marca (University of East Anglia, UK) who provided measurements of oxygen isotopes in extracted soil and plant waters using cavity ring-down spectroscopy (Chapter 3).
- Dr Jens Holtvoeth and Prof. Rich Pancost (University of Bristol, UK) who provided compound specific-isotope analysis and useful discussions on interpreting leaf wax  $\delta^2\text{H}$  data (Chapter 4).
- Dr Julia Tindall (University of Leeds, UK) who gave advice and provided simulations from HadCM3 for analysis, as well as assisting with analysis of HadCM3 model output (Chapter 4).

- Prof. Paul Valdes (University of Bristol, UK) who provided coding, training and technical assistance for implementing conservative dye-tracers in GCM simulations (Chapter 4).

Contributions and assistance not resulting in a co-authorship can be found in the Acknowledgements section.

Each of the three research chapters (Chapter 2, 3 and 4) have been written as individual research articles in preparation for submission to peer-reviewed journals. In each data chapter of the thesis, references to other data chapters are made using both the chapter number and the paper references. Chapter 2 has been formatted for submission to *Organic Geochemistry* (Rees-Owen et al., *in prep-a*) and Chapter 3 for *Earth Planetary Science Letters* (Rees-Owen et al., *in prep-b*). Chapter 4 has been prepared for submission to *Nature Geoscience* (Rees-Owen et al., *in prep-c*); the short format nature of this journal means that detailed discussion of the data produced and methods employed in this chapter may be found in Supplementary Information 3. For this reason, all supplementary material for each chapter is included as the final section within each chapter rather than as separate appendices. Each research chapter begins with a preface, detailing the intended journal and its status, and co-author contributions are noted.

## Chapter 2

# The last forests on Antarctica: reconstructing flora and temperatures from the Neogene Sirius Group, Transantarctic Mountains

### Preface

Chapter 2 was written in preparation for submission to *Organic Geochemistry*. The co-authors are my supervisors, colleagues and external collaborators (Fiona Gill, Rob Newton, Ruza Ivanovic, Jane Francis, James Riding, Christopher Vane and Raquel Lopes dos Santos). The work presented in this chapter is my own, including the background research, experiment design, set-up and execution, data analysis and presentation, and the written manuscript. My co-authors gave valuable advice and suggested improvements for all aspects of the work. Additionally, Fiona Gill provided technical support for the geochemical work carried out, and Christopher Vane and Raquel Lopes dos Santos provided analyses for the br-GDGT data.

## Abstract

Fossil-bearing deposits in the Transantarctic Mountains, Antarctica, indicate that, despite the cold and dynamic nature of the continent's climate, a tundra ecosystem flourished during periods of ice sheet retreat in the mid- to late Neogene (17 - 2.5 Ma), 480 km from the South Pole. There is contradictory evidence in the fossil record whether this flora was mixed angiosperm-conifer vegetation, or whether by this point, conifers had disappeared from the continent. Additionally, to date, temperature reconstructions have only been based on biological ranges, thus calling for a robust geochemical approach to understanding continental climate and environments. In order to address these questions we have analysed, for the first time, vascular plant and bacterial biomarkers in terrestrial sediments from the Transantarctic Mountains to reconstruct past temperatures and vegetation during a period of East Antarctic Ice Sheet retreat. From tetraether lipids (MBT'/CBT palaeothermometer), we conclude that continental summer temperatures were  $\sim 5$  °C, which is in agreement with previous reconstructions. This is warm enough to allow woody vegetation to survive even during the austral winter. Biomarkers from vascular plants indicate a low-diversity and spatially variable flora consisting of higher plants, mosses and algal mats growing in microenvironments in a glacial outwash system. Abietane-type compounds, a class of conifer biomarkers, are abundant which indicates that conifers, most likely Podocarpaceae, grew on the Antarctic continent well into the Neogene. This is supported by the palynological record, but not the macrofossil record on the continent and has implications for the evolution of vegetation on Antarctica.

## 2.1 Introduction

Since angiosperms first flourished on Antarctica in the late Cretaceous (85 million years ago; Ma; Cantrill and Poole, 2012; and references therein), Antarctic vegetation underwent a secular change, from a diverse fern-conifer dominated ecosystem, to a temperate rainforest during Eocene warmth, to a low-diversity tundra flora dominated

by angiosperms in the Neogene (Francis et al., 2008). This trend broadly correlates with long-term cooling seen from the mid-Eocene and the expansion of the Antarctic Ice Sheet (Zachos et al., 2001).

Generally, the Neogene Period (23 - 2.5 Ma) is characterised by atmospheric CO<sub>2</sub> levels similar to or lower than present, and warmer but fluctuating temperatures relative to today (Beerling and Royer, 2011). This interval is of particular interest in Antarctic science because of the complexity of both cryosphere (Cook et al., 2013, Pollard et al., 2015) and biosphere dynamics (e.g. Lewis et al., 2008) in this region. The scarcity of Neogene terrestrial deposits on Antarctica makes reconstructing vegetation difficult, but it appears that a low diversity mosaic tundra vegetation existed over a wide geographical range throughout the Oligocene to Middle Miocene (24 - 14 Ma; Prebble et al., 2006, Askin and Raine, 2000, Hill, 1989, Raine, 1998), and survived multiple episodes of glacial advance and retreat (Ashworth et al., 2007). Questions remain over both the timing of the disappearance of this tundra vegetation and its composition. In the McMurdo Dry Valleys at least, woody vegetation appears to have been rendered extinct by the expansion of the East Antarctic Ice Sheet at 13.8 Ma (Lewis et al., 2007, 2008). However, palynological data from DSDP Site 274 in the Ross Sea suggests that southern beech trees (*Nothofagus*) were present into the Pliocene (5 - 2.5 Ma; Fleming and Barron, 1996). The macrofossil record indicates that Antarctic flora was dominated by *Nothofagus* during the Neogene, but some pollen records suggest that conifers existed on Antarctica at least until ~15 Ma (Warny et al., 2009).

The Sirius Group in the Transantarctic Mountains has played a key role in reconstructing the Neogene flora of Antarctica. Fossil discoveries from Oliver Bluffs (85 °S, 166 °E; Francis and Hill, 1996) are some of the most important palaeobotanical discoveries on the continent in recent years. The age of these deposits has been the subject of a contentious debate (Barrett, 2013). Marine diatoms found at several Sirius Group locations throughout the Transantarctic Mountains suggest the deposits are 3 Ma (Webb and Harwood, 1991). However, it seems likely that the diatoms represent wind-blown contamination (McKay et al., 2008) and exposure dating of moraines at Oliver Bluffs suggests they formed at least 5 Ma and probably much earlier (Ackert,

Jr. and Kurz, 2004). Nonetheless, it is clear that these deposits represent a period of late Neogene Antarctic deglaciation, where the East Antarctic Ice Sheet had retreated far enough to allow a tundra shrub to grow 480 km from the South Pole. Not only do these sediments provide rare data on the evolution of vegetation on the Antarctic continent during the Neogene, but also insight into the Antarctic terrestrial climate during a warmer world.

The macrofossil and palynomorph record at Oliver Bluffs represent a low diversity angiosperm flora, including exceptionally preserved leaves and wood of *Nothofagus* (Carlquist, 1987, Francis and Hill, 1996, Hill et al., 1996, Hill and Trustwell, 1993, Webb and Harwood, 1987) as well as flowers, fruits, seeds and the remains of vascular plants with a cushion habit (Ashworth and Cantrill, 2004). Furthermore, at least five species of moss have been identified (Ashworth and Cantrill, 2004, Hill et al., 1996). There is no macrofossil record of coniferous plants at Oliver Bluffs, but rare bisaccate pollen grains suggest the presence of conifers, perhaps *Podocarpidites* (Askin and Raine, 2000). The low numbers of pollen grains is perhaps due to low pollen production, but the question of whether there were conifers in the interior of Antarctica has not been unequivocally answered. Resolving this issue would greatly enhance our understanding of Antarctic floral evolution.

Biomarkers from plants provide valuable information on terrestrial environments and climates and can be used to reconstruct past floras and depositional environments. Some, such as aliphatic wax lipids (e.g. *n*-alkanes, *n*-alkanols) are non-specific, whereas others, particularly the terpenoid family of compounds, provides valuable chemotaxonomic information. For example, tricyclic diterpenoids (e.g. abietanes) are characteristically produced by conifers, while non-steroidal pentacyclic triterpenoids (e.g. oleanane-type compounds) are specific to angiosperms (Otto and Wilde, 2001; and references therein). Using a biomarker approach to understand vegetation gives different insights into past floral changes where preservation biases in the macro- and microfossil record differ from those in the biomarker record. This has been used to some advantage in deep time settings, such as the Paleocene and Eocene Bighorn Basin, to gain a more complete knowledge of ancient vegetation (Diefendorf et al., 2011).

The fossil discoveries at Oliver Bluffs are thought to represent warm interglacials which allowed the flora to briefly return from coastal refugia (e.g. Askin and Markgraf, 1986). Temperatures for these warm periods have been reconstructed by analysis of the biological limits of fossil plants (Francis and Hill, 1996), weevils (Ashworth and Kuschel, 2003) and freshwater molluscs (Ashworth and Preece, 2003) found at Oliver Bluffs, suggesting temperatures were significantly warmer than the modern; i.e. 5 °C during the summer compared to  $\sim$ -3.4 °C for the present day. The distribution of branched glycerol dialkyl glycerol tetraether molecules, a suite of bacterial membrane lipids, can be used to empirically reconstruct soil pH and continental temperatures (known as the MBT'/CBT palaeothermometer, since followed by improved ratios (Peterse et al., 2012, Weijers et al., 2007). No geochemical thermometers have previously been applied to terrestrial Antarctic deposits during this interval.

This chapter describes the first biogeochemical study of the Sirius Group at Oliver Bluffs. We analyse biomarkers from higher plants to assess their preservation and potential as vegetation indicators which could resolve the apparent discrepancies between the macro- and microfossil record of conifers at Oliver Bluffs. The use of a geochemical thermometer provides an additional and robust dimension to our understanding of continental temperatures during Southern Hemisphere deglaciations. While the precise age of these deposits is not known, the results from this study inform our understanding of Antarctic climate and vegetation in a past warmer world.

## 2.2 Materials and Methods

### 2.2.1 Geological setting

The sediment samples are taken from the Meyer Desert Formation glacial deposits, which form the upper part of the Sirius Group in the Meyer Desert and Dominion Range region of the Transantarctic Mountains (Fig. 2.1, Mercer and Sutter, 1982). Samples were collected from Oliver Bluffs, which today is at the northern end of the Oliver Platform at latitude 85° 07' S and longitude 166° 35' E, 1760 masl. The site

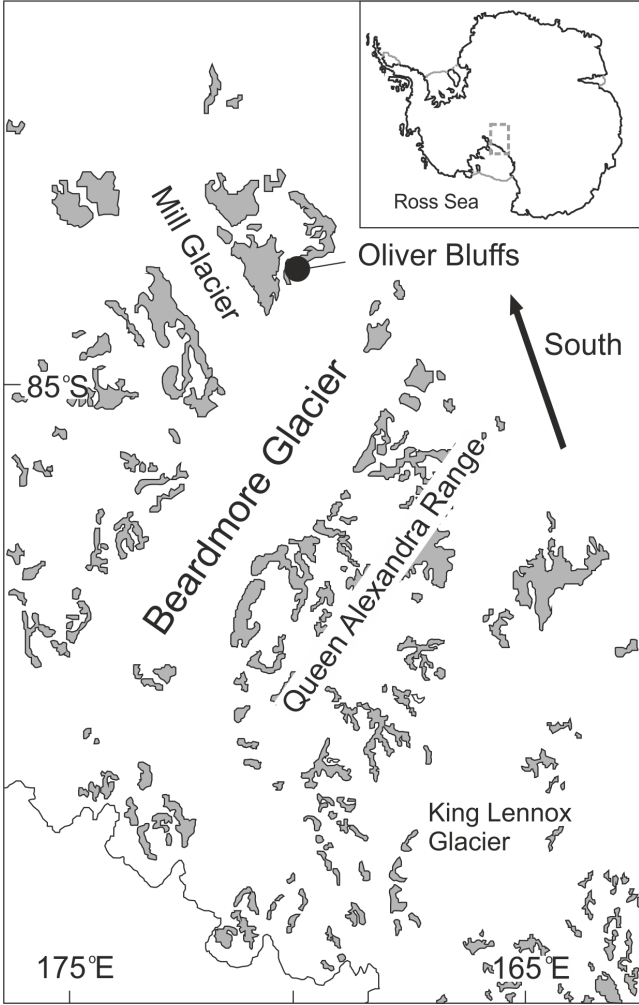


**Figure 2.1:** Map of Beardmore Glacier region with Oliver Bluffs marked. Grey areas denote outcrops. White areas denote ice-covered land and the Ross Ice Shelf.

was at a similarly high latitude during deposition (Lawver and Gahagan, 2003), but would have been at a considerably lower altitude (<700 masl), based on the biological constraints of the *in situ* plant macrofossils (Mercer, 1986). The section sampled is Member 2 of McKelvey et al. (1991), which includes fossil-bearing siltstones and sandstones, diamictites and mudstones, and is interpreted as representing periglacial or interglacial conditions.

### 2.2.2 Plant lipid analysis by Gas Chromatography/Mass Spectrometry

Prior to use, all glassware was solvent cleaned and furnace (400 °C, 4 hours) to avoid contamination. Sediment was dried and ground to <200 µm. An aliquot of sediment (20 - 25 g) was extracted using Soxhlet apparatus for 24 hours in DCM/MeOH (9:1, v/v). Sulphur was removed from the extract by the addition of activated copper wire (24 hours). The bulk of the solvent was removed using a rotary evaporator. Half of the total lipid extract (TLE) was archived; the other half was fractionated into four fractions (apolar, aromatic, aldehydes and ketones, polar) using column chromatography with activated silica gel and elution with hexane (4 ml), hexane/DCM (2:1; 2 ml), DCM (4 ml) and methanol (5 ml) respectively; adapted from Bendle et al. (2007). The polar fraction was derivatised by *bis*(trimethyl)trifluoroacetamide (BSTFA) in pyridine at 60 °C for 1 hour prior to analysis. Samples were dissolved in ethyl acetate before analysis by gas chromatography/mass spectrometry (GC/MS).

Lipid analysis by GC/MS was conducted at the University of Leeds using a Trace 1300 gas chromatograph coupled to an ISQ mass spectrometer (Thermo Scientific, UK) equipped with a non-polar fused silica capillary column (CPSil-5CB, 50 m x 0.32 mm x 0.12 mm; Agilent Technologies, USA). The temperature programme used was as follows: initial temperature 40 °C, increasing to 130 °C at a rate of 20 °C per minute, then rising to 300 °C at a rate of 4 °C per minute with a final isothermal hold at 300 °C for 25 minutes. Helium was used as the carrier gas. The sample was injected splitless with the injector temperature at 300 °C. The ion source and transfer line were maintained at 300

°C. The emission current was 50 A and the electron energy was 70 eV. The analyser was set to scan at  $m/z$  50-650 with a scan cycle time of 0.6 s. Data were collected and processed using the XCalibur software. Individual compounds were identified by interpretation of mass spectrometric fraction patterns and comparison of mass spectra and retention times with literature and library data. Lipids were quantified relative to internal standards.

### 2.2.3 GDGT analysis by Liquid Chromatography/Mass Spectrometry

Freeze-dried sediments were extracted using an automated solvent extractor (Dionex 200) operated at 100 °C and 7.6 x10<sup>6</sup> Pa with DCM: MeOH (9:1, v:v) to obtain a TLE. Internal standard C<sub>46</sub> GDGT was added to the TLE, which was separated into an apolar and polar fraction in an alumina oxide column (Al<sub>2</sub>O<sub>3</sub>), using *n*-hexane/DCM 9:1 and MeOH /DCM 1:1. The polar fraction was filtered through a polytetrafluoroethylene filter (PTFE - 0.45 μm) and analysed using a Thermo TSQ Quantiva MS instrument coupled to an Ultimate 3000 series μHPLC instrument. The chromatographic and MS conditions are described in Lopes dos Santos and Vane (2016). GDGT distributions were determined relative to internal standard.

Weijers et al. (2007) created two indices, the Methylation of Branched Tetraethers (MBT) and Cyclisation of Branched Tetraethers (CBT), which described the empirical relationship between the distribution of branched tetraether lipids, mean annual air temperature (MAAT), and soil pH. More recently, Peterse et al. (2012) recalibrated the proxy using an expanded global soils dataset, and refining the br-GDGTs used in the calibration. Here, we use the CBT index (equation 2.1) after Weijers et al. (2007) and use the revised MBT' index (equation 2.2; Peterse et al., 2012). Mean annual air temperature was calculated using two calibration equations (equations 2.3 and 2.4) from Peterse et al. (2012). The Branched Isoprenoidal Tetraether (BIT) index was calculated after Hopmans et al. (2004); equation 2.5.

$$CBT = \frac{-\log(Ib + IIb)}{(Ia + IIa)} \quad (2.1)$$

$$MBT' = \frac{(Ia + Ib + Ic)}{(Ia + Ib + Ic + IIa + IIb + IIc + IIIa)} \quad (2.2)$$

$$MAAT_a = -0.64 + 22.9 * MBT' \quad (2.3)$$

$$MAAT_b = 0.81 - 5.67 * CBT + 31 * MBT' \quad (2.4)$$

$$BIT = \frac{(I + II + III)}{(I + II + III + IV)} \quad (2.5)$$

Roman numerals in the equations refer to GDGT structures given in Weijers et al. (2007). The average standard deviation of the MBT' and CBT indices, based on duplicate injections of sample, is 0.013 and 0.051. This results in an analytical error in temperature estimates of ca. 0.3 and 0.6 °C for MAAT<sub>a</sub> and MAAT<sub>b</sub>, respectively. The root mean squared error of the mean annual temperature is 5.7 and 5.0 °C for MAAT<sub>a</sub> and MAAT<sub>b</sub> respectively, estimated for the MAAT calculations using the transfer functions in Peterse et al. (2012). Several factors may contribute to the relatively large scatter in the calibrations, but the uncertainty in temperature estimates is likely mainly systematic; application of the proxy on a local scale (such as this study) will result in much lower uncertainty, but an exact estimate of the error is hard to constrain (Peterse et al., 2012).

## 2.3 Results

### 2.3.1 Plant lipid contents

All lipid fractions analysed were dominated by plant-derived biomarkers, including a range of *n*-alkyl and terpenoid components; compound identifications are shown in Fig. 2.2 and the lipid contents are summarised in Table 2.1.

The apolar fraction is characterised by an *n*-alkane homologous series between C<sub>14</sub>

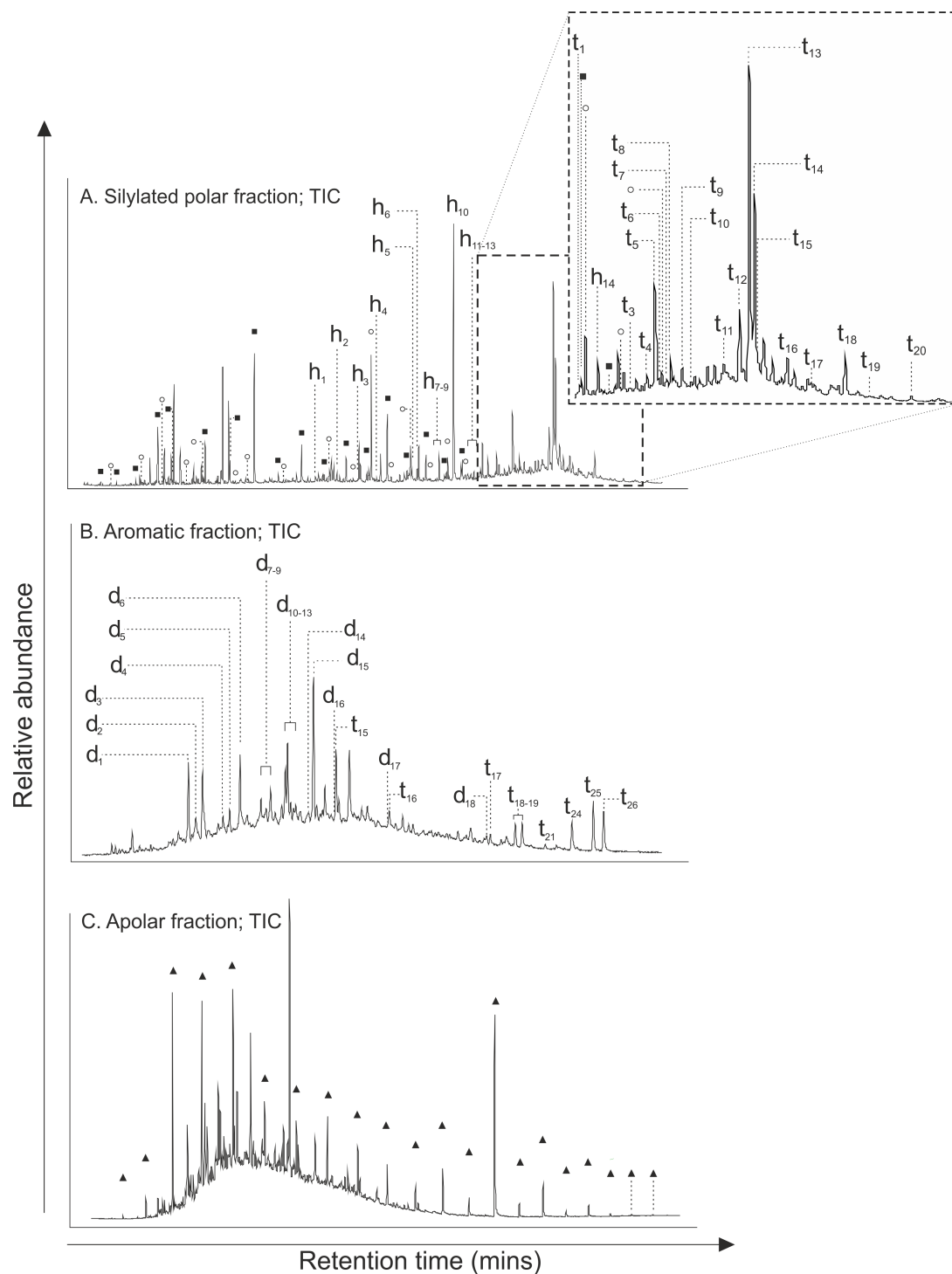


**Figure 2.2:** GC-MS (Total Ion Current; TIC) traces of polar, aromatic and apolar fractions from one sample from Oliver Bluffs, Transantarctic Mountains. For peak annotations see Table 2.1. ○ = alkanolic acid, ■ = alkanols, ▲ = alkanes.

and C<sub>34</sub>. Lipids were detected in concentrations between 0.02 - 84.3  $\mu\text{g g}^{-1}$  dry sediment; *n*-C<sub>13</sub> was detected in some samples in concentrations between 0.003 - 0.6  $\mu\text{g g}^{-1}$  dry sediment. The odd-even preference index (OEP) was 25.5 on average (Scalan and Smith, 1970) and the average carbon preference index (CPI; Bray and Evans, 1961) was 11.7, confirming a terrestrial plant origin (Fig. 2.3). The average chain length (ACL; Eglinton and Hamilton, 1967) ranged between 25.3 and 28.1 which is broadly consistent with modern trees (Diefendorf et al., 2011). The majority of samples had an *n*-alkane maximum at C<sub>27</sub> (n=11); however, the remainder were dominated by low chain-length alkanes (C<sub>17</sub>), suggesting algal input.

The polar fraction contained a homologous series of *n*-alkanols and *n*-alkanoic acids, ranging from C<sub>10</sub> to C<sub>30</sub>, and C<sub>9</sub> to C<sub>28</sub>, respectively. The *n*-alkanol series exhibited a strong even-odd predominance, had a CPI of 3.3 - 12.3 and the ACL ranged between 22.7 and 25.3. The dominant alkanol was C<sub>22</sub> in all samples. The alkanolic acid series exhibited a weaker even over odd predominance and had an average chain length ranging from 22.9 - 25.6. The majority of samples exhibited a bimodal distribution, maximising at C<sub>16</sub> and C<sub>22</sub>. The C<sub>21</sub> alkanolic acid was the most abundant lipid in one sample. In addition to the fatty acid homologous series, a homologous series of  $\alpha,\omega$ -alkanedioic acids (C<sub>14</sub> - C<sub>23</sub>) and several hydroxyl-fatty acids were found in numerous samples.

The polar fraction also contained numerous triterpenoids indicative of higher vascular plants including the steroids cholesterol, 5 $\beta$ -stigmastanol, 5  $\alpha$ -stigmastanol, 5 $\beta$ -sitosterol and campesterol, as well as the non-steroidal triterpenoids  $\beta$ -amyrin,  $\alpha$ -amyrin, taraxerol, betulin, betulinic acid and several unknown compounds.

The aromatic fraction contained a variety of aromatic diterpenoids and five di- and tri-aromatic *des-A*-triterpenoids, as well as two unidentified fully aromatised triterpenoids. Diterpenoids of the abietane class, which are typical of conifers (Otto and Wilde, 2001, Yamamoto et al., 2006), are relatively abundant, particularly dehydroabietane, norsimonellite, tetrahydroretene and two dehydroabietins (18-norabieta-8,11,13-triene and 19-norabieta-8,11,13-triene). Four trisnorabietatriene isomers were also iden-

tified along with several unknown diterpane compounds.

**Table 2.1:** Compounds identified in the sediments from Oliver Bluffs, Transantarctic Mountains. L = identified by comparison with the literature; M/R = identified by comparison of mass spectra or retention times with NIST and internal library; S = interpretation of mass spectra. (a) Rontani and Aubert (2004), (b) Otto and Simoneit (2001), (c) Philp (1985), (d) Simoneit and Mazurek (1982), (e) Simoneit (1977), (f) Enzell and Ryhage (1967), (g) AOCs lipid library, (h) Branco et al. (2004), (i) Sousa et al. (2006), (j) Lorenz et al. (2008), (k) Huang et al. (2013), (l) Trendel et al. (1989), (m) LaFlamme and Hites (1979).

No.	Compound name	MW	Composition	Fragments (m/z)	ID
I. Diacids and hydroxy-acids					
h1	C <sub>14</sub> diacid				S
h2	C <sub>15</sub> diacid				S
h3	C <sub>16</sub> diacid				S
h4	C <sub>17</sub> diacid				S
h5	C <sub>18</sub> diacid				S
h6	C <sub>19</sub> diacid				S
h7	22-hydroxydocosanoic acid methyl ester TMS	442	C <sub>23</sub> H <sub>45</sub> O <sub>3</sub> -TMS	75, 103, 129/131, 146, 159, 395, 427	L; [a]
h8	C <sub>20</sub> diacid				S
h9	3-hydroxytetracosanoic acid TMS	528	C <sub>24</sub> H <sub>47</sub> O <sub>3</sub> -TMS	73, 117, 129, 149, 159, 283, 411, 455	S
h10	1,21-heneicosandioic acid TMS	500	C <sub>21</sub> H <sub>38</sub> O <sub>4</sub> -TMS	75, 129, 149, 204, 217, 395, 469, 485	S

Table 2.1: continued

No.	Compound name	MW	Composition	Fragments (m/z)	ID
h11	C <sub>22</sub> diacid				S
h12	$\omega$ -hydroxytetracosanoic acid TMS	528	C <sub>24</sub> H <sub>47</sub> O <sub>3</sub> -TMS	73, 117, 129, 131/3, 146, 159, 423, 455	S
h13	3-hydroxyhexacosanoic acid TMS	514	C <sub>26</sub> H <sub>51</sub> O <sub>3</sub> -TMS	73, 129, 131, 159, 439, 483	S
h14	C <sub>23</sub> diacid				
II. Diterpenoids					
d1	Trisnorabietatriene isomer	228	C <sub>17</sub> H <sub>24</sub>	91, 105, 159, 171, 228	L [b]
d2	1,2,3,4-tetrahydroretene	238	C <sub>18</sub> H <sub>22</sub>	91, 165, 181, 223, 238	L [c]
d3	Trisnorabietatriene isomer	228	C <sub>17</sub> H <sub>24</sub>	105, 131, 159, 128	L [b]
d4	Norsimonellite	238	C <sub>18</sub> H <sub>22</sub>	152, 165, 181, 223, 238	L [d]
d5	Trisnorabietatriene isomer	228	C <sub>17</sub> H <sub>24</sub>	91, 105, 129/131, 159, 228	L [b]
d6	Trisnorabietatriene isomer	228	C <sub>17</sub> H <sub>24</sub>	91, 105, 129/131, 159, 228	L [b]
d7	Unknown diterpane	266	C <sub>20</sub> H <sub>26</sub>	57, 69, 152, 165, 181, 237, 266	S

Table 2.1: continued

No.	Compound name	MW	Composition	Fragments (m/z)	ID
d8	18-Norabieta-8,11,13-triene	256	C <sub>19</sub> H <sub>28</sub>	117, 129, 159, 185, 213, 241, 256	L [c,e]
d9	19-Norabieta-3,8,11,13-tetraene	254	C <sub>19</sub> H <sub>26</sub>	117, 129, 159, 241, 254	L [c]
d10	19-Norabieta-8,11,13-triene	256	C <sub>19</sub> H <sub>28</sub>	117, 129, 159, 185, 213, 241, 256	L [c,e]
d11	Isomer of d7	266	C <sub>20</sub> H <sub>26</sub>	57, 69, 152, 165 181, 237, 266	L [c]
d12	Isomer of d7	266	C <sub>20</sub> H <sub>26</sub>	57, 69, 152, 165 181, 237, 266	L [c]
d13	19-Norabieta-4,8,11,13-tetraene	254	C <sub>19</sub> H <sub>26</sub>	117, 129, 159, 241, 254	L [c]
d14	Dehydroabietane	270	C <sub>20</sub> H <sub>30</sub>	159, 173, 185, 200, 213, 241, 256, 270	L [f]
d15	Isomer of d7	266	C <sub>20</sub> H <sub>26</sub>	57, 69, 152, 165 181, 237, 266	L
d16	Unknown diterpene	236	-	91, 115, 152, 165, 193	L [c]
d17	Unknown diterpene	234	-	101, 204, 219	S
d18	Unknown diterpene	290	-	101, 205, 189	S

## III. Triterpenoids

Table 2.1: continued

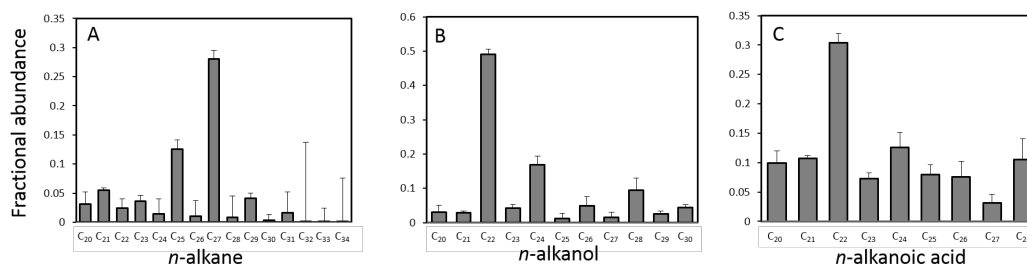
No.	Compound name	MW	Composition	Fragments (m/z)	ID
t1	Cholest-5-en-3 $\beta$ -ol (TMS)	458	C <sub>27</sub> H <sub>45</sub> O-TMS	73, 129, 273, 329, 353, 368, 443	M/R
t2	5 $\beta$ -stigmastanol (TMS)	488	C <sub>29</sub> H <sub>51</sub> O-TMS	57, 75, 215, 383, 398, 432, 473	M/R
t3	Lupeol (TMS)	498	C <sub>30</sub> H <sub>49</sub> O-TMS	73, 129, 175, 189, 369, 408, 482	L [g]
t4	Olean-12-en-3,11-dione	438	C <sub>30</sub> H <sub>46</sub> O <sub>2</sub>	77, 95, 105, 151, 189, 232, 423	L [h]
t5	24-ethyl-5 $\beta$ -cholest-5-en-3 $\beta$ -ol (TMS)	486	C <sub>29</sub> H <sub>49</sub> O-TMS	129, 255, 357, 381, 396, 471	M/R
t6	5 $\alpha$ -stigmastanol (TMS)	488	C <sub>29</sub> H <sub>51</sub> O-TMS	57, 75, 215, 255, 431, 473	M/R
t7	$\beta$ -amyirin (TMS)	498	C <sub>30</sub> H <sub>49</sub> O-TMS	55, 73, 129, 189, 203, 218, 257, 394	M/R
t8	C <sub>29.1</sub> sterol (TMS)	486	C <sub>29</sub> H <sub>49</sub> O-TMS	129, 157, 255, 453, 467	S
t9	Unknown triterpenoid (TMS)	-	-	73, 131, 189, 413, 441, 531	S
t10	C <sub>29.2</sub> sterol (TMS)	484	C <sub>29</sub> H <sub>47</sub> O-TMS	175, 257, 313, 328, 367, 395, 410, 484	S
t11	Unknown triterpenoid (TMS)	584	-	73, 129, 189, 203, 216, 424, 482, 496	S
t12	Uvaol (TMS)	586	C <sub>31</sub> H <sub>50</sub> O <sub>2</sub> -TMS	188, 203, 216, 391, 406, 426, 481, 496, 571	L [g]
t13	Betulin (TMS)	586	C <sub>30</sub> H <sub>48</sub> O <sub>2</sub> -TMS	73, 95, 189, 203, 393, 483, 496, 571	L [g]

Table 2.1: continued

No.	Compound name	MW	Composition	Fragments (m/z)	ID
t14	Unknown triterpenoid (TMS)	574	-	73, 95, 129, 257, 431, 484, 496, 512, 545, 574	S
t15	C <sub>30</sub> triterpenyl acid	600	-	73, 133, 189, 203, 320, 481, 585, 600	S
t16	$\alpha$ -amyrin (TMS)	498	C <sub>30</sub> H <sub>49</sub> O-TMS	55, 73, 129, 189, 203, 218, 257, 394	M/R
t17	Unknown triterpenoid (TMS)	586	?C <sub>30</sub> H <sub>48</sub> O <sub>2</sub> -TMS	73, 129, 189, 203, 395, 571	S
t18	Betulinic acid (TMS)	600	C <sub>30</sub> H <sub>47</sub> O <sub>3</sub> -TMS	73, 189, 202, 203, 320, 585	L [i]
t19	C <sub>31</sub> triterpenyl acid	614	-	73, 129, 159, 175, 189, 497, 599, 614	S
t20	Oleanolic acid (TMS)	600	C <sub>30</sub> H <sub>47</sub> O <sub>3</sub> -TMS	73, 173, 203, 320, 585	L [j]
t21	Unknown triterpene				S
t22	Unknown triterpene				S
t23	Unknown triterpene				S
t24	des-A-8,14-seconorlupa-5,7,13,15,17-hexaene	306	C <sub>23</sub> H <sub>30</sub>	119, 145, 187	L [k]
t24	des-A-dinoroleana-5,7,9,11,13-pentaene	292	C <sub>22</sub> H <sub>28</sub>	165, 168, 178, 193	L [k, l]
t25	des-A-dinorursa-5,7,9,11,13-pentaene	292	C <sub>22</sub> H <sub>28</sub>	165, 178, 193, 207	L [k, l]

Table 2.1: continued

No.	Compound name	MW	Composition	Fragments (m/z)	ID
t26	Unknown triterpene	290	C <sub>22</sub> H <sub>26</sub>	165, 247, 275	
t27	des-A-trinorlupa-5,7,9,11,13,15,17-heptaene	274	C <sub>21</sub> H <sub>22</sub>	202, 215, 231	L [k, m]
t28	des-A-trinorursa-5,7,9,11,13,15,17-heptaene	274	C <sub>21</sub> H <sub>22</sub>	189, 202, 215, 229, 259	L [k, l]
t29	des-A-trinorleana-5,7,9,11,13,15,17-heptaene	274	C <sub>21</sub> H <sub>22</sub>	189, 202, 218, 229, 259	L [k, m]



**Figure 2.3:** Average fractional abundance of n-alkanes, n-alkanols, n-alkanoic acids. Error bars = 1 sd.

### 2.3.2 Bacterial tetraether lipid distributions

Branched GDGTs were present in all samples. The total concentration of br-GDGT per sample ranged between 0.23 and 61.5 ng g<sup>-1</sup> dry sediment and averaged at 7.12 ng g<sup>-1</sup>. Sample WSU-13-6 was a major outlier (outside the outer fence; 3 x interquartile range added to the third quartile) with markedly higher br-GDGT abundances than other samples (total br-GDGT abundance 61.5 ng g<sup>-1</sup> sediment). GDGTs IIIa and IIa were the most abundant (mean of 32% each), followed by GDGT Ia (mean 18%), GDGT IIB (9%) and Ib (6%) (Fig. 2.4). Br-GDGTs IIC and IIIC were below the detection limit in several samples. The BIT index, a proxy for soil input, was calculated after Hopmans et al. (2004) and exceeded 0.99 in all samples. The CBT index ranged between 0.30-1.21, and MBT' ranged between 0.16-0.59.

Using the revised calibration in Peterse et al. (2012) (equation 2.3, MAAT<sub>b</sub>), reconstructed temperatures ranged between 3.1 and 12.7 °C, with a mean temperature of 4.5 ± 2.4 °C (error is standard deviation of sample mean). Using the alternative calibration from the same study (equation 2.4, MAAT<sub>a</sub>), reconstructed temperatures exhibited a larger range between -0.7 and 12.1 °C, with a mean temperature of 5.0 ± 2.5 °C (Fig. 2.5). The large range was caused by sample OBFL-04-14, which was a minor outlier (between the inner and outer fences; inner fence = 1.5 x interquartile range added to the third quartile). There was no analytical reason to reject this sample, and it was therefore included in the remainder of the study. Using both calibrations, sample WSU-13-6 was identified as a major outlier with a calculated temperature of ~12 °C. This could not be attributed to analytical error so was included in our analysis,

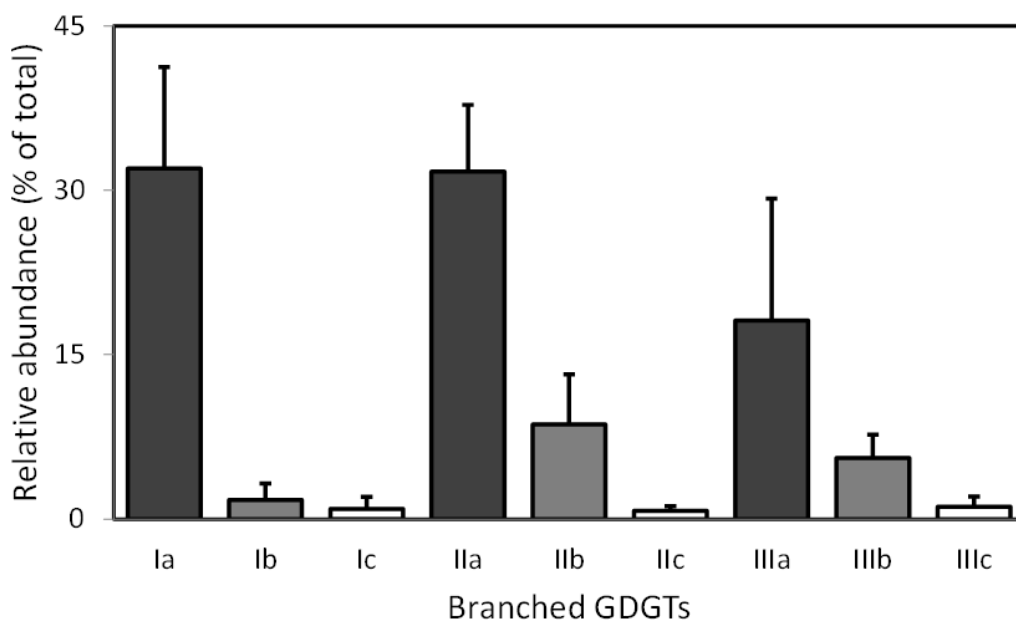


**Figure 2.4:** Average branched GDGT distributions in sediment samples ( $n=15$ ). Error bars = 1 sd.

although it is outside the proxy calibration error.

## 2.4 Discussion

### 2.4.1 Reconstructing vegetation from plant biomarkers

#### 2.4.1.1 Sources of plant biomarkers

**Aliphatic lipids** The high molecular weight (HMW) aliphatic lipids in the sediment were *n*-alkanes, *n*-alkanols and *n*-alkanoic acids in the range  $C_{22}$  to  $C_{34}$ , characteristic of epicuticular waxes from higher plants (Eglinton and Hamilton, 1967); this result is broadly consistent with the macrofossil record at Oliver Bluffs. The *n*-alkane distributions at Oliver Bluffs maximise strongly at  $C_{27}$ , with high abundances of  $C_{25}$ , and low abundances of the  $C_{29}$  and  $C_{31}$  homologues (Fig. 2.3). It is difficult to ascribe unambiguous origins to HMW aliphatic distributions, because large ranges have been documented within genera and species (e.g. Bush and McInerney, 2013, Stránský et al., 1967), and the aliphatic lipid record may also be biased towards angiosperm represen-

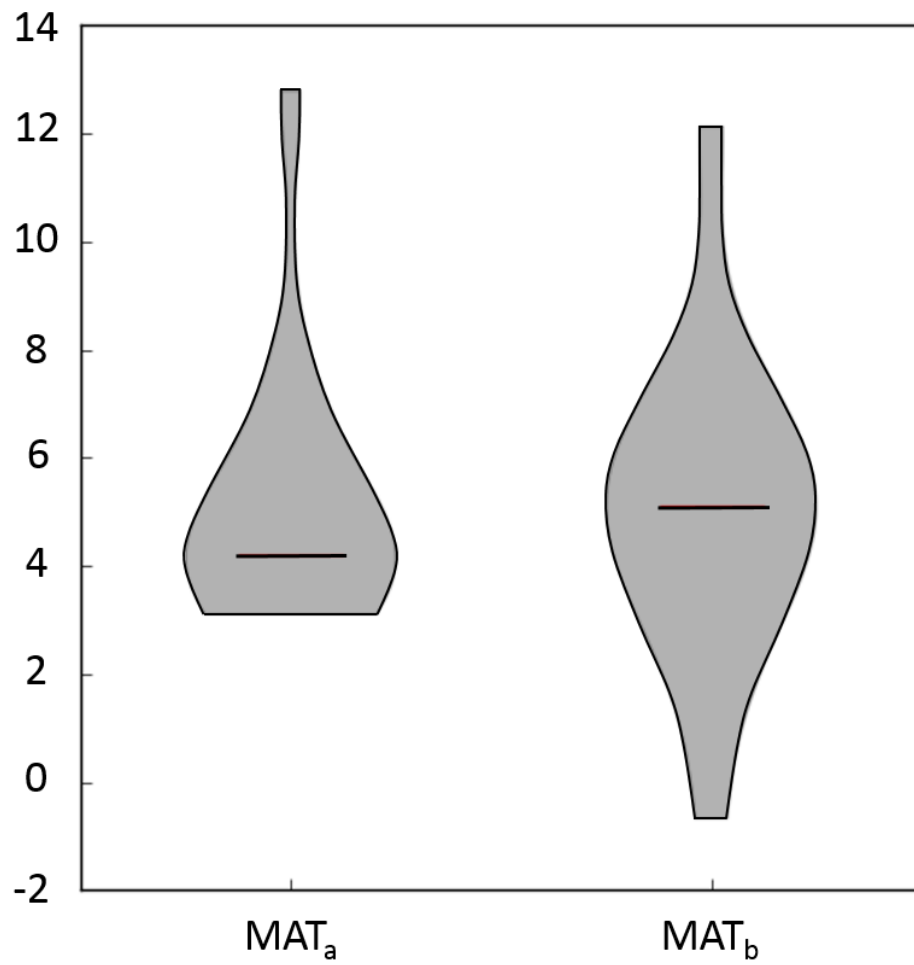


**Figure 2.5:** Distributions of reconstructed palaeotemperature for Oliver Bluffs using two calibrations from Peterse et al. (2012).

tation (Bush and McInerney, 2013, Diefendorf et al., 2011). However, the ACL index is at the lower end of the range for deciduous angiosperms reported in the literature (Diefendorf et al., 2011), which could suggest a mixed input from other higher plants. High abundances of the C<sub>27</sub> alkane have been reported in some sedges (Ficken et al., 1998), such as those found at Oliver Bluffs, although most graminoids are typically dominated by higher MW alkanes (e.g. Bush and McInerney, 2013). Similarly, the dominant chain lengths in alkanol and alkanolic acid series (C<sub>22</sub> alkanol for all and C<sub>22</sub> alkanolic acid for most samples) are low relative to those seen in modern leaf waxes and the sedimentary archive (Kolattukudy et al., 1976), and could reflect some input from mosses (Nierop et al., 2006). There is more variability in the distribution of low and medium MW aliphatic lipids at Oliver Bluffs. Several samples exhibited high abundances of the C<sub>16</sub> alkanolic acid, and the C<sub>17</sub> alkane is also abundant in a subset of these samples, which suggests that these samples have either a significant moss input (Nierop et al., 2006), or an algal input, or both (e.g. Cranwell, 1974). Abundant medium MW alkyl lipids are also indicative of peat bog bryophytes such as *Sphagnum* moss (Xie et al., 2000). Similarly, relatively high abundances of diacids in these samples may suggest a strong bryophyte input. Diacids could derive from the oxidation of  $\omega$ -hydroxyalkanoic acids, which are significant components of some liverwort cutin acids (Caldicott and Eglinton, 1976), as well as macromolecules in *Sphagnum* (Pancost et al., 2002). This interpretation is consistent with the Oliver Bluffs macrofossil record, which contains at least five poorly defined moss species as well as peat lenses, which are either a product of algal mats or mire deposits that represent poorly drained soil (Ashworth and Cantrill, 2004).

**Terpenoids** The steroid series at Oliver Bluffs consists of compounds with C<sub>27</sub> and C<sub>29</sub> backbones, suggesting that they originate from a higher plant source, although some C<sub>29</sub> sterols can also be synthesised by algae (Goodwin, 1974). The most abundant steroid was  $\beta$ -sitosterol, and the other identified steroids were in much lower abundance.

Polar triterpenoids of the lupane, oleanane and ursane classes are abundant in the polar fraction of the majority of samples, shown in Fig. 2.2; the majority were unaltered

natural products. Betulin and a compound we tentatively identify as uvaol were the most abundant triterpenoids (t13 and t12, respectively). Triterpenoids of these classes are characteristic of angiosperms (Simoneit et al., 1986) and suggest a high angiosperm input. Several triterpenyl acids were also detected, tentatively identified as betulinic acid and oleanolic acid as well as an unidentified triterpenyl acid (t18 - t20). Betulinic and oleanolic acid were in high abundance in some samples. Triterpenyl acids have been found in very high abundance in some *Sphagnum* mosses (Pancost et al., 2002); we speculate a possible moss source for these, although given their widespread distribution among angiosperm taxa, it is not possible to give a precise taxonomic assignment. Several di- and triaromatic triterpenes of the oleanane, ursane and lupane classes with A-ring (*des-A*) cleavage were identified (t24 - t29), and are also characteristic of angiosperms, (Hürlimann and Cherbuliez, 1981, Karrer, 1958, Karrer et al., 1977, Simoneit et al., 1986). The presence of *des-A*-triterpenoids suggests microbially mediated formation of these compounds (Huang et al., 1996, Trendel et al., 1989). The compounds identified here are similar to those identified in Late Cretaceous (100 - 66 Ma) and Paleocene (66 - 56 Ma) angiosperm fossils from Japan (Nakamura et al., 2010), which is consistent with the low level of oxidative degradation in our sediments and confirm a high angiosperm input to the sediment.

Diterpenoids are good chemotaxonomic biomarkers as they are major compounds in gymnosperms (Simoneit et al., 1986), and many classes of compounds have relatively high chemotaxonomic specificity (Otto and Wilde, 2001), although this is complicated at Oliver Bluffs by the lack of diterpenoid natural product precursors. The majority of the diterpenoids identified in the aromatic fraction were abietane-class compounds, which are widespread among conifers. Tetrahydroretene (d2) and the dehydroabietins 18-norabieta-8,11,13-triene and 19-norabieta-8,11,13-triene (d5, d6) have been identified as points on the diagenetic pathway for the degradation of abietic acid to retene (Marchand-Geneste and Carpy, 2003, Otto and Simoneit, 2001, 2002, Simoneit et al., 1986). Additionally, dehydroabietane and the norabietatetraenes are also thought to form during the diagenesis of abietic acid (cf. Hautevelle et al., 2006), so it seems likely these compounds originated from abietic acid. Under more reducing conditions, abi-

etic acid can undergo transformation to norabietanes like fichtelite (Otto and Simoneit, 2001), while bacterial degradation results in diterpenoid ketones and carboxylic acids (Biellmann et al., 1973b,a, Tavendale et al., 1997b,a). Their absence suggests an oxidative diagenetic pathway for diterpenoids in these sediments rather than biogenic or anaerobic alteration, in contrast to the triterpenoids. 18-norabieta-8,11,13-triene (d8) is also believed to be a derivative of 18-norferruginol (Stefanova et al., 2002), which itself is a diagenetic product of phenolic and ketophenolic abietanes such as ferruginol (Otto and Simoneit, 2001), and is found in all conifer families other than Pinaceae, although compounds in these families have not been identified here. The widespread distribution of normal abietane-class compounds among conifers means their source cannot be distinguished at a family level. However, abietanoic acids like abietic acid are predominantly found in Pinaceae resin (Otto and Wilde, 2001, Otto and Simoneit, 2001, 2002, Rezzi et al., 2005), though they are also found in low abundances across other conifer families (Hauteville et al., 2006). The geographical range of the Pinaceae family today is restricted to the Northern hemisphere, hence the diterpenoids identified at Oliver Bluffs come from another coniferous family.

#### **2.4.1.2 Depositional microenvironments**

Substantial variability is noted in the distributions of the classes of aliphatic lipids examined in this study between samples. In general, our samples cluster strongly into three groups based on aliphatic lipid distributions, which appear to represent several highly spatially heterogeneous distinct vegetation types, and support a complex sedimentary depositional regime consisting of microenvironments within a wide glacial outwash plain (summarised in Table 2.2). Group 1 consists of an input dominated by higher vascular plants (high C<sub>27</sub> alkane, low LMW alkanes), although high abundances of the C<sub>22</sub> alkanolic acid may indicate input from mosses. High abundances of triterpenoids suggests high angiosperm input, while low abundances of diterpenoids suggests very low input from conifer plants; these samples possibly correlate with the plant-colonized ridges of an outwash plain as described by Ashworth and Cantrill (2004). Samples in groups 2 and 3 exhibited high abundances of the C<sub>16</sub> alkanolic acid, and

**Table 2.2:** Differing biomarker distributions indicating microenvironments in the Beardmore Glacier region.

Group	Samples	Description
1	WSU-13-6, LCBA-05-5, SRB-07-6, OBFL-4-23, OBFL-04-29, OBFL-04-32, OBFL-04-25, SPBW-09-27, OBFL-04-13	High C <sub>27</sub> alkane and triterpenoids, low LMW alkanes and diterpenoids
2	OBFL-04-3, LCBA-05-17, OBFL-04-2	High C <sub>16</sub> alkanolic acid, low diterpenoids
3	OBFH-02-1, BNLB-12-3, LCBA-05-36, OBFL-04-20, SRB-07-5	High C <sub>16</sub> alkanolic acid, high C <sub>17</sub> alkane, low diterpenoids

the C<sub>17</sub> alkane is also abundant in group 3 samples, which suggests that these samples have either a significant moss input (Nierop et al., 2006), or an algal input (e.g. (Cranwell, 1974), possibly from waterlogged locations in abandoned meltwater channels. Low abundances of diterpenoids in group 2 samples implies little coniferous input, but group 3 samples have abundant triterpenoids and diterpenoids, indicating a mixed coniferous-angiosperm input. The variability in lipid distributions suggests that the vegetation recorded in our lipid record grew in a mosaic pattern of mires, cryptogram-herb and tundra shrub seen in Arctic islands and Tierra del Fuego, Chile, where the distribution of vegetation is a product of temperature, soil water balance and topography (Bliss and Matveyeva, 1992).

### 2.4.1.3 Coniferous input to sediment

The terpenoid record at Oliver Bluffs provides interesting insights into Antarctic vegetation. The high abundances of unaltered triterpenoids is consistent with both the macrofossil and palynomorph record which indicate a vegetation dominated by angiosperms, particularly *Nothofagus*. However, conifer-derived diterpenoids are reported here at Oliver Bluffs for the first time, supporting the presence of conifers on Antarctica well into the Neogene as suggested by the pollen record. While the abietane-class diterpenoids identified at Oliver Bluffs are generally not considered to be chemotaxonomically indicative beyond the division level, all coniferous pollen at Oliver Bluffs are

identified as Podocarpaceae (Askin and Raine, 2000), indicating a podocarp origin for these diterpenoids.

The uncertainty of the age of the strata at Oliver Bluffs makes it difficult to draw direct comparisons with other vegetation records. Earlier palynomorph records suggest that *Podocarpidites* species were the dominant Antarctic conifer throughout the Oligocene and Early Miocene (33 - 14 Ma; Askin and Raine, 2000, Kemp and Barrett, 1975, Prebble et al., 2006), and abundant *Podocarpidites* pollen has been identified between 17 Ma and 12 Ma in ANDRILL core AND-2A (Warny et al., 2009) which would support our interpretation. It is likely that these would have grown with a shrub or prostrate habit, similar to the prostrate *Nothofagus* fossils discovered at the same site (Francis and Hill, 1996); the pollen record also suggests that, with the exception of one or two warm intervals during the early Miocene, *Podocarpidites* grew as coniferous shrubs (Warny et al., 2009). Whilst it is possible that the Oliver Bluffs sediments are Pliocene (5 - 2.5 Ma) in age, the sole Pliocene palynomorph record (from DSDP Site 274; Fleming and Barron, 1996), only discusses *Nothofagus* pollen. This could provide a further constraint on the age of the sediment although a re-examination of the DSDP 274 pollen is necessary.

We note an apparent discrepancy between the preservation of macrofossil and lipid records at Oliver Bluffs. Many of the angiosperm-derived triterpenoids identified at Oliver Bluffs are unaltered natural products, with some evidence of diagenetic degradation. We did not identify any natural product precursors to the conifer-derived aromatic diterpenoids, suggesting that the diterpenoids were preferentially degraded relative to the triterpenoids. This is in contrast to the trend documented in the Miocene Clarkia Formation (Idaho, USA), attributed to the preferential taphonomic degradation of angiosperm over coniferous plant material (Otto et al., 2005). We suggest three possible explanations for this interpreted difference between the fossil and biomarker record:

1. The presence of relatively degraded diterpenoids alongside better preserved angiosperm-derived triterpenoids is due to the reworking of older organic matter from sediments with a high input of coniferous plant material.

2. The diterpenoids are geologically contemporaneous with the triterpenoids, but are transported (either fluviially or by aeolian processes) from a distal site with coniferous vegetation.
  
3. Different ecological niches for angiosperms and conifers existed within the glacial outwash plain (i.e. a mosaic of poorly- and well-drained soils; Ashworth and Cantrill, 2004), which could have had variable preservation potential relative to biomarker and macrofossil degradation.

It is difficult to distinguish between these three hypotheses. The palynomorph record may discount the first hypothesis: Askin and Markgraf (1986) suggested that some of the *Nothofagus* (angiosperm) pollen identified at Oliver Bluffs was reworked older Cenozoic palynomorphs (counter to explanation 1 above), although all pollen was deemed to be contemporaneous during later examinations (Ashworth and Cantrill, 2004). However, other biomarker classes indicate very low levels of reworking (e.g. very high abundances of fatty acids), suggesting that this hypothesis is unlikely. The lack of gymnosperm macrofossils and low abundances of *Podocarpidites* sp. pollen support the second explanation and may undermine the third. Podocarpaceae occupy a broad ecological range, generally preferring wet conditions (Veblen et al., 1995) but can survive in extreme environments including droughts, cold, and nutrient-poor soils (Coomes and Bellingham, 2011). In modern polar latitudes, deciduous shrubby plants are restricted to the most sheltered habitats, while evergreen plants can be found in much more exposed locations (Bliss and Matveyeva, 1992). Given this highly tolerant nature, it is difficult to understand why *Podocarpidites* sp. pollen should be substantially less abundant than angiosperm pollen if the two were coexistent at the same site. Hence we would favour the explanation that a Podocarpaceae-dominated vegetation existed in an upland site some distance from the Oliver Bluffs deposits, which could conceivably provide a mechanism for the preferential degradation of conifer biomarkers, as well as a lack of conifer macrofossils and a lower abundance of conifer pollen.

### 2.4.2 Temperature reconstruction from bacterial biomarkers

Using the br-GDGT based proxy MBT'/CBT paleothermometer, our results suggest a mean annual air temperature (MAAT) for the strata at Oliver Bluffs ranging between 3 and 12 °C, with a mean of 5 °C (Fig. 2.5). As the majority of the samples analysed (11 of the 15 soils) showed temperatures on the range of 3 - 5 °C, we speculate that this is the range of temperatures that mainly characterized the time period. The large calibration errors for this proxy mean that absolute temperature calculations must be interpreted cautiously (Peterse et al., 2012). However, our results are consistent with other temperature reconstructions from the Oliver Bluffs succession, giving summer temperatures of 5 °C based on tree ring analysis (Francis and Hill, 1996), fossil weevils (Ashworth and Kuschel, 2003) and freshwater molluscs (Ashworth and Preece, 2003) and MAAT of ~-12 °C based on palaeosol analysis (Retallack et al., 2001). A further constraint on the application of this proxy to high latitude soils could be the decoupling of air and soil temperatures by winter soil (Cline, 1997), which could result in reconstructed soil temperatures that differ markedly from the MAAT. Nevertheless, br-GDGT temperature calculations in modern high latitude soils closely match measured MAAT distributions (Peterse et al., 2009), supporting our absolute temperature reconstruction.

The palaeolatitude of Oliver Bluffs was highly likely to have been very similar to its latitude today (Lawver and Gahagan, 2003), which implies that during winter months, (a) the polar light regime would have caused surface temperatures to drop well below freezing, and (b) soil water availability would have been severely limited. Temperatures during these months would have dropped to -20 °C or lower, meaning that vegetation would have remained dormant for much of the year and soil bacterial activity would decrease although it continues under the snow (Männistö et al., 2012). We envisage that temperatures warm enough to induce snowmelt would have been reached in summer, allowing vegetation to flourish and soil bacteria activity to increase. Today, plant root and shoot growth in Antarctic and the Arctic can occur at low temperatures (0 - 5 °C; Billings et al., 1977) and plants are adapted to a rapid burst of growth following

snowmelt. Since br-GDGTs are membrane lipids produced by an unknown group of soil bacteria, likely Acidobacteria (Sinninghe Damsté et al., 2011, Weijers et al., 2007), it is possible that br-GDGT producing bacteria at Oliver Bluffs had a preferential summer growing season during the late Neogene. No seasonal pattern has been found in br-GDGT distributions at modern mid-latitudes (Weijers et al., 2011). However, at high latitudes, the MBT/CBT temperature reconstructions from a core containing br-GDGTs originating from coastal soils of the Wilkes Land sector of Antarctica showed a bias towards summer temperatures for the Early and Mid Eocene (Pross et al., 2012). Similarly, MBT/CBT based reconstructions for the Arctic during the Early Eocene are in good agreement with warmest month temperature reconstructions based on oxygen isotopes from biogenic phosphates of co-occurring terrestrial vertebrates (Weijers et al., 2007, Eberle et al., 2010). Based on the above, we suggest that the temperature calculations yielded by this study reflect a strong summer-seasonal or even warm monthly bias, meaning that MAAT over Antarctica were much cooler than 5 °C. Indeed, the vegetation reconstruction from this study supports this idea as it shows, consistent with the macrofossil record, a tundra shrub flora similar to those growing in present day cold high latitude environments.

## 2.5 Conclusions

This initial biogeochemical study of the Sirius Group at Oliver Bluffs shows new climatic and flora results, and the potential for further, more detailed study. Calculated temperatures are consistent with those reported from other temperature proxies recovered from the same site. Specifically, Antarctic summer surface air temperatures reconstructed using the MBT'/CBT proxy were around 5 °C, which is significantly higher than present day. This result is consistent with multiple temperature reconstructions from the same site, and is consistent with longer-term temperature records throughout the Neogene which suggest that continental summer temperatures ranged between 4 and 12 °C (Prebble et al., 2006, Warny et al., 2009). The bacterially-derived temperatures suggest that during the mid- to late-Neogene, Antarctica was perhaps

10 °C warmer than today in the summer. This would have been a cold, periglacial environment, which is supported by the sedimentology and flora at Oliver Bluffs (Ashworth and Cantrill, 2004, Retallack et al., 2001). The climate would have been strongly seasonal, where the onset of summer melt would have had a significant impact on the biological and hydrological regime of the outwash plain.

The aliphatic lipid record indicates a low diversity vegetation consisting of mosses, angiosperms and microalgal mats existing in a periglacial environment. The presence of aromatised diterpenoids provides the first geochemical evidence for the presence of conifers at or near this site, probably Podocarpaceae. These results contrast with the macrofossil record, which suggests that angiosperms were the only vascular higher plants present at the time, but support the palynomorph record from the same site (Askin and Raine, 2000). If the deposits at Oliver Bluffs are Miocene in age, then this result is consistent with marine cores from the Ross Sea (Warny et al., 2009); if they are Pliocene then this is a significant finding, indicating that the floral record of Antarctica is far from complete. Regardless, our data highlights the complexities of Antarctic biosphere dynamics. Additionally, this result emphasises the importance of using a multi-proxy approach when reconstructing vegetation because of taphonomic and transport biases in both the fossil and molecular record, and supports the use of chemotaxonomy as a complementary tool to palynology and palaeobotany.

## 2.6 Supplementary Information 1

**Table 2.3:** Summary of organic proxy data

Sample	% TOC	pH from CBT	MAAT <sub>a</sub> / °C	Depositional group
OBFH-02-1	2.5	6.1	7.4	3
BNLB-12-3	3.1	6.7	6.3	3
OBFL-04-3	2.8	6.2	3.9	2
WSU-13-6	1.9	5.5	12.8	1
LCBA-05-36	3.3			3
LCBA-05-5	0.9			1
LCBA-05-17	2.4	6.8	3.5	2
OBFL-04-2	2.8	5.6	3.1	2
SRB-07-6	2.2	7.3	4.1	1
OBFL-04-14	1.8	7.1	6.0	
OBFL-04-20	3.3			3
SRB-07-5	5.3	6.5	4.4	3
OBFL-4-23	2.0	7.1	4.6	1
OBFL-04-29	3.4	6.9	3.3	1
OBFL-04-32	2.2	7.3	4.0	1
OBFL-04-25			3.6	1
SPBW-09-27			4.2	1
OBFL-04-13			4.7	1

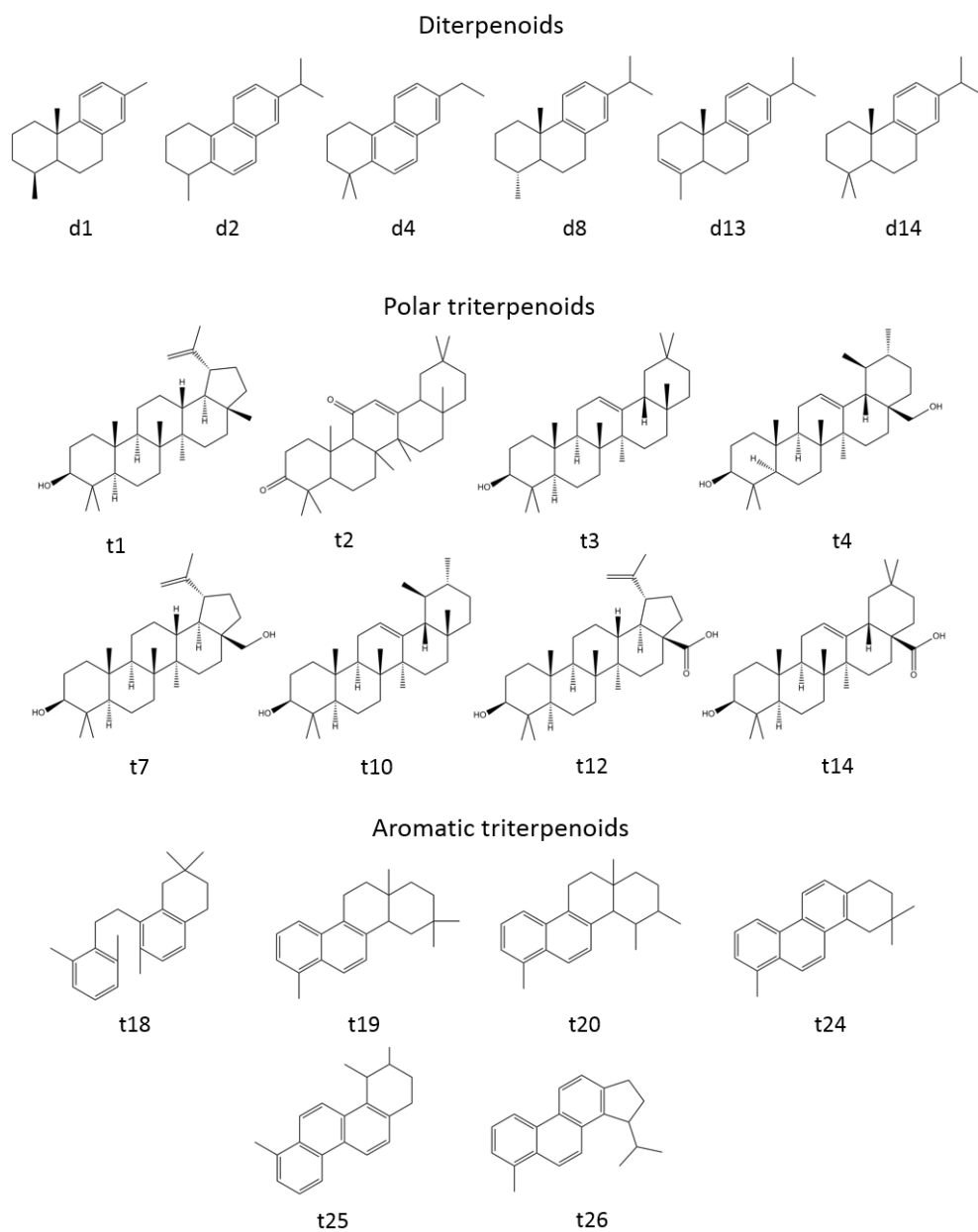


**Figure 2.6:** Structures of the terpenoid compounds identified in sediments at Oliver Bluffs.

## Chapter 3

# Climatic signals recorded in carbon and oxygen isotopes of fossil southern beech trees from Antarctica

### Preface

Chapter 3 has been prepared for submission to *Earth and Planetary Science Letters*. The co-authors are my supervisors and external collaborators: Rob Newton, Ruza Ivanovic, Jane Francis, James Riding, and Alina Marca. The work presented in this chapter is my own, including the background research, experiment design, set-up and execution, data analysis and presentation, and the written manuscript. My co-authors gave valuable advice and suggested improvements for all aspects of the work. Rob Newton gave technical support for the work carried out; in particular, with the isotopic measurements of tree ring cellulose. Alina Marca provided isotopic measurement of all waters.

## Abstract

Carbon and oxygen isotopes in tree rings are widely used to reconstruct palaeoclimate variables such as temperature during the Holocene (12 thousand years ago - present), and are used increasingly in deeper time. However, they also have excellent potential as archives of environmental isotopic signals such as the isotopic composition of precipitation and atmospheric CO<sub>2</sub>, which are much harder to reconstruct but can provide valuable information about hydrological and carbon cycling. Here we focus on a late Neogene (17 - 2.5 Ma) glacial deposit from the Transantarctic Mountains, Antarctica, from a period of significant ice sheet retreat. The deposits are characterised by a remarkable fossil floral assemblage, among which are a suite of exceptionally preserved southern beech twigs (*Nothofagus beardmorensis*), representative of a prostrate tundra shrub. Using cellulose- $\delta^{18}\text{O}$  in the fossil wood, we are able to reconstruct precipitation oxygen isotopes over the Antarctic interior and cellulose- $\delta^{13}\text{C}$  to reconstruct the isotopic signature of atmospheric CO<sub>2</sub> for the first time for this time period. This approach is calibrated by analysing tree ring isotopes in modern analogue *Nothofagus* in Chile at the southern limit of their current range. The results show that  $\delta^{18}\text{O}_{precip}$  over Antarctica was  $-16.0 \pm 4.2 \text{‰}$  (12 ‰ enriched relative to today), suggesting changes in the hydrological cycle linked to warmer temperatures. Atmospheric  $\delta^{13}\text{C}$  was  $-4.5 \pm 1.5 \text{‰}$ , which is significantly heavier than present day atmospheric  $\delta^{13}\text{C}$  and indicates substantial (possibly short-lived) changes to the carbon cycle through organic carbon sequestration.

## 3.1 Introduction

Tree ring stable isotope analysis is a powerful and widely-used tool for palaeoclimatic reconstructions, providing rare insights into terrestrial palaeoclimate at annual and seasonal resolution (McCarroll and Loader, 2004). The variables controlling the oxygen isotope composition of tree-ring cellulose are well understood and have been successfully described by numerical models based on plant physiology and its response to the envi-

ronment (eg. Roden and Ehleringer, 2000, Farquhar and Gan, 2003). Cellulose-oxygen isotopes are primarily governed by a combination of tightly-constrained biological fractionation factors, source water isotope composition and relative humidity (McCarroll and Loader, 2004). They are expressed as  $\delta^{18}\text{O}$ ; where delta notation is the conventional notation used for the ratio of isotopes (e.g.  $^{18}\text{O}/^{16}\text{O}$ ) in a sample ( $R$ ) relative to a standard ( $R_{std}$ ) such that  $\delta = (R/(R_{std} - 1)1000)$ , reported in per mil (‰). For oxygen isotopes, results are reported with respect to Vienna Standard Mean Ocean Water (VSMOW;  $R_{std} = 2.005 \times 10^{-3}$ ). Tree-ring cellulose  $\delta^{18}\text{O}$  ( $\delta^{18}\text{O}_{cell}$ ) is therefore an effective proxy for reconstructing global and regional hydrological change, for example, changes in basinal water regimes (Brienen et al., 2012) and atmospheric circulation (Zhu et al., 2012). Carbon isotopes in tree-ring cellulose (expressed as  $\delta^{13}\text{C}_{cell}$ , reported relative to the Vienna Pee Dee Belemnite standard) also have utility as a palaeoclimatic proxy. In general,  $\delta^{13}\text{C}_{cell}$  is largely controlled by the interplay between stomatal conductance and photosynthetic rate. With increased aridity or decreased precipitation, in order to conserve water, a plant will decrease stomatal conductance, which reduces the ratio of intracellular  $\text{CO}_2$  to atmospheric  $\text{CO}_2$  ( $c_i/c_a$ ), decreasing  $^{13}\text{C}$  discrimination and enriching  $\delta^{13}\text{C}_{cell}$  (Farquhar et al., 1982).

Both carbon and oxygen tree ring isotopes are increasingly being applied to older time periods (up to 53 Ma; Jahren and Sternberg, 2003, Schubert et al., 2012, Wolfe et al., 2012) as more fossil plants with adequate preservation are being recovered. One particular advantage of this growing dataset is the ability of tree ring isotopes to reconstruct climatic parameters that are much harder to access through marine sediments. These include environmental geochemical signals like precipitation isotopes (Ballantyne et al., 2006, Jahren and Sternberg, 2008, Jahren et al., 2009) and atmospheric carbon isotopes ( $\delta^{13}\text{C}_{atmos}$ ; Arens et al., 2000, Jahren et al., 2001). A notable example is the rich treasure trove of exceptionally well-preserved Eocene and Pliocene fossil wood from multiple kimberlite deposits in the Canadian High Arctic. These fossil recoveries have revealed unique details about Eocene and Pliocene palaeoclimate and hydrological cycling through their stable isotope records, such as reconstructing terrestrial temperatures and the isotopic composition of precipitation as well as providing insights into high

latitude climate variability (Ballantyne et al., 2006, 2010, Csank et al., 2011, Jähren and Sternberg, 2008, Jähren et al., 2009, Wolfe et al., 2012).

An exceptionally well-preserved suite of fossil wood of southern beech (*Nothofagus beardmorensis*) have been recovered from the Neogene Sirius Group deposits at the Oliver Bluffs in the Transantarctic Mountains, Antarctica (85° 07' S, 166° 35' E; Webb and Harwood, 1993, Hill et al., 1996, Francis and Hill, 1996), deposited at a similar latitude to today (Lawver and Gahagan, 2003). The fossil trees were deciduous and represent a tundra-like shrub. The plants likely had a prostrate life-habit, where stems grow horizontally to avoid freezing winds, similar to the extant *Salix arctica* in the High Arctic (Francis and Hill, 1996). Based on both geochemical (Rees-Owen et al., a; Chapter 2) and macrofossil-derived (Francis and Hill, 1996, Ashworth and Cantrill, 2004) palaeothermometers, continental summer temperatures were  $\sim 5$  °C, implying a weakened latitudinal temperature gradient compared to the present day, where the mean temperature December is -3.4 °C (McMurdo Station; 77° 51' S, 166° 40' E). Shallower gradients are supported by vegetation and marine proxy-based reconstructions, indicating, for example, a reduction of  $\sim 5.5$  °C in the meridional temperature gradient during the early Pliocene relative to today (Brierley et al., 2009, Pound et al., 2012).

The age of these sediments has been the subject of a protracted debate. The plant fossils have been biostratigraphically dated by close association with late Pliocene marine diatoms (Harwood, 1986, Webb et al., 1984), thought to indicate the incursion of seaways deep into the Antarctic interior. This relatively young age has been challenged by multiple studies that suggest the diatoms represent wind-blown contamination from the open ocean much further away (Burckle and Potter, 1996, Stroeve et al., 1996). Additionally, cosmogenic exposure dating suggests these sediments are much older (at least 5 Ma, but possibly as old as 17 Ma; Ackert, Jr. and Kurz, 2004); further details of this ongoing debate may be found in Barrett (2013).

Regardless of the age, the fossiliferous bed clearly represents a period of significant East Antarctic Ice Sheet (EAIS) retreat in response to warming temperatures (Francis and Hill, 1996, Mercer, 1986). Evidence for a periodically reduced ice sheet exists for

the mid-Miocene (17 - 15 Ma; Gasson et al., 2016, Griener et al., 2015, Levy et al., 2016, Warny et al., 2009), and increasingly both modelling (Austermann et al., 2015, Dolan et al., 2011, Pollard et al., 2015, Pollard and Deconto, 2016) and data (Cook et al., 2013) studies also suggest that at least partial EAIS retreat occurred during the Pliocene, driven by warmer sea surface temperatures (Pollard et al., 2015).

The objective of this study is to reconstruct  $\delta^{13}\text{C}_{atmos}$  and  $\delta^{18}\text{O}_{precip}$  during this brief period of warmth and EAIS retreat by measuring the carbon and oxygen isotopic composition of fossil plants from Oliver Bluffs. We use a simple process-based isotope model to calculate precipitation isotopes from fossil plants (Anderson et al., 2002) and apply an empirical transfer function to reconstruct  $\delta^{13}\text{C}_{atmos}$  (Arens et al., 2000). Although prostrate trees are beginning to be used in modern dendrochronological studies (e.g. Buras and Wilmking, 2014), no studies using tree ring isotopes in prostrate plants exist. We therefore examine the use of high latitude prostrate fossil trees for climatic reconstructions using modern analogue plants from Isla Navarino, Chile, where two extant deciduous *Nothofagus* species grow in both arborescent and prostrate form in a subpolar forest environment.

## 3.2 Materials and methods

### 3.2.1 Oliver Bluffs; fossil site

The fossil wood was sampled from a sedimentary succession at Oliver Bluffs in the Dominion Range of the Transantarctic Mountains (85° 07' S, 166° 35' E), which forms part of the Sirius Group sediments (Fig. 3.1). The fossil plant material occurs within one main bedding horizon in the central part of the exposure at Oliver Bluffs, on the eastern side of the upper valley of the Beardmore Glacier. The present elevation is approximately 1760 m above sea level, but deposition likely occurred at a much lower altitude (Webb and Harwood, 1993, Ackert, Jr. and Kurz, 2004). The sedimentary sequence consists of glacial diamictites, and are thought to be lodgement tills deposited by the ancestral Beardmore Glacier during glacial advance and retreat (McKelvey et al.,

1991). The fossiliferous bed containing fossil wood and leaves comprises poorly-sorted sandstones with silt lenses, representing an outwash deposit, in places burying poorly-developed glacial soils on a braided outwash plain (Ashworth and Cantrill, 2004). We envisage sporadic accretion of sediment over the plain, such that the fossiliferous bed is spatially heterogeneous, but as a whole is representative of a significant portion of the ice sheet retreat event.

The fossil wood fragments were first described as *Nothofagus* (Carlquist, 1987) and later identified as *Nothofagus beardmorensis* (Hill et al., 1996). Leaf remains and tree ring analyses suggest that these were deciduous prostrate shrubs, very similar to the *krummholz* *N. pumilio* and *N. antarctica*, which grow at the treeline in Tierra del Fuego, Chile (Francis and Hill, 1996). Due to the small ring size ( $<100 \mu\text{m}$ ), fossil wood fragments were sampled for isotope analysis in bulk or by pooling multiple rings together to give a decadal-resolution record.

### 3.2.2 Isla Navarino; modern analogue site

Isla Navarino ( $55^{\circ} 56' \text{ S}$ ,  $67^{\circ} 37' \text{ W}$ ; Fig. 3.1) is part of the Magellanic subpolar forests ecoregion which stretches west of the Andes down to Tierra del Fuego, Chile. The island has a maritime climate, with mean annual temperatures of  $6^{\circ}\text{C}$ , average summer highs of  $10^{\circ}\text{C}$  and winter averages of  $2^{\circ}\text{C}$ . Cool windy conditions prevail year round; Mean Annual Precipitation (MAP) is 400-500 mm, which is uniformly distributed throughout the year. The island vegetation is characterised by Magellanic forest dominated by *Nothofagus* trees to the north, and Magellanic moorland to the south.

Wood cores and rounds from branches (for prostrate trees) from 31 living trees were collected at five sites on Isla Navarino during the austral summer of 2013. Three species of *Nothofagus* trees grow on the island, one evergreen species (*N. betuloides*) and two deciduous species (*N. antarctica* and *N. pumilio*). Because the fossil plants from the Sirius Group sediments are deciduous (Hill et al., 1996), cores were taken from two deciduous *Nothofagus* species over an altitude transect from near sea-level to the treeline ( $\sim 600 \text{ m}$ ) at 5 sites (Table 3.1; Fig. 3.1). Over the transect, *Nothofagus*

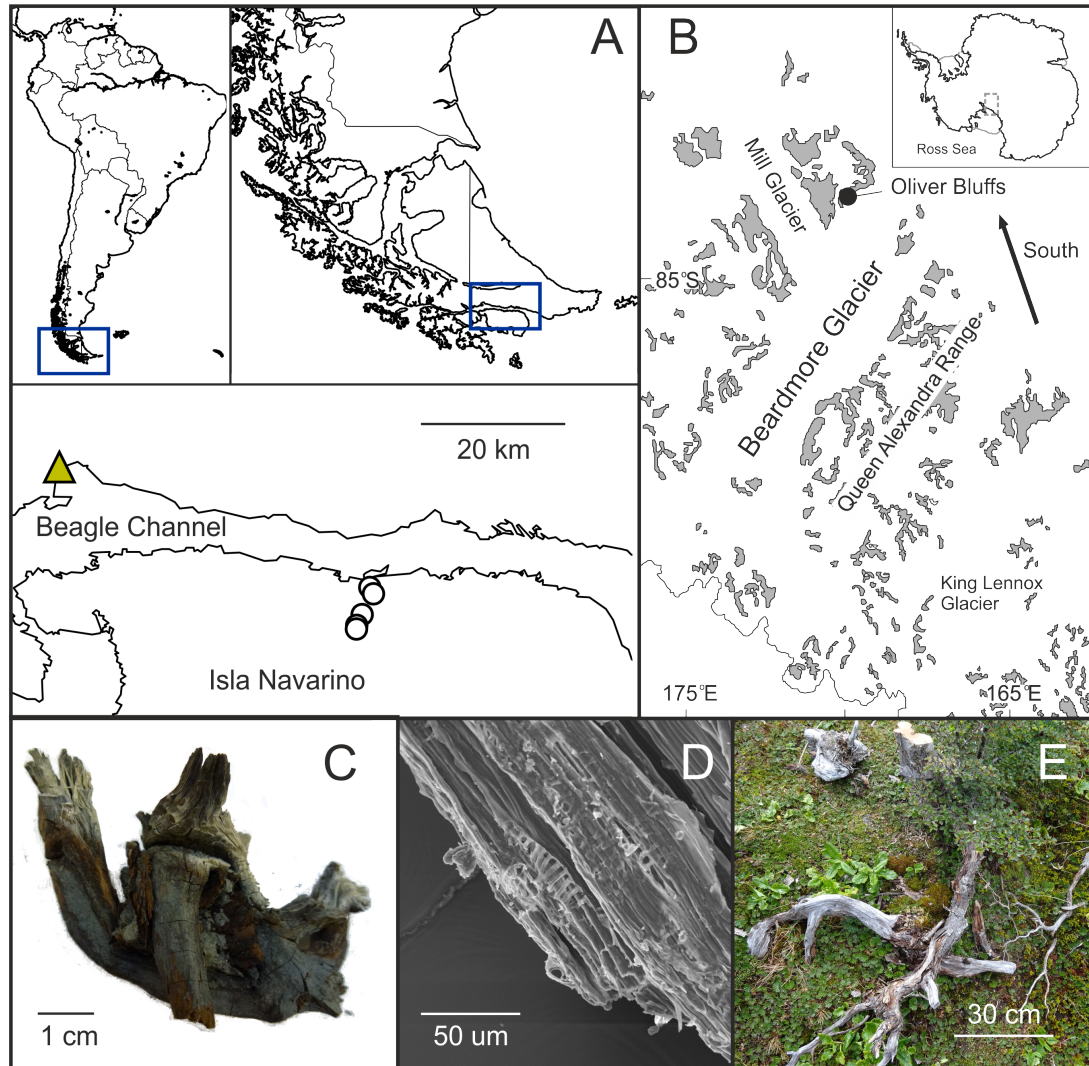


**Figure 3.1:** (A) Location of sampling sites on Isla Navarino in Tierra del Fuego, Chile. Yellow triangle = marks the location of the GNP station at Ushuaia; open circles = mark the tree ring sampling sites. (B) Fossil wood location at Oliver Bluffs (black filled circle), Transantarctic Mountains, Antarctica. White represents ice; grey shapes are Transantarctic Mountain outcrops. (C) Photograph of exceptionally preserved fossil *Nothofagus* from Oliver Bluffs. (D) Scanning Electron Microscope image of fossil *Nothofagus*, demonstrating excellent preservation of wood fibres. (E) Prostrate *Nothofagus antarctica* from Isla Navarino.

ranged in habit from arborescent (single stem and generally greater than 4 m in height) to *krummholz* form (i.e. prostrate, with a small trunk or stem and multiple branches lying horizontally upon the ground). Species were identified by leaf character (Moore, 1983) and sampled during the height of austral summer 2013 (January), when the trees were in full leaf. Arborescent trees were cored at chest height (~130 cm above the ground) using an increment wood corer with a diameter of 5 mm. Prostrate individuals were sampled from primary branches in order to match sampling from the fossil trees.

The core samples were dated to the calendar year of their formation and cross-dated using the techniques described in Stokes and Smiley (1968). As the austral growing season overlaps two calendar years, rings were assigned to the year when ring growth began (i.e. the last complete ring taken for each core in January 2013 was dated to austral summer 2011, as the 2012-2013 ring was still incomplete at the time of sampling).

The cores were air-dried, stored in plastic straws and a 30 year sequence was isolated for isotopic analysis. Tree rings are composed of earlywood and latewood; the former comprises large thin-walled cells made of stored photosynthates from the previous year and the latter comprises thicker-walled cells formed during summer. Therefore to sample at true annual resolution, it has been suggested that only latewood should be taken (Switsur et al., 1995). However, the rings in the prostrate plants in this study were too small to obtain sufficient latewood, so the entire ring was sampled each time; this approach has been used successfully to reconstruct hydrological change in the same region (Lavergne et al., 2016).

Soil and root samples were also collected, along with water from a stream network covering the altitude transect in order to estimate source water  $\delta^{18}\text{O}$ . Soils were sampled from 50 cm depth (where 90% of *Nothofagus* forest root mass is situated; Schulze et al., 1996), wrapped in cling film, stored in multiple airtight bags and frozen until required for water extraction. Source water samples were taken from fast-flowing streams, filtered (0.2  $\mu\text{m}$ ) and stored in McCartney vials. We also used temperature, precipitation and precipitation  $\delta^{18}\text{O}$  data from the nearby Global Network of Isotopes

in Precipitation (GNIP) station at Ushaia, Argentina (54° 46' 48" S; 68° 16' 48" W), approximately 50 km away.

### 3.2.3 Sample preparation and isotopic analysis

Except where otherwise indicated, the following procedures were all carried out in the University of Leeds Cohen Geochemistry laboratories, 2013 - 2016.

#### 3.2.3.1 Sample preservation

Exceptional preservation of the fossil *Nothofagus* utilised in this study is well documented (Francis and Hill 1996), and is supported by scanning electron microscope imaging (Fig 3.1D), which shows excellent retention of wood fibres. Although it is clear that some degradation of vessels has occurred, this should not impact the isotopic signal of the remaining cellulose; cellulose extracted from fossil trees significantly older than those used in this study (up to 53 Ma; Hook et al., 2014, 2015, Staccioli et al., 2014, Wolfe et al., 2012), was extracted in low yield (<5%; Hook et al., 2015), indicating a high degree of cellulose degradation, but showed no signs of isotopic alteration. Mineral contaminants in the form of microcrystalline calcite were detected in the Sirius Group fossil trees using energy dispersive X-ray spectroscopy, which could affect both  $\delta^{18}\text{O}$  and  $\delta^{13}\text{C}$ , but the delignification step during extraction is performed below pH 5, which removed all calcite (not shown). After extraction, cellulose was recovered as a white fluffy material (5 - 30% yield), which is a clear indication that cellulose is well-preserved and hence the fossil material is appropriate for isotope analysis.

#### 3.2.3.2 Cellulose isotope measurements

Cellulose was extracted from both modern and fossil samples using batch extraction equipment described by Wieloch et al. (2011). To summarise, ground wood samples were heated in aqueous NaOH solution (5%, 2 hours, 60 °C, repeated twice) to remove tannins, resins and fatty acids. Samples were then heated (60 °C) in acidified NaClO<sub>2</sub> (via glacial acetic acid; 7.5%, pH 4-5) for 10 hours; this step was repeated four times

to ensure complete delignification. Finally, we used a solution of NaOH (17%; 60 °C, 2 hours) to remove hemicelluloses, leaving  $\alpha$ -cellulose for analysis. Cellulose samples were homogenised using a Retsch MM301 Mixer Mill, then freeze-dried for 24 hours to remove ambient water. Samples were stored in Eppendorf vials and kept in a desiccator for >24 hours prior to isotope analysis.

In order to measure  $\delta^{18}\text{O}_{cell}$ , the milled, freeze-dried cellulose samples were weighed, packed into silver capsules and pyrolysed at 1450 °C. Oxygen isotope ratios were measured using an elemental analyser with a purge and trap column (Elementar vario PYROcube), coupled to an Isoprime isotope ratio-mass spectrometer. Ratios of  $^{18}\text{O}/^{16}\text{O}$  were converted to  $\delta^{18}\text{O}$  VSMOW with a one point linear calibration using IAEA-601 (benzoic acid;  $\delta^{18}\text{O} = +23.15 \pm 0.3\text{‰}$ ) with reference to cellulose from Sigma-Aldrich, UK (Lot#SLBD2972V; hereafter Leeds Sigma cellulose). The Leeds Sigma cellulose was analysed at the University of Leeds against IAEA-CH-3 cellulose (assuming  $\delta^{18}\text{O} = +31.9 \pm 0.5\text{‰}$ ; Hunsinger et al., 2010) and assigned a value of  $29.2 \pm 0.2\text{‰}$ . Standards were included at an interval of every twelve samples. Within-run reproducibility of an internal check standard was  $\pm 0.37 \text{‰}$ . For  $\delta^{13}\text{C}$  analysis, extracted cellulose samples were weighed and packed into tin capsules. Carbon isotope ratios were measured using an Elementar PyroCube elemental analyser coupled to an Isoprime mass spectrometer. The encapsulated samples were combusted at 1150 °C in pure oxygen. Ratios of  $^{13}\text{C}/^{12}\text{C}$  were calibrated to the international VPDB scale using in-house urea and C4 sucrose. These were assigned values of  $46.83 \pm 0.22\text{‰}$  and  $11.93 \pm 0.24\text{‰}$ , respectively after calibration using six replicates of each of the following international standards: IAEA-LSVEC ( $-46.479\text{‰}$ ), IAEA-CH7 ( $-31.83\text{‰}$ ), IAEA-CH6 ( $-10.45\text{‰}$ ) and IAEA-CO1 ( $+2.48\text{‰}$ ). The precision obtained for repeat analysis was better than  $\pm 0.2\text{‰}$  ( $\sigma$ ).

### 3.2.3.3 Water isotope measurements

Water was extracted from roots and soils by cryogenic vacuum distillation, following the procedure detailed by West et al. (2006). Extracted samples, along with stream

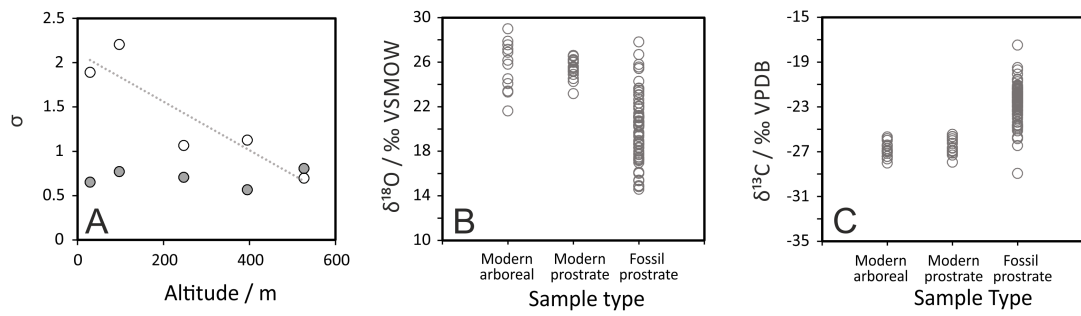


**Figure 3.2:** (A) Standard deviation of  $\delta^{13}\text{C}_{cell}$  (closed circles) and  $\delta^{18}\text{O}_{cell}$  (open circles) with altitude for *Nothofagus* from Isla Navarino, demonstrating a decrease in variability for  $\delta^{18}\text{O}_{cell}$  for prostrate trees. Dotted line is a linear trendline for the oxygen data. (B) Mean  $\delta^{18}\text{O}_{cell}$  data for modern *Nothofagus* separated into arboreal and prostrate form, and fossil *Nothofagus*. (C) As panel (B) but for  $\delta^{13}\text{C}_{cell}$ .

waters, were stored frozen until they were measured for water isotope ratios at the School of Environmental Sciences, University of East Anglia, UK. The  $^{18}\text{O}/^{16}\text{O}$  ratios were analysed using a Picarro L1102-i cavity ring-down spectroscopy analyser with a CTC Analytics autosampler. Measurements were calibrated by the application of linear regression of the analyses of IAEA calibration material (VSMOW, VSLAP and GISP). For each sample, 6 replicate injections were performed. The reproducibility of replicates was better than  $\pm 0.2$  ‰.

### 3.3 Results and discussion

#### 3.3.1 Oxygen and carbon isotope ratios in modern *Nothofagus*

Oxygen and carbon isotope ratios in modern *Nothofagus* trees over a range of morphologies were measured to provide a first order check on the ability of fossil prostrate *Nothofagus* plants to record long-term climate and environmental variables. Mean  $\delta^{18}\text{O}_{cell}$  for all sites over the sample period ranged between 24.1 and 26.9‰. There was no statistically significant difference between the two *Nothofagus* species ( $p > 0.7$ ; Students unpaired  $t$ -test). An enrichment in mean  $\delta^{18}\text{O}_{cell}$  with increasing altitude was expected due to increasing wind stress, which would be consistent with trends seen in global datasets of  $\delta^{18}\text{O}_{cell}$  and  $\delta^{18}\text{O}_{source}$ . However, there is no statistically significant difference between sites for mean  $\delta^{18}\text{O}_{cell}$ , and therefore for altitude and morphology

(i.e. prostrate or arboreal form), indicating that morphology does not impact absolute  $\delta^{18}\text{O}_{cell}$ . While inter-tree variability at all sites is consistent with studies using only arboreal trees ( $\sigma$  range = 0.7 - 2.2; Fig. 3.2), intriguingly, prostrate trees in this study exhibit much lower inter-tree variability than their arborescent counterparts ( $\sigma = 2.1$ ,  $\sigma = 0.8$ , for arboreal and prostrate morphologies, respectively). Prostrate plants are more aerodynamically decoupled from the atmosphere, and retain tight control over their microclimate (Barrera et al., 2000, Korner, 2003), which may reduce inter-tree variability in transpiration. We therefore speculate that the lower variability means that  $\delta^{18}\text{O}_{cell}$  in prostrate plants is a better archive of source water  $\delta^{18}\text{O}$  than in their arboreal counterparts.

Mean  $\delta^{13}\text{C}_{cell}$  for each site ranged between -27.2 and -26.7‰, (grand mean = -26.6  $\pm$  0.7 ‰), which is consistent with typical values for C3 land-plants (O’Leary, 1988). Mean inter-tree variability was low ( $\sigma$  range = 0.6 - 0.8 ‰;) and did not vary with altitude or morphology. In this case,  $\delta^{13}\text{C}_{cell}$  variability may be a function of carbon assimilation rate rather than transpiration (in support of findings by Farquhar et al. (1998) and Scheidegger et al. (2000), for example). Transpirational control would lead to co-varying carbon and oxygen isotope ratios with morphology, which is not seen here.

Generally, tree ring isotope studies are performed at annual resolution and require the construction of statistically representative chronologies between trees. Inter-series coherence at all sites was low for both  $\delta^{13}\text{C}$  and  $\delta^{18}\text{O}$ . An Expressed Population Signal (EPS; Wigley et al., 1984) was calculated for each sites  $\delta^{18}\text{O}$  and  $\delta^{13}\text{C}$  chronologies. This is a measure of how well a chronology constructed from a finite number of trees represents the hypothetical perfect or true chronology; a value of 0.85 is generally considered to be an acceptable confidence level. On the whole, EPS is highly sensitive to the number of trees in the chronology. However in this study, the EPS for each site was low (particularly for  $\delta^{13}\text{C}$ ) and did not improve with increasing sample size (0.43 - 0.69 for  $\delta^{18}\text{O}$ ; series were negatively correlated for  $\delta^{13}\text{C}$ ). This result contrasts with recent work by Lavergne et al. (2016), who found a strong common signal in  $\delta^{18}\text{O}$  series from *Nothofagus pumilio* in Northern Patagonia, and leads us to the conclusion

**Table 3.1:** Summary of sample sites on Isla Navarino with mean site  $\delta^{18}\text{O}_{soil}$ 

Site	Latitude	Longitude	Elevation / m	No. trees	$\delta^{18}\text{O}_{soil}$ / ‰
1	54° 56' 37" S	67° 39' 25" W	29	5	-11.51±0.25
2	54° 57' 04" S	67° 38' 58" W	97	4	-13.07±0.73
3	54° 58' 33" S	67° 40' 22" W	247	5	-10.48±1.17
4	54° 59' 19" S	67° 41' 02" W	395	7	-12.02±1.29
5	54° 59' 35" S	67° 41' 04" W	527	11	-11.96±0.58

that stand-level isotope signals on Isla Navarino may be dominated by tree-level effects due to microclimatic variations. Thus, *krummholz* *Nothofagus* in this region are not appropriate archives for constructing isotope chronologies at annual resolution. However, this does not prevent the plants from being good long-term archives of climate signals; the low inter-tree variability in the prostrate plants in particular suggests they may function well as a record of decadal resolution climate information and we test this hypothesis using a physiological model below. This result is particularly pertinent to the fossil plants in this study, where the tree ring widths are extremely narrow and do not provide sufficient material for analysis at annual resolution; data from the fossil plants is averaged at decadal scale resolution.

### 3.3.2 Source water $\delta^{18}\text{O}$ in modern *Nothofagus*

The isotopic composition of plant source water for the modern *Nothofagus* in this study was constrained by measuring  $\delta^{18}\text{O}$  of soil waters ( $\delta^{18}\text{O}_{soil}$ ; 50 cm; the recorded soil water depth for *Nothofagus*; Schulze et al., 1996) for the five sites, which ranged between  $-13.06 \pm 0.73$  ‰ and  $-10.56 \pm 1.17$  ‰ (1  $\sigma$ ; grand mean =  $-11.91 \pm 0.89$  ‰; Table 3.1). We also analysed  $\delta^{18}\text{O}$  from eight fast flowing streams and lakes across the sampling transect ( $\delta^{18}\text{O}_{stream}$ ), which ranged between -11.13 and -9.78 ‰ (mean =  $-10.78 \pm 0.41$  ‰). The  $\delta^{18}\text{O}$  data presented here only represent one years summer precipitation;  $\delta^{18}\text{O}_{precip}$  data from a nearby GNIP station (Ushuaia, record 1982-2002) were included in order to take into consideration summer and winter seasonal precipitation in this study. Mean summer precipitation was  $-9.9 \pm 0.9$  ‰; mean winter precipitation was  $-11.92 \pm 0.75$  ‰, which is not statistically different from the mean soil water  $\delta^{18}\text{O}$

( $p < 0.001$ ). Root water extracted from *Nothofagus* trees at three sites (mean =  $-10.50 \pm 0.54$  ‰) was isotopically similar to  $\delta^{18}\text{O}_{\text{stream}}$  and  $\delta^{18}\text{O}_{\text{precip}}$ , indicating that plants took up water from an annually integrated precipitation signal. From these observations we infer that plant source water  $\delta^{18}\text{O}$  ( $\delta^{18}\text{O}_{\text{source}}$ ) can be treated as  $\delta^{18}\text{O}_{\text{precip}}$ . There was no significant trend in  $\delta^{18}\text{O}$  of measured waters with altitude, which is most likely because of the small altitude range covered in this study (0-600 m). Sites 2 and 3  $\delta^{18}\text{O}_{\text{soil}}$  are statistically different from each other ( $p < 0.05$ ; one way ANOVA with post-hoc Tukey test) and site 2 is also significantly depleted relative to the stream and root water, suggesting an increased contribution from winter precipitation to soils.

### 3.3.3 Reconstructing ancient precipitation $\delta^{18}\text{O}$ from fossil *Nothofagus*

Mean  $\delta^{18}\text{O}_{\text{cell}}$  for the fossil plants was  $20.3 \pm 3.0$  ‰. The inter-tree variability is similar in magnitude to that seen in modern trees, but is greater than the inter-tree variability seen in the prostrate plants of this study. It seems likely that these data capture both significant temporal variability and climate variability. It is important to note that here, we are treating all fossils as being geologically contemporaneous as they were all collected from the same bed, but it is highly likely that our data may span multiple millennia. Ice sheet fluctuations during both the mid-Miocene and Pliocene occurred at orbital timescales (Greenop et al., 2014, Patterson et al., 2014); therefore the duration represented by the fossils must be less than 100 kyr, but long enough for poorly developed soils to form and woody plants to colonise the area. This is consistent with the larger variability in the fossil data compared to the modern. Mean  $\delta^{18}\text{O}_{\text{cell}}$  for the Sirius Group plant is significantly depleted by  $\sim 5$  ‰ ( $p < 0.001$ ) relative to the mean of the modern *Nothofagus* trees from Isla Navarino ( $25.5 \pm 1.5$  ‰). Broadly, there are two major controls on  $\delta^{18}\text{O}_{\text{cell}}$ , which could cause such an offset: evapotranspiration rates (controlled by relative humidity and stomatal conductance) and  $\delta^{18}\text{O}$  of the plants source water ( $\delta^{18}\text{O}_{\text{source}}$ ; McCarroll and Loader, 2004). From the modern data, plant source water is equal to precipitation  $\delta^{18}\text{O}$  within the uncertainty of precipitation variability (and where  $\delta^{18}\text{O}_{\text{precip}}$  is controlled by latitude, condensation temperature and

precipitation amount; Dansgaard, 1964), but there are additional processes that could modify this signal, including evaporation from soil or plants using groundwater as a moisture source. Depletion could result from a large decrease in stomatal conductance caused by increased Relative Humidity (RH), reducing evapotranspiration from leaves. However, RH on Isla Navarino is already high (65-75% in summer) and it is unlikely that there would have been significant increases in RH for Antarctica when summer temperatures are not predicted to have been much lower (Rees-Owen et al., a; Chapter 2). Alternatively, decreased  $\delta^{18}\text{O}_{cell}$  could be caused by a difference in  $\delta^{18}\text{O}_{precip}$ , which is consistent with the higher palaeolatitude of the fossil plants (85°S for the Sirius Group, 54°S for Isla Navarino). We test this hypothesis with a physiological model linking  $\delta^{18}\text{O}_{cell}$  with  $\delta^{18}\text{O}_{precip}$ .

There are multiple models of varying complexity linking  $\delta^{18}\text{O}_{cell}$ ,  $\delta^{18}\text{O}_{precip}$  and relative humidity and it is not clear whether more complex models provide better predictions than simpler ones. For the purposes of this study, we used a relatively simple model by Anderson et al., (2002) given by eq. 3.1, which was chosen because there are only two unconstrained parameters (RH and the fraction of leaf water not subject to fractionation,  $f$ ). This model has been used in multiple studies to reconstruct past precipitation isotopes (Csank et al., 2011, Hook et al., 2015, Wolfe et al., 2012):

$$\delta^{18}\text{O}_{source} = \delta^{18}\text{O}_{cell} - (1 - f)(1 - RH)(\epsilon_e + \epsilon_k) - \epsilon \quad (3.1)$$

where  $\epsilon$  is the biological fractionation factor associated with the formation of cellulose ( $+27 \pm 3 \text{ ‰}$ ; Sternberg and DeNiro, 1983),  $\epsilon_e$  is the equilibrium liquid-vapour fractionation for water and approximates  $\delta^{18}\text{O}$  of atmospheric vapour (11 ‰; Majoube, 1971) and the subscript *source* denotes source water. The kinetic liquid-vapour fractionation ( $\epsilon_k$ ) is dependent on leaf morphology and boundary layer vapour transport conditions; broad-leaf trees have quasi-laminar boundary layer conditions so  $\epsilon_k = 21 \text{ ‰}$  (Buhay et al., 1996). The parameter  $f$  is the fraction of leaf water not subject to evaporation (Allison et al., 1985), and also includes the isotopic alteration of carbon-bound oxygen via exchange with stem water (Rodén and Ehleringer, 1999).

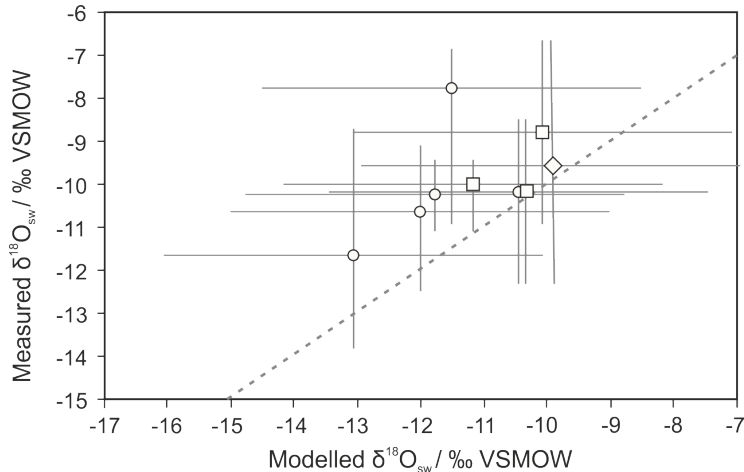


**Figure 3.3:** The relationship between modelled source water  $\delta^{18}\text{O}$  and measured  $\delta^{18}\text{O}_{\text{source}}$  from soils (circles), roots (squares) and Global Network of Isotopes in Precipitation  $\delta^{18}\text{O}_{\text{precip}}$  (summer precipitation; diamond). Modelled source water  $\delta^{18}\text{O}$  was calculated from measured  $\delta^{18}\text{O}_{\text{cell}}$  (modern *Nothofagus*) using the same method as Anderson et al. (2002). Markers give the mean modelled  $\delta^{18}\text{O}$ , y-error bars show the full measured data range, x-errors show fully propagated model errors, and a 1:1 ratio is given by the dotted line for comparison. Modelled data is calculated using  $\text{RH} = 0.7$ ,  $f = 0.2$ .

We tested the assumptions made by Anderson et al. (2002) using measured  $\delta^{18}\text{O}_{\text{cell}}$  from the modern analogue trees as input for the model (with  $\text{RH} = 0.7$ ,  $f = 0.2$  as in Allison et al., 1985) and compared the results against measured  $\delta^{18}\text{O}_{\text{source}}$  (i.e. soil and stream water) and  $\delta^{18}\text{O}_{\text{root}}$  from Isla Navarino and GNIP precipitation data from Ushuaia. The model over-predicted  $\delta^{18}\text{O}_{\text{source}}$  by between 0.2 and 2.9 ‰ (mean for all sites = 1.5 ‰; Fig. 3.3). This could be due to model parametrization; we chose a value of exactly 27 ‰ for the biological fraction factor  $\epsilon$ , but another value within the accepted range of 24 - 30 ‰ could equally be chosen (as in Anderson et al., 2002). Moreover, modelled  $\delta^{18}\text{O}_{\text{source}}$  was not statistically different from  $\delta^{18}\text{O}_{\text{root}}$ ,  $\delta^{18}\text{O}_{\text{stream}}$  or GNIP summer precipitation, indicating that the model works well for predicting  $\delta^{18}\text{O}_{\text{precip}}$  from measured  $\delta^{18}\text{O}_{\text{cell}}$ . We now apply the model to the fossil *Nothofagus* in order to calculate ancient  $\delta^{18}\text{O}_{\text{precip}}$ .

In order to apply the model to fossil *Nothofagus*, we applied a large range of values for RH that are consistent with measurements from high latitude modern analogue sites such as Isla Navarino (0.5 - 0.85) and using a random number generator with uniform distribution, we sampled between these constraints ( $n=1000$ ) to provide an estimate of

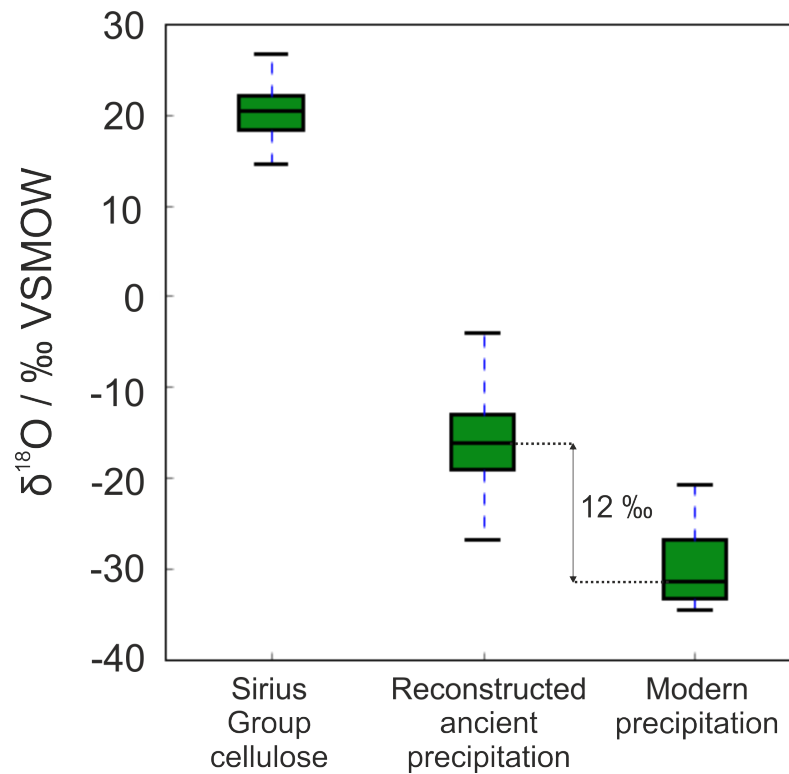


**Figure 3.4:** Cellulose  $\delta^{18}\text{O}$  from the Sirius Group fossil *Nothofagus*, with modelled  $\delta^{18}\text{O}$  of palaeo precipitation and modern Antarctic snow. Modern measurements from Masson-Delmotte et al. (2008); data restricted to  $>75^\circ\text{S}$  and below 700 masl. The median is given by the line, the first and third quartiles by the box, and the whiskers denote the full range of data.

the likely range of  $\delta^{18}\text{O}_{precip}$ . With this approach, we calculate that mean continental Antarctic palaeoprecipitation was  $-16 \pm 4.2 \text{‰}$  ( $1 \sigma$ ; ranging between  $-26$  and  $-3.5 \text{‰}$ ). Since  $\delta^{18}\text{O}_{cell}$  is strongly modified by ambient relative humidity, the large range in our results is consistent with the conservative (i.e. wide) humidity range used in this study.

In the present day,  $\delta^{18}\text{O}_{precip}$  over East Antarctica is highly variable, ranging from  $-55 \text{‰}$  at the highest elevations and furthest from the coast, to  $-25 \text{‰}$  near sea level at lower latitudes ( $<75^\circ\text{S}$ ; Masson-Delmotte et al., 2008). However, there is considerable uncertainty surrounding the palaeoaltitude of the *Nothofagus* fossils sampled in this study (Ackert, Jr. and Kurz, 2004), which makes it difficult to provide context for the reconstructed  $\delta^{18}\text{O}_{precip}$  values. We therefore compared our record to measured Antarctic  $\delta^{18}\text{O}_{precip}$  from sites above  $75^\circ\text{S}$  and less than 700 m above sea level (masl; the height of the timberline on Isla Navarino; Masson-Delmotte et al., 2008), representing a reasonable habitat range. Reconstructed  $\delta^{18}\text{O}_{precip}$  was significantly enriched by  $\sim 12$

‰ relative to modern  $\delta^{18}\text{O}_{precip}$  (ancient mean = -16 ‰, modern mean = -28 ‰;  $p < 0.001$ ; Fig. 3.4). Growth experiments have suggested that plant  $\delta^2\text{H}$  (and therefore by extension,  $\delta^{18}\text{O}$ ) can be significantly enriched in plants grown under continuous light, analogous to the polar light regime (Yang et al., 2009; Supplementary Information 2). Therefore, part of the enrichment in the Sirius Group specimens could be accounted for by the continuous light regime experienced by the Antarctic plants during the growing season, which would increase  $\delta^{18}\text{O}_{cell}$  via continuous transpiration, as opposed to the light regime on Isla Navarino, where plants undergo a diurnal transpiration-respiration cycle. However, the plants used by Yang et al. (2009) have a relatively high transpiration rate because of the relatively warm growing temperatures used in their experimental study. We suggest that the transpiration rate for the Sirius Group plants would likely be much lower because of the cold summer temperatures ( $\sim 5^\circ\text{C}$ , compared to  $\sim 20^\circ\text{C}$  in the environment used by Yang et al., 2009). Furthermore, *Nothofagus* have been documented as having significantly tighter stomatal control of transpiration than co-existing conifers (Fernández et al., 2009), as used by Yang et al. (2009). Therefore it seems likely that there is much lower enrichment due to continuous light in the Sirius Group fossils (see Supplementary Information 2 for further discussion).

Our result has implications for regional and global climate during periods of ice sheet retreat in the Neogene. A significant enrichment in precipitation isotopes implies a considerable change in some of the atmospheric processes of the hydrological cycle. Plausible mechanisms include increased temperatures affecting fractionation during condensation, or changes in rainout patterns due to shifts in source moisture region or different atmospheric circulation patterns leading to a shortened vapour transport pathway. As previously discussed, warmer Antarctic temperatures (relative to today) are consistent with multiple contemporaneous terrestrial temperature proxies, which suggest that summer temperatures reached  $5^\circ\text{C}$  during the period of study (Ashworth and Preece, 2003, Ashworth and Kuschel, 2003, Ashworth and Cantrill, 2004, Rees-Owen et al., a; Chapter 2). This result is also consistent with both age scenarios for the site: during both the mid-Miocene and Pliocene, sea surface temperatures in the Southern Ocean were several degrees warmer than today (Clark et al., 2013, McKay

et al., 2012, Warny et al., 2009) and there is evidence for reduced sea ice cover (Warny et al., 2009, Whitehead et al., 2005). However, previous work by Feakins et al. (2012) suggests that the relationship between temperature and precipitation isotopes earlier in the Miocene (20 - 15 Ma) on the Antarctic coast was different from the modern, driven by increased evaporation from a warmer Southern Ocean. This implies that other factors may also influence the hydrological cycle at this time, which is plausible within the context of a warmer Neogene world, where warmer Southern Ocean temperatures could drive an increase in evaporation from high latitude moisture sources. Equally, the smaller ice sheet could well have influenced regional atmospheric circulation patterns, and changes in global atmospheric circulation are documented for the Pliocene (Brierley et al., 2009). These variables are likely to be important for understanding the full significance of our data, but are unconstrained, and a full exploration of hydrological changes is beyond the scope of this study. These questions could be more fully answered through further data collection to reduce proxy uncertainty, and the use of a coupled ocean-atmosphere climate model to investigate hydrodynamic changes.

### 3.3.4 Reconstructing atmospheric $\delta^{13}\text{C}$ from fossil *Nothofagus*

Mean  $\delta^{13}\text{C}_{cell}$  was  $-22.6 \pm 1.9 \text{‰}$  ( $1 \sigma$ ). The inter-tree variability here is much larger than in either the arboreal or prostrate plants from Isla Navarino ( $-26.6 \pm 0.7 \text{‰}$ ), which again is consistent with the dataset spanning millennial timescales. This range of values is significantly enriched by  $\sim 4 \text{‰}$  ( $p < 0.001$ ) relative to the mean values seen in the modern *Nothofagus* trees (Fig. 3.2).

Scarring on the bark (Francis and Hill, 1996) implies strong winds and paleosol analysis suggests MAP was 120-220 mm (Retallack et al., 2001), which is considerably lower than MAP on Isla Navarino (400-500 mm). Both of these factors would lead to water stress, reducing stomatal conductance and hence enriching  $\delta^{13}\text{C}_{cell}$ . This is consistent with the decrease in  $^{13}\text{C}$  discrimination seen in our fossil plants relative to the modern, although fossil *Nothofagus* leaves associated with the wood fragments are large in size indicating that the plants were not living in a marginal habitat (Hill et al.,

1996) and thus any water stress could not have been too severe.

In studies of modern plants along precipitation gradients, leaf  $\delta^{13}\text{C}$  decreased by less than 1‰ per 200 mm increase in MAP (Gouveia and Freitas, 2009, Stewart et al., 1995). While leaf and cellulose  $\delta^{13}\text{C}$  are not directly comparable, their isotopic compositions are controlled by the same environmental factors. It is therefore unlikely that more than 1‰ of the enrichment in the fossil plants is due to water stress and associated decreases in stomatal conductance and in the ratio of intercellular to atmospheric  $\text{CO}_2$  concentration ( $c_i/c_a$ ). Instead, we infer that the enrichment must be caused by  $\delta^{13}\text{C}$  enrichment of atmospheric  $\text{CO}_2$ .

Similar to oxygen isotopes, this interpretation of our findings could be affected by plant growth under continuous light, which has also been shown to affect  $\delta^{13}\text{C}_{cell}$  (Yang et al., 2009). The 24 hour transpiration cycle results in a higher  $c_i/c_a$  and greater discrimination against  $^{13}\text{C}$ . Thus,  $\delta^{13}\text{C}_{cell}$  decreases by 1 - 4‰ (Jagels and Day, 2004, Smith et al., 1976, Yang et al., 2009). As previously mentioned, transpiration rate is partly determined by temperature and the fossil *Nothofagus* experienced much colder temperatures than the growth experiment conifers (Yang et al., 2009). It is therefore unlikely that growth under the polar light regime significantly affected the carbon isotope data from the fossil plants. Additionally, any continuous light-induced depletion in  $\delta^{13}\text{C}_{cell}$  for the fossil plants would increase the offset between modern and fossil *Nothofagus*  $\delta^{13}\text{C}_{cell}$ , requiring a larger shift in  $\delta^{13}\text{C}_{atmos}$ .

By analysing a large dataset of published plant  $\delta^{13}\text{C}$  measurements, Arens et al. (2000) derived an empirical relationship between  $\delta^{13}\text{C}_{atmos}$  and  $\delta^{13}\text{C}_{plant}$  (eq. 3.2;  $r = 0.95$ ,  $r^2 = 0.91$ ). In order to verify this relationship's predictive ability, we first converted  $\delta^{13}\text{C}_{cell}$  to wholewood  $\delta^{13}\text{C}$  ( $\delta^{13}\text{C}_{ww}$ ) using the relationship in eq. 3.3 (Loader et al., 2003), and then applied the transfer function to  $\delta^{13}\text{C}_{cell}$  from modern *Nothofagus* plants.

$$\delta^{13}\text{C}_{atmos} = \frac{(\delta^{13}\text{C}_{plant} + 18.67)}{1.1} \quad (3.2)$$

$$\delta^{13}C_{ww} = \delta^{13}C_{cell} - 1 \quad (3.3)$$

This analysis yielded means of  $-8.3 \pm 0.2 \text{ ‰}$  from arboreal trees and  $-8.0 \pm 0.2 \text{ ‰}$  for prostrate plants (standard error of the mean; s.e.m;  $n=14$  for both). Mean  $\delta^{13}C_{atmos}$  over the thirty year period sampled in our modern data is  $-7.96 \pm 0.24 \text{ ‰}$  (1 s.e.m; 1982-2012; data from Keeling et al., 2010; and NOAA Earth System Research Laboratory). Both of our reconstructed  $\delta^{13}C_{atmos}$  values are statistically indistinguishable from measured  $\delta^{13}C_{atmos}$  values ( $p>0.37$  for arboreal,  $p>0.9$  for prostrate) indicating that the method successfully predicts  $\delta^{13}C_{atmos}$ , within error. By applying the same method to ancient wood, we calculate that  $\delta^{13}C_{atmos}$  was  $-4.4 \pm 0.1 \text{ ‰}$  (1 s.e.m). There is considerable variability ( $\sigma = 1.2\text{‰}$ ) in our land-plant based  $\delta^{13}C_{atmos}$  results, which again is likely due to integration over multi-millennial timescales.

There are few palaeorecords of  $\delta^{13}C_{atmos}$  with which to compare our results, but the range of our record (between  $-7.9$  and  $-1.6 \text{ ‰}$ ) is greater than that seen in recent records of  $\delta^{13}C_{atmos}$  from Antarctic ice cores over the last glacial-interglacial cycle (between  $-7.0$  and  $-6.2 \text{ ‰}$ ; Eggleston et al., 2016). In contrast, a similarly large range is seen in  $\delta^{13}C_{atmos}$  calculated from land plants using the same method as this study during the Early Cretaceous (between  $-3$  and  $-8 \text{ ‰}$ ; Jahren et al., 2001), thought to have been caused by rapid methane hydrate release, which is unlikely to have influenced carbon cycling during the Neogene.

Our result is also strikingly different from both the pre-industrial  $\delta^{13}C_{atmos}$  value of  $-6.5 \text{ ‰}$  and the modern value of  $-8.0 \text{ ‰}$ , indicating a change in carbon cycling (Eggleston et al., 2016). A record of  $\delta^{13}C_{atmos}$  for the last 65 Ma has been reconstructed from benthic foraminiferal  $\delta^{13}C$  (Tippie et al., 2010), which provides points of comparison for both possible age scenarios for the fossil wood (i.e. 17 - 15 Ma or 3 Ma). Tippie et al. (2010) also produced a record of  $\delta^{13}C_{atmos}$  based on planktonic foraminifera, but because of large uncertainties over several factors influencing planktonic  $\delta^{13}C$  (such as effects of photosymbionts, depth of production and recrystallization after burial), this record was considered by the authors to be much less robust than the benthic record

and is not discussed here.

Reconstructed  $\delta^{13}\text{C}_{atmos}$  from fossil *Nothofagus* is considerably enriched relative to values from the benthic foraminifera record for both possible age scenarios (-6.3 ‰ for the Pliocene, between -5.6 and -5.3 ‰ for the mid-Miocene, see Fig. 3.5; Tipple et al., 2010). The benthic  $\delta^{13}\text{C}_{atmos}$  curve was constructed using a 3 Myr moving average (mean; Tipple et al., 2010), which implicitly smooths out any short-lived variability, and the size of the dissolved inorganic carbon pool in the ocean would serve to dampen the response of carbon isotope ratios in benthic foraminifera to rapid or large atmospheric changes. Decoupling of benthic and atmospheric  $\delta^{13}\text{C}$  on glacial-interglacial timescales during the Pleistocene is seen in both data and model studies (Eggleson et al., 2016, Köhler et al., 2010): certain processes that enrich  $\delta^{13}\text{C}_{atmos}$ , such as increased marine export and decreased ocean stratification, will deplete benthic  $\delta^{13}\text{C}$ , while increased terrestrial carbon storage will enrich both  $\delta^{13}\text{C}$  pools (Köhler et al., 2010). It is not clear whether these mechanisms would have a similar impact on the timescales of the Cenozoic curve, but this does provide a plausible explanation for part of the positive offset between the land-plant and benthic foraminifera reconstructions. Nevertheless, an enrichment on the order of 1-2 ‰ in atmospheric  $\delta^{13}\text{C}$  relative to pre-industrial values implies a significant change in carbon cycling during a period of EAIS retreat; we now discuss potential mechanisms for the two age scenarios.

Warmth in the Pliocene has been well-documented. Sea surface temperatures in the Early Pliocene were  $\sim 5 - 7^\circ\text{C}$  warmer in the mid-latitudes relative to the present, and meridional temperature gradients were considerably weaker (Fedorov et al., 2015). Increased sea surface temperatures would decrease equilibrium fractionation, enriching  $\delta^{13}\text{C}_{atmos}$  somewhat due to solubility effects (Vogel et al., 1970, Zhang et al., 1995, Lourantou et al., 2010). However, dust and iron fertilisation in the Southern Ocean, today a significant driver of primary productivity and therefore changes in  $\delta^{13}\text{C}_{atmos}$ , was much lower during the Pliocene (Martínez-García et al., 2011), which would have reduced export of  $^{13}\text{C}$ -depleted waters to the deep ocean. A strengthening of the Atlantic Meridional Overturning Circulation (AMOC) has been inferred from marine

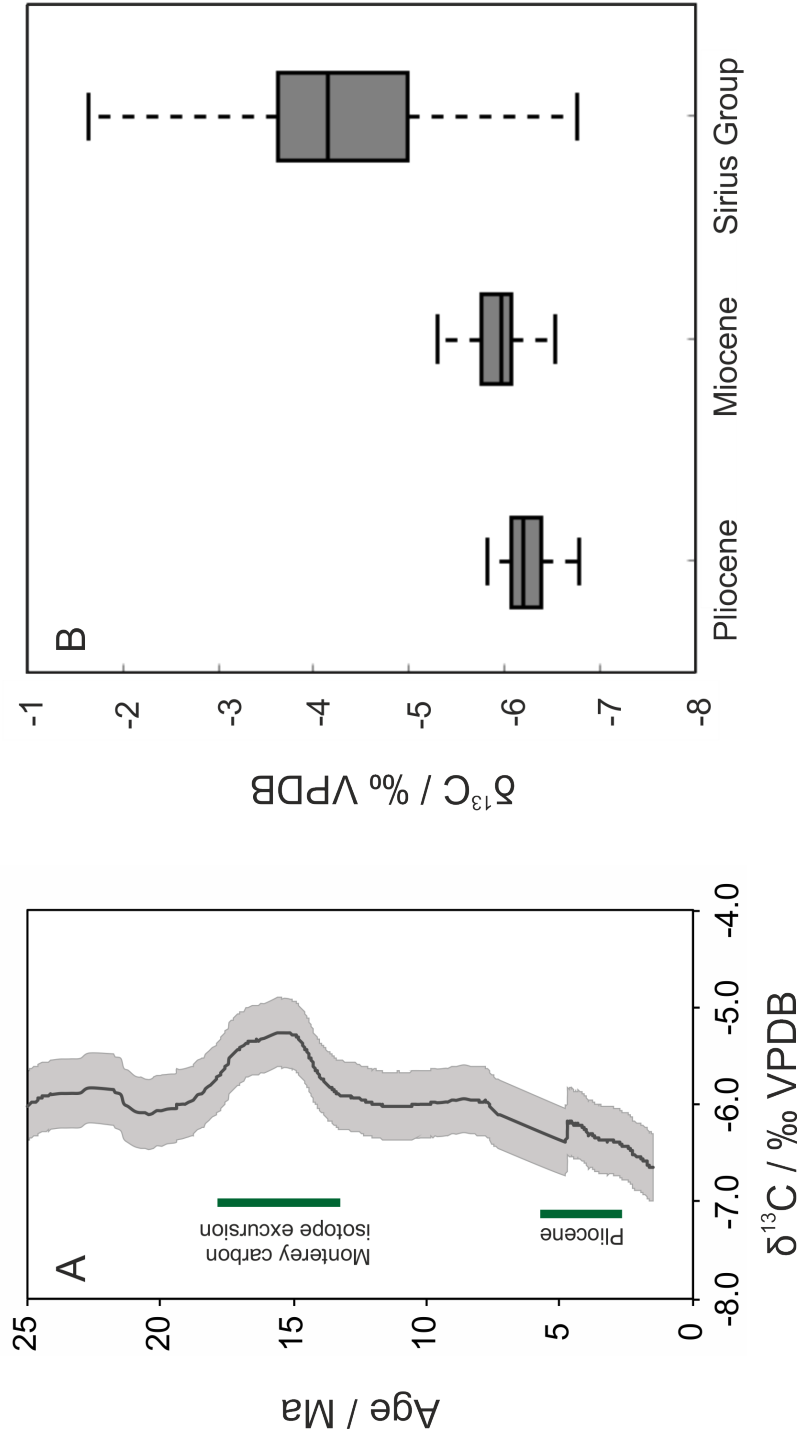


**Figure 3.5:** **A)** Atmospheric  $\delta^{13}\text{C}$  through time based on the benthic  $\delta^{13}\text{C}$  records (Tippie et al., 2010). Dark grey line gives the 3 Ma moving average, and 95% confidence intervals are given by the grey shading. **B)** Reconstructed  $\delta^{13}\text{C}_{\text{atmos}}$  for the Sirius Group, with  $\delta^{13}\text{C}_{\text{atmos}}$  for the mid-Miocene and Pliocene based on benthic  $\delta^{13}\text{C}$  records (Tippie et al., 2010). The median is given by the line, the first and third quartiles by the box, and the whiskers denote the full range of data.

ocean circulation proxy data (Dowsett et al., 2009, Frank et al., 2002, Frenz et al., 2006, McKay et al., 2012, Raymo et al., 1996, Ravelo and Andreasen, 2000), although this is not replicated well in modelling studies (Zhang et al., 2013). It has been proposed that a stronger AMOC would result in greater upwelling of  $^{13}\text{C}$ -depleted deep waters in the Southern Ocean, which would again result in more negative  $\delta^{13}\text{C}_{atmos}$  (Köhler et al., 2010); in general, multiple models have found that, on glacial-interglacial timescales,  $\delta^{13}\text{C}_{atmos}$  is negatively correlated with increasing ocean ventilation (Menviel et al., 2015). Regardless, none of these explanations can explain the high  $\delta^{13}\text{C}_{atmos}$  seen in this record, which implies a significant perturbation in the carbon cycle, such as increased sequestration of organic carbon in the oceans, that is not seen in the global benthic  $\delta^{13}\text{C}$  record for the Pliocene (Zachos et al., 2001). In fact, when put into the context of Cenozoic climate evolution, the benthic  $\delta^{13}\text{C}_{atmos}$  curve records a continuous decrease in  $\delta^{13}\text{C}_{atmos}$  (Tippie et al., 2010), in line with an overall cooling throughout the Pliocene; our result is not consistent with this scenario.

The alternative age scenario for the fossil plants is a mid-Miocene age, correlated with plant fossils from the McMurdo Dry Valleys, which are dated to  $\sim 14$  Ma (Lewis et al., 2007, 2008). At first glance, our carbon isotope data appears to be consistent with carbon isotope data from this time period (benthic foraminifera and bulk carbonate). A mid-Miocene age corresponds to the tail end of a significant perturbation in the carbon cycle between 16.9 and 13.6 Ma (Badger et al., 2013, Holbourn et al., 2007) known as the Monterey Excursion and captured in the  $\delta^{13}\text{C}_{atmos}$  reconstruction by Tippie et al. (2010), although the latter point is somewhat circular as the  $\delta^{13}\text{C}_{atmos}$  record is based on marine  $\delta^{13}\text{C}$ . The event is expressed globally as a broad positive carbon isotope excursion in bulk carbonate, benthic and planktonic foraminiferal records (Vincent and Berger, 1985, Holbourn et al., 2007). Within the broader excursion, there are multiple short-lived positive excursions of between 1 and 1.5 ‰, some lasting as little as 40 kyr (Badger et al., 2013). There are complex links between these maxima and EAIS fluctuations: several of the carbon isotope maxima coincide with periods of low  $\text{CO}_2$  ( $< 300$  ppmv) and Antarctic Ice Sheet maxima, but others correlate with high atmospheric  $\text{CO}_2$  levels and ice sheet minima ( $\geq 500$  ppmv; Holbourn et al., 2014, 2015,

Levy et al., 2016). Broadly, the ice sheet fluctuations are driven by orbital forcing (Griener et al., 2015, Holbourn et al., 2005, Passchier et al., 2013b), but are strongly modulated by changes in atmospheric CO<sub>2</sub> (Gasson et al., 2016, Levy et al., 2016). Our  $\delta^{13}\text{C}_{atmos}$  data represent an anomalously heavy and highly variable atmospheric carbon pool during a period of EAIS retreat, of a magnitude and timescale compatible with middle Miocene carbon cycle dynamics. Multiple mechanisms to explain these carbon maxima have been proposed, though it is not clear to what extent they are driven by changes in the terrestrial or marine carbon cycle (Diester-Haass, 2009). Traditionally, the positive excursions are interpreted as the result of increased organic matter burial in marine settings, leading to a drawdown of atmospheric carbon dioxide (Badger et al., 2013, Flower and Kennett, 1994, Katz et al., 2005, Shevenell et al., 2004, Woodruff and Savin, 1989) and thus an increase in  $\delta^{13}\text{C}_{atmos}$ , although this scenario is not necessarily consistent with a reduced ice sheet. Carbon isotope maxima in the benthic  $\delta^{13}\text{C}$  record coincide with productivity maxima in the Pacific and Southern Ocean, which would increase  $\delta^{13}\text{C}_{atmos}$  (Diester-Haass et al., 2013). Increases in terrestrial carbon sequestration have not been discussed in great detail as a mechanism for the excursions, but a denser vegetation cover than today is modelled globally for the mid-Miocene (Krapp and Jungclauss, 2011) and would also be consistent with our result. In summary, the results from our fossil tree-derived  $\delta^{13}\text{C}_{atmos}$  reconstruction are in good agreement with proposed mechanisms for global carbon cycling during the mid-Miocene, in contrast to those for the Pliocene, and may provide additional constraints on the age of the Sirius Group fossils.

### 3.4 Conclusions

By testing a simple physiological model linking  $\delta^{18}\text{O}_{cell}$  with  $\delta^{18}\text{O}_{precip}$  in two species of modern *Nothofagus* plants, which grow in both arboreal and prostrate form, we found that  $\delta^{18}\text{O}_{cell}$  of prostrate *Nothofagus* faithfully records  $\delta^{18}\text{O}_{precip}$  at multi-year resolution. Hitherto, most tree ring stable isotope analyses have been applied to trees with an arboreal habit in temperate and tropical environments. Therefore, it was pre-

viously unclear whether the assumptions made in process-based isotope models hold true for *krummholz*-type plants, such as those from Oliver Bluffs, which feature growth asymmetry that could affect isotopic signals via resource partitioning. Our findings demonstrate that prostrate trees are potentially suitable archives for recording climatological means over longer periods (on the order of decades). This result opens up high latitude and altitude end-member environments in both palaeo and modern times for tree ring isotope analysis.

The carbon and oxygen isotopic composition of exceptionally well-preserved fossil wood from the Transantarctic Mountains, Antarctica, provide new insights into Neogene hydrological and carbon cycling. The oxygen isotope record indicates that during a period of EAIS ice sheet retreat in which small prostrate shrubs colonised the exposed glacial landscape close to the South Pole, the hydrological cycle was markedly different to today with precipitation significantly enriched in  $^{18}\text{O}$  by  $\sim 12\text{‰}$  relative to modern precipitation over the continent. While the enrichment may be temperature driven alone, our result correlates well with the result of Feakins et al. (2012), suggesting that moisture source regions may have been different in the past. However, it is not possible to distinguish between these two possibilities or some combination of both based on the geochemical data alone.

Our record also reveals that the time period represented by the fossils was characterised by an anomalously heavy and variable atmospheric  $\delta^{13}\text{C}$ , indicating a dynamic carbon cycle during a period of EAIS retreat. This result is consistent with high amplitude, orbitally driven climate-carbon cycle fluctuations in the mid-Miocene and may correspond to documented EAIS fluctuations associated with rapid carbon cycle changes (Levy et al., 2016).

## 3.5 Supplementary Information 2

### 3.5.1 Modification of carbon and oxygen isotopes by continuous light

A recent study (Yang et al., 2009) suggested that hydrogen and carbon isotope fractionations in plants could be significantly affected by growth under continuous light, analogous to plant growth at very high latitudes under a polar light regime. Here, we discuss the potential impact of growth under continuous light on the measured isotope ratios in fossil *Nothofagus*.

Our reconstruction of  $\delta^{18}\text{O}_{precip}$  from ancient tree ring cellulose suggests that during a period of warming and Neogene ice sheet retreat, Antarctic  $\delta^{18}\text{O}_{precip}$  was significantly enriched ( $\sim 12\text{‰}$ ) relative to modern precipitation over the continent. Part of this enrichment could be due to the continuous light regime experienced by the plant during the growing season. While no data exists for  $\delta^{18}\text{O}$ , an enrichment in  $\delta^2\text{H}$  of 15 - 40 ‰ has been documented in plant species grown in continuous light experiments (Yang et al., 2009); using an equilibrium fractionation factor of 8 to convert between  $\delta^{18}\text{O}$  and  $\delta^2\text{H}$ , this would imply an enrichment of 2 - 5 ‰ in oxygen isotope space.

This decrease in discrimination against the heavier isotope is believed to be caused by enhanced water loss during a 24 hr transpiration cycle. However, it must be emphasised that while the light regime may have been similar, the fossil *Nothofagus* plants in this study grew under very different conditions to those used in the growth experiments. During the late Neogene, the Antarctic interior was covered by a tundra shrub; low summer temperatures ( $\sim 5\text{ °C}$ ), low precipitation rates and high wind stress mean that photosynthetic and transpiration rates would have been significantly lower during the growth season, evidenced by the extremely narrow growth rings of the fossil *Nothofagus* (Francis and Hill, 1996). In contrast, deciduous conifers in the experiments of Yang et al. (2009) were grown at much higher temperatures and lower water stress. This would considerably reduce the transpiration rate for Antarctic plants versus those used in the growth experiment, decreasing water loss, and consequentially reducing any potential leaf water isotope enrichment. We therefore conclude that the majority of the

enrichment signal in our ancient  $\delta^{18}\text{O}_{precip}$  reconstruction is caused by changes in the hydrological cycle, not in plant isotope fractionation. The same study also recorded more negative values in plant  $\delta^{13}\text{C}$  in plants grown under continuous light relative to those grown under diurnal light, due to increased internal  $\text{CO}_2$  concentrations which would impact our estimations of palaeo- $\delta^{13}\text{C}$ - $\text{CO}_2$  (Jagels and Day, 2004, Smith et al., 1976, Yang et al., 2009). For similar reasons, however, we believe that the lower transpiration rates in the Antarctic fossil plants would lead to smaller increases in  $c_i/c_a$  and would have a much smaller impact on  $\delta^{13}\text{C}_{cell}$ .

**Table 3.2:** Isotope and morphology data for modern *Nothofagus* trees from Isla Navarino. \*p is *N. pumilio* and a is *N. antarctica*.

Tree	$\delta^{18}\text{O}_{cell}$ / ‰ VSMOW	$\delta^{13}\text{C}_{cell}$ / ‰ VPDB	Altitude	Trunk diameter / m	Height / m	Morphology	Species*
O-1-2-1	27.89	-27.14	29	1.11	16	arboreal	p
O-1-4-2	28.99	-26.87	29	1.16	21	arboreal	p
O-2-1-2	24.07	-25.67	29	2.02	27	arboreal	a
O-2-3-1	26.18	-26.94	29	1.24	26	arboreal	a
O-2-4-1	27.56	-25.98	29	0.51	17	arboreal	p
O-3-1-3	26.89	-26.49	97	0.72	16	arboreal	p
O-3-6-1	23.41	-26.40	97	2.75	21	arboreal	p
O-4-1-1	24.51	-27.41	97	0.52	26	arboreal	p
O-4-5-2	21.62	-28.00	97	0.6	14	arboreal	p
W-1-2-2	25.82	-27.41	247	0.76	13	arboreal	p
W-1-2-3	27.15	-26.72	247	0.76	13	arboreal	p
W-1-4-1	23.32	-27.00	247	0.63	11	arboreal	p

Table 3.2: continued

Tree	$\delta^{18}\text{O}_{cell} / \text{‰ VSMOW}$	$\delta^{13}\text{C}_{cell} / \text{‰ VPDB}$	Altitude	Trunk diameter / m	Height / m	Morphology	Species*
W-1-6-1	26.23	-25.83	247	0.74	18	arboreal	a
W-1-7-2	24.27	-27.63	247	0.65	17	arboreal	a
W-2-1-1	25.56	-27.10	395	0.44	1.2	prostrate	a
W-2-1-2	26.53	-26.25	395	0.44	1.2	prostrate	a
W-2-2-2	24.91	-26.67	395	0.4	0.7	prostrate	a
W-2-5-2	25.59	-26.95	395	0.54	5	prostrate	a
W-2-6-1	25.99	-26.89	395	0.5	3	prostrate	a
W-2-7-1	25.22	-27.30	395	0.34	1	prostrate	a
W-3-2-2	23.17	-25.65	395	0.33	3	prostrate	a
W-4-1-1	25.38	-27.93	527	0.03	0.03	prostrate	a
W-4-2-1	25.16	-26.89	527	0.26	0.5	prostrate	a
W-4-5-1	26.61	-25.22	527	0.3	0.4	prostrate	a
W-4-6-1	25.57	-25.84	527	0.32	1	prostrate	a

Table 3.2: continued

Tree	$\delta^{18}\text{O}_{cell} / \text{‰ VSMOW}$	$\delta^{13}\text{C}_{cell} / \text{‰ VPDB}$	Altitude	Trunk diameter / m	Height / m	Morphology	Species*
W-4-7-1	25.5	-26.94	527	0.62	2	prostrate	p
W-5-1-1	26.12	-26.28	527	0.24	1	prostrate	p
W-5-2-1	26.2	-25.43	527	0.33	0.5	prostrate	a
W-5-2-2	24.53	-26.63	527	0.33	0.5	prostrate	p
W-5-6-1	25.98	-26.00	527	0.45	0.8	prostrate	p
C-1-2-2	26.21	-25.64	527	0.19	0.6	prostrate	p
C-1-3-1	25.16	-26.89	527	0.28	0.8	prostrate	p

**Table 3.3:** Isotopic data for Sirius Group samples.

Sample	$\delta^{13}\text{C}_{cell} / \text{‰}$	$\delta^{18}\text{O}_{cell} / \text{‰}$
SRB-07-03	-25.83	
SRB-07-03	-25.13	27.82
OBFH-02-07	-22.51	
OBFL-04-06	-20.57	20.18
OBFL-04-06	-21.91	18.97
OBFL-04-06	-21.85	21.82
OBFL-04-06	-21.51	21.00
OBFL-04-06	-21.33	23.67
SRB-07-1	-21.84	20.33
SRB-07-1	-22.38	19.47
SRB-07-1	-22.13	23.08
SRB-07-1	-24.59	
SRB-07-1	-22.12	
SRB-07-1	-22.07	
SRB-07-1	-22.65	24.28
SRB-07-1	-23.11	22.00
OBFL-04-4		17.81
OBFL-04-12	-22.01	16.98
OBFL-04-12	-21.22	20.75
OBFL-04-12	-21.72	18.61
OBFL-04-18	-20.06	20.25
OBFL-04-18	-19.70	21.11

**Table 3.3:** continued

Sample	$\delta^{13}\text{C}_{cell} / \text{‰}$	$\delta^{18}\text{O}_{cell} / \text{‰}$
OBFL-04-18	-19.47	25.43
OBFL-04-16	-22.58	
OBFL-04-16	-22.91	
OBFL-04-16	-22.79	20.33
LCBA-05-06	-21.36	23.31
LCBA-05-06	-21.19	26.69
OBFL-04-23		17.17
OBFL-04-23	-22.74	16.12
OBFL-04-23	-22.86	
OBFL-04-23	-22.33	
OBFL-04-23	-24.62	
OBFL-04-23	-17.48	
OBFL-04-23	-24.05	
OBFL-04-23	-24.35	
OBFL-04-23	-25.69	
OBFL-04-23	-23.60	15.35
WSU-13-1	-24.67	
FBCP-14-7	-22.94	
FBCP-14-7		22.33
FBCP-14-7	-21.32	20.62
FBCP-14-7	-21.80	23.64
FBCP-14-7		25.56

**Table 3.3:** continued

Sample	$\delta^{13}\text{C}_{cell} / \text{‰}$	$\delta^{18}\text{O}_{cell} / \text{‰}$
LRB-08-4	-21.66	
SBPW-09-18	-21.65	
SBPW-09-18	-21.69	
SBPW-09-16	-24.81	21.12
SRB-07-2	-21.66	16.02
SRB-07-2	-21.64	
SRB-07-2	-21.77	
SRB-07-2	-21.45	
SRB-17-4	-23.87	
BNLB-12-1	-24.79	
BNLB-12-1		14.92
LLW-06-4	-22.54	20.60
LLW-06-4	-22.15	18.31
LLW-06-4	-22.20	21.22
LLW-06-4	-22.39	21.15
LLW-06-4	-22.63	20.58
LLW-06-4	-22.24	20.38
LLW-06-4	-21.35	20.67
LLW-06-4	-21.76	19.33
LLW-06-1		14.59
LLW-06-1	-20.52	18.71
LLW-06-1	-20.74	18.36

**Table 3.3:** continued

Sample	$\delta^{13}\text{C}_{cell} / \text{‰}$	$\delta^{18}\text{O}_{cell} / \text{‰}$
LLW-06-2	-21.04	
LLW-06-2	-21.39	18.01
LLW-06-2	-24.96	17.37
FBCP-14-2	-23.00	18.86
FBCP-14-2	-22.36	21.43
FBCP-14-3	-21.97	17.50
FBCP-14-3	-23.40	17.26
FBCP-14-3	-23.43	21.03
FBCP-14-1	-22.51	15.41
FBCP-14-1	-23.24	18.63
FBCP-14-1	-22.49	17.69
LLW-06-3	-23.71	19.71
LLW-06-3	-22.98	
LLW-06-3	-22.02	14.82
FBCP-14-6	-23.27	22.65
FBCP-14-6	-23.28	
FBCP-14-5	-23.63	
FBCP-14-5	-21.36	22.06
FBCP-14-4	-21.11	22.33
FBCP-14-4	-21.88	23.49
FBCP-14-4	-21.77	19.64
<b>Mean</b>	-22.38	20.14

**Table 3.3:** continued

Sample	$\delta^{13}\text{C}_{cell} / \text{‰}$	$\delta^{18}\text{O}_{cell} / \text{‰}$
<b>s.d.</b>	1.41	2.95
<b>s.e.m.</b>	0.16	0.38

## Chapter 4

# Smaller ice sheets drive a shift in the Antarctic temperature-water isotope relationship in a warmer world

### Preface

Chapter 4 has been prepared for submission to *Nature Geoscience*. The co-authors are my supervisors, colleagues and external collaborators: Rob Newton, Ruza Ivanovic, Jane Francis, James Riding, Julia Tindall, Rich Pancost, Jens Holtvoeth and Paul Valdes. The work presented in this chapter is my own, including the background research, experiment design, set-up and execution, data analysis and presentation, and the written manuscript. My co-authors gave valuable advice and suggested improvements for all aspects of the work. In particular, Ruza Ivanovic assisted with running the climate model and analysing climate model output. Julia Tindall provided simulations for analysis and Paul Valdes assisted with the implementation of dye-tracers in the model. Jens Holtvoeth and Rich Pancost provided compound-specific isotope analyses as well as useful discussion on their interpretation. This paper was written

more collaboratively than the other chapters appearing in this thesis; Rob Newton and Ruza Ivanovic assisted with the structure of the manuscript and with identifying the key arguments to develop and emphasise.

## Abstract

During the mid- to late Neogene (17 - 2.5 million years ago), episodic retreat of the Antarctic Ice Sheet (AIS) coincided with periods of higher-than-present atmospheric CO<sub>2</sub>, indicating ice sheet sensitivity to climatic conditions similar to those projected for the coming decades. Climate-ice sheet feedbacks mean that glacial climates are sensitive to ice sheet change, impacting temperature and moisture availability. Understanding the Antarctic hydrological cycle during past AIS retreat is therefore critical for understanding hydrological change in future warming scenarios. Here we use plant compound isotopes ( $\delta^{18}\text{O}$  and  $\delta^2\text{H}$ ) from terrestrial sediments to reconstruct precipitation isotopes and assess mechanisms for change using an isotope-enabled General Circulation Model. Tree ring  $\delta^{18}\text{O}$  and leaf wax  $\delta^2\text{H}$  translate to values of -16‰ and -170‰, respectively, for precipitation falling over the continent, significantly higher than modern day values (-30 ‰ and -240 ‰). Combining these independent proxy measurements with climate simulations, we find that the shrinking AIS induced a change in precipitation regime where moisture fell as rain over deglaciated coastal areas, with an associated isotopic depletion of inland snow, relative to modern. Our findings are likely to be indicative of future hydrological change over Antarctica. Furthermore, examining the spatial distribution of ice sheet isotopes in model runs shows that interpretations of ice core records may underestimate interglacial temperatures, depending on the location of the core relative to the ice sheet margin.

## 4.1 Introduction

Much of the mid- to late-Neogene (17 - 2.5 million years ago; Ma) is characterised by fluctuations in Antarctic Ice Sheet (AIS) volume and extent, particularly the mid-

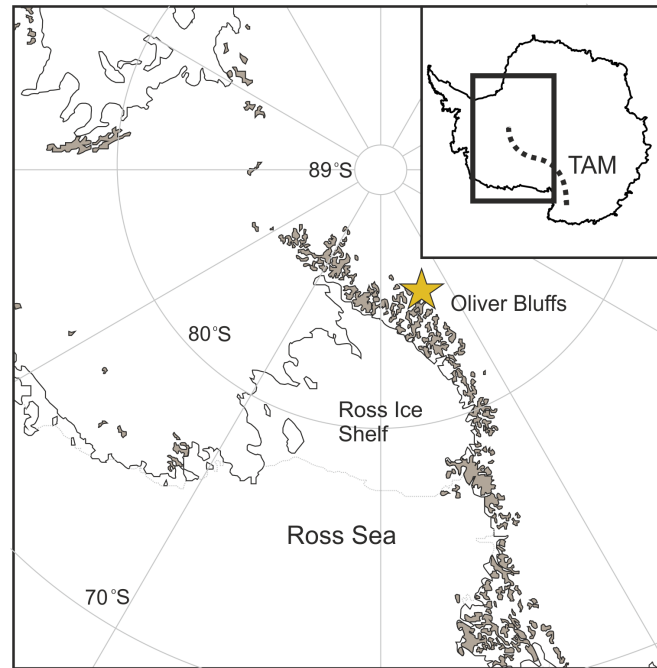


**Figure 4.1:** Location of the Sirius Group sediments at Oliver Bluffs (yellow star), which is on the poleward side of the Transantarctic Mountains (TAM). Grey shading shows rocky outcrops of the mountains.

Miocene (17 - 15 Ma; Gasson et al., 2016, Levy et al., 2016, Warny et al., 2009), and Pliocene (5 - 2.5 Ma; Austermann et al., 2015, Cook et al., 2013). Ice sheet retreat is linked to atmospheric CO<sub>2</sub> levels above 400 ppmv (Beerling and Royer, 2011, Gasson et al., 2016, Levy et al., 2016) as well as to variations in the Earth's orbit (Patterson et al., 2014); the former trigger being highly relevant to twenty-first century climate.

There are intriguing climate feedbacks associated with ice sheet retreat: glacial climates are highly sensitive to ice sheet change (Ullman et al., 2014) in part because of the impact that topography has on temperature and atmospheric circulation, while moisture availability and net precipitation are an important limiting factor on ice sheet growth (Shevenell et al., 2008). These changes may also impact the isotopic composition of precipitation falling over the ice sheet (Rees-Owen et al., b; Chapter 3), which could also affect interpretations of interglacial climate from ice core records by introducing spatial variability into the empirical temperature-isotope relationship used to calculate temperature records (Sime et al., 2009). Plant fossils, pollen, and biomarkers recovered from the terrestrial Sirius Group sediments in the Transantarctic Mountains record a

warmer climate and the existence of a tundra vegetation during a period of Neogene AIS retreat 480 km from the South Pole (Fig. 4.1; Askin and Markgraf, 1986, Francis and Hill, 1996, Rees-Owen et al., a; Chapter 2). Clearly, understanding the Antarctic hydrological cycle during such an episode of reduced ice is critical for understanding the fundamental behaviour of the climate system, and potentially also for improving projections of our own warming world (Pollard and Deconto, 2016).

## 4.2 Reconstructing precipitation isotopes

Oxygen and hydrogen isotope ratios in precipitation ( $\delta^{18}\text{O}_{precip}$  and  $\delta^2\text{H}_{precip}$ , respectively) act as a tracer of the hydrological cycle, giving quantitative insight into evaporative and transport processes (Dansgaard, 1964). The isotopic composition of precipitation at mid- and high latitudes is largely governed by latitudinal and vertical temperature gradients, as well as distance from the evaporative source region (Gat, 1996). Thus,  $\sim 55$  million year old geological records of  $\delta^2\text{H}_{precip}$  from the Arctic reveal considerably higher poleward moisture transport and rainout at high latitudes relative to the present day, during a period of abrupt climate change and carbon release to the atmosphere (Pagani et al., 2006). Precipitation isotopes can be reconstructed using  $\delta^{18}\text{O}_{precip}$  and  $\delta^2\text{H}_{precip}$  in plant compounds (tree ring cellulose and plant leaf waxes; McCarroll and Loader, 2004, Sachse et al., 2012). Accordingly, we are able to use cellulose  $\delta^{18}\text{O}_{precip}$  and plant leaf wax  $\delta^2\text{H}$  to reconstruct a multi-proxy record of precipitation isotopes during Neogene AIS retreat, thus giving a unique insight into Antarctic hydrological cycling.

The Sirius Group sediments at Oliver Bluffs provide an exceptional geological archive of terrestrial Antarctic climate during a period of AIS retreat under  $\text{CO}_2$  levels in the range 400 - 500 ppmv (Beerling and Royer, 2011, Levy et al., 2016), similar to today and projections for near-future changes (next 40 years, IPCC, 2013). The studied plant fossil-bearing interval is a mixed coarse sand and gravel unit representing glacial outwash over a poorly developed soil horizon that formed on top of glacial moraine, sandwiched between fluvio-glacial lodgement tillites; it represents periglacial or inter-

glacial conditions and likely formed over a geologically short period of time (McKelvey et al., 1991). Fossil and geochemical evidence show continental summer temperatures reached 5 °C and tundra-like vegetation was able to survive (Francis and Hill, 1996, Rees-Owen et al., a; , Chapter 2). The timing of this episode of retreat is uncertain, and may coincide with periodic warming and ice sheet fluctuations from the Pliocene (5 - 2.5 Ma; Cook et al., 2013) or the mid-Miocene (17 - 15 Ma; Lewis et al., 2007, 2008). This age uncertainty is not problematic for our aims: these time periods share characteristics which make them equally useful for an investigation into the style of Antarctic hydrological cycle change in a warmer world (see Supplementary Information 3). The Sirius Group sediments capture a snapshot of an episode of such retreat at a critical location and therefore have the potential to provide key insights into the response of Antarctic climate to a reduced ice sheet. Recent work using tree ring cellulose oxygen isotope analysis has shown that during this period of warmth, the oxygen isotope composition of precipitation ( $\delta^{18}\text{O}_{precip}$ ) falling over the Antarctic continent was  $-16.2 \pm 4.2$  ‰ (Rees-Owen et al., b; Chapter 3). Palaeoprecipitation was therefore  $\sim 12$  ‰ enriched in the heavy isotope relative to modern-day precipitation, markedly different to current high latitude precipitation ( $p < 0.001$ ). This is an intriguing result, which suggests that the hydrological cycle was functioning very differently in response to warmer temperatures and a reduced Antarctic ice sheet. Hydrological cycle change will impact both the oxygen and hydrogen isotope composition of precipitation in a similar way. To fully explore the mechanisms behind isotopic change and as a check on the veracity of our cellulose oxygen measurements we therefore reconstructed  $\delta^2\text{H}_{precip}$ . This enables a deeper investigation of hydrological cycling by providing independent data to support the tree ring isotope result, as well as comparing the results to modern relationships between the two parameters (Craig, 1961), prior to investigating the significance of these changes with an isotope enabled GCM.

Plant compound isotope analysis in the form of plant leaf wax hydrogen isotopes (hereafter  $\delta^2\text{H}_{leaf}$ ) from sedimentary lipids provide independent evidence for hydrological change during Neogene East Antarctic Ice Sheet (EAIS) retreat. The isotopic composition of precipitation is a dominant component of the  $\delta^2\text{H}_{leaf}$  signal, along with

various biological fractionation factors (Sachse et al., 2012). Applications of this proxy to ancient sediments have been able to reconstruct changes in rainout patterns and moisture source region for high latitude hydrological cycling during warmer climates 55 Ma (Pagani et al., 2006) and 20-15 Ma (Feakins et al., 2012). Previous work identified C<sub>23</sub> to C<sub>31</sub> *n*-alkanes in the terrestrial sediments at the same site in the Sirius Group at Oliver Bluffs, Transantarctic Mountains (Rees-Owen et al., a; Chapter 2). The strong odd-over-even preference indicates that the leaf waxes are derived from the epicuticular waxes of plant leaves, likely forming during the growth season in the austral summer and deposited *in situ* to the terrestrial sediments or transported a short distance (Rees-Owen et al., a; , Chapter 2). We selected the C<sub>27</sub> *n*-alkane for the  $\delta^2\text{H}_{leaf}$ -based reconstruction of palaeoprecipitation as it is the most abundant; while fractionation factors vary with *n*-alkane chain length, previous work has found that this does not greatly bias the result (Sachse et al., 2012).  $\delta^2\text{H}_{leaf}$  values range between -298 and -254 ‰ with a mean of  $-275 \pm 10$  ‰ (1 s.d., n = 14). Isotopic variability between samples and within the *n*-alkane homologous series indicates that the isotopic signal is unaltered (Schimmelmann et al., 2006; Supplementary Information 3).

In order to calculate palaeoprecipitation isotope ratios, the measured  $\delta^2\text{H}_{leaf}$  values are adjusted for the enrichment factor ( $\epsilon$ ) between precipitation and leaf waxes (Sessions et al., 1999). Global calibration studies on modern plants indicate that for the *n*-C<sub>27</sub> alkane,  $\epsilon = -108 \pm 25$  ‰ (1 s.d., n = 79; Sachse et al., 2012). Plants grown under continuous light in greenhouse experiments (Yang et al., 2009) have exhibited smaller fractionations, attributed to a continuous transpiration cycle. However, measured real world high latitude fractionations are not significantly different to the global dataset (Yang et al., 2011), and the cold growing season temperatures of the Sirius Group plants means that transpiration rates were likely lower (see Supplementary Information 2 for further discussion). We therefore apply the mean modern value of  $\epsilon = -108$  ‰, which is similar to fractionations applied in early Miocene Antarctic reconstructions (Feakins et al., 2012). This yields mean palaeoprecipitation values for continental Antarctica of  $167 \pm 27$ ‰ (error is compounded standard deviation; Fig. 4.2).

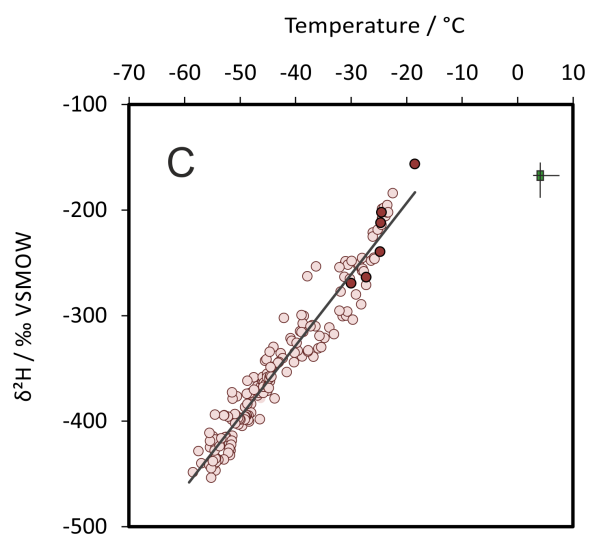
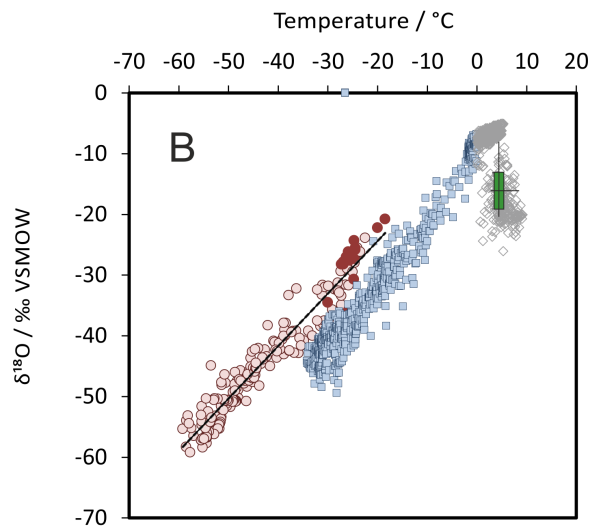
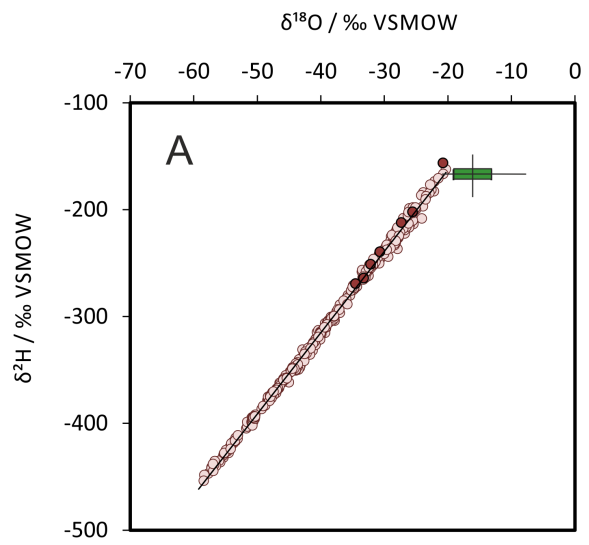


**Figure 4.2 (previous page):** (A) The relationship between  $\delta^{18}\text{O}$  and  $\delta^2\text{H}$  for modern Antarctic snow (open pink circles) demonstrating the linear relationship between  $\delta^{18}\text{O}$  and  $\delta^2\text{H}$  at high latitude (local meteoric water line). Filled red circles are modern data for sites south of  $75^\circ\text{S}$  and below 700 m above sea level. Sirius Group data is summarised by the green box and whisker plot in the x- and y- directions showing median (line), 25th and 75th percentiles (box) and range (error bars). Modern data from Masson-Delmotte et al. (2008). (B)  $\delta^{18}\text{O}$  versus temperature for modern Antarctic snow (Masson-Delmotte et al., 2008), Sirius Group data (green box and whiskers, as in panel A) and data from the palaeo HadCM3 climate model simulation (blue squares for grid cells where surface temperature  $< 0^\circ\text{C}$  and grey diamonds for surface temperature  $> 0^\circ\text{C}$ ). (C)  $\delta^2\text{H}$  and surface air temperature in modern Antarctic snow (Masson-Delmotte et al., 2008), with Sirius Group data indicated by the box and whisker plot, as in panel (A).

Modern precipitation falling over Antarctica ranges between  $-453$  and  $-156\text{‰}$  ( $\delta^2\text{H}_{precip}$ ), depending on a complex interplay of temperature, season, distance from the coast and altitude. In contrast, our Neogene  $\delta^2\text{H}_{precip}$  estimates are significantly enriched from modern values by  $\sim 100\text{‰}$  ( $p < 0.001$ , Supplementary Figure 4.7). Presently,  $\delta^{18}\text{O}$  and  $\delta^2\text{H}$  over Antarctica exhibit a linear relationship, based on mass dependencies for each isotope, known as the local meteoric water line (given as  $\delta^2\text{H} = 7.75 * \delta^{18}\text{O} - 4.93$ ; LMWL;  $R^2 = 0.998$ ,  $n=789$ , Masson-Delmotte et al., 2008). The combined  $\delta^2\text{H}_{precip}$  and  $\delta^{18}\text{O}_{precip}$  from Oliver Bluffs are consistent with this relationship (Fig. 4.2A), which is a first order check on the consistency our two datasets, and provides further confirmation that neither dataset are isotopically altered. At high latitude, precipitation isotopes are controlled by the temperature difference between the sites of evaporation and condensation, because of the temperature-dependence of isotope fractionation (Dansgaard, 1964). Over Antarctica, precipitation isotopes exhibit a strong linear relationship with temperature, which is the basis for ice core temperature reconstructions (Jouzel et al., 1997, Masson-Delmotte et al., 2008). Therefore, in warmer climates, precipitation isotopes at high latitudes are expected to be heavier; our data are qualitatively consistent with the warmer palaeotemperatures for this site (mean summer temperature of  $5^\circ\text{C}$  from multiple independent proxies; Ashworth and Preece, 2003, Ashworth and Kuschel, 2003, Francis and Hill, 1996, Rees-Owen et al., a; Chapter 2). However, for both isotope systems, our palaeoprecipitation data is markedly offset from this linear relationship such that using modern isotope-temperature (hereafter  $\delta$ -T) relationships would under-predict temperature by  $\sim 20^\circ\text{C}$  (Figs. 4.2B and 4.2C).

The  $\delta$ -T relationship during both the more recent Quaternary interglacials and the older Early Miocene has been shown to vary temporally and spatially (Feakins et al., 2012, Jouzel et al., 1997, Lee et al., 2008). The variation in slope is itself temperature-dependent (Sime et al., 2009), owing to changes in sea ice, evaporative source and rates of atmospheric overturning. Thus it is plausible that such changes would occur during even warmer periods of Earth's history, such as the interval discussed in this study. This is important because understanding the mechanism behind this shift will aid fundamental understanding of the polar hydrological cycle in a warmer world. Combining the proxy-data results with an isotope-enabled General Circulation Model (GCM) will enable a more rigorous examination of the climate and hydrological response to ice sheet reduction.

### 4.3 Changes in moisture delivery to the continent

To this end, we employ the oxygen isotope-enabled atmosphere-ocean-vegetation general circulation model HadCM3 to explore our results (Cox, 2001, Gordon et al., 2000, Pope et al., 2000). This climate model has been shown to represent  $\delta^{18}\text{O}_{precip}$  in the preindustrial well (Tindall et al., 2009) and has been used to investigate a number of palaeoclimates, including the Pliocene (5 - 2.5 Ma; Tindall and Haywood, 2015) and the warmer, older Eocene (56 - 34 Ma; Tindall et al., 2010). As the age uncertainty of the Sirius Group sediments precludes using a model with age-specific boundary conditions, we use previously published simulations with boundary conditions matching the mid-Pliocene (Tindall and Haywood, 2015), including elevated  $\text{CO}_2$  (405 ppmv) and a reduced Antarctic ice sheet with respect to the preindustrial. The purpose of the modelling was to examine if the features seen in the temperature and precipitation isotope reconstructions were consistent with the direction of change in the model data. Thus, this warmer, reduced-ice world is a reasonable idealised scenario for better understanding the climate recorded by the Sirius Group (see Supplementary Information 3 for further discussion).

Over the entire continent, the model simulates a mean  $\delta^{18}\text{O}_{precip}$  of  $-20.6 \pm 14.0$

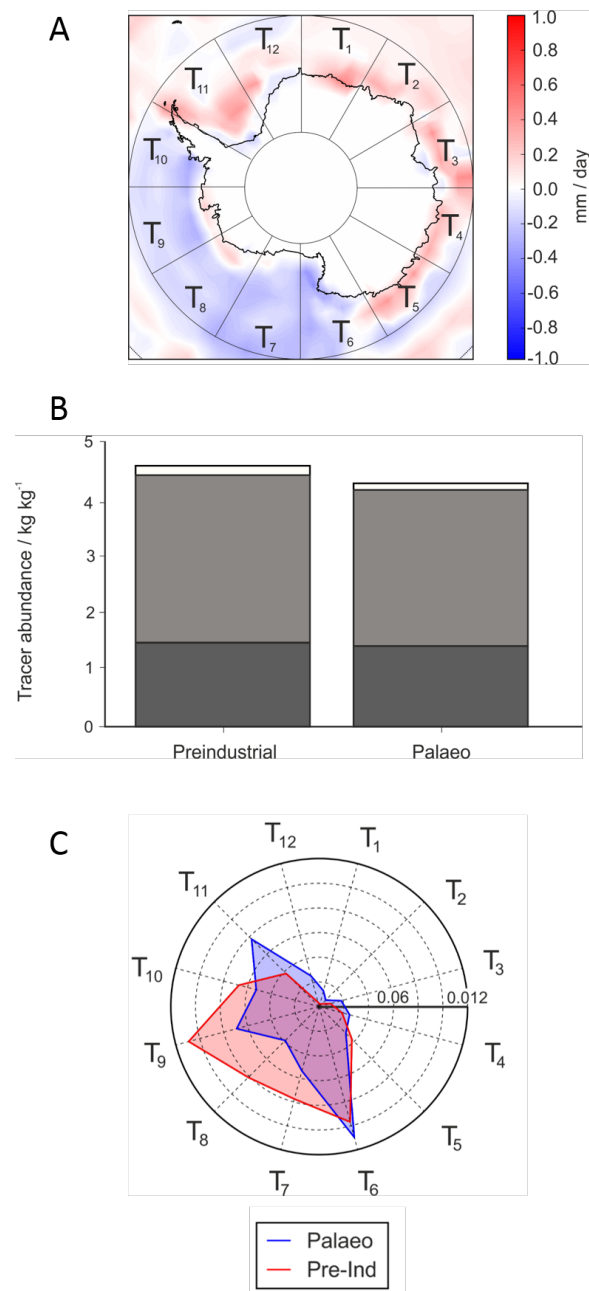


**Figure 4.3:** (A) Tracer initialisation sectors (T1-T12; see Methods). Each tracer was initialised at the surface of the labelled sectors. The tracer sectors overlay the mean difference in summer evaporation from the sea surface of the palaeo scenario with respect to the preindustrial (simulations a and b; see Methods). (B) Stacked bar charts of absolute tracer abundance for latitudinal sectors where white = 0 - 30 °S, light grey = 30 - 60 °S, dark grey = 60 - 80 °S. (C) Tracer abundance profiles for the preindustrial and palaeo simulations for a set of grid cells on East Antarctica representative of the Sirius Group site (see Supplementary Information 3). Tracer amounts were calculated on the 10<sup>th</sup> day of the simulation, which is the residence time of water vapour in the atmosphere.

‰ (error = 1 s.d.), broadly consistent with the enrichment in our palaeoprecipitation reconstruction ( $\delta^{18}\text{O}_{precip} = -16.2 \pm 4.2$  ‰ Supplementary Figure 4.7). In ice-free areas of Antarctica (i.e. grid boxes which were ice-covered in the preindustrial control but under palaeo boundary conditions are land), which are most similar to our fossil site, the climate model simulates a mean  $\delta^{18}\text{O}_{precip}$  of  $-24.2 \pm 9.4$  ‰ (error = 1 s.d.), an enrichment of  $\sim 7$  ‰ relative to the preindustrial. Furthermore, an offset from the  $\delta$ -T linear relationship (similar to that seen in our geochemical data) is evident in ice-free areas of Antarctica (Fig. 4.2B; Tindall and Haywood, 2015). The key factors influencing the distribution of isotopes in modern Antarctic precipitation are the origin of moisture, and spatial changes of the condensation temperature (Masson-Delmotte et al., 2008). From both the enrichment and offset  $\delta$ -T relationship in the proxy and model results, we infer a marked shift in the structure of the hydrological cycle during Neogene ice sheet retreat.

Presently, Antarctic precipitation is dominated by moisture from the mid-latitudes (up to 66%; 30 - 60° S), while up to a fifth is sourced from high latitude oceans above 60° S (Delaygue et al., 2000). One hypothesis to explain our observations is that the enrichment in precipitation isotopes is a result of a change to an evaporative source region closer to the coast (i.e. more moisture from higher latitudes), as this would alter the evaporation temperature as well as the amount of precipitation along the water transport path. This mechanism is similar to the source change mechanism invoked for Antarctic hydrological change during the Early Miocene (Feakins et al., 2012). We explored this hypothesis by implementing conservative dye-tracers in the model, which track the movement of air parcels through the atmosphere. The addition of atmospheric tracers is an effective way of tracing changes in moisture source, and the preindustrial simulation models the modern latitudinal distribution of moisture sources well (Fig. 4.3B). In the reduced-ice, warmer world simulation, there is an overall decrease in the amount of tracer reaching the continent, but based on our model experiments, there is no significant change in latitudinal moisture source (Fig. 4.3B). This indicates that changing source region is not responsible for the observed shift towards more positive precipitation isotope compositions. Alternatively, changes in

short-range moisture transport pathways caused by shifting local source regions could be responsible. Indeed, there are subtle changes in the evaporative source regions of Antarctic precipitation from the polar oceans to the Oliver Bluffs region. Our tracer experiments show that there is an increase by a factor of two in moisture sourced from the Weddell Sea region (Tracer 11) and corresponding decrease in moisture from the Ross, Amundsen and Bellingshausen Seas (Tracers 7-10) relative to the preindustrial. These changes in delivery are accompanied by a respective increase and decrease in evaporation from the sea surface (Figs. 4.3C and 4.4D).

The increase in moisture delivery from the Weddell Sea region may be linked to changes in atmospheric circulation in the lower atmosphere driven by the reduction in ice sheet extent; there are notable changes in wind vector direction and reductions in vector strength over ice-free areas (Supplementary Fig. 4.8). This would allow increased penetration of moisture via low-pressure systems further into the continent. Currently, the height of the Transantarctic Mountains and ice sheet at the edge of the continent prevents penetration of much moisture into the interior (Turner and Marshall, 2011), but the palaeo-orography would have been much lower (Ackert, Jr. and Kurz, 2004). However, while evaporative enrichment in the Weddell Sea would recharge atmospheric vapour with the heavy isotope (a shift away from the traditional Rayleigh distillation model) we do not see the expected corresponding shift to more positive values for water vapour  $\delta^{18}\text{O}$  (as in Lee et al., 2008; Fig. 4.4B and D). This suggests that these small changes in evaporative source cannot explain the observed shift in the  $\delta$ -T relationship. This result contrasts with Antarctic hydrological change seen in the Early Miocene ascribed to a latitudinal shift in moisture source region (Feakins et al., 2012), although this previous study used an idealised general circulation model without continents or ice sheets, so cannot capture changes in atmospheric circulation or moisture delivery related to Antarctic orography or ice sheet extent. As the large changes in the temperature-isotope relationship cannot be caused by source region changes, we surmise that the different relationship must therefore be driven by changing transport and rainout patterns.

Having discounted long- and short-range changes in moisture source region, we infer

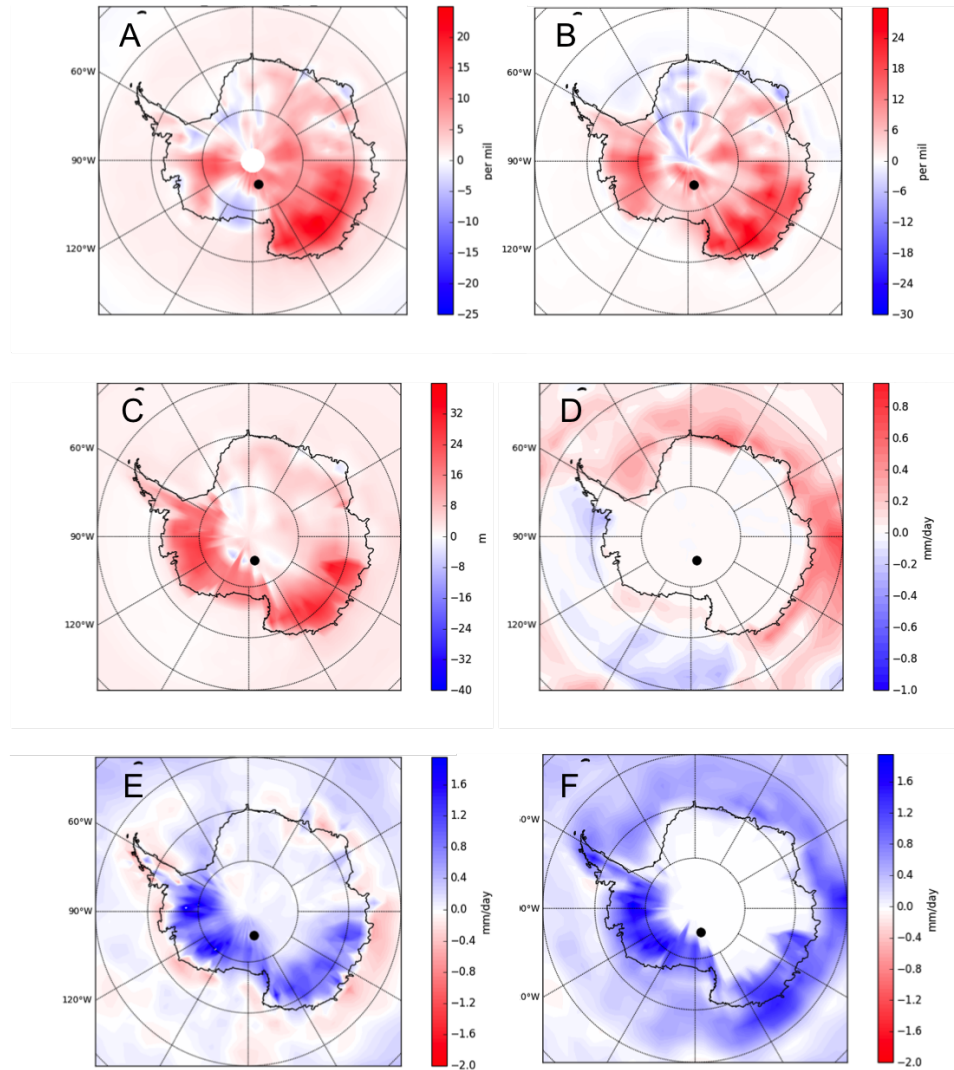


**Figure 4.4:** Mean summer difference in the palaeo scenario with respect to the preindustrial (simulations a and b; see Methods) for **(A)** precipitation  $\delta^{18}\text{O}$ ; **(B)** atmospheric vapour  $\delta^{18}\text{O}$  in the lower atmosphere; **(C)** surface temperature; **(D)** evaporation from the sea; **(E)** total precipitation; **(F)** precipitation falling as rain. Climate fields are calculated from a 30 year climate mean (last 30 years of the simulations). The Sirius Group site is shown by the black dot. Note reversed scalebar in **E** and **F**.

a switch to a different precipitation regime. Analysis of the model results, which present a good match to measured  $\delta^{18}\text{O}$  and surface temperature data (Rees-Owen et al., a,b; Chapters 2 and 3), show that much of the positive shift in the temperature-isotope relationship can be explained by change occurring in the areas of Antarctica that have been fully deglaciated. The ice-free regions experience greater warming than the rest of the continent (Fig. 4.4C Tindall and Haywood, 2015). The regions of warming are also subject to an increase in precipitation (Fig. 4.4E), as well as a change in the type of precipitation: the fraction of precipitation made up by rain increases, particularly over the coast (Fig. 4.4F). Changing the type of precipitation considerably affects  $\delta^{18}\text{O}_{precip}$ . Unlike snow, rain undergoes post-condensation exchange with the vapour parcel, which enriches the heavy isotopes in the rain and depletes those in the vapour parcel, therefore  $\delta^{18}\text{O}_{rain}$  is more positive than  $\delta^{18}\text{O}_{snow}$  (Field et al., 2010; see discussion in Supplementary Information 3). In the palaeo simulation, isotopically heavy rain falling over the coast depletes the vapour parcel relative to the pre-industrial simulation, where precipitation only falls as snow. As the depleted vapour parcel moves inland over deglaciated regions of Antarctica, precipitation falling as either rain or snow is then offset (lighter) relative to pure Rayleigh distillation  $\delta$ -T relationship (summarised in Fig. 4.5). This mechanism is the inverse of results from the Last Glacial Maximum where an increase in precipitation falling as snow resulted in relatively enriched vapour (Lee et al., 2008).

In the palaeo model, the whole continent volume weighted precipitation average is  $\sim 11$  ‰ more positive than the preindustrial. Therefore in order to maintain isotope mass balance, we infer the advection of depleted vapour away from the continent. This conclusion is supported by the results from the dye-tracer experiments, where less tracer reaches the continent in the palaeo simulation than in the pre-industrial control (Fig. 4.3B).

As a further test of this hypothesis, we examined the results of a simulation with a pre-industrial (full) EAIS but elevated (400 ppmv)  $\text{CO}_2$  (Supplementary Information 3, Supplementary Fig. 4.9). Very little change in the temperature-isotope relationship was found, indicating that the main driver behind this mechanism is ice sheet removal.

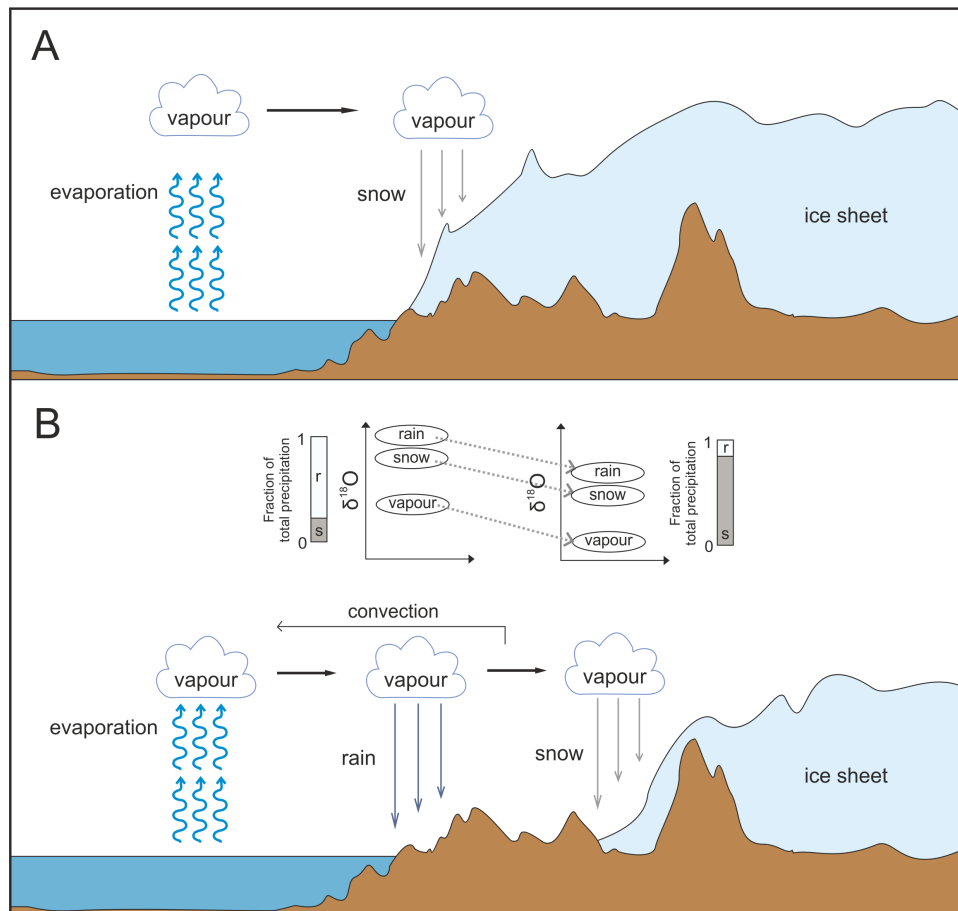


**Figure 4.5:** (A) Current precipitation regime over Antarctica, where all precipitation falls as snow. (B) Inferred precipitation regime under reduced ice sheet conditions where precipitation falls as rain over deglaciated coastal areas, depleting the remaining vapour as it moves inland relative to scenario (A).

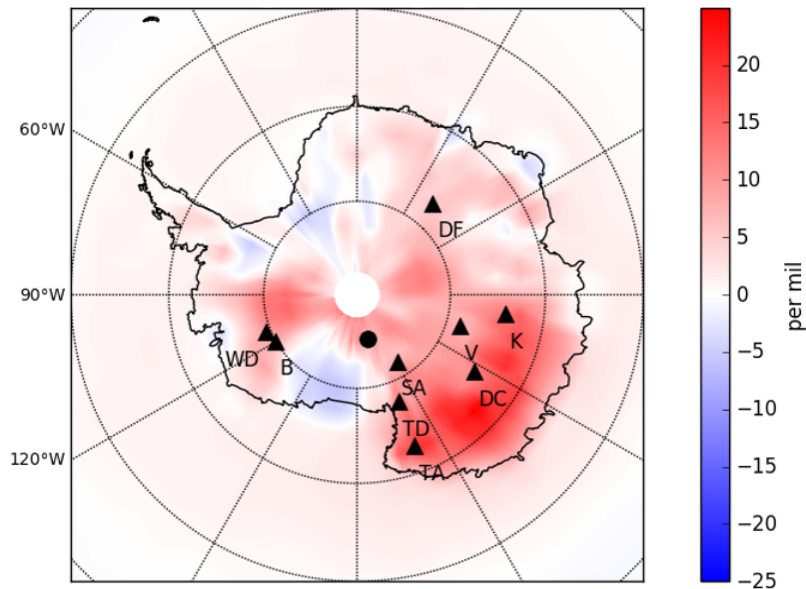


**Figure 4.6:** Mean summer difference for precipitation  $\delta^{18}\text{O}$  (repeat of Fig. 4.4A) in the palaeo scenario with respect to the preindustrial (simulations a and b; see Methods) and the locations of ice cores with records longer than 1000 years . B = Byrd, DF = Dome Fuji, DC = EPICA Dome C, K = Komsomaskay, SA = Siple Dome A, TD = Taylor Dome, TA = TALDICE, V = Vostok, W = WAIS Divide. Climate means are calculated from the last 30 years of the simulations.

Our findings are highly relevant to future warming scenarios: ice sheet modelling predicts that significant EAIS retreat could occur by 2100 (Pollard and Deconto, 2016), which in turn could severely impact the Antarctic hydrological cycle, with increasing temperatures leading to more precipitation and moisture falling as rain rather than snow. This has implications for predicting future ice sheet-climate feedbacks and ice sheet changes, which are partly dependent on moisture regime (Ligtenberg et al., 2013, Shevenell et al., 2008), as well as continental runoff and marine productivity.

Just as importantly, these findings have strong implications for the interpretation of ice cores, particularly during periods of deglaciation and warm interglacials. The loss of the West Antarctic Ice Sheet (e.g. Marine Isotope Stage 11; Raymo and Mitrovica, 2012) and parts of the East Antarctic Ice Sheet (e.g. the Last Interglacial; Bradley et al., 2013) could induce similar, if smaller changes in the temperature-isotope relationship (Sime et al., 2009), particularly for marginal cores proximal to deglaciated areas such as the Byrd, WAIS Divide or Taylor Dome ice cores (Fig. 4.6). Following

this through, it seems highly probable that a similar principle applies to ice core records from Greenland, which experienced substantial ice volume loss during interglacials (up to 50%; Stone et al., 2013, de Vernal and Hillaire-Marcel, 2008). However, with respect to this study,  $\delta^{18}\text{O}_{precip}$  over Greenland is much less well represented by HadCM3 than Antarctica  $\delta^{18}\text{O}_{precip}$  (Tindall et al., 2009), for reasons that are not well understood. Therefore it is not possible to test this hypothesis with any certainty. Temperatures derived from ice core  $\delta^{18}\text{O}$  and  $\delta^2\text{H}$  records may therefore be severely under-estimated (by up to 25 °C), which indicates large gaps in our understanding of warmer-than-present climates. Clearly, this knowledge gap needs to be addressed in order to fully assess the impact of such warmer climates.

## 4.4 Conclusions

During a period of significant Neogene EAIS retreat, we find strong model and geological evidence for a change in hydrological regime driven by ice sheet shrinkage. Plant compound isotopes ( $\delta^{18}\text{O}$  from tree ring cellulose,  $\delta^2\text{H}$  from leaf waxes) form the basis of precipitation isotope calculations showing enrichment in both isotope systems, consistent with warmer temperatures (Rees-Owen et al., a,b; Chapters 2 and 3). Combined with geochemical temperature reconstructions, we find our data is significantly offset from the well-established modern relationship, used as the basis for the interpretation of ice-core records (Dansgaard, 1964, Masson-Delmotte et al., 2008) This indicates a large shift in hydrological dynamics. Model experiments using an atmospheric dye-tracer show that changes in evaporative source region to a more local moisture source is an insignificant mechanism in terms of explaining such a hydrological shift. Instead, we find evidence for a strikingly different precipitation regime, where a switch to liquid precipitation from snow alters the isotopic fingerprint of Antarctic continental precipitation, driven by warmer temperatures over areas of ice sheet loss. Our findings offer valuable insights into hydrological processes during periods of ice sheet retreat, and have implications for Antarctic hydrological cycling in future warming scenarios. Moreover, this result has particular relevance for our interpretation of ice core records during in-

terglacials and indicates that ice-core based temperature reconstructions during these warm periods may be severely underestimated.

## 4.5 Methods

### 4.5.1 Proxy data

#### 4.5.1.1 Tree ring isotopes

The tree ring cellulose oxygen isotope data used in this study is taken from Rees-Owen et al. (b; Chapter 3).

#### 4.5.1.2 Leaf wax isotopes

Samples analysed for plant leaf wax isotopes are the same as those in Chapter 2 (Rees-Owen et al., a) and extraction methods can be found in the same location. Lipids (*n*-alkanes) in the apolar fraction were analysed for compound specific-isotope ratios ( $\delta^{13}\text{C}$  and  $\delta^2\text{H}$ ) at the Organic Geochemistry Unit, University of Bristol. The stable hydrogen isotope composition of individual *n*-alkanes was measured in duplicate or triplicate by gas chromatography-isotope ratio monitoring mass spectrometry (GC-irmMS), using a Thermo Scientific Trace Ultra gas chromatograph (GC) linked *via* a Thermo Scientific GC Isolink and ConFlo IV interface to a Delta V Plus isotope ratio monitoring mass spectrometer (irmMS, Thermo Scientific, Bremen, Germany). The GC was fitted with a PTV splitless injector and a Zebron (ZB-1) fused silica column (30 m, 0.25 mm I.D., 0.25  $\mu\text{m}$  df; Phenomenex), using helium as the carrier gas (flow: 1.4 ml min<sup>-1</sup>). The GC temperature was programmed from 70 to 300 °C at 10 °C min<sup>-1</sup> and hold at 300 °C for 8 minutes. Data acquisition was controlled by Isodat (Thermo Scientific) software and raw data was processed using the Isodat dynamic background integration Workspace software. Stable carbon isotopes ratios of the *n*-alkanes were determined in duplicate using an Agilent Technologies 7890A GC coupled to an Isoprime 100 irmMS via an Isoprime GC5 combustion interface. The GC was fitted with a split/splitless injector and a non-polar RTX-1 fused silica column (50 m, 0.32 mm I.D., 0.17  $\mu\text{m}$  df; Thames Restek). Samples were injected in splitless mode and the carrier gas was helium (flow: 2 ml min<sup>-1</sup>). The GC temperature was programmed from 70 to 130 °C at 20 °C min<sup>-1</sup>, then to 300 °C at 4 °C min<sup>-1</sup> and held at 300 °C for 25 minutes.

IsoVantage (Isoprime) software was used for data acquisition and processing.

Isotope ratios are given as  $\delta^2\text{H}$  and  $\delta^{13}\text{C}$  values relative to the reference gases ( $\text{H}_2$ ,  $\text{CO}_2$ ) calibrated from reference standard mixtures with known isotopic values for hydrogen and carbon (Schimmelmann, Indiana University, USA). Ratios are reported relative to the Vienna Standard Mean Ocean Water (VSMOW;  $\delta^2\text{H}$ ) and the Vienna Pee Dee Belemnite (VPDB;  $\delta^{13}\text{C}$ ) standards. The average standard deviation for hydrogen isotope duplicate and triplicate analyses of the  $\text{C}_{25}$  and  $\text{C}_{29}$  *n*-alkane was  $\pm 5 \text{‰}$  and  $\pm 4 \text{‰}$ , respectively, and  $\pm 2 \text{‰}$  for the dominant  $\text{C}_{27}$  *n*-alkane. The average standard deviation for carbon isotope duplicate analyses of the  $\text{C}_{27}$  and  $\text{C}_{29}$  *n*-alkane was  $\pm 0.2 \text{‰}$ , and  $\pm 0.3 \text{‰}$  for the  $\text{C}_{25}$  *n*-alkane.

Leaf wax  $\delta^2\text{H}$  was then converted to precipitation  $\delta^2\text{H}$  by the addition of the enrichment factor  $\epsilon$  (where  $\epsilon = -108 \pm 25 \text{‰}$ ). See Supplementary Information 3 for a discussion of  $\epsilon$  values.

## 4.5.2 Climate modelling

### 4.5.2.1 Model description

The model used in this study is version 4.5 of the Hadley Centre General Circulation Model (HadCM3) as described by Gordon et al. (2000) and Pope et al. (2000). HadCM3 is a fully coupled ocean-atmosphere-vegetation GCM. The ocean model has a resolution of  $1.25^\circ \times 1.25^\circ$  with 20 vertical levels, giving highest vertical resolution towards the ocean surface (Johns et al., 1997), and has a timestep of 1 hour. The atmosphere model has a coarser resolution at  $3.75^\circ \times 2.5^\circ$  with 19 vertical levels based on the hybrid vertical coordinate scheme by Simmons and Burridge (1981). The version of HadCM3 used here includes the MOSES2 land surface exchange scheme with the TRIFFID dynamic vegetation model (Cox, 2001), which means that the climate and vegetation interact fully. The convection scheme is given by Gregory and Rowntree (1990). The atmosphere and ocean grids are aligned and coupling occurs once per model-day, where both models pass across the fluxes accumulated over the previous model-day. Oxygen isotope tracers are included throughout the hydrological cycle (Tindall et al., 2009).

HadCM3 is no longer considered a state of the art GCM, but its relatively fast model speed compared with the more highly resolved and complex models ( $\sim 70$  model years per wallclock day on the N8 Polaris Tier 2 supercomputer facility) means it is highly suitable for a study such as this, which requires millennial-length model simulations to spin-up the palaeoclimate state. It has been shown to represent a realistic and stable atmospheric and oceanic climate (Gordon et al., 2000, Sime et al., 2006), and is able to replicate observed estimates of poleward atmospheric and oceanic heat transport very well for modern times (Cooper and Gordon, 2002, Dong and Sutton, 2002). The oxygen isotope component of the model provides a good representation of oxygen isotopes in precipitation and sea water for the pre-industrial, and matches well with proxy data for the Pliocene (Tindall et al., 2009, Tindall and Haywood, 2015). The isotope-enabled model has been used in a number of palaeoclimate studies including the Quaternary, Pliocene and Eocene (Tindall et al., 2010, Tindall and Haywood, 2015, Holloway et al., 2016), and notably has been run as part of the Pliocene Model Inter-comparison Project (PlioMIP; Bragg et al., 2012, Haywood et al., 2010, 2011, 2016). In general, the models simulated climate are in good agreement with reconstructions from palaeoclimate proxies, although there are some discrepancies, e.g. under-predictions of Northern Hemisphere high-latitude terrestrial warming and Pliocene sea surface temperature in the North Atlantic (a problem common to many PlioMIP models; Bragg et al., 2012, Dowsett et al., 2012, Salzmann et al., 2013). However, of particular relevance to this study, HadCM3 represents the broad-scale features of high southern latitude ocean and atmospheric circulation well (Turner et al., 2006) and has been used to model Antarctica during the Pliocene in multiple studies (e.g. Dolan et al., 2011). It is for these reasons that we chose to use this model.

#### 4.5.2.2 Addition of tracers

In order to examine changes in moisture source region, we implemented conservative air dye-tracers in the model, which tags an air parcel initiated at the surface. As tracer-spiked air circulates around the Southern Hemisphere, it is possible to directly track the movement of air parcels and quantify changes in moisture delivery to the

Antarctic continent, though we highlight that the dye-tracers are an approximation for moisture transport. Since  $\delta^{18}\text{O}$  is a moisture source tracer, but one that behaves less conservatively because it is affected by fractionation processes, the two tracer schemes are complementary.

The isotopic signal in our tree ring and leaf wax isotope results are most likely a summer precipitation signal (see Supplementary Information 3), so only changes in atmospheric circulation during the Austral summer were examined in the tracer experiments (specifically December, taken as representative of summer precipitation). Tracer experiments were run in parallel to the steady-state climate simulations (see 5.2.3). The Southern Hemisphere was divided into sectors and a different dye was applied to the surface of every sector at the very start of each tracer simulation. Figure 4.3A and Supplementary Fig. 4.10 show the sectors that the different tracers were initialised in:

1. Tracers (T) 1 - 12 were applied to the surface between 59 and 80 °S, where the circumference was divided into twelve equal longitudinal sectors (e.g. T11 was applied between 30 and 60 °W).
2. Tracer 13 was applied to the surface at all longitudes between 0 and 30 °S.
3. Tracer 14 was applied to the surface at all longitudes between 30 and 60 °S.

### 4.5.2.3 Experimental design

To examine the interaction between East Antarctic Ice Sheet and the Antarctic hydrological cycle, we performed three HadCM3 simulations (preindustrial, palaeo, palaeoCO<sub>2</sub>), along with additional tracer simulations which branch from the preindustrial and palaeo simulations; see the palaeo-dye simulation (d). The palaeo and preindustrial simulations were run for 2500 years. Results are presented for climate means calculated from the final 30 years. The majority of discussion in the main text refers to the palaeo simulation (b), and when anomalies (or climate differences) are discussed, these are the palaeo simulation (b) with respect to the preindustrial simulation (a), i.e., (b) minus

(a). The preindustrial and palaeoCO<sub>2</sub> simulations are otherwise referred to occasionally for comparison and in the supplementary material.

(a) Preindustrial: A control experiment was run with standardised preindustrial boundary conditions based on the HadCM3 public release spin-up simulation published by Gordon et al. (2000). These include a modern continental configuration, fully developed ice-sheets and modern orbital parameters. Atmospheric CO<sub>2</sub> was set to 280 ppmv and trace greenhouse gases were set to standard preindustrial levels (761 ppb methane, 269 ppb nitrous oxide). Vegetation was based on the Wilson and Henderson-Sellers (1985) archive of land-cover. This simulation provides a reference point for comparison to the idealised, reduced-ice, warm world simulation (simulation b).

(b) Palaeo: A palaeo simulation, previously published by Tindall and Haywood (2015), which was set up with mid-Pliocene Warm Period (mPWP) boundary conditions (see Supplementary Information 3). The palaeo simulation was initialised from a standard pre-industrial  $\delta^{18}\text{O}$  model run, which had been run for several millennia, based on simulations by Tindall et al. (2009). The experiment was then reconfigured into a Pliocene Model Intercomparison Project (PlioMIP) compliant experiment (Bragg et al., 2012, Haywood et al., 2011) by using the PRISM3D dataset (Dowsett et al., 2010) to change the ice sheets, the orography and vegetation parameters; while the continental configuration (coastlines), ocean bathymetry and river outflow points were kept as pre-industrial. The PRISM3D dataset includes an orography very similar to the modern, except for areas of the Andes, which are slightly lower than the present day (Dowsett et al., 2010). The West Antarctic Ice Sheet is fully removed (deglaciated) and in East Antarctica, the ice sheet is approximately one third smaller (for full details see Dowsett et al., 2010, Haywood et al., 2010, 2011). Atmospheric CO<sub>2</sub> levels were set to 405 ppmv and orbital parameters were set to 3.205 Ma (Prescott et al., 2014), which are near-modern. The version of HadCM3 in this study uses the TRIFFID dynamic vegetation model (Cox, 2001) such that the vegetation is prognostic and interacts

with the climate (thus making them consistent) and the relative proportions of vegetation types evolve throughout the simulation.

- (c) PalaeoCO<sub>2</sub> - An intermediate simulation was run in order to distinguish between the impacts of greenhouse-gas controlled radiative forcing and ice sheet extent on Antarctic climate. Atmospheric CO<sub>2</sub> was set to 405 ppmv at the end of the preindustrial simulation (a), all other boundary conditions were kept the same as in (a), and the simulation was run for a further 500 years, which was sufficient for the surface climate to reach steady state.
- (d) For the dye-tracer enabled simulations, the long palaeo and pre-industrial simulations used in this study were run for a further 30 years each. Dye experiments were then initialised from the December start dumps of every year of this extension period, and run for 15 days. This enabled us to repeat the experiment 30 times, one for each year, in order to calculate the climate mean state and thus try to reduce any uncertainty or bias in the result caused by meteorological events in the model that are unrepresentative of the background climate state in (e.g. a large storm beginning on December 1<sup>st</sup>). The residence time of water in the atmosphere is  $\sim 10$  days, hence experiments were run for 15 days, also ensuring that the tracer had not become too mixed and diluted to trace coherent pathways. Climate means (for all 30 years of each time period) were calculated for the 10th and 15th day of the experiments. An area consisting of 9 grid squares approximating the Sirius Group site were picked and tracer concentrations calculated (Supplementary Figure 4.11).

Note, dye tracers were not implemented in simulation (c), since it was a diagnostic tool for deconstructing the cause of the modelled climate signal, and implementing the dye tracers comes at significant extra computational cost (slower by a factor of eight).

## 4.6 Supplementary Information 3

### 4.6.1 Proxy reconstruction of precipitation isotopes

#### 4.6.1.1 Sample selection

The Sirius Group sediments at Oliver Bluffs are located on the poleward flanks of the Transantarctic Mountains. Sediment samples for leaf wax hydrogen isotope analysis were the same as those selected for GDGT-based palaeothermometry and biomarker vegetation analysis in Chapter 2 (Rees-Owen et al., a); these were selected to span the lateral extent of the fossiliferous bed.

#### 4.6.1.2 Biomarker discussion

Rees-Owen et al. (a) (Chapter 2) reported the biomarker abundances for C<sub>21</sub> to C<sub>31</sub> *n*-alkanes in the Sirius Group sediments. The strong odd-over-even preference of the long chain lipids, with a dominant chain length of C<sub>27</sub>, is characteristic of terrestrial plants. In two samples (OB5 and OB14), low abundances of alkanes precluded robust measurement of hydrogen isotope values for all long chain *n*-alkanes. We selected *n*-C<sub>27</sub> for isotope analysis as it was the most abundant *n*-alkane in all samples, and it provided the most robust data (high signal to noise; all peak heights were greater than 1000 mV), although *n*-C<sub>25</sub> and *n*-C<sub>29</sub> also produced reasonably robust results which mirrored the *n*-C<sub>27</sub> values. *n*-C<sub>31</sub> and *n*-C<sub>23</sub> were either not abundant enough or co-eluted with unresolved compounds, which meant there was a low signal-to-noise ratio, and did not produce reliable data (see Supplementary Table 4.1).

**Preservation** There are several lines of reasoning which suggest that isotopic signal of the leaf waxes in this study are isotopically unaltered.  $\delta^2\text{H}$  values of most lipid biomarkers appear to be unaffected up until the onset of catagenesis and the exceptional preservation of contemporaneous plant fossils (used for  $\delta^{18}\text{O}_{precip}$  calculations in Rees-Owen et al., b; Chapter 3) indicates that burial has not generally affected the sedimentary archive at Oliver Bluffs. The excellent preservation of a broad range

of plant lipids also precludes diagenetic alteration (discussed in Rees-Owen et al., a; Chapter 2). To summarise, diagenesis would convert *n*-alkanoic acids to *n*-alkanes, but *n*-alkanoic acids are very abundant in the Sirius Group sediments. Similarly, other natural product compounds (such as polar triterpenoids) are abundant, suggesting that very little degradation has occurred. Diagenesis could also impact the isotopic signal of leaf waxes through hydrogen exchange, which would lead to homogenous isotope values (Schimmelmann et al., 2006). Here, offsets of 40 - 50 ‰ between samples suggest that the primary signal has not been altered. Furthermore, long chain *n*-alkanes are the most isotopically conservative hydrogen moiety as they contain the most recalcitrant C-H bonds of the compound classes used for compound specific  $\delta^2\text{H}$  analysis (Sessions et al., 2004).

**Calculating palaeoprecipitation isotopes** The compound-specific hydrogen isotope composition of leaf waxes (*n*-alkanes, *n*-alkanoic acids, *n*-alcohols) has been shown to record precipitation  $\delta^2\text{H}$  well (Sessions et al., 1999, Sachse et al., 2004). The hydrogen isotopic composition of precipitation may be calculated from  $\delta^2\text{H}$  measurements of leaf wax alkanes by the application of an enrichment factor,  $\epsilon$ , defined as the apparent fractionation between lipid and precipitation water, given by equation 4.1:

$$\epsilon = \frac{(\delta^2 H_{lipid} + 1)}{(\delta^2 H_{source} + 1)} - 1 \quad (4.1)$$

where the subscript *lipid* refers to the leaf wax alkane and *source* to source water, assumed to be precipitation. In higher plants,  $\epsilon$  incorporates multiple biological and environmental fractionations, including soil water fractionation, leaf-water transpiration and biosynthetic fractionation (a full discussion of these processes was laid out by Sachse et al., 2012). In order to select the most appropriate value for  $\epsilon$ , the plant source of the leaf waxes must be constrained, as there is considerable variability between  $\epsilon$  for different plant life-forms (Sachse et al., 2012).

The macrofossil and lipid record (Rees-Owen et al., a; Chapter 2) for the Sirius

Group indicates that the palaeovegetation comprised a spatially heterogeneous mixture of angiosperms, gymnosperms and bryophytes. Measurements of leaf wax carbon isotopes ( $\delta^{13}\text{C}_{leaf}$ ) are recommended to confirm the origin of leaf waxes and to rule out significant vegetation changes in palaeoenvironmental applications (Sachse et al., 2012); such as between trees, C<sub>3</sub> and C<sub>4</sub> grasses. Very little variability is expected in  $\delta^{13}\text{C}_{leaf}$  for the Sirius Group as the sediments analysed here represent a small timeframe, although the vegetation was spatially heterogeneous (Rees-Owen et al., a; Chapter 2). Mean  $\delta^{13}\text{C}_{leaf}$  was  $-29.9 \pm 0.2 \text{ ‰}$  (error = 1  $\sigma$ ). After the removal of unreliable data-points (defined as having a standard deviation  $> 0.5\text{‰}$ ), the *n*-C<sub>25</sub> and *n*-C<sub>29</sub> lipids give mean  $\delta^{13}\text{C}_{leaf}$  of  $-30.3 \pm 0.3 \text{ ‰}$  and  $-29.7 \pm 0.2 \text{ ‰}$  respectively, which are not statistically different from each other (see Supplementary Table 4.1). Overall, our results confirm that the leaf waxes originate from C<sub>3</sub> higher plants, and the low variability indicates that while the macrofossil record may be spatially heterogeneous, there is little isotopic vegetational change.

Angiosperms produce up to 10 times as many leaf waxes as gymnosperms (Diefendorf et al., 2010) and bryophytes typically only produce mid-chain length leaf waxes (Pancost et al., 2002), indicating that the average angiosperm apparent fractionation of  $-113 \pm 30 \text{ ‰}$  may be appropriate. The Sirius Group macrofossil record also indicates that the woody vegetation had a prostrate or shrubby life-form; a global compilation of data shows that the enrichment factors for *n*-C<sub>27</sub> in trees and shrubs are not significantly different (mean  $-108 \pm 25\text{‰}$  and  $105 \pm 31\text{‰}$  respectively; Sachse et al., 2012), and neither are they significantly different from the angiosperm apparent fractionation. However, the apparent fractionations for trees and shrubs differ for the *n*-C<sub>29</sub> alkane (mean tree value  $-121 \pm 22\text{‰}$ ; mean shrub value  $-99 \pm 32\text{‰}$ ; Sachse et al., 2012). The large difference between trees and shrubs for *n*-C<sub>29</sub> is attributed to the fact that shrubs are very common in dry and arid regions, and the D-enriched nature of shrub-derived leaf waxes is attributed to increased evaporative enrichment of leaf waters (Sachse et al., 2012). Why this should impact the *n*-C<sub>29</sub> and not the *n*-C<sub>27</sub> alkane is not clear. As discussed by Rees-Owen et al. (b); (Chapter 3), the size of the fossil *Nothofagus* leaves

from the Sirius Group indicates that the plants were not water-stressed, so the  $\epsilon$  value for trees is most appropriate (i.e.  $\epsilon = -108 \pm 25 \text{ ‰}$ ). Plants grown under continuous light conditions in greenhouse experiments have exhibited smaller values of  $\epsilon$  relative to plants grown under diurnal conditions (Yang et al., 2009), attributed to a 24 hour transpiration cycle. However, transpiration is dependent on both temperature and relative humidity. Temperatures for the Sirius Group were low ( $5 \text{ °C}$ ) and relative humidity for analogous modern environments in South Chile is very high (above 70 % year round), so it is likely that transpiration rates for the Sirius Group were much lower than those in the growth experiment by Yang et al. (2009). Therefore a value for  $\epsilon$  based on the global dataset is appropriate, and we use  $\epsilon = -108 \pm 25 \text{ ‰}$ .

Measured  $\delta^2\text{H}$  for the  $n\text{-C}_{27}$  alkane range between  $-298$  and  $-254 \text{ ‰}$ . We therefore convert the measured  $\delta^2\text{H}$  values to  $\delta^2\text{H}_{precip}$  using  $\epsilon = -108 \pm 25 \text{ ‰}$ . From this, we calculate that  $\delta^2\text{H}_{precip}$  ranged between  $-190$  and  $-146 \text{ ‰}$ , with a mean of  $-167 \pm 27 \text{ ‰}$ . The error is the propagated standard deviation based on the standard deviation of reported  $\epsilon$  for  $n\text{-C}_{27}$  alkane for trees ( $\epsilon = -108 \pm 25 \text{ ‰}$ ,  $n = 79$ ) and mean  $\delta^2\text{H}_{leaf}$  for the Sirius Group ( $\delta^2\text{H}_{leaf} = -275 \pm 10$ ,  $n = 14$ ).

**Seasonality of leaf wax production** There is considerable seasonal variation in the isotopic composition of precipitation (Dansgaard, 1964), therefore the seasonality of leaf wax biosynthesis will impact the interpretation of  $\delta^2\text{H}_{leaf}$  results. Broadleaf deciduous species form cuticle (and therefore leaf waxes) during the brief period of leaf expansion, and the majority of leaf wax formation reduces after this first period (Kolattukudy, 1970, Hauke and Schreiber, 1998). Several studies record varying  $\delta^2\text{H}_{leaf}$  throughout the growing season, owing to short-term changes in leaf and soil water  $\delta^2\text{H}$  (Lockheart et al., 1997, Sachse et al., 2009) or reworking of leaf waxes due to environmental stresses (Bacic et al., 2005). However, other research has shown that leaf wax  $\delta^2\text{H}$  in deciduous trees record  $\delta^2\text{H}_{precip}$  at first leaf flush, early in the growing season rather than integrating over the full growing season (Tipple et al., 2013). Deciduous shrubs in the High Arctic have a full complement of leaves within 2 - 3 weeks of the start of the growing season and become dormant within 50 - 60 days (Bliss and Matveyeva,

1992), although how this affects high latitude leaf wax formation is not clear. Based on the polar light regime, we infer that the growing season would last for no longer than 2 months (between the months December and February). The climate model used in this study predicts increased precipitation over Antarctica (>200 % increase in some areas), but the majority of this increase comes from summer precipitation (Tindall and Haywood, 2015). Therefore in our interpretation, we assume the leaf wax isotope signal integrates summer precipitation, although there is likely some bias towards more depleted (winter) precipitation isotope values because of a snow melt memory effect (Bliss and Matveyeva, 1992).

#### **4.6.2 Modelling hydrological change**

We discuss several climate model experiments in order to evaluate the climate proxy data presented in this study. Firstly, we compare palaeoprecipitation isotope values reconstructed from measured tree ring oxygen isotopes and biomarker hydrogen isotopes to values predicted by an isotope enabled General Circulation Model (GCM) in an idealised, reduced-ice, warmer world scenario (see Methods section 4.5.2). We then examine climate diagnostics within the model and implement a conservative atmospheric dye-tracer in order to examine atmospheric and hydrological changes in greater detail.

##### **4.6.2.1 Choice of boundary conditions**

The use of a full GCM for palaeoclimate modelling requires the input of boundary conditions that are not simulated as prognostics by the model, such as: ice sheet surface elevation and extent, land surface cover, continental configuration (coastlines), ocean bathymetry, land surface orography, solar insolation and atmospheric trace gases. The age uncertainty association with the Sirius Group (i.e. an age of 17 - 15 Ma *vs.* 5 - 2.5 Ma) means there is uncertainty around some of these boundary conditions; in particular, land surface orography and solar insolation. We used a mid-Pliocene Warm Period (mPWP; see Methods 4.5.2) simulation for practical and theoretical reasons, with the caveat that the modelling results are discussed in terms of an idealised reduced-ice,

warmer world scenario.

This is justified since the clearest implication from the Sirius Group sediments and fossils is that there was a significantly reduced Antarctic Ice Sheet during plant growth and sediment deposition and based on current understanding of radiative forcing and albedo, as well as atmospheric dynamics, it is likely that this is an important control on Antarctic climate (e.g. Lewis et al., 2007, 2008). The PRISM3D dataset, reconstructed for 3.264 - 3.025 Ma, includes the complete deglaciation of the West Antarctic Ice Sheet, and a significantly smaller East Antarctic Ice Sheet with most ice removal occurring in the Wilkes and Aurora sub-glacial basins (Dowsett et al., 2010, Haywood et al., 2010). Atmospheric CO<sub>2</sub> in the model (405 ppmv) is the same as reconstructed Pliocene CO<sub>2</sub> values (~400 - 450 ppm; Beerling and Royer, 2011). Atmospheric CO<sub>2</sub> during the mid-Miocene may have been much lower, although there is large uncertainty associated with this estimate (120 - 500 ppmv; Beerling and Royer, 2011), and we know climate was necessarily warmer in order for there to be vegetated land in the Oliver Bluffs region. Moreover, geological evidence indicates that episodes of maximum ice sheet loss during the mid-Miocene occurred when atmospheric CO<sub>2</sub> was at least 500 ppmv (Levy et al., 2016). Therefore, the elevated atmospheric CO<sub>2</sub> in the model (with respect to preindustrial) and reduced ice extent is consistent with both age scenarios for the Sirius Group.

There is greater uncertainty with regards to the continental configuration and orography in the model. Between 17 Ma and 2.7 Ma several tectonic reorganisations occurred that could have led to large changes in oceanic and atmospheric circulation, including the uplift of several mountain ranges and the closure of the Panama seaway (Bradshaw et al., 2012). The palaeo simulations use a pre-industrial continental configuration, which could have a small impact on ocean circulation, but modelling studies have suggested that orographic and marine gateway changes would only have had a regional effect on climate, e.g., Andean uplift in the late Miocene resulted in warmer temperatures only in that region (Bradshaw et al., 2012). Thus, any effect on Antarctic climate from imprecisely represented orography in the models boundary conditions are likely to be caused by local changes rather than orographic differences further afield,

or bathymetric uncertainty.

We emphasise that the boundary conditions used in this study are an approximation for a reduced-ice, warmer world scenario that may be Pliocene (5 - 2.5 Ma) or Miocene (17 - 15 Ma) in age, even though they are more consistent with a Pliocene age range for the Sirius Group (3 Ma).

#### **4.6.2.2 Isotopic composition of rain and snow**

Isotope theory predicts that the isotopic composition of snow will be heavier than rain condensed from an identical water vapour parcel, because there is increased fractionation during the vapour-solid transition relative to the vapour-liquid transition (i.e. the fractionation factor  $\alpha$  is larger for the condensation of solids than liquids; Merlivat and Nief, 1967). The isotope scheme used in this version of HadCM3 only applies the vapour-solid fractionation factor for condensation temperatures below  $-20\text{ }^{\circ}\text{C}$  (Tindall et al., 2009); at temperatures higher than this, the difference in equilibrium fractionation between liquid and solid is small (Dansgaard, 1964). Above this temperature in the model, differences in  $\delta^{18}\text{O}$  between rain and snow falling over Antarctica are dependent on differences in the condensation temperature, along with vapour-exchange processes as the precipitation falls. Thus it follows that for areas of Antarctica that have had ice sheet removed, precipitation will be heavier (ie. it will have a higher apparent condensation temperature) than solid precipitation (snow).

## 4.6.3 Supplementary figures

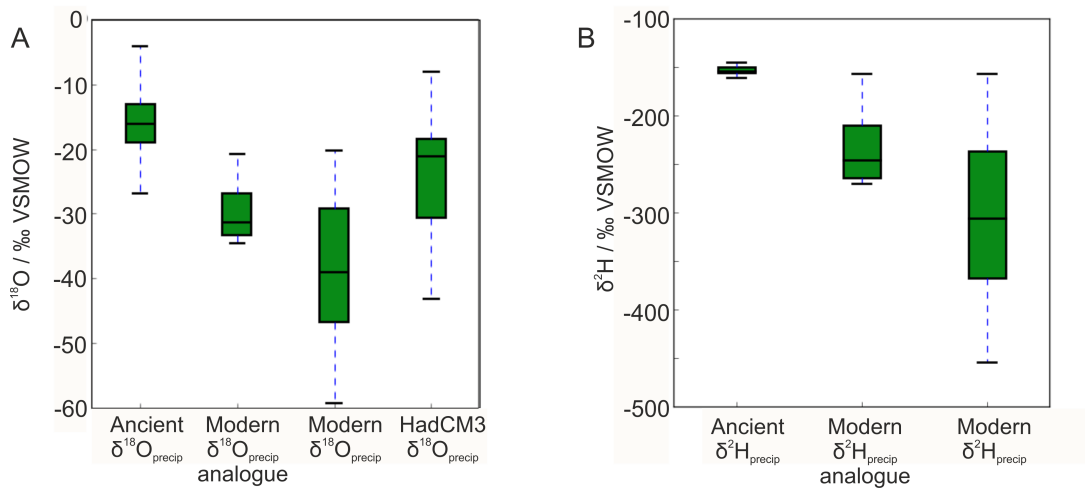


**Figure 4.7:** (A)  $\delta^{18}\text{O}$  from the Sirius Group precipitation, modern Antarctic precipitation at sites above  $75^\circ\text{S}$  and below 700 masl, precipitation over the entire continent, and simulated precipitation for deglaciated regions from the HadCM3 palaeo simulation. (B) from the Sirius Group precipitation, modern Antarctic precipitation at sites above  $75^\circ\text{S}$  and below 700 masl, precipitation over the entire continent. Modern data from Masson-Delmotte et al. (2008).

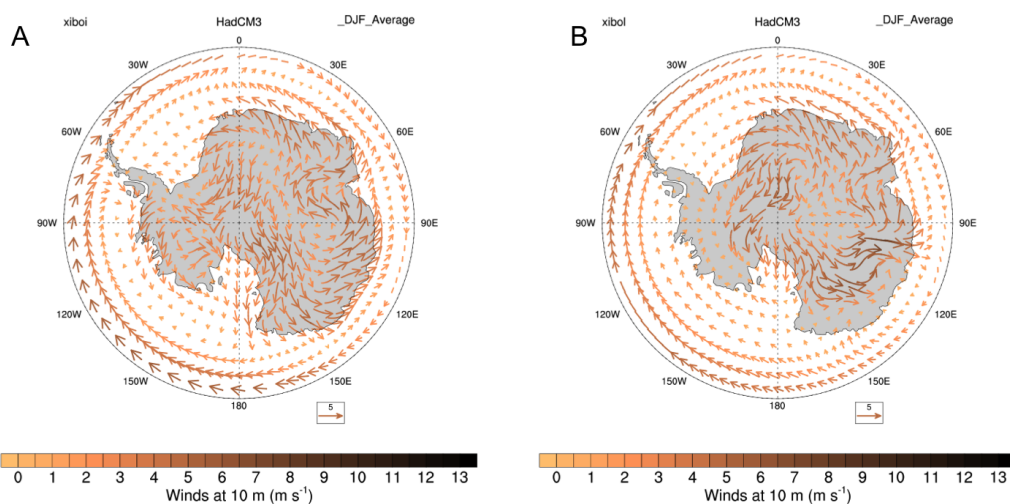


**Figure 4.8:** Seasonal (summer) mean surface wind vectors for (A) preindustrial and (B) palaeo simulations.

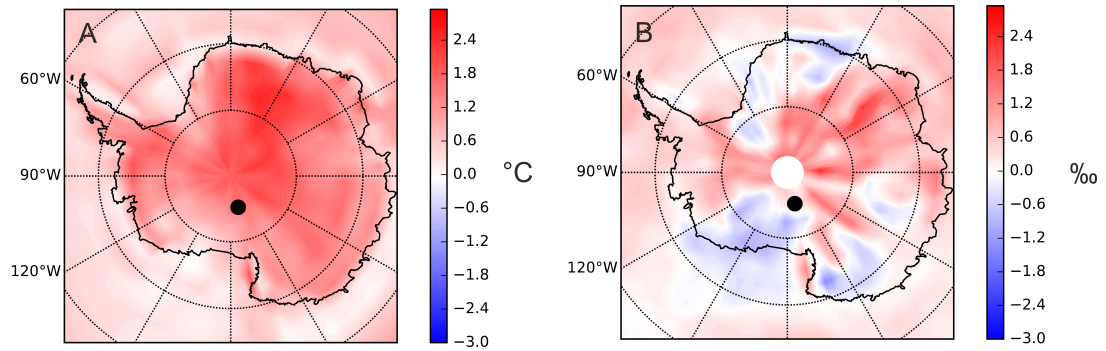


**Figure 4.9:** (A) Mean summer temperature difference for the intermediate simulation (c) with respect to the preindustrial (a) for a 30 year climate mean (taken from the last 30 years of the simulation). (B) Mean summer precipitation  $\delta^{18}\text{O}$  difference for the intermediate simulation (c) with respect to the preindustrial (a) for a 30 year climate mean (taken from the last 30 years of the simulation).

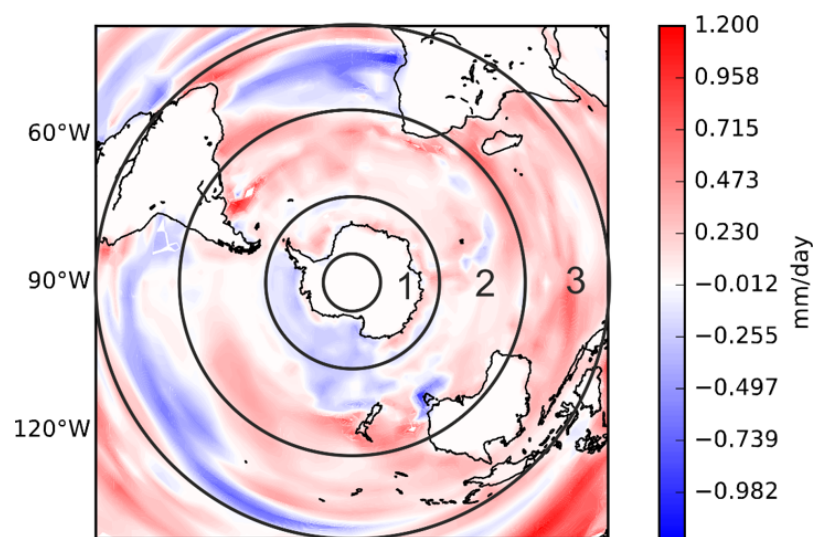


**Figure 4.10:** Latitudinal bounds for tracers superimposed over the mean summer evaporation difference for the palaeo simulation with respect to the preindustrial.

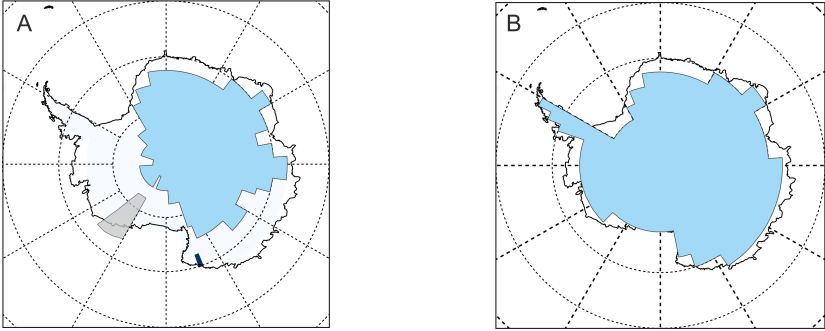


**Figure 4.11:** (A) Ice sheet extent for palaeo boundary conditions; the grey box shows the grid boxes used to calculate tracer concentrations. (B) Ice sheet extent for preindustrial boundary conditions.

## 4.6.4 Supplementary tables

**Table 4.1:** Plant leaf wax  $\delta^{13}\text{C}$  results of the samples used in this study. Data for the  $n\text{-C}_{23}$ ,  $n\text{-C}_{25}$ ,  $n\text{-C}_{27}$ ,  $n\text{-C}_{29}$  and  $n\text{-C}_{31}$  alkanes is given for each, along with the analytical error (standard deviation for duplicate or triplicate measurements). All numbers are in per mille (‰).

sample ID	$n\text{-C}_{23}$	$\sigma$	$n\text{-C}_{25}$	$\sigma$	$n\text{-C}_{27}$	$\sigma$	$n\text{-C}_{29}$	$\sigma$	$n\text{-C}_{31}$	$\sigma$
OBFH-02-1	-		-30.8	0.2	-30.5	0.2	-29.7	0.1	-	
BNLB-12-3	-28.6	0.5	-29.5	0.5	-29.6	0.2	-29.3	0.1	-30.7	0.1
OBFL-04-3	-31.7	0.7	-31.9	0.3	-29.9	0.3	-30.0	0.1	-	
WSU-13-6	-30.0	0.3	-29.6	0.2	-29.0	0.3	-29.2	0.3	-31.5	0.7
LCBA-05-36										
LCBA-05-5	-28.7	1.0	-29.8	0.4	-28.2	0.3	-29.2	1.0	-27.9	0.9
LCBA-05-17	-		-30.3	0.01	-31.3	0.4	-32.5	0.2	-34.3	0.05
OBFL-04-2	-		-30.2	1.4	-31.5	0.4	-30.1	0.4	-	
SRB-07-6	-		-29.1	1.1	-29.8	0.3	-29.4	0.6	-	
SRB-07-5										
OBFL-4-23	-30.8	0.8	-31.0	0.5	-31.3	0.2	-30.7	0.1	-31.8	0.6
OBFL-04-29	-29.0	0.5	-29.8	0.3	-30.0	0.1	-31.9	0.1	-33.6	0.5
OBFL-04-32	-29.5	0.7	-30.1	0.1	-28.9	0.04	-28.3	0.3	-	
OBFL-04-25	-29.8	0.01	-29.5	0.2	-28.9	0.0	-28.7	0.2	-	
SPBW-09-27	-30.2	0.6	-29.9	0.2	-29.5	0.2	-29.2	0.4	-30.8	0.3
OBFL-04-13	-30.7	0.2	-30.5	0.4	-30.4	0.1	-30.0	0.05	-	

**Table 4.2:** Plant leaf wax  $\delta^2\text{H}$  results of the samples used in this study. Data for the  $n\text{-C}_{23}$ ,  $n\text{-C}_{25}$ ,  $n\text{-C}_{27}$ ,  $n\text{-C}_{29}$  and  $n\text{-C}_{31}$  alkanes is given for each, along with the analytical error (standard deviation for duplicate or triplicate measurements). All numbers are in per mille (‰).

sample ID	$n\text{-C}_{23}$	$\sigma$	$n\text{-C}_{25}$	$\sigma$	$n\text{-C}_{27}$	$\sigma$	$n\text{-C}_{29}$	$\sigma$	$n\text{-C}_{31}$	$\sigma$
OBFH-02-1	-164.6	14.6	-264.5	7.5	-265.9	1.4	-267.4	-	-200.8	1.8
BNLB-12-3	-178.8	11.5	-283.3	5.9	-298.9	1.0	-284.3	7.5	-284.5	1.8
OBFL-04-3	-217.9	5.5	-278.3	0.6	-275.9	0.2	-266.1	8.9	-251.2	1.2
WSU-13-6	-228.0	24.0	-308.8	0.5	-290.4	0.9	-294.2	4.0	-294.3	13.9
LCBA-05-36										
LCBA-05-5	-200.1	22.3	-250.3	1.2	-254.0	0.5	-261.5	0.3	-252.1	1.5
LCBA-05-17	-228.5	14.2	-263.6	15.2	-269.1	3.2	-266.7	8.3	-270.5	4.9
OBFL-04-2	-261.5	3.8	-235.2	5.4	-276.2	4.8	-231.6	5.3	-149.7	11.1
SRB-07-6	-264.2	-	-263.9	7.5	-274.7	4.0	-269.0	1.9	-269.2	-
SRB-07-5										
OBFL-4-23	-281.5	11.6	-283.7	4.5	-273.0	0.3	-273.3	1.7	-266.5	1.8
OBFL-04-29	-235.8	27.9	-279.8	4.4	-281.4	0.7	-285.3	0.8	-281.2	3.8
OBFL-04-32	-234.8	13.3	-277.7	2.1	-269.4	1.5	-276.4	1.2	-285.3	5.9
OBFL-04-25	-282.6	2.8	-281.7	0.7	-277.1	1.2	-281.5	2.4	-273.0	7.9
SPBW-09-27	-313.4	1.7	-284.4	6.3	-273.4	1.0	-273.5	6.4	-262.4	17.7
OBFL-04-13	-265.9	8.5	-284.4	3.8	-275.2	0.5	-277.6	3.1	-279.2	5.6

## Chapter 5

# Conclusions, wider implications and future work

### 5.1 Revisiting the aims and objectives

The aim of this thesis was to explore in detail Antarctic vegetation and climate during a period of East Antarctic Ice Sheet (EAIS) retreat. This overall aim was broken down into six research questions in Chapter 1 (see table 5.1, reproduced from Chapter 1). Each research chapter (Chapters 2, 3 and 4) dealt with at least one research question, using a combination of geochemical techniques and climate modelling with a general circulation model. In this chapter I summarise the results presented. The overall conclusions and wider implications are discussed, and the possibilities for future work are reviewed.

### 5.2 Answering the research questions

#### 5.2.1 Can a geochemical approach advance understanding of local and regional vegetation community structures? (Chapter 2)

In agreement with the macrofossil record (Ashworth and Cantrill, 2004), vegetation reconstructions using higher plant-derived biomarkers indicate a diverse vegetation,

**Table 5.1:** Research questions addressed in this thesis (reproduced from Chapter 1).

Research question	Chapter
1. Can a geochemical approach advance understanding of local and regional vegetation community structures?	2
2. What were continental temperatures during EAIS retreat?	2
3. Can oxygen isotopes in Antarctic fossil prostrate trees be used to trace hydrological change?	3
4. Were there changes in carbon cycling during EAIS retreat?	3
5. Was there a different hydrological cycle during EAIS retreat?	4

consisting of woody plants (angiosperms), which grew alongside mosses and cushion plants, as well as peat-forming plants (possibly *Sphagnum* mosses) and algal mats. There is considerable local spatial heterogeneity in the plant distributions; i.e. some samples are dominated by angiosperm input, others by peat-forming plants or algal mats. The patchy distribution is analogous to mosaic patterns seen in the Arctic, where local variations in drainage, temperature and nutrient availability control local plant growth (Bliss and Matveyeva, 1992).

While evidence for the persistence of angiosperms on Antarctica into the Neogene is very clear, discrepancies between the pollen and plant macrofossil record at Oliver Bluffs (Ashworth and Cantrill, 2004, Askin and Markgraf, 1986, Francis and Hill, 1996) and elsewhere on Antarctica (Ashworth et al., 2007, Hambrey et al., 2003, Lewis et al., 2008) have raised questions over the presence of conifers on the continent. The presence of conifer-specific biomarkers in the Sirius Group sediments support conifer growth (possibly podocarp) on the continent, albeit at a site proximal to Oliver Bluffs where aeolian or water-driven transport delivered lipids to the sediments. A similar discrepancy is seen between the Miocene macrofossil record in the McMurdo Dry Valleys (Ashworth and Cantrill, 2004, Ashworth et al., 2007, Lewis et al., 2008), which did not find evidence for conifers, and the ANDRILL-2A core in the Ross Sea, which included abundant coniferous palynomorphs (Griener et al., 2015, Warny et al., 2009). This would suggest that during the Neogene, conifers occupied a specific niche, such as upland sites, which have since been obscured by ice sheet expansion.

This thesis is the first organic geochemical study of Antarctic vegetation. It has provided new floral results that provide novel constraints on questions around the evolution of vegetation on Antarctica. Importantly, in contrast to the macrofossil record, the presence of aromatised diterpenoids show clearly the presence of conifers at or near the Oliver Bluffs site, probably Podocarpaceae. As discussed, the age of the deposits presents some difficulty. If these results date from the Miocene, then this result is highly consistent with marine sediment-derived pollen records showing Podocarpaceae on the Antarctic coast (Warny et al., 2009). However, if they are Pliocene, then the results are much more significant and suggest that present understanding of Antarctic vegetational evolution is lacking. Moreover, these new data highlight the complexities of Antarctic biosphere dynamics, and shows the value of using chemotaxonomy to study ancient vegetation. This result also highlights the importance of using a multi-method approach for understanding the evolution of vegetation, where taphonomic biases can skew the fossil record, but have no effect on the lipid record (and *vice versa*).

### **5.2.2 What were continental temperatures during EAIS retreat? (Chapter 2)**

To fully examine Antarctic climate during EAIS retreat, it is necessary to have precise constraints on continental temperatures. Previous studies reconstructing Neogene Antarctic continental temperatures relied on the lower temperature limits of modern relatives of fossils found in the Sirius group strata (freshwater molluscs, listroderine weevils, extant *Nothofagus* species; Ashworth and Preece, 2003, Ashworth and Kuschel, 2003, Francis and Hill, 1996, Hill and Jordan, 1996, Hill and Trustwell, 1993, Hill et al., 1996, Webb and Harwood, 1993). However, fossil-derived temperature reconstructions are generally found to be less precise than geochemical temperature reconstructions (Ballantyne et al., 2005). Using a geochemical palaeothermometer could provide further constraints on continental temperatures. To this end, the MBT<sup>c</sup>/CBT palaeothermometer, based on distributions of soil bacteria-derived cell membrane lipids (br-GDGTs; Weijers et al., 2007, Sinninghe Damsté et al., 2011), was applied to Sirius Group sediments.

Application of this proxy to Sirius Group strata gives a temperature of  $5.0 \pm 2.5$  °C, normally assumed to be the mean annual air temperature. Given the polar light regime and therefore extremely cold winter temperatures, it seems likely that there was a strong summer bias in the production of bacterial lipids. Similar high latitude studies (in both hemispheres) during the Eocene also inferred a summer bias in the proxy at these latitudes (Eberle et al., 2010, Pross et al., 2012, Weijers et al., 2007). Therefore, a strong summer-seasonal or even warm monthly bias seems probable for the temperature calculations in this study. The reconstructed temperatures are in good agreement with the lower summer temperature limits inferred from fossil plants, molluscs and insects ( $\sim 5$  °C; Ashworth and Preece, 2003, Ashworth and Kuschel, 2003, Francis and Hill, 1996, Hill and Jordan, 1996, Hill and Trustwell, 1993, Hill et al., 1996, Webb and Harwood, 1993).

These findings are also in generally good agreement with longer-term pollen-based records of Antarctic temperatures throughout the Neogene, suggesting continental summer temperatures of 4 - 12 °C (Prebble et al., 2006, Warny et al., 2009). This indicates that during the mid- to late-Neogene, Antarctica was at least 10 °C warmer than today (present-day summer temperatures of -3.4 °C), with a strongly seasonal climate. For the majority of the year, temperatures would have been well below freezing such that most vegetation remained dormant. For at least two months of the year summer temperatures reached levels warm enough to sustain photosynthesis and provide sufficient water, significantly impacting the biological and hydrological regime of the deglaciated areas of the continent.

### **5.2.3 Can oxygen isotopes in Antarctic fossil prostrate trees be used to trace hydrological change? (Chapter 3)**

In combination with fossil data, the biomarker evidence in Chapter 2 indicates that a tundra shrub grew during EAIS retreat, when summer temperatures reached  $\sim 5$  °C. This poses intriguing questions over the nature of the hydrological cycle that could have supported such vegetation, and whether it functioned differently in response to

the warmer temperatures and reduced ice sheet. For reconstructing past hydrological cycling, the prostrate *Nothofagus* trees recovered from the Sirius Group sediments therefore present a unique opportunity to examine hydrological change on Antarctica through the reconstruction of precipitation isotopes from tree ring cellulose. This approach not only provides novel insights into Antarctic palaeoclimate, but also presents a challenge, as prostrate trees have never before been utilised in tree ring isotope studies. Nearest living relatives of the fossil *Nothofagus* growing in both arboreal and prostrate form at the southernmost limit of their range (Tierra del Fuego, Chile) offer an opportunity to test whether tree ring cellulose oxygen isotopes ( $\delta^{18}\text{O}_{\text{cell}}$ ) in prostrate trees function as a proxy for precipitation isotopes ( $\delta^{18}\text{O}_{\text{precip}}$ ).

Measurements of  $\delta^{18}\text{O}_{\text{cell}}$  extracted from two species of modern *Nothofagus* do appear to record  $\delta^{18}\text{O}_{\text{precip}}$ . In particular, using the model linking  $\delta^{18}\text{O}_{\text{cell}}$  and  $\delta^{18}\text{O}_{\text{precip}}$  by Anderson et al. (2002), it can be shown that over a climate mean period (30 years), both arboreal and prostrate trees recorded  $\delta^{18}\text{O}_{\text{precip}}$  reasonably well. Prostrate trees exhibited considerably lower inter-tree variability, likely due to their short stature and decreased path length (Barrera et al., 2000, Korner, 2003), which implies that morphology does not have an impact on  $\delta^{18}\text{O}_{\text{cell}}$ . Thus it is concluded that they are highly suitable archives of long-term (averaged) climate records. This result is particularly important because it potentially makes end-member (high altitude and latitude) environments more accessible for tree ring isotope-based climate reconstructions using prostrate trees.

Application of the same technique to the Antarctic fossil *Nothofagus* yields intriguing results, giving  $\delta^{18}\text{O}_{\text{precip}}$  of -16 ‰. This is significantly depleted relative to  $\delta^{18}\text{O}_{\text{precip}}$  at Tierra del Fuego, consistent with the very high latitude of the Antarctic plants. Furthermore, comparison with modern Antarctic  $\delta^{18}\text{O}_{\text{precip}}$  (mean -28 ‰; Masson-Delmotte et al., 2008) suggests that Neogene palaeoprecipitation over Antarctica was significantly enriched relative to the present day (Fig. 5.1). This result is indicative of a markedly different Antarctic hydrological cycle, and it is tempting to invoke a number of plausible mechanisms as its cause:

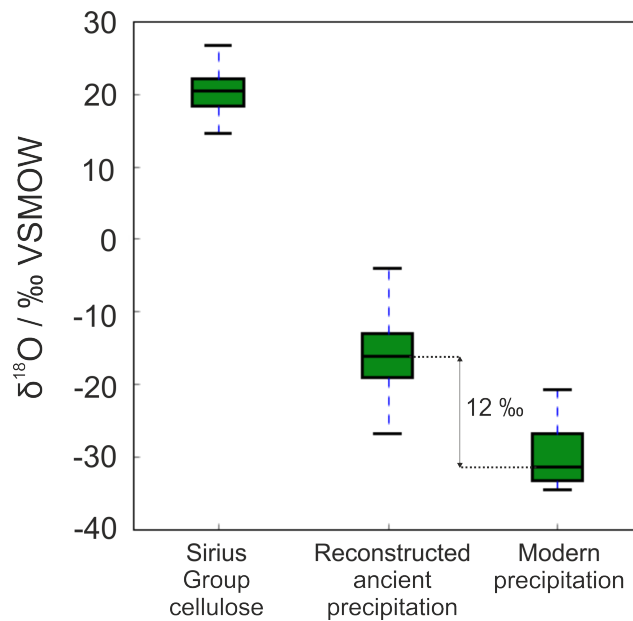


**Figure 5.1:** Cellulose  $\delta^{18}\text{O}$  from the Sirius Group fossil *Nothofagus*, with modelled  $\delta^{18}\text{O}$  of palaeo precipitation and modern Antarctic snow. Modern measurements from Masson-Delmotte et al. (2008); data restricted to  $>75^\circ\text{S}$  and below 700 masl. The median is given by the line, the first and third quartiles by the box, and the whiskers denote the full range of data. Reproduced from Chapter 3.

1. Increased condensation temperatures leading to decreased discrimination against  $^{18}\text{O}$ ;
2. Change to a local, high latitude moisture source region, which would considerably shorten vapour transport pathways;
3. Change in atmospheric circulation, altering transport and delivery of moisture.

The list of proposed mechanisms is not exhaustive, and full consideration of mechanisms using an isotope-enabled general circulation model was later used to shed light on these new data (Chapter 4).

#### 5.2.4 Were there changes in carbon cycling during EAIS retreat? (Chapter 3)

There appears to have been long-term coupling between the carbon cycle and EAIS dynamics throughout the Neogene (Shevenell et al., 2008). In particular, the EAIS exhibited a threshold for collapse at atmospheric  $\text{CO}_2$  levels above  $\sim 500$  ppmv during the

mid-Miocene (Gasson et al., 2016, Levy et al., 2016) and perhaps 400 ppmv during the Pliocene (Beerling and Royer, 2011). Reconstructing atmospheric carbon isotope ratios ( $\delta^{13}\text{C}_{atmos}$ ) from tree ring carbon isotope ratios ( $\delta^{13}\text{C}_{cell}$ ) could elucidate the carbon cycling mechanisms at play during EAIS retreat, as well as provide broad constraints on the age of the fossil plants by correlation with other records of  $\delta^{13}\text{C}_{atmos}$ .

Atmospheric  $\delta^{13}\text{C}$  is rarely reconstructed from plants because of concerns about competing environmental effects (Farquhar et al., 1989a). Thus, the ability of modern *Nothofagus* to record  $\delta^{13}\text{C}_{atmos}$  was first tested. Similar to the oxygen isotope results from Chapter 3 (research question 3), we find that at interannual resolution,  $\delta^{13}\text{C}_{cell}$  in two species of *Nothofagus* is dominated by tree-level rather than stand-level signals. However, again in agreement with the oxygen isotope results, the  $\delta^{13}\text{C}_{cell}$  climate mean (30 years) is an excellent record of mean  $\delta^{13}\text{C}_{atmos}$  (measured  $\delta^{13}\text{C}_{atmos} = -7.96 \pm 0.24$  ‰; reconstructed  $\delta^{13}\text{C}_{atmos} = 8.3 \pm 0.2$  ‰ from arboreal trees,  $-8.0 \pm 0.2$  ‰ from prostrate).

While it is impossible to completely rule out the effect of environmental controls on  $\delta^{13}\text{C}_{cell}$  and therefore  $\delta^{13}\text{C}_{atmos}$ , the reconstructed palaeo-archive of  $\delta^{13}\text{C}_{atmos}$  from Antarctic fossil plants shows that  $\delta^{13}\text{C}_{atmos}$  was significantly enriched ( $-4.4$  ‰) relative to modern  $\delta^{13}\text{C}_{atmos}$  ( $-7.96$  ‰). It is difficult to draw direct comparisons between the findings from this study and the Cenozoic record of  $\delta^{13}\text{C}_{atmos}$  based on marine biogenic carbonates because the timescale represented by the plant-based record is considerably shorter than the 3 Ma smoothing period of the marine record (Tippie et al., 2010). Moreover, the size of the dissolved inorganic carbon pool in the ocean would serve to dampen the response of carbon isotope ratios in benthic foraminifera to rapid and large atmospheric changes. Nevertheless, the plant-based  $\delta^{13}\text{C}_{atmos}$  record presented in this thesis is closer to calculated  $\delta^{13}\text{C}_{atmos}$  values for the mid-Miocene than the Pliocene (Tippie et al., 2010), and is very consistent with large, short-lived positive carbon isotope excursions seen in the middle-Miocene benthic carbon isotope record which correspond to EAIS minima (Holbourn et al., 2014, 2015, Levy et al., 2016). The  $\delta^{13}\text{C}_{atmos}$  data clearly represent an anomalously heavy and highly variable atmospheric carbon pool during a period of EAIS retreat, of a magnitude and timescale that is com-

patible with middle Miocene carbon cycle dynamics. These findings cannot definitively explain why such an increase in  $\delta^{13}\text{C}_{atmos}$  would occur, but if (as is suggested by the EAIS and  $\text{CO}_2$  record by Levy et al., 2016) this corresponds to a positive excursion in the marine record too, some mechanisms that would serve to deplete  $\delta^{13}\text{C}_{atmos}$ , but that are inconsistent with elevated  $\text{CO}_2$  could be discounted; for example, increased organic matter burial in marine sediments resulting in  $\text{CO}_2$  drawdown (e.g. Badger et al., 2013).

### 5.2.5 Was there a different hydrological cycle during EAIS retreat? (Chapter 4)

Chapter 3 (research question 3) presented tree ring  $\delta^{18}\text{O}_{cell}$  data which suggested that precipitation isotopes on Antarctica during a period of EAIS retreat (mean = -16 ‰) were significantly enriched relative to the modern (mean = -28 ‰; Masson-Delmotte et al., 2008). This is an intriguing result from which we can infer a markedly different Antarctic hydrological cycle compared to the present day. Chapter 4 builds on this result in two ways: firstly, by employing a second, independent proxy for precipitation (hydrogen isotopes,  $\delta^2\text{H}_{precip}$ ), which enables a deeper analysis of hydrological cycling; and secondly, climate analysis using HadCM3, an oxygen isotope-enabled atmosphere-ocean-vegetation General Circulation Model (GCM), to explore mechanisms underlying this hydrological change.

The leaf wax hydrogen isotope-based reconstructions of  $\delta^2\text{H}_{precip}$  are in good agreement with the  $\delta^{18}\text{O}_{precip}$  analysis from Chapter 3. This second dataset is also significantly enriched relative to modern Antarctic precipitation (-240 ‰ for modern, Masson-Delmotte et al., 2008; -170 ‰ for a warmer world with a reduced AIS, this study). The two datasets are internally consistent, giving confidence that both are recording a primary signal (Fig. 5.2A). Furthermore, by including the temperature calculations from Chapter 2, both isotope systems exhibit a significant shift away from the modern linear temperature-isotope relationship (Figs. 5.2B and C), indicating a considerable reorganisation of the Antarctic hydrological cycle.

To examine these data further, simulations from the isotope-enabled GCM HadCM3 were analysed (summarised below and discussed in more detail in Supplementary Information 3):

- (a) Preindustrial: A control experiment run with standardised preindustrial boundary conditions including a modern continental configuration, full ice-sheets and modern orbital parameters. Atmospheric CO<sub>2</sub> was set to 280 ppmv.
- (b) Palaeo: A palaeo simulation, previously published by Tindall and Haywood (2015), which was set up with mid-Pliocene Warm Period (mPWP) boundary conditions: 1/3 smaller ice sheet, mPWP vegetation and orography, and atmospheric CO<sub>2</sub> was set to 405 ppmv. The continental configuration (coastlines), ocean bathymetry and river outflow points were kept as pre-industrial.
- (c) PalaeoCO<sub>2</sub> - An intermediate simulation run in order to distinguish between the impacts of greenhouse-gas controlled radiative forcing and ice sheet extent on Antarctic climate. Atmospheric CO<sub>2</sub> was set to 405 ppmv at the end of the preindustrial simulation (a), all other boundary conditions were kept the same as in (a).
- (d) Dye-tracer enabled simulations: Surface air parcels were tagged in the model as an approximation for tracing moisture sources, run only for simulations (a) and (b).

Interrogation of the model results shows that whilst precipitation over the Polar Plateau maintains the same linear relationship, in good agreement with the proxy data, HadCM3 simulates a shift in the temperature-isotope relationship over deglaciated regions of Antarctica remarkably similar to that seen in the isotope data. In contrast to work on the early- to mid-Miocene by Feakins et al. (2012), results from modelling experiments using atmospheric tracers to tag (or dye) air parcels suggest that very little change in moisture source region occurred. Some increases in moisture derived from the Weddell Sea (with corresponding decreases from the Ross Sea region) may play a small role. More importantly, however, corresponding large increases in temperature

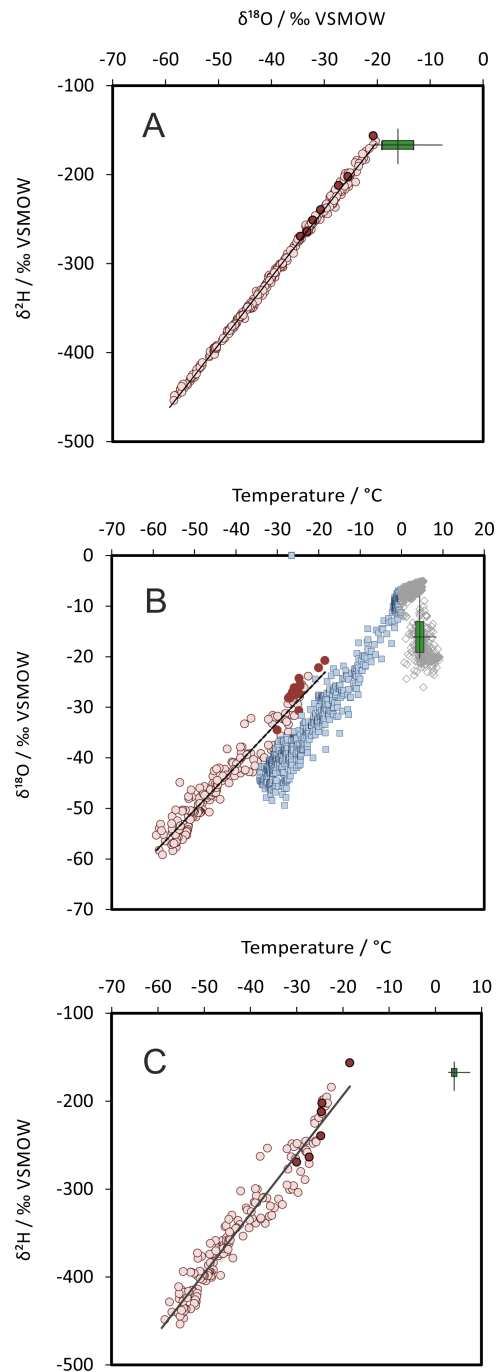


**Figure 5.2:** (A) The relationship between  $\delta^{18}\text{O}$  and  $\delta^2\text{H}$  for modern Antarctic snow (open pink circles) demonstrating the linear relationship between  $\delta^{18}\text{O}$  and  $\delta^2\text{H}$  at high latitude (local meteoric water line). Filled red circles are modern data for sites south of  $75^\circ\text{S}$  and below 700 m above sea level. Sirius Group data is summarised by the green box and whisker plot in the x- and y- directions showing median (line), 25<sup>th</sup> and 75<sup>th</sup> (box) and range (error bars). Modern data from Masson-Delmotte et al. (2008). (B)  $\delta^{18}\text{O}$  versus temperature for modern Antarctic snow (Masson-Delmotte et al., 2008), Sirius Group data (green box and whiskers, as in panel A) and data from the palaeo HadCM3 climate model simulation (blue squares for grid cells where surface temperature  $< 0^\circ\text{C}$  and grey diamonds for surface temperature  $> 0^\circ\text{C}$ ). (C)  $\delta^2\text{H}$  and surface air temperature in modern Antarctic snow (Masson-Delmotte et al., 2008), with Sirius Group data indicated by the box and whisker plot, as in panel (A). Reproduced from Chapter 4.

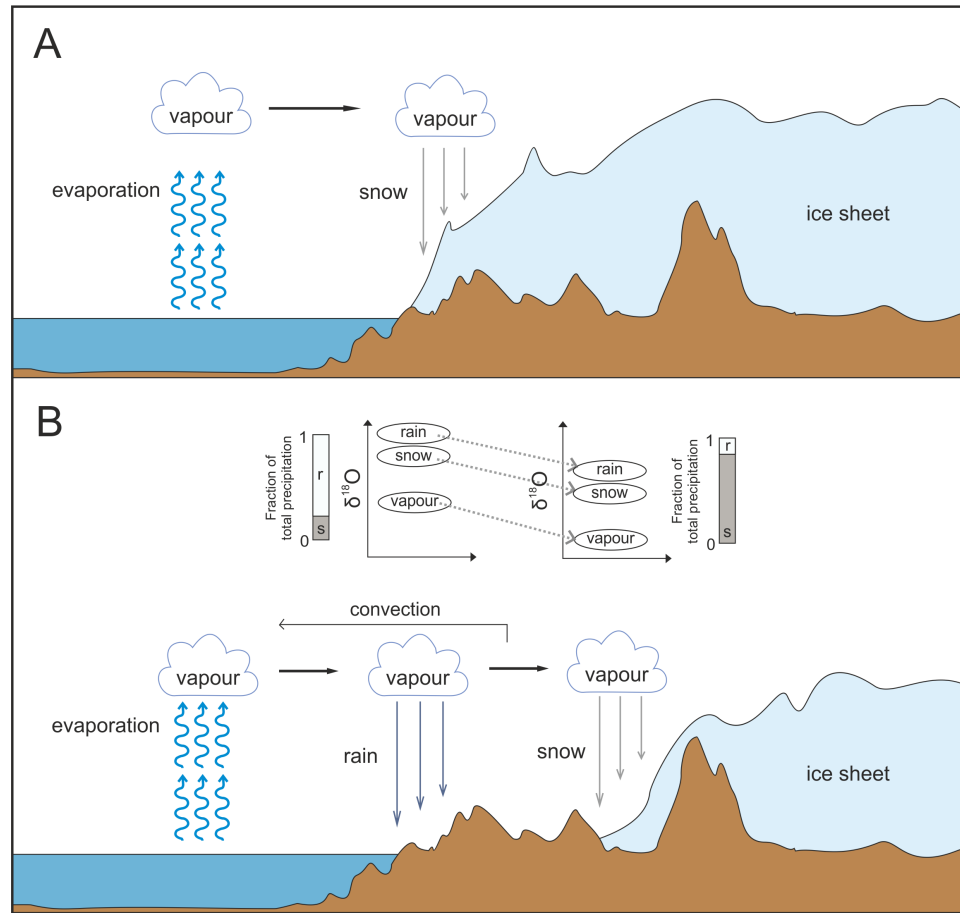


**Figure 5.3:** (A) Current precipitation regime over Antarctica, where all precipitation falls as snow. (B) Inferred precipitation regime under reduced ice sheet conditions where precipitation falls as rain over deglaciated coastal areas, depleting the remaining vapour as it moves inland relative to scenario (A). Reproduced from Chapter 4.

(up to 16 °C) and changes to precipitation (condensing as rain and snow over these deglaciated regions) imply significant local climatic shifts may be the driving force. Both the equivalent HadCM3 pre-industrial and intermediate simulation with full ice sheet and elevated CO<sub>2</sub> (405 ppmv) maintain the traditional linear temperature-isotope relationship. These results show that the Antarctic hydrological cycle and climate is highly sensitive to ice sheet extent and perhaps far less directly sensitive to radiative forcing. From the combined data and model findings of Chapters 3 and 4, I propose a general mechanism for a switch in hydrological regime at high latitudes regions that have undergone deglaciation (given in Fig. 5.3), described below.

**Present day regime:** A one-stage process, in which precipitation falls as snow over the coast; transport of moisture further inland is precluded by the orography of

both the Transantarctic Mountains and the ice sheet. The isotopic composition of the precipitation is governed by temperature, with secondary controls by altitude, and distance from the coast (Dansgaard, 1964). This mechanism produces the well-known empirical linear temperature-isotope relationship, which is widely used in reconstructions of temperatures from ice core records (e.g. Bradley et al., 2013).

**Reduced ice regime:** A two-stage process. Decreasing surface albedo upon after removal of the ice sheet leads to highly elevated temperatures over deglaciated regions. Condensation temperatures over the coastal regions in particular are sufficiently warm that over these ice-free areas, water precipitates as rain instead of snow. The isotopically heavier rain (Field et al., 2010) depletes the remaining water vapour such that precipitation falling further inland (as snow) is relatively more depleted than snow condensing from an identical vapour parcel under the present-day regime.

This is the first study to provide a comprehensive analysis of Antarctic hydrological cycling using both data and an isotope-enabled fully coupled ocean-atmosphere GCM.

### 5.2.6 What are the bigger implications of this work?

The ice sheet driven hydrological switch discussed in Chapter 4 (Rees-Owen et al., *in prep-c*) clearly has numerous implications for understanding both the past, and future of Earth's climate. These are listed below (and discussed further in section 5.4):

#### **Implication 1: Temperature reconstructions of Quaternary interglacials from ice core records**

Numerous records show that there are regions of the Antarctica that are particularly prone to deglaciation (Raymo and Mitrovica, 2012). The change in the ratio of rain to snow may be dependent on ice sheet extent, among other, untested variables, including ice sheet elevation, sea ice extent and the height of the inversion. However, isotope-based temperature calculations from ice core records proximal to these deglaciation-prone regions may underestimate the temperature of Quaternary interglacials by up to 20° C. Specifically, the following core locations are particularly likely to be affected: Taylor Dome, WAIS Divide and Byrd Land. This is broadly in agreement with analysis

by Sime et al. (2009) who found spatial variability in the temperature-isotope relationship over the Polar Plateau also leading to underprediction of interglacial temperatures.

**Implication 2: Past oxygen isotope composition of sea-water**

Estimates of past sea level changes are frequently based on the  $\delta^{18}\text{O}$  signal of benthic foraminifera (Miller et al., 2012, Rohling et al., 2014), which in part record  $\delta^{18}\text{O}$  of sea-water, itself governed by ice volume. These calculations are underpinned by the assumption that the isotopic budget of the Antarctic Ice Sheet does not vary with climate. Recently, Winnick and Caves (2015) proposed that during the mid-Pliocene Warm Period (mPWP; 3.3 - 2.9 Ma), the Antarctic ice sheet  $\delta^{18}\text{O}$  was 1 - 4 ‰ higher than present day as a result of warmer Antarctic temperatures, and as a result, estimates of mPWP sea level from benthic  $\delta^{18}\text{O}$  may be too high. The enrichment in precipitation isotopes from Chapters 3 and 4 support these conclusions to some extent, but the effect may be somewhat modulated by the precipitation regime switch. This suggests that Antarctic Ice Sheet  $\delta^{18}\text{O}$  was still elevated relative to the present day, but less so than predicted by Winnick and Caves (2015). However, it should be emphasised here that these data are representative only of one episode of ice sheet retreat, and clearly there are many climate signals and mechanisms that require resolving to quantify the effect for each specific time period.

**Implication 3: Ice sheet-climate feedbacks** A switch to precipitation falling as rain over deglaciated regions of Antarctica may have as yet-unexplored consequences with respect to ice sheet-climate feedback mechanisms. Precipitation falling as rain would affect existing snow and ice melt, firstly and most simply because rain is warmer than snow and hence may encourage further snow melt. Secondly, if rain were falling on pre-existing ice, then further feedback mechanisms could be implemented, such as enhancing hydrofracturing and meltwater ponds. Meltwater ponds also have lower albedo relative to a frozen ice surface (0.15 - 0.45 for meltwater, 0.52 - 0.87 for snow-covered ice; Polashenski et al., 2012), which would further enhance positive feedbacks. An exploration of these effects is beyond the scope of this thesis, but their implication is clear: we need to know whether a precipitation regime switch negatively affects ice sheet regrowth following collapse.

**Implication 4: Hydrological cycling under future warming scenarios** Given implication 3 (above), it seems clear that AIS retreat instigates hydrology-based feedbacks that could play a role in determining ice sheet regrowth (or indeed, further ice sheet retreat). The future of the AIS under increasing anthropogenically induced radiative forcing in the coming decades and centuries is uncertain (Pritchard et al., 2012, Shepherd et al., 2012). However, recent ice sheet model developments suggest that the AIS does exhibit considerable sensitivity to greenhouse gas forcing under some future emissions scenarios (Pollard et al., 2015, Pollard and Deconto, 2016). Therefore the two-stage precipitation mechanism proposed in Chapter 4 could play an important role in future AIS retreat scenarios, although clearly this mechanism needs to be explored in far greater detail.

### 5.3 Scientific advances and overall conclusions

The work in this thesis was intended to address several unknowns and outstanding uncertainties surrounding Antarctic palaeoclimate and vegetation during AIS retreat, summarised in Table 5.2. The combination of diverse geochemical techniques applied to the unique samples used in this investigation, and general circulation modelling, allowed new, broad-ranging information to inform and take forwards our understanding of Antarctic palaeoclimate. Multiple scientific advancements have been made while carrying out the research for this thesis and are summarised below (Table 5.3).

With a few notable exceptions focused on the early Miocene (Feakins et al., 2012, Warny et al., 2009), previous studies documenting Neogene Antarctic terrestrial climate change have largely been limited to qualitative comparisons between fossils found in numerous terrestrial deposits and their nearest living relatives (Ashworth and Preece, 2003, Ashworth and Kuschel, 2003, Francis and Hill, 1996, Hill and Jordan, 1996, Hill and Trustwell, 1993, Hill et al., 1996, Webb and Harwood, 1993), or similar qualitative comparisons between palaeosols and modern high latitude soils (Retallack et al., 2001). Although each of the proxies used have their own associated uncertainties (discussed in

**Table 5.2:** Summary of the outstanding uncertainties in the published research undertaken to understand Antarctic palaeoclimate and vegetation during EAIS retreat, forming the basis of this thesis. Reproduced from Chapter 1.

Outstanding uncertainties in the research carried out to date
1. Uncertainties over the composition of Neogene Antarctic vegetation communities due to discrepancies between the macrofossil and pollen record in both terrestrial and marine geological records.
2. Lack of geochemical-based temperature data to provide more precise, quantitative estimates of continental temperatures during ice sheet retreat.
3. Prostrate fossil trees could provide novel proxy archives of environmental signals but it is unknown whether tree ring isotopes in prostrate trees or shrubs record climate signals.
4. Limited understanding of carbon cycle dynamics during EAIS retreat, although ice sheet fluctuations are known to be linked to atmospheric CO <sub>2</sub> levels.
5. No constraints in hydrological change during EAIS retreat or detailed examination of Antarctic climate response to EAIS retreat: the only Neogene Antarctic hydrological reconstruction to date is too early (20 - 15 Ma) and has no temporal resolution.

detail in Chapters 2, 3 and 4 and corresponding Supplementary Information sections 2 and 3), the data presented here represent the first quantitative geochemical study of a Neogene Antarctic setting. Unfortunately, poor temporal resolution within the studied horizon precludes an in-depth analysis of climate evolution during such an ice sheet retreat event. Nevertheless, the approach for reconstructing climatic change used in this thesis (documented particularly in Chapter 4) still provides a detailed understanding of many of the studied climatic changes.

When considered together, the climate proxy data presented in this investigation (temperature in Chapter 2, precipitation isotopes in Chapters 3 and 4) provide clear and internally consistent evidence for climatic and hydrological change on the continent during EAIS retreat. In short, these data show strong evidence for a warmer, wetter Antarctica. Furthermore, these conditions supported a low diversity mixed vegetation (Chapter 2), and correspond to a clearly dynamic carbon cycle, evidenced by anomalously high and variable atmospheric  $\delta^{13}\text{C}$  (Chapter 3). The carbon cycle dynamics are probably linked to fluctuations in atmospheric CO<sub>2</sub>, which itself is tightly coupled to the

**Table 5.3:** Summary of the progress made in advancing the science of this field and in addressing the uncertainties raised in Table 5.2.

Progress made in this thesis	Chapter
1. For the first time, biomarker analysis was applied to the Sirius Group sediments to successfully constrain vegetation communities growing on the continent.	2
2. The MBT'/CBT palaeothermometer was used to reconstruct continental temperatures on Antarctica, giving summer temperatures of 5 °C. This is the first application of a quantitative palaeothermometer to terrestrial Antarctic Neogene sediments.	2
3. The same data was used to support previous conclusions that at high latitudes, the MBT'/CBT proxy has a strong summer bias, in contrast to the mid-latitudes, where it records mean annual air temperatures.	2
4. Tree ring cellulose isotopes (carbon and oxygen) in modern analogue prostrate <i>Nothofagus</i> trees from Tierra del Fuego, Chile, suggested for the first time that prostrate plants record climate signals.	3
5. Atmospheric $\delta^{13}\text{C}$ was reconstructed using tree ring $\delta^{13}\text{C}$ from fossil <i>Nothofagus</i> from the Sirius Group, giving $\delta^{13}\text{C} = 4.5\text{‰}$ . This was used to broadly infer carbon cycle dynamics during EAIS retreat.	3
6. The same data was used as a novel constraint on the Sirius group age problem.	3
7. Two proxies for precipitation isotopes (tree ring $\delta^{18}\text{O}$ and plant leaf wax $\delta^2\text{H}$ ) were used in combination for the first time.	4
8. The same data provided novel constraints on Antarctic hydrological cycling specifically during a period of Neogene EAIS retreat.	4
9. The modelling experiments presented here are the first to examine Antarctic hydrological cycling in detail and particularly to examine the impact of ice sheet reduction on Antarctic climate.	4
10. For the first time, atmospheric tracers were used to trace Neogene atmospheric circulation and moisture delivery changes, challenging previous hypotheses that changes in $\delta^{18}\text{O}$ were due to changes in moisture source.	4

fate of the AIS (Holbourn et al., 2015, Levy et al., 2016), although from the geochemical data, further direct links to Antarctic *climate* (i.e. temperature and hydrological cycling) are unclear. The climate proxy data is borne out by experiments from a fully

coupled isotope enabled atmosphere-ocean-vegetation GCM (Chapter 4), which show increased continental temperatures (of a similar order of magnitude as suggested by the presented proxy data) as well as markedly different hydrological cycling. Importantly, the intermediate HadCM3 simulation (full preindustrial ice sheet, atmospheric CO<sub>2</sub> = 405 ppmv) strongly suggests that Antarctic continental climate is governed far more strongly by the extent of the ice sheet than by greenhouse gas radiative forcing, implying numerous feedbacks that should be explored further such as changes in albedo and its impact on temperature and hydrological cycling or different atmospheric circulation due to changed orography driving temperature and precipitation. In some respects, this final result could be anticipated from the presented proxy and fossil data as there is a large difference in surface albedo between shrub/bare soil and ice sheet (Bonfils et al., 2012). However, the value of using an isotope-enabled GCM approach is clear; this approach incorporates complex physical processes and interactions and enables a quantitative analysis of the climate system.

These final conclusions are ultimately limited by the seemingly intractable Sirius Group age problem. Much of the climate information derived from both the geochemical and climate modelling components of this thesis functions well as a test of hypothetical warmer, reduced ice world scenarios. There is clear relevance for understanding future warming scenarios as well as many palaeoclimate time periods (Chapter 4 and section 5.2.6). However, even more robust conclusions could be drawn from both the geochemical and climate modelling data if broader boundary conditions (e.g. latitudinal temperature gradients, specific carbon cycle dynamics) associated with the age of the sampled sediments and fossils were known. Similarly, inferences from the vegetation and carbon cycle data (Chapters 2 and 3) would be powerful if stronger links and correlations to other, geographically disparate records (e.g. pollen in Antarctic marine sediments, global  $\delta^{13}\text{C}$  records) could be drawn. It seems somewhat naive to ask for a better age model, which are never easy to develop in the first place. Nevertheless, better geological age constraints are very obviously needed so that the novel datasets produced in this work can inform more realistic climate simulations and geochemical data collection from both the terrestrial and marine realms. Such experiments and

data would provide more in-depth analysis of some of the questions posed in this thesis (particularly relating to ice sheet-hydrological cycle links) and provide much-needed sensitivity testing for some of the conclusions.

Within the limitations discussed throughout the thesis (Chapters 1 - 4), this study provides detailed knowledge on Antarctic climate and vegetation during a period of Neogene AIS retreat. A mixed (angiosperm and conifer) tundra shrub persisted well into the Neogene, supported by warmer summer temperatures and increased precipitation over deglaciated regions of Antarctica. Following on from this, some of the outstanding uncertainties and limitations should be addressed in future work in order to shore up or refute these main conclusions.

## **5.4 Future work**

There are multiple possible directions to take in order to improve or expand the work presented here. In this section, I discuss several ways in which the existing knowledge within this thesis could be put to better use via further geochemical and modelling work. Such additional research would address some of the specific limitations of this thesis and test the conclusions in each chapter, thus improving upon the existing work. Additionally, Section 5.4.4 discusses some other, bigger picture directions that could lead on from these results, which would expand the scope of some of the developments presented in this thesis significantly.

### **5.4.1 Dating improvements**

It would be extremely advantageous to constrain the age of the Sirius Group sediments. Much of the data presented in this thesis is valuable to several branches of palaeoclimate science, and would be much more so if the data could be compared robustly with and included in other datasets. For example, sea level and ice volume records based on benthic foraminifera  $\delta^{18}\text{O}$  assume a constant ice sheet  $\delta^{18}\text{O}$  through time, which introduces additional uncertainty into benthic foraminifera-based ice volume reconstructions. Our

finding that Antarctic precipitation  $\delta^{18}\text{O}$  and  $\delta^2\text{H}$  was significantly higher during AIS retreat (Chapters 3 and 4) implies that ice sheet  $\delta^{18}\text{O}$  was probably much higher during warm intervals in the past. This would seriously affect past records of sea level and climate change, as found by Winnick and Caves (2015) but requires a robust age model before it can be integrated fully into long term palaeoclimate records. Furthermore, and perhaps more importantly, finding a solution to the Sirius age issue would resolve a decades-long debate on EAIS stability during the Pliocene. Three possible routes past the dating issue could resolve the problem:

1. Uranium (U) series dating has recently been used to date organic matter in Quaternary Age fossil wood fragments from North America (Allard et al., 2012). Application of the technique to organic matter is dependent upon the material being isolated from surrounding isotopic fluxes such that the material only contains authigenic U. It is plausible that this holds true for the Sirius Group wood as the exceptional preservation and very low degree of permineralisation suggests that the fossils have existed in a persistently arid environment since shortly after deposition. Two test fragments of the Sirius Group wood are currently being analysed for lead concentrations at the University of Bristol (by collaborator Dr. David Richards), and may prove this dating technique to be feasible.
2. Foraminifera have been recorded in the sedimentary layer directly below the wood-bearing horizon at Oliver Bluffs (Ashworth and Cantrill, 2004), and unlike the marine diatoms previously used to date the Sirius Group, there is no uncertainty over their provenance in the sediment (i.e., they are very likely not windblown; Barrett, 2013). The only reported foraminifera are agglutinated, but much of the foraminifera record for the Sirius group at Oliver Bluffs is unpublished (J. Francis, pers. comm. 2015) and it is therefore unclear whether any calcareous foraminifera are present. If any calcareous foraminifera are present in these underlying sediments, then strontium isotope ( $^{87}\text{Sr}/^{86}\text{Sr}$ ) analysis should provide a solution to the ageing problem by comparison with the Cenozoic strontium isotope record (Elderfield, 1986).

3. A re-examination of Pliocene marine sediments from around Antarctica could provide additional insights. Based on diatom and radiolarian biostratigraphy, Fleming and Barron (1996) found *Nothofagus* pollen in three samples dating to c. 3 Ma in the DSDP Site 274 core near Cape Adare. By their analysis, previous studies looking at Pliocene marine sediments had used inadequate techniques to examine Pliocene palynology, and results suggesting barren palynology were actually inconclusive. While the presence of *Nothofagus* pollen in Pliocene Antarctic marine sediments cannot directly date the Sirius Group sediments in this thesis, it could give credence to a Pliocene age

#### 5.4.2 How representative are the geochemical results in this thesis?

In this thesis, I have made the assumption that the data from the Sirius Group at Oliver Bluffs are representative of large-scale Antarctic change. This could be the case, as the isotope and temperature data from Chapters 2, 3 and 4 are broadly consistent with the modelling data. However, it cannot be conclusively resolved from these data alone. Therefore expanding the spatial and temporal range of geochemical data to other episodes of AIS retreat would provide information not only on the general representability of the results presented in this thesis, but also on the degree of climate variability between episodes of retreat.

It has been noted that there were further plant fossils from other horizons at Oliver Bluffs (B. Duncan, pers. comm. 2015). These plants likely represent other episodes of AIS retreat, and therefore other interglacials. It would greatly enhance the scope of the work presented in Chapter 4 to test whether the ice sheet-driven hydrological change was consistent between interglacials by applying a similar analysis (temperature and precipitation isotope reconstructions) to these horizons too. Similarly, numerous plant fossils are noted from multiple locations in the McMurdo Dry Valleys, including Friis Hills and the Olympus Range (Ashworth et al., 2007, Lewis et al., 2008; B. Duncan, pers. comm. 2015, J. Francis, pers. comm., 2013). Some of these fossil-bearing deposits are very well dated; while they also represent different AIS retreat events, analysis of

their cellulose and leaf wax isotopes would provide an idea of the spatial variability of hydrological change during AIS retreat.

Furthermore, a biomarker analysis (with emphasis on terpenoids) of the same deposits (above) could provide further detail on questions around the evolution of vegetation on Antarctica. A planned future drilling expedition to Friis Hills (R. McKay, pers. comm., 2015), where a very well-dated terrestrial sequence contains multiple plant fossil-bearing horizons would give very clear insight on the interplay between vegetation (particularly the presence/absence of conifers on the continent), environment and climate.

### 5.4.3 Improved climate modelling

While the results in Chapter 4 suggest that the main driver of Antarctic hydrological change during EAIS retreat was the reduced ice sheet extent and volume, there are several boundary conditions in HadCM3 that could have an effect on this result. Most of this boundary condition uncertainty stems from the age uncertainty of the Sirius Group deposits. Although the mid-Pliocene Warm Period boundary conditions used in the simulations for this thesis remain a reasonable test of hydrological cycling in a reduced ice volume world, running simulations with mid-Miocene specific boundary conditions (continental configuration, land-sea mask and orography) would provide a further check on the representability of the results. This could be a time-consuming task as currently there are no mid-Miocene boundary conditions for HadCM3, and the challenge is not only in the technical implementation of new boundary conditions, but also in the establishment of detailed palaeogeographies.

The orbital parameters for the palaeo HadCM3 simulations in this thesis are very similar to present day orbital parameters. High latitude climates are affected to varying degrees by different orbital configurations. For example, high latitude insolation is directly correlated with obliquity, and high latitude seasonality is dependent on precession of the Earth's rotational axis. Moreover, ice sheet retreat during both the mid-Miocene and Pliocene appears to be orbitally driven (Greenop et al., 2014, Patterson et al.,

2014). Given the age uncertainty, it would be interesting to run a series of simulations with identical boundary conditions while varying the orbital configurations in order to further elucidate the true impact of ice sheet retreat on Antarctic climate as opposed to other climate factors.

#### **5.4.4 Expanding the scope of the work**

This section deals briefly with some of the broader implications of this thesis in an attempt to consider the bigger picture of the climate system as opposed to improving the existing work. The suggestions for future work are not intended to be an exhaustive list, but are merely intended to illustrate certain possibilities that could yield important novel data.

##### **5.4.4.1 Sensitivity testing**

Multiple improvements could be made to broaden the scope and impact of this work, particularly through the use of climate modelling. From Chapter 4, in particular, it seems clear that the Antarctic hydrological cycle is sensitive to ice sheet extent. Partly due to time constraints, it was not feasible to fully explore this concept during the course of my investigation. One possible remedy would be to run a series of simulations testing the sensitivity of the hydrological cycle to different ice sheet configurations; such simulations have been run here at the University of Leeds, but without oxygen isotopes in the hydrological cycle (D. Hill, pers. comm., 2014). Extending these pre-existing HadCM3 simulations with the inclusion of water isotopes throughout the climate system would be a relatively simple way of gaining valuable insight to the sensitivity and variability of climate in response to changes in ice sheets.

A more complex means of addressing the same concept would be to use an isotope-enabled ice sheet model (such as that used by Gasson et al., 2016) coupled to a high resolution isotope enabled GCM. The ice sheet model would include currently accepted mechanisms for retreat and the climate model would account for ice-sheet climate feedbacks, including feedbacks related to the new precipitation regime proposed in

Chapter 4. Furthermore, the isotope-enabled component of both models would allow the impact of changes in precipitation isotopes on other factors such as ice sheet  $\delta^{18}\text{O}$  and therefore past sea level changes, as well as constraining the impact of the switch in precipitation regime on ice core records (see section 5.2.6) to be assessed. This is likely to be very computationally expensive, however, and beyond current modelling capabilities. If (or when) possible, the most efficient way of running these simulations to establish their usefulness would be using snapshot simulations. If this approach proved fruitful, and given the wide-ranging implications for some of the work in this thesis, it would not be extravagant to consider running transient simulations, forced by evolving  $\text{CO}_2$ , to cover entire ice sheet retreat scenarios. Furthermore, this approach could go some way towards resolving outstanding questions over whether ice core records during the Quaternary were affected by the precipitation regime switch mechanism.

#### **5.4.4.2 Did a switch in precipitation regime occur over Greenland?**

Finally, it would be very interesting to explore whether the precipitation regime switch seen in the Antarctic data is applicable to the Greenland Ice Sheet (GIS) and climate, specifically during the Quaternary. The GIS is particularly sensitive to climate warming (Cuffey and Marshall, 2000, Stone et al., 2013, de Vernal and Hillaire-Marcel, 2008) and during some interglacial periods, such as the Last Interglacial, underwent severe retreat (van de Berg et al., 2011). Pollen records from around the continent indicate that during these periods of GIS collapse, the deglaciated land was colonised by vegetation (de Vernal and Hillaire-Marcel, 2008), which, similarly to Oliver Bluffs, would considerably affect surface albedo. A clear advance on the hydrological cycle work presented in Chapters 3 and 4 would therefore be to reconstruct precipitation isotope data from Greenland (either from leaf wax hydrogen isotope analysis in marine cores or the use of oxygen isotopes in fossil plant material) along with temperature reconstructions, and test for the presence of this mechanism on Greenland during GIS retreat. As the GIS is more susceptible to collapse than the AIS, one could hypothesise that the precipitation regime switch mechanism could play a far stronger role in governing precipitation isotopes and therefore isotope ratios in ice core records. This could then be tested further

using a similar modelling approach to that taken in Chapter 4 and would provide important information for improving our understanding of ice sheet-climate interactions, in the past and in the future.

# References

- R. P. Ackert, Jr. and M. D. Kurz. Age and uplift rates of Sirius Group sediments in the Dominion Range, Antarctica, from surface exposure dating and geomorphology. *Global and Planetary Change*, 42:207–225, 2004.
- G. Allard, M. Roy, B. Ghaleb, P. J. H. Richard, A. C. Larouche, J. J. Veillette, and M. Parent. Constraining the age of the last interglacial-glacial transition in the Hudson Bay lowlands (Canada) using U-Th dating of buried wood. *Quaternary Geochronology*, 7(1):37–47, 2012.
- G. B. Allison, J. R. Gat, and F. W. J. Leaney. The relationship between deuterium and oxygen-18 delta values in leaf water. *Chemical Geology (Isotope Geoscience Section)*, 58:145–156, 1985.
- J. B. Anderson, S. Warny, R. A. Askin, J. S. Wellner, S. M. Bohaty, A. E. Kirshner, D. N. Livsey, A. R. Simms, T. R. Smith, W. Ehrmann, L. A. Lawver, D. Barbeau, S. W. Wise, D. K. Kulhanek, F. M. Weaver, and W. Majewski. Progressive Cenozoic cooling and the demise of Antarctica’s last refugium. *Proceedings of the National Academy of Sciences*, 108(28):11356–11360, 2011.
- W. T. Anderson, S. M. Bernasconi, J. A. McKenzie, M. Saurer, and F. Schweingruber. Model evaluation for reconstructing the oxygen isotopic composition in precipitation from tree ring cellulose over the last century. *Chemical Geology*, 182(2-4):121–137, 2002.
- N. C. Arens, A. H. Jahren, and R. Amundson. Can C3 plants faithfully record the carbon isotopic composition of atmospheric carbon dioxide? *Paleobiology*, 26(1):137–164, 2000.
- A. C. Ashworth and D. J. Cantrill. Neogene vegetation of the Meyer Desert Formation (Sirius Group) Transantarctic Mountains, Antarctica. *Palaeogeography, Palaeoclimatology, Palaeoecology*, 213(1-2):65–82, 2004.
- A. C. Ashworth, A. R. Lewis, D. R. Marchant, R. A. Askin, D. J. Cantrill, J. E. Francis, M. J. Leng, A. E. Newton, J. I. Raine, M. Williams, and A. P. Wolfe. The Neogene biota of the Transantarctic Mountains. In *Related Publications from ANDRILL Affiliates*, page 5. 2007.
- A. C. Ashworth and G. Kuschel. Fossil weevils (Coleoptera: Curculionidae) from latitude 85S Antarctica. *Palaeogeography, Palaeoclimatology, Palaeoecology*, 191(2):191–202, 2003.
- A. C. Ashworth and R. C. Preece. The first freshwater molluscs from Antarctica. *Journal Molluscan Studies*, 69(1):89–92, 2003.
- R. A. Askin and V. Markgraf. Palynomorphs from the Sirius Formation, Dominion Range, Antarctica. *Antarctic Journal of the United States*, 21(5):34–35, 1986.

- R. A. Askin and J. I. Raine. Oligocene and Early Miocene Terrestrial Palynology of the , Cape Roberts Drillhole CRP-2/2A, Victoria Land Basin, Antarctica. *Terra Antarctica*, 7(4):493–501, 2000.
- J. Austermann, D. Pollard, J. X. Mitrovica, R. Moucha, A. M. Forte, R. M. DeConto, D. B. Rowley, and M. E. Raymo. The impact of dynamic topography change on Antarctic ice sheet stability during the mid-Pliocene warm period. *Geology*, 43(10):927–930, 2015.
- T. Bacic, L. Krstin, J. Rosa, and Z. Popvic. Epicuticular wax on stomata of damaged silver fir trees [*Abies alba* Mill.]. *Acta Societatis Botanicorum Poloniae*, 74(2):159–166, 2005.
- M. P. S. Badger, C. H. Lear, R. D. Pancost, G. L. Foster, T. R. Bailey, M. J. Leng, and H. A. Abels. CO<sub>2</sub> drawdown following the middle Miocene expansion of the Antarctic Ice Sheet. *Paleoceanography*, 28(1):42–53, 2013.
- A. P. Ballantyne, M. Lavine, T. J. Crowley, J. Liu, and P. B. Baker. Meta-analysis of tropical surface temperatures during the Last Glacial Maximum. *Geophysical Research Letters*, 32(5):1–4, 2005.
- A. P. Ballantyne, N. Rybczynski, P. A. Baker, C. R. Harington, and D. White. Pliocene Arctic temperature constraints from the growth rings and isotopic composition of fossil larch. *Palaeogeography Palaeoclimatology Palaeoecology*, 242(3-4):188–200, 2006.
- A. P. Ballantyne, D. R. Greenwood, J. S. Sinninghe Damste, A. Z. Csank, J. J. Eberle, and N. Rybczynski. Significantly warmer Arctic surface temperatures during the Pliocene indicated by multiple independent proxies. *Geology*, 38(7):603–606, 2010.
- M. M. Barbour and G. D. Farquhar. Relative humidity- and ABA-induced variation in carbon and oxygen isotope ratios of cotton leaves. *Plant, Cell & Environment*, 23(5):473–485, 2001.
- M. M. Barbour, U. Schurr, B. K. Henry, S. C. Wong, and G. D. Farquhar. Variation in the oxygen isotope ratio of phloem sap sucrose from castor bean. Evidence in support of the Pecllet effect. *Plant Physiology*, 123(2):671–679, 2000.
- M. M. Barbour, A. S. Walcroft, and G. D. Farquhar. Seasonal variation in d13C and d18O of cellulose from growth rings of *Pinus radiata*. *Plant, Cell & Environment*, 25(11):1483–1499, 2002.
- M. M. Barbour, J. S. Roden, G. D. Farquhar, and J. R. Ehleringer. Expressing leaf water and cellulose oxygen isotope ratios as enrichment above source water reveals evidence of a Pecllet effect. *Oecologia*, 138:426–435, 2004.
- M. D. Barrera, J. L. Frangi, L. L. Richter, M. H. Perdomo, and B. Pinedo, Luis. Structural and functional changes in *Nothofagus pumilio* forests along an altitudinal gradient in Tierra del Fuego, Argentina. *Journal of Vegetation Science*, 11:179–188, 2000.
- P. J. Barrett. Resolving views on Antarctic Neogene glacial history the Sirius debate. *Earth and Environmental Science Transactions of the Royal Society of Edinburgh*, 104(May 2013):31–53, 2013.
- D. J. Beerling and D. L. Royer. Convergent Cenozoic CO<sub>2</sub> history. *Nature Geoscience*, 4(7):418–420, 2011.
- J. A. P. Bendle, K. Kawamura, K. Yamazaki, and T. Niwai. Latitudinal distribution of terrestrial lipid biomarkers and n-alkane compound-specific stable carbon isotope ratios in the atmosphere over the western Pacific and Southern Ocean. *Geochimica et Cosmochimica Acta*, 71(24):5934–5955, 2007.

- R. A. Berner. The carbon cycle and carbon dioxide over Phanerozoic time: the role of land plants. *Philosophical Transactions of the Royal Society B: Biological Sciences*, 353(1365):75–82, 1998.
- J. Biellmann, G. Branlant, M. Gero-Robert, and M. Poiret. Dégradation bactérienne de l'acide déhydroabiétique par un Pseudomonas et une Alcaligenes. *Tetrahedron*, 29(9):1237–1241, 1973a.
- J. Biellmann, G. Branlant, M. Gero-Robert, and M. Poiret. Dégradation bactérienne de l'acide déhydroabiétique par Flavobacterium resinovorum. *Tetrahedron*, 29(9):1227–1236, 1973b.
- W. D. Billings, K. M. Peterson, S. G. R., and A. W. Trent. Root Growth, Respiration, and Carbon Dioxide Evolution in an Arctic Tundra Soil. *Arctic and Alpine Research*, 9(2):129–37, 1977.
- L. C. Bliss and N. V. Matveyeva. Circumpolar Arctic vegetation. In *Arctic ecosystems in a changing climate: an ecophysiological perspective*, pages 59–86. 1992.
- C. J. W. Bonfils, T. J. Phillips, D. M. Lawrence, P. Cameron-Smith, W. J. Riley, and Z. M. Subin. On the influence of shrub height and expansion on northern high latitude climate. *Environmental Research Letters*, 7(1):015503, 2012.
- S. L. Bradley, M. Siddall, G. A. Milne, V. Masson-Delmotte, and E. W. Wolff. Combining ice core records and ice sheet models to explore the evolution of the East Antarctic Ice sheet during the Last Interglacial period. *Global and Planetary Change*, 100:278–290, 2013.
- C. D. Bradshaw, D. J. Lunt, R. Flecker, U. Salzmann, M. J. Pound, A. M. Haywood, and J. T. Eronen. The relative roles of CO<sub>2</sub> and palaeogeography in determining Late Miocene climate: results from a terrestrial model-data comparison. *Climate of the Past Discussions*, 8(2):715–786, 2012.
- F. J. Bragg, D. J. Lunt, and A. M. Haywood. Mid-Pliocene climate modelled using the UK Hadley Centre Model: PlioMIP Experiments 1 and 2. *Geoscientific Model Development*, 5(5):1109–1125, 2012.
- A. Branco, A. C. Pinto, and R. B. Filho. Chemical constituents from Vellozia graminifolia (Velloziaceae). *Anais da Academia Brasileira de Ciências*, 76(3):505–518, 2004.
- E. E. Bray and E. D. Evans. Distribution of n-Paraffins as a clue to Recognition of Source Beds. *Geochimica et Cosmochimica Acta*, 22(1):2–15, 1961.
- R. J. W. Brienen, G. Helle, T. L. Pons, J.-L. Guyot, and M. Gloor. Oxygen isotopes in tree rings are a good proxy for Amazon precipitation and El Niño-Southern Oscillation variability. *Proceedings of the National Academy of Sciences*, 109(42):16957–16962, 2012.
- C. M. Brierley, A. V. Fedorov, Z. Liu, T. D. Herbert, K. T. Lawrence, and J. P. LaRiviere. Greatly Expanded Tropical Warm Pool and Weakened Hadley Circulation in the Early Pliocene. *Science*, 323(5922), 2009.
- J.-P. Brunel, G. R. Walker, C. D. Walker, J. C. Dighton, and A. Kennett-Smith. Using stable isotopes of water to trace plant water uptake. In *Stable isotopes in plant nutrition, soil fertility and environmental studies*, pages 543–551. 1991.
- W. M. Buhay, T. W. D. Edwards, and R. Aravena. Evaluating kinetic fractionation factors used for ecologic and paleoclimatic reconstructions from oxygen and hydrogen isotope ratios in plant water and cellulose. *Geochimica et Cosmochimica Acta*, 60(12):2209–2218, 1996.
- A. Buras and M. Wilmking. Straight lines or eccentric eggs? A comparison of radial and spatial ring width measurements and its implications for climate transfer functions. *Dendrochronologia*, 32(4):313–326, 2014.

- L. H. Burckle and N. Potter. Pliocene-Pleistocene diatoms in Paleozoic and Mesozoic sedimentary and igneous rocks from Antarctica : A Sirius problem solved Pliocene-Pleistocene diatoms in Paleozoic and Mesozoic sedimentary and igneous rocks from Antarctica : A Sirius problem solved. *Geology*, 24:235–238, 1996.
- R. T. Bush and F. A. McInerney. Leaf wax n-alkane distributions in and across modern plants : Implications for paleoecology and chemotaxonomy. *Geochimica et Cosmochimica Acta*, 117:161–179, 2013.
- A. B. Caldicott and G. Eglinton. Cutin acids from bryophytes: An ??-1 hydroxy alkanolic acid in two liverwort species. *Phytochemistry*, 15(7):1139–1143, 1976.
- D. J. Cantrill and I. Poole. *The vegetation of Antarctic through geological time*. Cambridge University Press, Cambridge, 2012.
- S. Carlquist. Pliocene Nothofagus wood from the Transantarctic mountains. *Aliso*, 11: 571–583, 1987.
- N. A. Clark, M. Williams, D. J. Hill, P. G. Quilty, J. L. Smellie, J. Zalasiewicz, M. J. Leng, and M. A. Ellis. Fossil proxies of near-shore sea surface temperatures and seasonality from the late Neogene Antarctic shelf. *Naturwissenschaften*, 100:699–722, 2013.
- D. W. Cline. Snow surface energy exchanges and snowmelt at a continental, midlatitude Alpine site. *Water Resources Research*, 33(4):689–701, 1997.
- C. P. Cook, D. J. Hill, T. van de Flierdt, T. Williams, S. R. Hemming, A. M. Dolan, E. L. Pierce, C. Escutia, D. M. Harwood, G. Cortese, and J. J. Gonzales. Sea surface temperature control on the distribution of far-traveled Southern Ocean ice-rafted detritus during the Pliocene. *Paleoceanography*, 29(6):533–548, 2014.
- C. P. Cook, T. van de Flierdt, T. Williams, S. R. Hemming, M. Iwai, M. Kobayashi, F. J. Jimenez-Espejo, C. Escutia, J. J. González, B.-K. Khim, R. M. McKay, S. Passchier, S. M. Bohaty, C. R. Riesselman, L. Tauxe, S. Sugisaki, A. L. Galindo, M. O. Patterson, F. Sangiorgi, E. L. Pierce, H. Brinkhuis, A. Klaus, A. Fehr, J. A. P. Bendle, P. K. Bijl, S. a. Carr, R. B. Dunbar, J. A. Flores, T. G. Hayden, K. Katsuki, G. S. Kong, M. Nakai, M. P. Olney, S. F. Pekar, J. Pross, U. Röhl, T. Sakai, P. K. Shrivastava, C. E. Stickley, S. Tuo, K. Welsh, and M. Yamane. Dynamic behaviour of the East Antarctic ice sheet during Pliocene warmth. *Nature Geoscience*, 6(9): 765–769, 2013.
- D. A. Coomes and P. J. Bellingham. Temperate and tropical podocarps: how ecologically alike are they. *Ecology of the Podocarpaceae in tropical forests*, (1989):119–140, 2011.
- C. Cooper and C. Gordon. North Atlantic oceanic decadal variability in the Hadley Centre coupled model. *Journal of Climate*, 15(3):45–72, 2002.
- P. M. Cox. Description of the "TRIFFID" Dynamic Global Vegetation Model. Technical report, 2001.
- H. Craig. Standard for reporting concentrations of deuterium and oxygen-18 in natural waters. *Science*, 133(3467):1833–1834, 1961.
- H. Craig and L. I. Gordon. Deuterium and oxygen-18 variations in the ocean and marine atmosphere. In E. Tongiogi, editor, *In Proc. Stable isotopes in oceanographic studies and paleotemperatures*, pages 9–130, Spoleto, Italy, 1965.
- P. A. Cranwell. Monocarboxylic acids in lake sediments: indicators, derived from terrestrial and aquatic biota, of paleoenvironmental trophic levels. *Chemical Geology*, 14, 1974.

- R. M. M. Crawford. Plant survival in cold habitats. In *Tundra-taiga biology: Human, plant, and animal survival in the Arctic*, pages 146–163. Oxford University Press, 2014.
- A. Z. Csank, W. P. Patterson, B. M. Eglinton, N. Rybczynski, and J. F. Basinger. Climate variability in the Early Pliocene Arctic: Annually resolved evidence from stable isotope values of sub-fossil wood, Ellesmere Island, Canada. *Palaeogeography Palaeoclimatology Palaeoecology*, 308(3-4):339–349, 2011.
- K. M. Cuffey and S. J. Marshall. Substantial contribution to sea-level rise during the last interglacial from the Greenland ice sheet. *Nature*, 404:591–4, 2000.
- W. Dansgaard. Stable isotopes in precipitation. *Tellus*, 16(4):436–468, 1964.
- T. E. Dawson and J. R. Ehleringer. Gender-specific physiology, carbon isotope discrimination, and habitat distribution in Box Elder, *Acer Negundo*. *Ecology*, 74(3):798–815, 1993.
- T. E. Dawson and J. S. Pate. Seasonal water uptake and movement in root systems of Australian phraeatophytic plants of dimorphic root morphology: a stable isotope investigation. *Oecologia*, 107:13–20, 1996.
- B. de Boer, L. J. Lourens, and R. S. W. van de Wal. Persistent 400,000-year variability of Antarctic ice volume and the carbon cycle is revealed throughout the Plio-Pleistocene. *Nature Communications*, 5:2999, 2014.
- A. de Vernal and C. Hillaire-Marcel. Natural Variability of Greenland Climate, Vegetation, and Ice Volume During the Past Million Years. *Science*, 320(5883):1622–1625, 2008.
- G. Delaygue, V. Masson, J. Jouzel, R. D. Koster, and R. J. Healy. The origin of Antarctic precipitation: A modelling approach. *Tellus, Series B: Chemical and Physical Meteorology*, 52:19–36, 2000.
- A. F. Diefendorf, K. E. Mueller, S. L. Wing, P. L. Koch, and K. H. Freeman. Global patterns in leaf  $^{13}\text{C}$  discrimination and implications for studies of past and future climate. *PNAS*, 107(13):5738–5743, 2010.
- A. F. Diefendorf, K. H. Freeman, S. L. Wing, and H. V. Graham. Production of n-alkyl lipids in living plants and implications for the geologic past. *Geochimica et Cosmochimica Acta*, 75(23):7472–7485, 2011.
- L. Diester-Haass, K. Billups, I. Jacquemin, K. C. Emeis, V. Lefebvre, and L. François. Paleoproductivity during the middle Miocene carbon isotope events: A data-model approach. *Paleoceanography*, 28(2):334–346, 2013.
- A. M. Dolan, A. M. Haywood, D. J. Hill, H. J. Dowsett, S. J. Hunter, D. J. Lunt, and S. J. Pickering. Sensitivity of Pliocene ice sheets to orbital forcing. *Palaeogeography, Palaeoclimatology, Palaeoecology*, 309(1):98–110, 2011.
- B. Dong and R. T. Sutton. Variability in North Atlantic heat content and heat transport in a coupled ocean-atmosphere GCM. *Climate Dynamics*, 19(5-6):485–497, 2002.
- G. Dongmann, H. W. Nurnberg, H. Forstel, and K. Wagener. On the enrichment of  $\text{H}_2\text{-}^{18}\text{O}$  in the leaves of transpiring plants. *Radiation and Environmental Biophysics*, 11:41–52, 1974.
- H. J. Dowsett, M. M. Robinson, and K. M. Foley. Pliocene three-dimensional global ocean temperature reconstruction. *Climate of the Past Discussions*, 5(4):1901–1928, 2009.
- H. J. Dowsett, M. M. Robinson, A. M. Haywood, U. Salzmann, D. J. Hill, L. E. Sohl, M. A. Chandler, M. Williams, K. M. Foley, and D. K. Stoll. The PRISM3D paleoenvironmental reconstruction. *Stratigraphy*, 7:123–139, 2010.

- H. J. Dowsett, M. M. Robinson, A. M. Haywood, D. J. Hill, A. M. Dolan, D. K. Stoll, W.-L. Chan, A. Abe-Ouchi, M. A. Chandler, N. A. Rosenbloom, B. L. Otto-Bliesner, F. J. Bragg, D. J. Lunt, K. M. Foley, and C. R. Riesselman. Assessing confidence in Pliocene sea surface temperatures to evaluate predictive models. *Nature Climate Change*, 2(5):365–371, 2012.
- J. J. Eberle, H. C. Fricke, J. D. Humphrey, L. Hackett, M. G. Newbrey, and J. H. Hutchison. Seasonal variability in Arctic temperatures during early Eocene time. 2010.
- S. Eggleston, J. Schmitt, B. Bereiter, R. Schneider, and H. Fischer. Evolution of the stable carbon isotope composition of atmospheric CO<sub>2</sub> over the last glacial cycle. *Paleoceanography*, pages n/a–n/a, 2016.
- G. Eglinton and R. J. Hamilton. Leaf Epicuticular Waxes. *Science*, 156(3780):1322–1335, 1967.
- H. Elderfield. Strontium isotope stratigraphy. *Palaeogeography, Palaeoclimatology, Palaeoecology*, 57:71–90, 1986.
- C. R. Enzell and R. Ryhage. Mass spectrometric studies of diterpenes. 5. Aromatic diterpenes. *Arkiv For Kemi*, 27(3):213, 1967.
- S. Epstein, P. Thompson, and C. J. Yapp. Oxygen and Hydrogen Isotopic Ratios in Plant Cellulose. *Science*, 198(4323):1209–1215, 1977.
- C. Escutia, M. A. Bárcena, R. G. Lucchi, O. Romero, A. M. Balleger, J. J. Gonzalez, and D. M. Harwood. Circum-Antarctic warming events between 4 and 3.5Ma recorded in marine sediments from the Prydz Bay (ODP Leg 188) and the Antarctic Peninsula (ODP Leg 178) margins. *Global and Planetary Change*, 69(3):170–184, 2009.
- G. D. Farquhar and K. S. Gan. On the progressive enrichment of the oxygen isotopic composition along a leaf. *Plant Cell Environment*, 26(6):801–819, 2003.
- G. D. Farquhar and J. Lloyd. Isotope effects in CO<sub>2</sub> exchange. In J. R. Ehleringer, A. E. Hall, and G. Farquhar, editors, *Stable isotopes and plant carbon-water relations*, pages 47–70. 1993a.
- G. D. Farquhar and J. Lloyd. Carbon and oxygen isotope effects in the exchange of carbon dioxide between terrestrial plants and the atmosphere. In J. R. Ehleringer, A. E. Hall, and G. D. Farquhar, editors, *Stable isotopes and plant carbon-water relations*, pages 47–70. Academic Press, San Diego, California, 1993b.
- G. D. Farquhar, M. H. O'Leary, and J. A. Berry. On the Relationship between Carbon Isotope Discrimination and the Inter-Cellular Carbon-Dioxide Concentration in Leaves. *Plant Physiology*, 9(2):121–137, 1982.
- G. D. Farquhar, J. R. Ehleringer, and K. T. Hubick. Carbon isotope discrimination and photosynthesis. *Annual Review of Plant Physiology and Plant Molecular Biology*, 40:503–537, 1989a.
- G. D. Farquhar, K. T. Hubick, A. G. Condon, and R. A. Richards. Carbon isotope discrimination and water use efficiency. In P. W. Rundel, J. R. Ehleringer, and K. A. Nagy, editors, *Stable isotopes in ecological research*, pages 21–46. Springer-Verlag, New York, 1989b.
- G. D. Farquhar, M. M. Barbour, and B. K. Henry. Interpretation of oxygen isotope composition of leaf material. *Stable Isotopes: Integration of Biological, Ecological, and Geochemical Processes*, pages 27–48, 1998.
- S. J. Feakins, P. B. DeMenocal, and T. I. Eglinton. Biomarker records of late Neogene changes in northeast African vegetation. *Geology*, 33(12):977–980, 2005.

- S. J. Feakins, T. I. Eglinton, and P. B. DeMenocal. A comparison of biomarker records of northeast African vegetation from lacustrine and marine sediments (ca. 3.40 Ma). *Organic Geochemistry*, 38(10):1607–1624, 2007.
- S. J. Feakins, S. Warny, and J.-e. Lee. Hydrologic cycling over Antarctica during the middle Miocene warming. *Nature Geoscience*, 5(8):557–560, 2012.
- A. V. Fedorov, N. J. Burls, K. T. Lawrence, and L. C. Peterson. Tightly linked zonal and meridional sea surface temperature gradients over the past five million years. *Nature Geoscience*, 8(12):975–980, 2015.
- M. E. Fernández, J. Gyenge, and T. Schlichter. Water flux and canopy conductance of natural versus planted forests in Patagonia, South America. *Trees - Structure and Function*, 23(2):415–427, 2009.
- K. J. Ficken, K. E. Barber, and G. Eglinton. Lipid biomarker,  $\delta^{13}\text{C}$  and plant macrofossil stratigraphy of a Scottish montane peat bog over the last two millennia. *Organic Geochemistry*, 28(3):217–237, 1998.
- R. D. Field, D. B. A. Jones, and D. P. Brown. Effects of postcondensation exchange on the isotopic composition of water in the atmosphere. *Journal of Geophysical Research Atmospheres*, 115(24):1–16, 2010.
- C. R. Fielding, G. H. Browne, B. Field, F. Florindo, D. M. Harwood, L. A. Krissek, R. H. Levy, K. S. Panter, S. Passchier, and S. F. Pekar. Sequence stratigraphy of the ANDRILL AND-2A drillcore, Antarctica: A long-term, ice-proximal record of Early to Mid-Miocene climate, sea-level and glacial dynamism. *Palaeogeography, Palaeoclimatology, Palaeoecology*, 305(1-4):337–351, 2011.
- R. F. Fleming and J. A. Barron. Evidence of Pliocene *Nothofagus* in Antarctica from Pliocene marine sedimentary deposits ( DSDP Site 274 ). *Marine Micropaleontology*, 27(95):227–236, 1996.
- B. P. Flower and J. P. Kennett. The middle Miocene climatic transition: East Antarctic ice sheet development, deep ocean circulation and global carbon cycling. *Palaeogeography, Palaeoclimatology, Palaeoecology*, 108(3-4):537–555, 1994.
- G. L. Foster, C. H. Lear, and J. W. B. Rae. The evolution of  $p\text{CO}_2$ , ice volume and climate during the middle Miocene. *Earth and Planetary Science Letters*, 341-344: 243–254, 2012.
- J. E. Francis and R. S. Hill. Fossil Plants from the Pliocene Sirius Group , Transantarctic Evidence for Mountains : Climate from Growth Rings and Fossil Leaves. *PALAIOS*, 11(4):389–396, 1996.
- J. E. Francis, A. M. Haywood, A. C. Ashworth, and P. J. Valdes. Tundra environments in the Neogene Sirius Group, Antarctica: evidence from the geological record and coupled atmosphere-vegetation models. *Journal of the Geological Society*, 164(2): 317–322, 2007.
- J. E. Francis, A. C. Ashworth, D. J. Cantrill, J. A. Crame, J. Howe, R. Stephens, and A.-M. Tosolini. 100 millions years of Antarctic climate evolution: Evidence from fossil plants. In A. K. Cooper, P. Barrett, B. Stoey, E. Stump, and W. Wise, editors, *Antarctica: A keystone in a changing world*, pages 19–28. National Academies Press, Washington D. C., 2008.
- M. Frank, N. Whiteley, S. Kastan, J. R. Hein, and K. O’Nions. North Atlantic Deep Water export to the Southern Ocean over the past 14 Myr: Evidence from Nd and Pb isotopes in ferromanganese crusts. *Paleoceanography*, 17(2):1–9, 2002.
- M. Frenz, R. Henrich, and B. Zychla. Carbonate preservation patterns at the Ceara Rise - Evidence for the Pliocene super conveyor. *Marine Geology*, 232(3-4):173–180, 2006.

- K. S. Gan, S. C. Wong, J. W. H. Yong, and G. D. Farquhar. 18O spatial patterns of vein xylem water, leaf water, and dry matter in cotton leaves. *Plant Physiology*, 130(2):1008–1021, 2002.
- A. I. Garcia-Cervigon Morales, J. M. Olano Mendoza, M. Eugenio Gozalbo, and J. J. Camarero Martinez. Arboreal and prostrate conifers coexisting in Mediterranean high mountains differ in their climatic responses. *Dendrochronologia*, 30(4):279–286, 2012.
- E. Gasson, R. M. DeConto, D. Pollard, and R. H. Levy. Dynamic Antarctic ice sheet during the early to mid-Miocene. *Proceedings of the National Academy of Sciences*, (34):201516130, 2016.
- J. R. Gat. Oxygen and hydrogen isotopes in the hydrologic cycle. *Annual Review Earth Planetary Science*, 24:225–262, 1996.
- J. R. Gat and C. Bowser. The heavy isotope enrichment of water in coupled evaporative systems. *Stable isotope geochemistry: A tribute to Samuel Epstein*, 3:159–168, 1991.
- T. W. Goodwin. Sterols. In *Algal physiology and biochemistry*, pages 266–280. 1974.
- C. Gordon, C. Cooper, C. A. Senior, H. Banks, J. M. Gregory, T. C. Johns, J. F. B. Mitchell, and R. A. Wood. The simulation of SST, sea ice extents and ocean heat transports in a version of the Hadley Centre coupled model without flux adjustments. *Climate Dynamics*, 16(2-3):147–168, 2000.
- A. C. Gouveia and H. Freitas. Modulation of leaf attributes and water use efficiency in *Quercus suber* along a rainfall gradient. *Trees - Structure and Function*, 23(2):267–275, 2009.
- R. Greenop, G. L. Foster, P. A. Wilson, and C. H. Lear. Middle Miocene climate instability associated with high-amplitude CO<sub>2</sub> variability. *Paleoceanography*, 29(9):845–853, 2014.
- D. Gregory and P. R. Rowntree. A Mass Flux Convection Scheme with Representation of Cloud Ensemble Characteristics and Stability-Dependent Closure. *Monthly Weather Review*, 118(7):1483–1506, 1990.
- K. W. Griener, S. Warny, R. A. Askin, and G. Acton. Early to middle Miocene vegetation history of Antarctica supports eccentricity-paced warming intervals during the Antarctic icehouse phase. *Global and Planetary Change*, 127:67–78, 2015.
- D. R. Grocke, S. P. Hesselbo, and H. C. Jenkyns. Carbon-isotope composition of Lower Cretaceous fossil wood: ocean-atm chemistry and relation to sea level change. *Geology*, 27(2):155–158, 1999.
- M. J. Hambrey, P.-N. Webb, D. M. Harwood, and L. A. Krissek. Neogene glacial record from the Sirius Group of the Shackleton Glacier region, central Transantarctic Mountains, Antarctica. *Bulletin of the Geological Society of America*, 115(8):994–1015, 2003.
- M. A. Hansen, S. Passchier, B.-K. Khim, B. Song, and T. Williams. Threshold behavior of a marine-based sector of the East Antarctic Ice Sheet in response to early Pliocene ocean warming. *Paleoceanography*, 30(6):789–801, 2015.
- R. Hantemirov, S. Shiyatov, and L. Gorlanova. Dendroclimatic study of Siberian juniper. *Dendrochronologia*, 29(2):119–122, 2011.
- D. M. Harwood. *Diatom biostratigraphy and paleoecology with a Cenozoic history of Antarctic ice sheets*. PhD thesis, Ohio State University, 1986.
- V. Hauke and L. Schreiber. Ontogenetic and seasonal development of wax composition and cuticular transpiration of ivy (*Hedera helix* L.) sun and shade leaves. *Planta*, 207(1):67–75, 1998.

- D. W. Hauptvogel and S. Passchier. Early-Middle Miocene (17-14Ma) Antarctic ice dynamics reconstructed from the heavy mineral provenance in the AND-2A drill core, Ross Sea, Antarctica. *Global and Planetary Change*, 82-83:38–50, 2012.
- Y. Hautevelle, R. Michels, F. Malartre, and A. Trouiller. Vascular plant biomarkers as proxies for palaeoflora and palaeoclimatic changes at the Dogger/Malm transition of the Paris Basin (France). *Organic Geochemistry*, 37(5):610–625, 2006.
- A. M. Haywood, H. J. Dowsett, B. Otto-Bliesner, M. A. Chandler, A. M. Dolan, D. J. Hill, D. J. Lunt, M. M. Robinson, N. Rosenbloom, U. Salzmann, and L. E. Sohl. Pliocene Model Intercomparison Project (PlioMIP): experimental design and boundary conditions (Experiment 1). *Geoscientific Model Development*, 3(1):227–242, 2010.
- A. M. Haywood, H. J. Dowsett, M. M. Robinson, D. K. Stoll, A. M. Dolan, D. J. Lunt, B. L. Otto-Bliesner, and M. A. Chandler. Pliocene Model Intercomparison Project (PlioMIP): experimental design and boundary conditions (Experiment 2). *Geoscientific Model Development*, 4(3):571–577, 2011.
- A. M. Haywood, H. J. Dowsett, A. M. Dolan, D. Rowley, A. Abe-Ouchi, B. Otto-Bliesner, M. A. Chandler, S. J. Hunter, D. J. Lunt, M. Pound, and U. Salzmann. The Pliocene Model Intercomparison Project (PlioMIP) Phase 2: scientific objectives and experimental design. *Climate of the Past*, 12(3):663–675, 2016.
- B. R. Helliker and J. R. Ehleringer. Establishing a grassland signature in veins:  $^{18}\text{O}$  in the leaf water of C3 and C4 grasses. *PNAS*, 97(14):7894–7898, 2000.
- R. S. Hill. Fossil leaf. *Antarctic Cenozoic History from the CIROS-1 Drillhole, McMurdo Sound, Antarctica*, pages 143–144, 1989.
- R. S. Hill and G. J. Jordan. Macrofossils as indicators of Plio-Pleistocene climates in Tasmania and Antarctica. *Papers and Proceedings of the Royal Society of Tasmania*, 130(2):9–15, 1996.
- R. S. Hill and E. M. Trustwell. Nothofagus fossils in the Sirius Group, Transantarctic Mountains: Leaves and pollen and their climatic implications. *Antarctic Research Series*, 60:67–73, 1993.
- R. S. Hill, D. M. Harwood, and P.-N. Webb. Nothofagus beardmorensis (Nothofagaceae), a new species based on leaves from the Pliocene Sirius Group, Transantarctic Mountains, Antarctica. *Review of Palaeobotany and Palynology*, 94:11–24, 1996.
- A. Holbourn, W. Kuhnt, M. Schulz, and H. Erlenkeuser. Impacts of orbital forcing and atmospheric carbon dioxide on Miocene ice-sheet expansion. *Nature*, 438(7067):483–7, 2005.
- A. Holbourn, W. Kuhnt, M. Schulz, J. A. Flores, and N. Andersen. Orbitally-paced climate evolution during the middle Miocene "Monterey" carbon-isotope excursion. *Earth and Planetary Science Letters*, 261(3-4):534–550, 2007.
- A. Holbourn, W. Kuhnt, S. Clemens, W. Prell, and N. Andersen. Middle to late Miocene stepwise climate cooling: Evidence from a high-resolution deep water isotope curve spanning 8 million years. *Paleoceanography*, 28(4):688–699, 2013.
- A. Holbourn, W. Kuhnt, M. Lyle, L. Schneider, O. Romero, and N. Andersen. Middle Miocene climate cooling linked to intensification of eastern equatorial Pacific upwelling. *Geology*, 42(1):19–22, 2014.
- A. Holbourn, W. Kuhnt, K. G. D. Kochhann, N. Andersen, and K. J. Sebastian Meier. Global perturbation of the carbon cycle at the onset of the Miocene Climatic Optimum. *Geology*, 43(2):123–126, 2015.
- M. M. Holland and C. M. Bitz. Polar amplification of climate change in coupled models. *Climate Dynamics*, 21(3-4):221–232, 2003.

- M. D. Holloway, L. C. Sime, J. S. Singarayer, J. C. Tindall, and P. J. Valdes. Reconstructing paleosalinity from  $\delta^{18}\text{O}$ : Coupled model simulations of the Last Glacial Maximum, Last Interglacial and Late Holocene. *Quaternary Science Reviews*, 131: 350–364, 2016.
- B. A. Hook, J. Halfar, Z. Gedalof, J. Bollmann, and D. J. Schulze. Stable isotope paleoclimatology of the earliest Eocene using kimberlite-hosted mummified wood from the Canadian Subarctic. *Biogeosciences Discussions*, 11(11):16269–16308, 2014.
- B. A. Hook, J. Halfar, J. Bollmann, Z. Gedalof, M. Azizur Rahman, J. Reyes, and D. J. Schulze. Extraction of  $\alpha$ -cellulose from mummified wood for stable isotopic analysis. *Chemical Geology*, 405:19–27, 2015.
- P. J. Hopley, J. D. Marshall, G. P. Weedon, A. G. Latham, A. I. R. Herries, and K. L. Kuykendall. Orbital forcing and the spread of C4 grasses in the late Neogene: stable isotope evidence from South African speleothems. *Journal of Human Evolution*, 53(5):620–634, 2007.
- E. C. Hopmans, J. W. Weijers, E. Schefuß, L. Herfort, J. S. Sinninghe Damsté, and S. Schouten. A novel proxy for terrestrial organic matter in sediments based on branched and isoprenoid tetraether lipids. 2004.
- X. Huang, J. Xue, X. Wang, P. A. Meyers, J. Huang, and S. Xie. Paleoclimate influence on early diagenesis of plant triterpenes in the Dajiuhu peatland, central China. *Geochimica et Cosmochimica Acta*, 123:106–119, 2013.
- Y. Huang, M. J. Lockheart, G. A. Logan, and G. Eglinton. Isotope and molecular evidence for the diverse origins of carboxylic acids in leaf fossils and sediments from the Miocene Lake Clarkia deposit, Idaho, U.S.A. *Organic Geochemistry*, 24(3):289–299, 1996.
- G. B. Hunsinger, W. M. Hagopian, and A. H. Jahren. Offline oxygen isotope analysis of organic compounds with high N:O. *Rapid Communications in Mass Spectrometry*, 24(21):3182–3186, 2010.
- H. Hürlimann and E. Cherbuliez. Konstitution und Vorkommen der organischen Pflanzenstoffe. *Ergänzungsband 2*, 1, 1981.
- F. Iacoviello, G. Giorgetti, I. Turbanti Memmi, and S. Passchier. Early Miocene Antarctic glacial history: new insights from heavy mineral analysis from ANDRILL AND-2A drill core sediments. *International Journal of Earth Sciences*, 104(3):853–872, 2015.
- IPCC. Climate Change 2013: The Physical Science Basis. Contribution of Working Group I to the Fifth Assessment Report of the Intergovernmental Panel on Climate Change. Technical report, 2013.
- T. H. Jacka and W. F. Budd. Detection of temperature and sea-ice-extent changes in the Antarctic and Southern Ocean, 1949–96. *Annals of Glaciology*, 27(1):553–59, 1998.
- R. Jagels and M. Day. The adaptive physiology of *Metasequoia* to Eocene high-latitude environments. In *The evolution of plant physiology*, page 401. 2004.
- A. H. Jahren and L. S. L. Sternberg. Humidity estimate for the middle Eocene Arctic rain forest. *Geology*, 31(5):463–466, 2003.
- A. H. Jahren and L. S. L. Sternberg. Annual patterns within tree rings of the Arctic middle Eocene (ca. 45 Ma): Isotopic signatures of precipitation, relative humidity, and deciduousness. *Geology*, 36(2):99–102, 2008.
- A. H. Jahren, N. C. Arens, G. Sarmiento, J. Guerrero, and R. Amundson. Terrestrial record of methane hydrate dissociation in the Early Cretaceous. *Geology*, 29(2): 159–162, 2001.

- A. H. Jahren, M. C. Byrne, H. V. Graham, L. S. L. Sternberg, and R. E. Summons. The environmental water of the middle Eocene Arctic: Evidence from  $\delta D$ ,  $\delta^{18}O$  and  $\delta^{13}C$  within specific compounds. *Palaeogeography Palaeoclimatology Palaeoecology*, 271(1-2):96–103, 2009.
- T. C. Johns, R. E. Carnell, J. F. Crossley, J. M. Gregory, J. F. B. Mitchell, C. A. Senior, S. F. B. Tett, and R. A. Wood. The second Hadley Centre coupled ocean-atmosphere GCM: model description, spinup and validation. *Climate Dynamics*, 13(2):103–134, 1997.
- J. Jouzel, R. B. Alley, K. M. Cuffey, W. Dansgaard, P. Grootes, G. Hoffmann, S. J. Johnsen, R. D. Koster, D. Peel, C. A. Shuman, M. Stievenard, M. Stuiver, and J. White. Validity of the Temperature Reconstruction from Water Isotopes in Ice Cores. *J. Geophys. Res.*, 102(C12):26471–26487, 1997.
- R. J. G. Kaandorp, H. B. Vonhof, F. P. Wesselingh, L. R. Pittman, D. Kroon, and J. E. van Hinte. Seasonal Amazonian rainfall variation in the Miocene climate optimum. *Palaeogeography, Palaeoclimatology, Palaeoecology*, 221(1-2):1–6, 2005.
- P. Karrer. *Konstitution und Vorkommen der Organischen Pflanzenstoffe*. 1958.
- W. Karrer, E. Cherbuliez, and C. H. Eugster. Konstitution und Vorkommen der Organischen Pflanzenstoffe. In *Erganzungsband 1*. 1977.
- M. E. Katz, J. D. Wright, K. G. Miller, B. S. Cramer, K. Fennel, and P. G. Falkowski. Biological overprint of the geological carbon cycle. *Marine Geology*, 217(3-4):323–338, 2005.
- R. F. Keeling, S. C. Piper, A. F. Bollenbacher, and A. F. Walker. Monthly atmospheric  $^{13}C/^{12}C$  isotopic ratios for 11 SIO stations. In *Trends: A Compendium of Data on Global Change*. 2010.
- E. M. Kemp and P. J. Barrett. Antarctic glaciation and early Tertiary vegetation. *Nature*, 258:507–508, 1975.
- P. Köhler, H. Fischer, and J. Schmitt. Atmospheric  $d^{13}CO_2$  and its relation to  $pCO_2$  and deep ocean  $d^{13}C$  during the late Pleistocene. *Paleoceanography*, 25(1):PA1213, 2010.
- P. E. Kolattukudy. Biosynthesis of Cuticular Lipids. *Annual Review of Plant Physiology*, 21(1):163–192, 1970.
- P. E. Kolattukudy, R. Croteau, and J. S. Buckner. Biochemistry of plant waxes. In *Chemistry and biochemistry of natural waxes*. 1976.
- C. Korner. Plant ecology at high elevations. In *Alpine plant life: functional plant ecology of high mountain ecosystems*, pages 1–7. 2003.
- M. Krapp and J. H. Jungclauss. The Middle Miocene climate as modelled in an atmosphere-ocean-biosphere model. *Climate of the Past*, 7(4):1169–1188, 2011.
- G. Krinner, O. Magand, I. Simmonds, C. Genthon, and J. L. Dufresne. Simulated Antarctic precipitation and surface mass balance at the end of the twentieth and twenty-first centuries. *Climate Dynamics*, 28(2-3):215–230, 2007.
- W. M. Kürschner, Z. Kvacek, and D. L. Dilcher. The impact of Miocene atmospheric carbon dioxide fluctuations on climate and the evolution of terrestrial ecosystems. *Proceedings of the National Academy of Sciences of the United States of America*, 105(2):449–53, 2008.
- R. E. LaFlamme and R. A. Hites. Tetra- and pentacyclic, naturally occurring, aromatic hydrocarbons in recent sediments. *Geochimica et Cosmochimica Acta*, 43(310):1687–1691, 1979.

- A. Lavergne, V. Daux, R. Villalba, M. Pierre, M. Stievenard, F. Vimeux, and A. M. Srur. Are the oxygen isotopic compositions of *Fitzroya cupressoides* and *Nothofagus pumilio* cellulose promising proxies for climate reconstructions in northern Patagonia? *Journal of Geophysical Research: Biogeosciences*, pages n/a–n/a, 2016.
- L. A. Lawver and L. M. Gahagan. Evolution of Cenozoic seaways in the circum-Antarctic region. *Palaeogeography, Palaeoclimatology, Palaeoecology*, 198(1-2):11–37, 2003.
- J.-E. Lee, I. Fung, D. J. DePaolo, and B. L. Otto-Bliesner. Water isotopes during the Last Glacial Maximum: New general circulation model calculations. *Journal of Geophysical Research*, 113(D19):D19109, 2008.
- R. H. Levy, D. M. Harwood, F. Florindo, F. Sangiorgi, R. Tripathi, H. von Eynatten, E. Gasson, G. Kuhn, A. Tripathi, R. M. DeConto, C. R. Fielding, B. Field, N. Golledge, R. M. McKay, T. R. Naish, M. P. Olney, D. Pollard, S. Schouten, F. Talarico, S. Warny, V. Willmott, G. Acton, K. Panter, T. Paulsen, and M. Taviani. Antarctic ice sheet sensitivity to atmospheric CO<sub>2</sub> variations in the early to mid-Miocene. *Proceedings of the National Academy of Sciences*, 113(13):3453–3458, 2016.
- A. R. Lewis, D. R. Marchant, A. C. Ashworth, S. R. Hemming, and M. L. Machlus. Major middle Miocene global climate change: Evidence from East Antarctica and the Transantarctic Mountains. *Geological Society of America Bulletin*, 119(11-12):1449–1461, 2007.
- A. R. Lewis, D. R. Marchant, A. C. Ashworth, L. Hedenäs, S. R. Hemming, J. V. Johnson, M. J. Leng, M. L. Machlus, A. E. Newton, J. I. Raine, J. K. Willenbring, M. Williams, and A. P. Wolfe. Mid-Miocene cooling and the extinction of tundra in continental Antarctica. *Proceedings of the National Academy of Sciences of the United States of America*, 105(31):10676–80, 2008.
- S. R. M. Ligtenberg, W. J. van de Berg, M. R. van den Broeke, J. G. L. Rae, and E. van Meijgaard. Future surface mass balance of the Antarctic ice sheet and its influence on sea level change, simulated by a regional atmospheric climate model. *Climate Dynamics*, 41(3-4):867–884, 2013.
- N. J. Loader, I. Robertson, and D. McCarroll. Comparison of stable carbon isotope ratios in the whole wood, cellulose and lignin of oak tree-rings. *Palaeogeography, Palaeoclimatology, Palaeoecology*, 196(3-4):395–407, 2003.
- M. J. Lockheart, P. F. van Bergen, and R. P. Evershed. Variations in the stable carbon isotope compositions of individual lipids from the leaves of modern angiosperms: implications for the study of sedimentary organic matter. *Organic Geochemistry*, 26(1):137–153, 1997.
- R. A. Lopes dos Santos and C. H. Vane. Signatures of tetraether lipids reveal anthropogenic overprinting of natural organic matter in sediments of the Thames Estuary, UK. *Organic Geochemistry*, 93:68–76, 2016.
- P. Lorenz, M. Berger, J. Bertrams, K. Wende, K. Wenzel, U. Lindequist, U. Meyer, and F. C. Stintzing. Natural wax constituents of a supercritical fluid CO<sub>2</sub> extract from quince (*Cydonia oblonga* Mill.) pomace. *Analytical and Bioanalytical Chemistry*, 391(2):633–646, 2008.
- A. Lourantou, J. V. Lavriè, P. Köhler, J. M. Barnola, D. Paillard, E. Michel, D. Raynaud, and J. Chappellaz. Constraint of the CO<sub>2</sub> rise by new atmospheric carbon isotopic measurements during the last deglaciation. *Global Biogeochemical Cycles*, 24(2):1–15, 2010.
- M. Majoube. Oxygen-18 and deuterium fractionation between water and steam. *Journal de Chimie Physique et de Physico-Chimie Biologique*, 68(10):1423, 1971.

- M. K. Männistö, S. Rawat, V. Starovoytov, and M. M. Häggblom. *Granulicella arctica* sp. nov., *Granulicella mallensis* sp. nov., *Granulicella tundricola* sp. nov. and *Granulicella sapmiensis* sp. nov., novel acidobacteria from tundra soil. *International journal of systematic and evolutionary microbiology*, 62(Pt 9):2097–106, 2012.
- N. Marchand-Geneste and A. Carpy. Theoretical study of the thermal degradation pathways of abietane skeleton diterpenoids: aromatization to retene. *Journal of Molecular Structure: THEOCHEM*, 635(1):55–82, 2003.
- D. R. Marchant, C. C. Swisher, D. R. Lux, D. P. West, and G. H. Denton. Pliocene Paleoclimate and East Antarctic Ice-Sheet History from Surficial Ash Deposits. *Science*, 260(5108):667–670, 1993a.
- D. R. Marchant, G. H. Denton, D. E. Sugden, and C. C. Swisher. Miocene Glacial Stratigraphy and Landscape Evolution of the Western Asgard Range, Antarctica. *Geografiska Annaler. Series A, Physical Geography*, 75(4):303, 1993b.
- D. R. Marchant, G. H. Denton, and C. C. Swisher. Miocene-Pliocene-Pleistocene Glacial History of Arena Valley, Quartermain Mountains, Antarctica. *Geografiska Annaler. Series A, Physical Geography*, 75(4):269, 1993c.
- D. R. Marchant, G. H. Denton, C. C. Swisher III, and N. Potter Jr. Late Cenozoic Antarctic paleoclimate reconstructed from volcanic ashes in the Late Cenozoic Antarctic paleoclimate reconstructed from volcanic ashes in the Dry Valleys region of southern Victoria Land. *Geological Society of America Bulletin*, 108(2):181–194, 1996.
- A. Martínez-García, A. Rosell-Melé, S. L. Jaccard, W. Geibert, D. M. Sigman, and G. H. Haug. Southern Ocean dust-climate coupling over the past four million years. *Nature*, 476(7360):312–315, 2011.
- V. Masson-Delmotte, S. Hou, A. Ekaykin, J. Jouzel, A. Aristarain, R. T. Bernardo, D. Bromwich, O. Cattani, M. Delmotte, S. Falourd, M. Frezzotti, H. Gallée, L. Genoni, E. Isaksson, A. Landais, M. M. Helsen, G. Hoffmann, J. Lopez, V. Morgan, H. Motoyama, D. Noone, H. Oerter, J. R. Petit, A. Royer, R. Uemura, G. A. Schmidt, E. Schlosser, J. C. Simões, E. J. Steig, B. Stenni, M. Stievenard, M. R. van den Broeke, R. S. W. van de Wal, W. J. van de Berg, F. Vimeux, and J. W. C. White. A Review of Antarctic Surface Snow Isotopic Composition: Observations, Atmospheric Circulation, and Isotopic Modeling\*. *Journal of Climate*, 21(13):3359–3387, 2008.
- D. McCarroll and N. J. Loader. Stable isotopes in tree rings. *Quaternary Science Reviews*, 23:771–801, 2004.
- R. M. McKay, P. J. Barrett, M. A. Harper, and M. J. Hannah. Atmospheric transport and concentration of diatoms in surficial and glacial sediments of the Allan Hills, Transantarctic Mountains. *Palaeogeography, Palaeoclimatology, Palaeoecology*, 260(1):168–183, 2008.
- R. M. McKay, T. R. Naish, L. Carter, C. R. Riesselman, R. B. Dunbar, C. Sjunneskog, D. Winter, F. Sangiorgi, C. Warren, M. Pagani, S. Schouten, V. Willmott, R. H. Levy, R. M. DeConto, and R. D. Powell. Antarctic and Southern Ocean influences on Late Pliocene global cooling. *Proceedings of the National Academy of Sciences of the United States of America*, 109(17):6423–8, 2012.
- B. C. McKelvey, P. N. Webb, D. M. Harwood, and M. C. G. Mabin. The Dominion Range Sirius Group: a record of the late Pliocene-early Pleistocene Beardmore Glacier. In *Geological Evolution of Antarctica*, pages 675–682. 1991.
- L. Menviel, A. Mouchet, K. J. Meissner, F. Joos, and M. H. England. Impact of oceanic circulation changes on atmospheric  $\delta^{13}\text{C}$  CO<sub>2</sub>. *Global Biogeochemical Cycles*, (Dic): n/a–n/a, 2015.

- J. H. Mercer. Southernmost Chile : A modern analog of the southern shores of the Ross Embayment during Pliocene warm intervals. *Antarctic Journal of the United States*, 21(5):103–105, 1986.
- J. H. Mercer and J. F. Sutter. Late Miocene-earliest Pliocene glaciation in southern Argentina: Implications for global ice-sheet history. *Palaeogeography Palaeoclimatology Palaeoecology*, 38:185–206, 1982.
- L. Merlivat and G. Nief. Fractionnement isotopique lors des changements d'état solide-vapeur et liquide-vapeur de l'eau à des températures inférieures à 0 C. *Tellus A*, 19(1), 1967.
- K. G. Miller, J. D. Wright, J. V. Browning, A. Kulpecz, M. Kominz, T. R. Naish, B. S. Cramer, Y. Rosenthal, W. R. Peltier, and S. Sosdian. High tide of the warm Pliocene: Implications of global sea level for Antarctic deglaciation. *Geology*, 40(5):407–410, 2012.
- D. M. Moore. *Flora of Tierra del Fuego*. Anthony Nelson, Oswesrty, 1983.
- T. R. Naish, R. Powell, R. H. Levy, G. B. Wilson, R. P. Scherer, F. Talarico, L. A. Krissek, F. Niessen, M. Pompilio, T. Wilson, L. Carter, R. M. DeConto, P. Huybers, R. M. McKay, D. Pollard, J. Ross, D. Winter, P. Barrett, G. H. Browne, R. Cody, E. Cowan, J. Crampton, G. Dunbar, N. Dunbar, F. Florindo, C. Gebhardt, I. Graham, M. J. Hannah, D. Hansaraj, D. M. Harwood, D. Helling, S. A. Henrys, L. Hinnov, G. Kuhn, P. Kyle, A. Läufer, P. Maffioli, D. Magens, K. Mandernack, W. C. McIntosh, C. Millan, R. Morin, C. Ohneiser, T. Paulsen, D. Persico, I. Raine, J. Reed, C. R. Riesselman, L. Sagnotti, D. Schmitt, C. Sjunneskog, P. Strong, M. Taviani, S. Vogel, T. Wilch, and T. Williams. Obliquity-paced Pliocene West Antarctic ice sheet oscillations. *Nature*, 458(7236):322–8, 2009.
- H. Nakamura, K. Sawada, and M. Takahashi. Aliphatic and aromatic terpenoid biomarkers in Cretaceous and Paleogene angiosperm fossils from Japan. *Organic Geochemistry*, 41(9):975–980, 2010.
- K. G. J. Nierop, B. Jansen, J. A. Hageman, and J. M. Verstraten. The complementarity of extractable and ester-bound lipids in a soil profile under pine. *Plant and Soil*, 286(1-2):269–285, 2006.
- M. H. O'Leary. Carbon isotopes in photosynthesis. *BioScience*, 38(5):328–336, 1988.
- A. Otto and B. R. T. Simoneit. Chemosystematics and diagenesis of terpenoids in fossil conifer species and sediment from the Eocene Zeitz formation, Saxony, Germany. *Geochimica et Cosmochimica Acta*, 65(20):3505–3527, 2001.
- A. Otto and B. R. Simoneit. Biomarkers of Holocene buried conifer logs from Bella Coola and north Vancouver, British Columbia, Canada. *Organic Geochemistry*, 33(11):1241–1251, 2002.
- A. Otto and V. Wilde. Sesqui-, di-, and triterpenoids as chemosystematic markers in extant conifers: A review. *The Botanical Review*, 67(2):141–238, 2001.
- A. Otto, B. R. T. Simoneit, and W. C. Rember. Conifer and angiosperm biomarkers in clay sediments and fossil plants from the Miocene Clarkia Formation, Idaho, USA. *Organic Geochemistry*, 36:907–922, 2005.
- M. Pagani, N. Pedentchouk, M. Huber, A. Sluijs, S. Schouten, H. Brinkhuis, J. S. S. Damsté, and G. R. Dickens. Arctic hydrology during global warming at the Palaeocene/Eocene thermal maximum. *Nature*, 442(7103):671–675, 2006.
- M. Pagani, Z. Liu, J. LaRiviere, and A. C. Ravelo. High Earth-system climate sensitivity determined from Pliocene carbon dioxide concentrations. *Nature Geoscience*, 3(1):27–30, 2010.

- R. D. Pancost, M. Baas, B. van Geel, and J. S. Sinninghe Damsté. Biomarkers as proxies for plant inputs to peats: An example from a sub-boreal ombrotrophic bog. *Organic Geochemistry*, 33(7):675–690, 2002.
- F. S. Paolo, H. A. Fricker, and L. Padman. Volume loss from Antarctic ice shelves is accelerating. *Science*, 348(6232):327–331, 2015.
- S. Passchier. Variability in Geochemical Provenance and Weathering History of Sirius Group Strata, Transantarctic Mountains: Implications for Antarctic Glacial History. *Journal of Sedimentary Research*, 74(5):607–619, 2004.
- S. Passchier, G. H. Browne, B. Field, C. R. Fielding, L. A. Krissek, K. Panter, and S. F. Pekar. Early and middle Miocene Antarctic glacial history from the sedimentary facies distribution in the AND-2A drill hole, Ross Sea, Antarctica. *Bulletin of the Geological Society of America*, 123(11-12):2352–2365, 2011.
- S. Passchier, S. M. Bohaty, F. J. Jiménez-Espejo, J. Pross, U. Röhl, T. Van De Flierdt, C. Escutia, and H. Brinkhuis. Early Eocene to Middle Miocene cooling and aridification of east antarctica. *Geochemistry, Geophysics, Geosystems*, 14(5):1399–1410, 2013a.
- S. Passchier, C. J. Falk, and F. Florindo. Orbitally paced shifts in the particle size of Antarctic continental shelf sediments in response to ice dynamics during the Miocene climatic optimum. *Geosphere*, 9(1):54–62, 2013b.
- S. Passchier. Provenance of the Sirius Group and related Upper Cenozoic glacial deposits from the Transantarctic Mountains, Antarctica: Relation to landscape evolution and ice-sheet drainage. *Sedimentary Geology*, 144:263–290, 2001.
- M. O. Patterson, R. M. McKay, T. R. Naish, C. Escutia, F. J. Jimenez-Espejo, M. E. Raymo, S. R. Meyers, L. Tauxe, H. Brinkhuis, and I. E. . Scientists. Orbital forcing of the East Antarctic ice sheet during the Pliocene and Early Pleistocene. *Nature Geosci*, 7(11):841–847, 2014.
- S. F. Pekar and R. M. DeConto. High-resolution ice-volume estimates for the early Miocene: Evidence for a dynamic ice sheet in Antarctica. *Palaeogeography, Palaeoclimatology, Palaeoecology*, 231(1-2):101–109, 2006.
- F. Peterse, J.-H. Kim, S. Schouten, D. K. Kristensen, N. Koç, and J. S. Sinninghe Damsté. Constraints on the application of the MBT/CBT palaeothermometer at high latitude environments (Svalbard, Norway). *Organic Geochemistry*, 40(6):692–699, 2009.
- F. Peterse, J. van der Meer, S. Schouten, J. W. H. Weijers, N. Fierer, R. B. Jackson, J. H. Kim, and J. S. Sinninghe Damsté. Revised calibration of the MBT-CBT paleotemperature proxy based on branched tetraether membrane lipids in surface soils. *Geochimica et Cosmochimica Acta*, 96:215–229, 2012.
- R. P. Philp. *Fossil fuel biomarkers: Applications and spectra*. 1985.
- C. Polashenski, D. Perovich, and Z. Courville. The mechanisms of sea ice melt pond formation and evolution. *Journal of Geophysical Research: Oceans*, 117(C1):n/a–n/a, 2012.
- D. Pollard, R. M. DeConto, and R. B. Alley. Potential Antarctic Ice Sheet retreat driven by hydrofracturing and ice cliff failure. *Earth and Planetary Science Letters*, 412:112–121, 2015.
- D. Pollard and R. M. DeConto. Modelling West Antarctic ice sheet growth and collapse through the past five million years. *Nature*, 458(7236):329–32, 2009.
- D. Pollard and R. M. DeConto. Contribution of Antarctica to past and future sea-level rise. *Nature*, 531(7596):591–597, 2016.

- V. D. Pope, M. L. Gallani, P. R. Rowntree, and R. A. Stratton. The impact of new physical parametrizations in the Hadley Centre climate model: HadAM3. *Climate Dynamics*, 16(2-3):123–146, 2000.
- M. J. Pound, A. M. Haywood, U. Salzmann, and J. B. Riding. Global vegetation dynamics and latitudinal temperature gradients during the Mid to Late Miocene (15.975–33Ma). *Earth-Science Reviews*, 112(1-2):1–22, 2012.
- J. G. Prebble, J. I. Raine, P. J. Barrett, and M. J. Hannah. Vegetation and climate from two Oligocene glacioeustatic sedimentary cycles (31 and 24 Ma) cored by the Cape Roberts Project, Victoria Land Basin, Antarctica. *Palaeogeography, Palaeoclimatology, Palaeoecology*, 231(1-2):41–57, 2006.
- C. L. Prescott, A. M. Haywood, A. M. Dolan, S. J. Hunter, J. O. Pope, and S. J. Pickering. Assessing orbitally-forced interglacial climate variability during the mid-Pliocene Warm Period. *Earth and Planetary Science Letters*, 400:261–271, 2014.
- H. D. Pritchard, S. R. M. Ligtenberg, H. A. Fricker, D. G. Vaughan, M. R. van den Broeke, and L. Padman. Antarctic ice-sheet loss driven by basal melting of ice shelves. *Nature*, 484(7395):502–505, 2012.
- J. Pross, L. Contreras, P. K. Bijl, D. R. Greenwood, S. M. Bohaty, S. Schouten, J. A. P. Bendle, U. Röhl, L. Tauxe, J. I. Raine, C. E. Huck, T. van de Flierdt, S. S. R. Jamieson, C. E. Stickley, B. van de Schootbrugge, C. Escutia, H. Brinkhuis, A. Klaus, A. Fehr, T. Williams, S. A. Carr, R. B. Dunbar, J. J. González, T. G. Hayden, M. Iwai, F. J. Jimenez-Espejo, K. Katsuki, G. Soo Kong, R. M. McKay, M. Nakai, M. P. Olney, S. Passchier, S. F. Pekar, C. R. Riesselman, U. Röhl, T. Sakai, P. K. Shrivastava, C. E. Stickley, S. Sugisaki, S. Tuo, K. Welsh, and M. Yamane. Persistent near-tropical warmth on the Antarctic continent during the early Eocene epoch. *Nature*, 488(7409):73–77, 2012.
- J. I. Raine. Terrestrial Palynomorphs from Cape Roberts Project Drillhole CRP-1, Ross Sea, Antarctica. *Terra Antarctica*, 5(3):539–548, 1998.
- A. C. Ravelo and D. H. Andreasen. Enhanced circulation during a warm period. *Geophysical Research Letters*, 27(7):1001–1004, 2000.
- M. E. Raymo, B. Grant, M. Horowitz, and G. H. Rau. Mid-Pliocene warmth: stronger greenhouse and stronger conveyor. *Marine Micropaleontology*, 27(1-4):313–326, 1996.
- M. E. Raymo and J. X. Mitrovica. Collapse of polar ice sheets during the stage 11 interglacial. *Nature*, 483(7390):453–456, 2012.
- R. L. Rees-Owen, F. Gill, R. J. Newton, R. Ivanovic, J. E. Francis, J. B. Riding, C. H. Vane, and R. A. Lopes dos Santos. The last forests on Antarctica: reconstructing flora and temperatures from the Neogene Sirius Group, Transantarctic Mountains. *in prep-a*, a.
- R. L. Rees-Owen, R. J. Newton, R. Ivanovic, J. B. Riding, J. E. Francis, and A. Marca. Climatic signals recorded in carbon and oxygen isotopes of fossil southern beech trees from Antarctica. *in prep-b*, b.
- B. T. I. Reinardy, C. Escutia, M. Iwai, F. J. Jimenez-Espejo, C. P. Cook, T. van de Flierdt, and H. Brinkhuis. Repeated advance and retreat of the East Antarctic Ice Sheet on the continental shelf during the early Pliocene warm period. *Palaeogeography, Palaeoclimatology, Palaeoecology*, 422:65–84, 2015.
- G. J. Retallack, E. S. Krull, and J. G. Bockheim. New grounds for reassessing palaeoclimate of the Sirius Group, Antarctica. *Journal of the Geological Society, London*, 158:925–935, 2001.

- S. Rezzi, A. Bighelli, V. Castola, and J. Casanova. Composition and chemical variability of the oleoresin of *Pinus nigra* ssp. *laricio* from Corsica. *Industrial Crops and Products*, 21(1):71–79, 2005.
- J. S. Roden and J. R. Ehleringer. Observations of hydrogen and oxygen isotopes in leaf water confirm the Craig-Gordon model under wide-ranging environmental conditions. *Plant Physiology*, 120(4):1165–1174, 1999.
- J. S. Roden and J. R. Ehleringer. Hydrogen and oxygen isotope ratios of tree ring cellulose for field-grown riparian trees. *Oecologia*, 123(4):481–489, 2000.
- E. J. Rohling, M. Medina-Elizalde, J. G. Shepherd, M. Siddall, and J. D. Stanford. Sea surface and high-latitude temperature sensitivity to radiative forcing of climate over several glacial cycles. *Journal of Climate*, 25(5):1635–1656, 2012.
- E. J. Rohling, G. L. Foster, K. M. Grant, G. Marino, A. P. Roberts, M. E. Tamisiea, and F. Williams. Sea-level and deep-sea-temperature variability over the past 5.3 million years. *Nature*, 508(7497):477–482, 2014.
- J.-F. Rontani and C. Aubert. Trimethylsilyl transfer during electron ionization mass spectral fragmentation of some  $\omega$ -hydroxycarboxylic and  $\omega$ -dicarboxylic acid trimethylsilyl derivatives and the effect of chain length. *Rapid Communications in Mass Spectrometry*, 18:1889–1895, 2004.
- D. Sachse, J. Radke, and G. Gleixner. Hydrogen isotope ratios of recent lacustrine sedimentary n-alkanes record modern climate variability. *Geochimica et Cosmochimica Acta*, 68(23):4877–4889, 2004.
- D. Sachse, A. Kahmen, and G. Gleixner. Significant seasonal variation in the hydrogen isotopic composition of leaf-wax lipids for two deciduous tree ecosystems (*Fagus sylvatica* and *Acer pseudoplatanus*). *Organic Geochemistry*, 40(6):732–742, 2009.
- D. Sachse, I. Billault, G. J. Bowen, Y. Chikaraishi, T. E. Dawson, S. J. Feakins, K. H. Freeman, C. R. Magill, F. A. McInerney, M. T. J. J. van der Meer, P. J. Polissar, R. J. Robins, J. P. Sachs, H.-L. Schmidt, A. L. Sessions, J. W. C. White, J. B. West, and A. Kahmen. Molecular paleohydrology: interpreting the hydrogen-isotopic composition of lipid biomarkers from photosynthesizing organisms. *Annual Review of Earth and Planetary Sciences*, 40:221–249, 2012.
- U. Salzmann, A. M. Dolan, A. M. Haywood, W.-L. Chan, J. Voss, D. J. Hill, A. Abe-Ouchi, B. Otto-Bliesner, F. J. Bragg, M. A. Chandler, C. Contoux, H. J. Dowsett, A. Jost, Y. Kamae, G. Lohmann, D. J. Lunt, S. J. Pickering, M. J. Pound, G. Ramstein, N. A. Rosenbloom, L. Sohl, C. Stepanek, H. Ueda, and Z. Zhang. Challenges in quantifying Pliocene terrestrial warming revealed by datamodel discord. *Nature Climate Change*, 3(11):969–974, 2013.
- M. Saurer, K. Aellen, and R. T. W. Siegwolf. Correlating  $\delta^{13}\text{C}$  and  $\delta^{18}\text{O}$  in cellulose of trees. *Plant, Cell and Environment*, 20(12):1543–1550, 1997.
- E. S. Scalan and J. E. Smith. An improved measure of the odd-even predominance in the normal alkanes of sediment extracts and petroleum. *Geochimica et Cosmochimica Acta*, 34(5):611–620, 1970.
- Y. Scheidegger, M. Saurer, M. Bahn, and R. T. W. Siegwolf. Linking stable oxygen and carbon isotopes with stomatal conductance and photosynthetic capacity: a conceptual model. *Oecologia*, 125(3):350–357, 2000.
- A. Schimmelmann, A. L. Sessions, and M. Mastalerz. Hydrogen Isotopic (D/H) Composition of Organic Matter During Diagenesis and Thermal Maturation. *Annual Review of Earth and Planetary Sciences*, 34(1):501–533, 2006.

- B. A. Schubert, A. H. Jahren, J. J. Eberle, L. S. L. Sternberg, and D. A. Eberth. A summertime rainy season in the Arctic forests of the Eocene. *Geology*, 40(6):523–526, 2012.
- E. D. Schulze, H. A. Mooney, O. E. Sala, E. Jobbagy, N. Buchmann, G. Bauer, J. Canadell, R. B. Jackson, J. Loreti, M. Oesterheld, and J. R. Ehleringer. Rooting depth, water availability, and vegetation cover along an aridity gradient in Patagonia. *Oecologia*, 108(3):503–511, 1996.
- F. Schweingruber. *Wood structure and environment*. 2007.
- P. Sepulchre, G. Ramstein, F. Fluteau, M. Schuster, J.-J. Tiercelin, and M. Brunet. Tectonic Uplift and Eastern Africa Aridification. *Science*, 313(5792):1419–1423, 2006.
- A. L. Sessions, T. W. Burgoyne, A. Schimmelmann, and J. M. Hayes. Fractionation of hydrogen isotopes in lipid biosynthesis. *Organic Geochemistry*, 30:1193–1200, 1999.
- A. L. Sessions, S. P. Sylva, R. E. Summons, and J. M. Hayes. Isotopic exchange of carbon-bound hydrogen over geologic timescales. *Geochimica et Cosmochimica Acta*, 68(7):1545–1559, 2004.
- A. Shepherd, E. R. Ivins, G. A. V. R. Barletta, M. J. Bentley, S. Bettadpur, K. H. Briggs, D. H. Bromwich, R. Forsberg, N. Galin, M. Horwath, S. Jacobs, I. Joughin, M. A. King, J. T. M. Lenaerts, J. Li, S. R. M. Ligtenberg, A. Luckman, S. B. Luthcke, M. McMillan, R. Meister, G. Milne, J. Mouginot, A. Muir, J. P. Nicolas, J. Paden, A. J. Payne, H. Pritchard, E. Rignot, H. Rott, L. S. Sorensen, T. A. Scambos, B. Scheuchl, E. J. O. Schrama, B. Smith, A. V. Sundal, J. H. van Angelen, W. J. van de Berg, M. R. van den Broeke, D. G. Vaughan, I. Velicogna, J. Wahr, P. L. Whitehouse, D. J. Wingham, D. Yi, D. Young, and H. J. Zwally. A Reconciled Estimate of Ice-Sheet Mass Balance. *Science*, 338(6111):1183–1189, 2012.
- A. E. Shevenell, J. P. Kennett, and D. W. Lea. Middle Miocene Southern Ocean cooling and Antarctic cryosphere expansion. *Science*, 305(5691):1766–1770, 2004.
- A. E. Shevenell, J. P. Kennett, and D. W. Lea. Middle Miocene ice sheet dynamics, deep-sea temperatures, and carbon cycling: A Southern Ocean perspective. *Geochemistry, Geophysics, Geosystems*, 9(2), 2008.
- L. C. Sime, E. W. Wolff, K. I. C. Oliver, and J. C. Tindall. Evidence for warmer interglacials in East Antarctic ice cores. *Nature*, 462(7271):342–345, 2009.
- L. C. Sime, D. P. Stevens, K. J. Heywood, and K. I. C. Oliver. A Decomposition of the Atlantic Meridional Overturning. *Journal of Physical Oceanography*, 36(12):2253–2270, 2006.
- A. J. Simmons and D. M. Burridge. An Energy and Angular-Momentum Conserving Vertical Finite-Difference Scheme and Hybrid Vertical Coordinates. *Monthly Weather Review*, 109(4):758–766, 1981.
- B. R. T. Simoneit. Diterpenoid compounds and other lipids in deep-sea sediments and their geochemical significance. *Geochimica et Cosmochimica Acta*, 41(4):463–476, 1977.
- B. R. T. Simoneit and M. A. Mazurek. Organic matter of the troposphere II. Natural background of biogenic lipid matter in aerosols over the rural western united states. *Atmospheric Environment (1967)*, 16(9):2139–2159, 1982.
- B. R. T. Simoneit, J. O. Grimalt, T. G. Wang, R. E. Cox, P. G. Hatcher, and A. Nissenbaum. Cyclic terpenoids of contemporary resinous plant detritus and of fossil woods, ambers and coals. *Organic Geochemistry*, 10(4-6):877–889, 1986.
- J. S. Singarayer and P. J. Valdes. High-latitude climate sensitivity to ice-sheet forcing over the last 120 kyr. *Quaternary Science Reviews*, 29(1-2):43–55, 2010.

- J. S. Sinninghe Damsté, W. I. C. Rijpstra, E. C. Hopmans, J. W. H. Weijers, B. U. Foessel, J. Overmann, and S. N. Dedysh. 13,16-Dimethyl octacosanedioic acid (isodiabolic acid), a common membrane-spanning lipid of Acidobacteria subdivisions 1 and 3. *Applied and environmental microbiology*, 77(12):4147–54, 2011.
- B. N. Smith, J. Oliver, and C. McMillan. Influence of carbon source, oxygen concentration, light intensity and temperature on  $^{13}\text{C}/^{12}\text{C}$  ratios in plant tissues. *Botanical Gazette*, 137(2):99–104, 1976.
- A. F. Sousa, P. C. R. O. Pinto, A. J. D. Silvestre, and C. P. Neto. Triterpenic and other lipophilic components from industrial cork byproducts. *Journal of Agricultural and Food Chemistry*, 54(18):6888–6893, 2006.
- G. Staccioli, I. Santoni, and B. Pizzo. Decay of fossil wood from kimberlite pipes of Lac de Gras in the Canadian sub-Arctic area. *Annales de Paléontologie*, 100(1):87–94, 2014.
- M. Stefanova, D. R. Oros, A. Otto, and B. R. T. Simoneit. Polar aromatic biomarkers in the Miocene Maritza-East lignite, Bulgaria. *Organic Geochemistry*, 33(9):1079–1091, 2002.
- L. S. L. Sternberg and M. J. DeNiro. Isotopic Composition of Cellulose from C3, C4, and CAM Plants Growing Near One Another. *Science*, 220(4600):947–949, 1983.
- L. S. L. Sternberg, M. J. DeNiro, and R. A. Savidge. Oxygen Isotope Exchange between Metabolites and Water during Biochemical Reactions Leading to Cellulose Synthesis. *Plant Physiology*, 82(2):423–7, 1986.
- G. R. Stewart, M. H. Turnbull, S. Schmidt, and P. D. Erskine.  $^{13}\text{C}$  Natural Abundance in Plant Communities Along a Rainfall Gradient: a Biological Integrator of Water Availability. *Australian Journal of Plant Physiology*, 22(1):51–55, 1995.
- M. A. Stokes and T. L. Smiley. *An introduction to tree-ring dating*. The University of Chicago Press, Chicago and London, 1968.
- E. J. Stone, D. J. Lunt, J. D. Annan, and J. C. Hargreaves. Quantification of the Greenland ice sheet contribution to Last Interglacial sea level rise. *Climate of the Past*, 9(2):621–639, 2013.
- K. Stránský, M. Streibl, and V. Herout. On natural waxes. VI. Distribution of wax hydrocarbons in plants at different evolutionary levels. *Collection of Czechoslovak Chemical Communications*, 32(9):3213–3220, 1967.
- A. P. Stroeven, M. L. Prentice, and J. Kleman. On marine microfossil transport and pathways in Antarctica during the late Neogene: Evidence from the Sirius Group at Mount Fleming. *Geology*, 24(8):727–730, 1996.
- D. E. Sugden, G. H. Denton, and R. Marchant. Landscape evolution of the Dry Valleys, Transantarctic Mountains: Tectonic implications. *Journal of Geophysical Research:Solid Earth*, 100(B6):9949–9967, 1995.
- V. R. Switsur, J. S. Waterhouse, E. M. Field, A. H. C. Carter, and N. J. Loader. Stable isotope studies in tree rings from oak techniques and some preliminary results. *Paläoklimaforschung*, 15:129–140, 1995.
- M. H. Tavendale, P. N. McFarlane, K. L. Mackie, A. L. Wilkins, and A. G. Langdon. The fate of resin acids-2. The fate of resin acids and resin acid derived neutral compounds in anaerobic sediments. *Chemosphere*, 35(10):2153–2166, 1997a.
- M. H. Tavendale, P. N. McFarlane, K. L. Mackie, A. L. Wilkins, and A. G. Langdon. The fate of resin acids-1. The biotransformation and degradation of deuterium labelled dehydroabietic acid in anaerobic sediments. *Chemosphere*, 35(10):2137–2151, 1997b.

- M. Taviani, M. J. Hannah, D. M. Harwood, S. E. Ishman, K. Johnson, M. P. Olney, C. R. Riesselman, E. Tuzzi, R. A. Askin, A. G. Beu, S. Blair, V. Cantarelli, A. Ceregato, S. Corrado, B. A. R. Mohr, S. H. H. Nielsen, D. Persico, S. Petrushak, J. I. Raine, S. Warny, and T. A.-S. S. Team. Palaeontological characterisation and analysis of the AND-2A core, ANDRILL Southern McMurdo Sound Project. *Terra Antarctica*, 15(1):113–144, 2008.
- J. C. Tindall, P. J. Valdes, and L. C. Sime. Stable water isotopes in HadCM3: Isotopic signature of El Niño-Southern Oscillation and the tropical amount effect. *Journal of Geophysical Research Atmospheres*, 114(4):1–12, 2009.
- J. C. Tindall and A. M. Haywood. Modeling oxygen isotopes in the Pliocene: Large-scale features over the land and ocean. *Paleoceanography*, 30(9):1183–1201, 2015.
- J. C. Tindall, R. Flecker, P. Valdes, D. N. Schmidt, P. Markwick, and J. Harris. Modelling the oxygen isotope distribution of ancient seawater using a coupled ocean-atmosphere GCM: Implications for reconstructing early Eocene climate. *Earth and Planetary Science Letters*, 292(3-4):265–273, 2010.
- B. J. Tipple, S. R. Meyers, and M. Pagani. Carbon isotope ratio of Cenozoic CO<sub>2</sub> : A comparative evaluation of available geochemical proxies. *Paleoceanography*, 25(3):n/a–n/a, 2010.
- B. J. Tipple, M. A. Berke, C. E. Doman, S. Khachatryan, and J. R. Ehleringer. Leaf-wax n-alkanes record the plant-water environment at leaf flush. *Proceedings of the National Academy of Sciences of the United States of America*, 110(7):2659–64, 2013.
- J. M. Trendel, F. Lohmann, J. P. Kintzinger, P. Albrecht, A. Chiarone, C. Riche, M. Cesario, J. Guilhem, and C. Pascard. Identification of des-A-triterpenoid hydrocarbons occurring in surface sediments. *Tetrahedron*, 45(14):4457–4470, 1989.
- J. Turner and G. J. Marshall. The high latitude climates and change mechanisms. In *Climate Change in the Polar Regions*, pages 137–138. Cambridge University Press, 2011.
- J. Turner, W. M. Connolley, T. A. Lachlan-Cope, and G. J. Marshall. The performance of the Hadley Centre climate model (HADCM3) in high southern latitudes. *International Journal of Climatology*, 26(1):91–112, 2006.
- D. J. Ullman, A. N. Legrande, A. E. Carlson, F. S. Anslow, and J. M. Licciardi. Assessing the impact of laurentide ice sheet topography on glacial climate. *Climate of the Past*, 10(2):487–507, 2014.
- W. J. van de Berg, M. van den Broeke, J. Ettema, E. van Meijgaard, and F. Kaspar. Significant contribution of insolation to Eemian melting of the Greenland ice sheet. *Nature Geoscience*, 4(10):679–683, 2011.
- T. T. Veblen, B. R. Burns, T. Kitzberger, A. Lara, and R. Villalba. The ecology of the conifers of southern South America. In N. J. Enright and R. S. Hill, editors, *The Ecology of the Southern Conifers*, pages 120–155. 1995.
- T. T. Veblen, C. Donoso, T. Kitzberger, and A. J. Rebertus. Ecology of southern Chilean and Argentinian Nothofagus forests. In T. T. Veblen, R. S. Hill, and J. Read, editors, *The Ecology and Biogeography of Nothofagus Forests*, pages 293 – 353. Yale University Press, 1996.
- E. Vincent and W. H. Berger. Carbon dioxide and polar cooling in the Miocene: the Monterey hypothesis. *The Carbon Cycle and Atmospheric CO<sub>2</sub>: Natural Variations Archean to Present*, 32:455–468, 1985.
- J. C. Vogel, P. M. Grootes, and W. G. Mook. Isotopic fractionation between gaseous and dissolved carbon dioxide. *Z. Phys.*, 230:225–238, 1970.

- X.-F. Wang and D. Yakir. Temporal and spatial variations in the oxygen-18 content of leaf water in different plant species. *Plant, Cell & Environment*, 18(12):1377–1385, 1995.
- S. Warny, R. A. Askin, M. J. Hannah, B. A. R. Mohr, J. I. Raine, D. M. Harwood, and F. Florindo. Palynomorphs from a sediment core reveal a sudden remarkably warm Antarctica during the middle Miocene. *Geology*, 37(10):955–958, 2009.
- S. Warny and R. A. Askin. Last Remnants of Cenozoic Vegetation and Organic-Walled Phytoplankton in the Antarctic Peninsula’s Icehouse World. In *Tectonic, Climatic, and Cryospheric Evolution of the Antarctic Peninsula*, pages 167–192. 2011.
- S. Warny, J. H. Wrenn, P. J. Bart, and R. A. Askin. Palynology of the NBP0301A transect in the Northern Basin, Western Ross Sea, Antarctica: A late Pliocene record. *Palynology*, 30(1):151–182, 2006.
- P. N. Webb and D. M. Harwood. Terrestrial flora of the Sirius Formation: its significance for Late Cenozoic glacial history. *Antarctic Journal of the United States*, 22(4):7–11, 1987.
- P.-N. Webb and D. M. Harwood. Pliocene Fossil Nothofagus (Southern Beech) from Antarctica: Phytogeography, Dispersal Strategies, and Survival in High Latitude Glacial-Deglacial Environments. In *Forest Development in Cold Climates*, pages 135–165. 1993.
- P. N. Webb, D. M. Harwood, B. C. McKelvey, J. H. Mercer, and L. D. Stott. Geology Cenozoic marine sedimentation and ice-volume variation on the East Antarctic craton. *Geology*, 12(5):287–291, 1984.
- P.-N. Webb, D. M. Harwood, M. G. C. Mabin, and B. C. McKelvey. A marine and terrestrial Sirius Group succession, middle Beardmore Glacier-Queen Alexandra Range, Transantarctic Mountains, Antarctica. *Marine Micropaleontology*, 27(1-4):273–297, 1996.
- P.-N. Webb and D. M. Harwood. Late Cenozoic glacial history of the Ross embayment, Antarctica. *Quaternary Science Reviews*, 10(2-3):215–223, 1991.
- J. W. Weijers, S. Schouten, J. C. van den Donker, E. C. Hopmans, and J. S. Sinninghe Damsté. Environmental controls on bacterial tetraether membrane lipid distribution in soils. *Geochimica et Cosmochimica Acta*, 71(3):703–713, 2007.
- J. W. Weijers, B. Bernhardt, F. Peterse, J. P. Werne, J. A. J. Dungait, S. Schouten, and J. S. Sinninghe Damsté. Absence of seasonal patterns in MBTCBT indices in mid-latitude soils. *Geochimica et Cosmochimica Acta*, 75(11):3179–3190, 2011.
- A. G. West, S. J. Patrickson, and J. R. Ehleringer. Water extraction times for plant and soil materials used in stable isotope analysis. *Rapid Communications in Mass Spectrometry*, 20(8):1317–1321, 2006.
- J. M. Whitehead, S. Wotherspoon, and S. M. Bohaty. Minimal Antarctic sea ice during the Pliocene. *Geology*, 33(2):137–140, 2005.
- T. Wieloch, G. Helle, I. Heinrich, M. Voigt, and P. Schyma. A novel device for batch-wise isolation of  $\alpha$ -cellulose from small-amount wholewood samples. *Dendrochronologia*, 29(2):115–117, 2011.
- T. M. L. Wigley, K. R. Briffa, and P. D. Jones. On the Average Value of Correlated Time Series, with Applications in Dendroclimatology and Hydrometeorology. *Journal of Climate and Applied Meteorology*, 23(2):201–213, 1984.

- T. Williams, T. van de Flierdt, S. R. Hemming, E. Chung, M. Roy, and S. L. Goldstein. Evidence for iceberg armadas from East Antarctica in the Southern Ocean during the late Miocene and early Pliocene. *Earth and Planetary Science Letters*, 290(3-4): 351–361, 2010.
- M. F. Wilson and A. Henderson-Sellers. A global archive of land cover and soils data for use in general-circulation climate models. *Journal of Climatology*, 5(2):119–143, 1985.
- M. J. Winnick and J. K. Caves. Oxygen isotope mass-balance constraints on Pliocene sea level and East Antarctic Ice Sheet stability. *Geology*, 43(10):879–882, 2015.
- A. P. Wolfe, A. Z. Csank, A. V. Reyes, R. C. McKellar, R. Tappert, and K. Muehlenbachs. Pristine early eocene wood buried deeply in kimberlite from northern Canada. *PLoS one*, 7(9):e45537, 2012.
- F. Woodruff and S. M. Savin. Miocene deepwater oceanography. *Paleoceanography*, 4(1):87–140, 1989.
- S. Xie, C. J. Nott, L. A. Avsejs, F. Volders, D. Maddy, F. M. Chambers, A. Gledhill, J. F. Carter, and R. P. Evershed. Palaeoclimate records in compound-specific  $\delta D$  values of a lipid biomarker in ombrotrophic peat. *Organic Geochemistry*, 31(10): 1053–1057, 2000.
- D. Yakir and M. J. DeNiro. Oxygen and Hydrogen Isotope Fractionation during Cellulose Metabolism in *Lemna gibba* L. *Plant Physiology*, 93(1):325–32, 1990.
- S. Yamamoto, A. Otto, G. Krumbiegel, and B. R. T. Simoneit. The natural product biomarkers in succinite, glessite and stantienite ambers from Bitterfeld, Germany. *Review of Palaeobotany and Palynology*, 140(1):27–49, 2006.
- H. Yang, M. Pagani, D. E. G. Briggs, M. A. Equiza, R. Jagels, Q. Leng, and B. A. Lepage. Carbon and hydrogen isotope fractionation under continuous light: implications for paleoenvironmental interpretations of the High Arctic during Paleogene warming. *Oecologia*, 160(3):461–470, 2009.
- H. Yang, W. Liu, Q. Leng, M. T. Hren, and M. Pagani. Variation in n-alkane  $\delta D$  values from terrestrial plants at high latitude: Implications for paleoclimate reconstruction. *Organic Geochemistry*, 42(3):283–288, 2011.
- J. C. Zachos, M. Pagani, L. Sloan, E. Thomas, and K. Billups. Trends, rhythms, and aberrations in global climate 65 Ma to present. *Science*, 292(5517):686–93, 2001.
- C. Zhang, Y. Wang, T. Deng, X. Wang, D. Biasatti, Y. Xu, and Q. Li. C4 expansion in the central Inner Mongolia during the latest Miocene and early Pliocene. *Earth and Planetary Science Letters*, 287(3-4):311–319, 2009.
- J. Zhang, P. D. Quay, and D. O. Wilbur. Carbon-Isotope Fractionation During Gas-Water Exchange and Dissolution of  $CO_2$ . *Geochimica et Cosmochimica Acta*, 59(1): 107–114, 1995.
- Z. S. Zhang, K. H. Nisancioglu, M. A. Chandler, A. M. Haywood, B. L. Otto-Bliesner, G. Ramstein, C. Stepanek, A. Abe-Ouchi, W. L. Chan, F. J. Bragg, C. Contoux, A. M. Dolan, D. J. Hill, A. Jost, Y. Kamae, G. Lohmann, D. J. Lunt, N. A. Rosenbloom, L. E. Sohl, and H. Ueda. Mid-pliocene Atlantic Meridional Overturning Circulation not unlike modern. *Climate of the Past*, 9(4):1495–1504, 2013.
- M. F. Zhu, L. Stott, B. Buckley, K. Yoshimura, and K. Ra. Indo-Pacific Warm Pool convection and ENSO since 1867 derived from Cambodian pine tree cellulose oxygen isotopes. *Journal of Geophysical Research-Atmospheres*, 117, 2012.



---